

Universidade do Minho
Escola de Engenharia

Tiago Sanches Franco

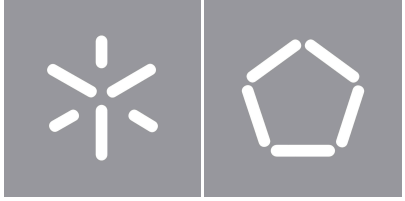
Clinical Decision Support System to Electrostimulation Treatments for Muscle Rehabilitation in the Elderly

October, 2024

Clinical Decision Support System to Electrostimulation Treatments for Muscle Rehabilitation in the Elderly

Tiago Sanches Franco

UMinho | 2024



University of Minho
School of Engineering

Tiago Sanches Franco

Clinical Decision Support System to Electrostimulation Treatments for Muscle Rehabilitation in the Elderly

PhD Thesis
Doctorate in Informatics

Thesis supervised by
Pedro Manuel Rangel Santos Henriques
Paulo Alexandre Vara Alves

october 2024

Copyright and Terms of Use for Third Party Work

This dissertation reports on academic work that can be used by third parties as long as the internationally accepted standards and good practices are respected concerning copyright and related rights.

This work can thereafter be used under the terms established in the license below.

Readers needing authorization conditions not provided for in the indicated licensing should contact the author through the RepositóriUM of the University of Minho.

License granted to users of this work:



CC BY-NC-SA

https://creativecommons.org/licenses/by-nc-sa/4.0/

Acknowledgements

With deep gratitude, I would like to sincerely thank everyone who was part of this challenging doctoral journey. This work results from the support, dedication, and generosity of many.

First and foremost, I am incredibly thankful to my supervisor, Professor Pedro Henriques, and my co-supervisor, Professor Paulo Alves. Their knowledge, patience, and consistent guidance led me through each step of this journey. I am equally grateful to Professor Maria João Varanda Pereira, who provided weekly support alongside my supervisors. Thank you for the trust you placed in me and the challenges you presented, which have shaped me both as a researcher and a person.

To my partner and love, Laís Fabiana Serafini, who was by my side through moments of exhaustion, joy, and achievement. I offer my deepest thanks for your essential support, understanding, and patience throughout this journey.

I am also grateful to my father and mother, whose attentiveness and care have been a constant source of strength, even from afar. To my sister, whose encouraging words have supported me not only in this work but throughout my life, I am deeply thankful.

To the participants in the experimental studies, thank you for generously sharing your time and commitment to help advance this project. Without your involvement, this work would not have been possible.

I would also like to thank Professors Paulo Leitão, Tiago Pedrosa, and José Rufino, who played key roles in the NanoStim project, along with students Leonardo Sestrem de Oliveira, Felipe Gimenez da Silva, Raul Kaizer, and João Gonçalves, who contributed significantly to the project.

I am also thankful to physiotherapists Nelson Azevedo and Elsa Costa for their technical and scientific support throughout the NanoStim project.

My sincere thanks to Ana Carolina Cardoso De Sousa and the Research Centre for Biomedical Engi-

neering members at the Universitat Politècnica de Catalunya. I am grateful for your warm welcome and professionalism, which provided a stimulating environment.

To all my colleagues at the Research Centre in Digitalization and Intelligent Robotics (CeDRI), with whom I shared countless conversations, discussions, and cups of coffee, thank you for your friendship.

Finally, I am grateful to the Foundation for Science and Technology (FCT), Portugal for the PhD scholarship grant number *2020.05704.BD*, which made this research possible and allowed me to focus entirely on my studies.

This work was supported European Regional Development Fund (ERDF) through the Operational Programme for Competitiveness and Internationalization (COMPETE 2020), under Portugal 2020, in the framework of the NanoStim (POCI-01-0247-FEDER-045908) project. This work was supported by national funds through FCT/MCTES (PIDDAC): CeDRI, UIDB/05757/2020 and UIDP/05757/2020; SusTEC, LA/P/0007/2020; Centro ALGORITMI, UIDB/00319/2020.

This work reflects the contributions of each of you, and I am sincerely grateful.

Statement of Integrity

I hereby declare having conducted this academic work with integrity.

I confirm that I have not used plagiarism or any form of undue use of information or falsification of results along the process leading to its elaboration.

I further declare that I have fully acknowledged the Code of Ethical Conduct of the University of Minho.

University of Minho, Braga, october 2024

Tiago Sanches Franco

Abstract

The aging population poses increasing challenges to healthcare systems, particularly regarding long-term muscular rehabilitation services for the elderly. Conditions such as sarcopenia and knee osteoarthritis, which are common in this age group, compromise mobility and quality of life, making rehabilitation essential for ensuring active aging. Neuromuscular electrical stimulation has proven to be an effective intervention, but its proper application depends on personalized parameterization and continuous monitoring. This PhD project presents an innovative solution to this scenario: a Clinical Decision Support System (CDSS) aimed at electrostimulation treatments. Developed within the scope of the NanoStim project, CDSS integrates Industry 4.0 technologies to create an efficient, portable, and cost-effective wearable system, allowing treatment to be conducted at home, with increased accessibility and reduced clinical visits. A system architecture with sensitive data protection for home treatment scenarios is proposed. The system processes real-time muscle fatigue metrics, interprets knee extension exercises, and adjusts electrostimulation in a personalized manner. Three experimental studies validated CDSS. In the first, the system demonstrated the ability to synchronize biofeedback data and remove artifacts from the electromyographic signal. In the second, the accuracy of the mobile application in processing muscle fatigue metrics in real-time was demonstrated. In the third, the CDSS was compared with a gold-standard motion capture system, and responsive electrostimulation modes based on real-time biofeedback were tested. Finally, a statistical correlation analysis was conducted between the fatigue levels predicted by the CDSS and the participants' subjective feedback. The CDSS received ethical approvals from different institutions and clearance for sensitive data storage. The analyzed results show that CDSS has the potential to innovate in the field of remote muscular rehabilitation and improve the quality of life for the elderly through personalized treatments.

Keywords Biofeedback, Decision Support, Electrostimulation, Remote Rehabilitation, Wearable Device

Resumo

O envelhecimento da população impõe desafios crescentes aos sistemas de saúde, especialmente no que diz respeito aos serviços de reabilitação muscular de longo prazo para idosos. Condições como sarcopenia e osteoartrite do joelho, comuns nessa faixa etária, comprometem a mobilidade e a qualidade de vida, tornando a reabilitação essencial para garantir um envelhecimento ativo. A eletroestimulação neuromuscular tem se mostrado uma intervenção eficaz, mas a sua aplicação adequada depende de uma parametrização personalizada e acompanhamento contínuo. Esta tese de doutoramento apresenta uma solução inovadora para esse cenário: um Sistema de Suporte à Decisão Clínico (SSDC) para tratamentos de eletroestimulação. Desenvolvido no âmbito do projeto NanoStim, o SSDC integra tecnologias da Indústria 4.0 para criar um sistema wearable eficiente, portátil e de baixo custo, permitindo que o tratamento seja realizado em casa, com maior acessibilidade e redução de consultas clínicas. Assim, é proposto uma arquitetura de sistema com proteção de dados sensíveis para o cenário de tratamento ao domiciliar. O sistema processa em tempo real métricas relacionadas a fadiga muscular, interpreta o exercício de extensão de joelho e ajusta a eletroestimulação de forma personalizada. Três estudos experimentais validaram o SSDC. No primeiro, o sistema demonstrou a capacidade de sincronizar os dados de biofeedback e remover artefatos do sinal eletromiográfico. No segundo, foi evidenciada a precisão da aplicação móvel em processar métricas de fadiga muscular em tempo real. No terceiro, o SSDC foi comparado com um sistema padrão-ouro de captura de movimento, foram testados modos de eletroestimulação responsivos ao biofeedback coletado em tempo real. Por fim, foi realizado uma análise estatística de correlação entre o nível de fadiga previsto pelo SSDC com o feedback subjetivos dos participantes. O SSDC recebeu aprovações éticas de diferentes instituições e aprovação para armazenamento de dados sensíveis. Os resultados analisados mostram que o SSDC tem potencial de inovar a área de reabilitação muscular remota e melhorar a qualidade de vida dos idosos por meio de tratamentos personalizados.

Palavras-chave Biofeedback, Dispositivo Vestível, Eletroestimulação, Reabilitação Remota, Suporte a Decisão

Contents

1 Introduction **1**

1.1 Motivation and Relevance 1

1.2 Research Objectives 3

1.3 Research methodology 5

1.3.1 Design Science Research Methodology for IS 5

1.3.2 Cross-Industry Standard Process for Data Mining 7

1.4 Document Structure 8

2 Background **9**

2.1 Aging and Functional Impairment 9

2.2 Electrical Stimulation as a Rehabilitation Tool 12

2.3 Decision Support System 15

2.3.1 Clinical Decision Support Systems 17

2.3.2 Rule-Based Reasoning 19

2.3.3 Case-Based Reasoning 20

2.3.4 Model-Based Reasoning 21

2.3.5 Machine Learning-Based Reasoning 21

3 State of the Art **23**

3.1 Methodology 23

3.1.1 Keywords Identification 23

3.1.2 Systematic Literature Review Approach 25

3.2 Research Trends Over Time 28

3.3 Systematic Literature Review 33

3.3.1 RQ_01: What are the main characteristics of the system architecture? 36

3.3.2 RQ_02: What data is used and how is it acquired? 37

3.3.3 RQ_03: How is sensitive data protected? . . . 39
3.3.4 RQ_04: What are the reasoning methods used in these systems? . . . 39
3.3.5 RQ_05: How do systems modify electrical stimulation? . . . 40
3.3.6 RQ_06: How were the systems validated? . . . 41
3.4 Conclusions . . . 41

4 myHealth System 43
4.1 Design . . . 43
4.1.1 Treatment Scenarios . . . 43
4.1.2 System Architecture . . . 46
4.1.3 Sensitive Data Protection . . . 48
4.1.4 Database Modeling . . . 50
4.2 Prototyping . . . 53
4.2.1 Cloud Infrastructure . . . 53
4.2.2 Wearable Device . . . 53
4.2.3 Mobile Application . . . 56
4.2.4 Communication Between the Wearable System and the Mobile App . . . 58
4.2.5 System Panel . . . 61

5 Intelligent Features for Treatment Customization 64
5.1 Movement Recognition . . . 64
5.1.1 Mathematical Model . . . 65
5.1.2 Knee Extension Exercise . . . 67
5.2 Muscle Fatigue Monitor . . . 71
5.2.1 Fatigue Metrics . . . 71
5.2.2 Normalization and Calibration . . . 76
5.3 Stimulation Modes . . . 77
5.3.1 Commercial Stimulator . . . 78
5.3.2 Raising the Leg Stimulator . . . 79
5.3.3 Range of Angle Stimulator . . . 80
5.4 Rule-based Stimulation . . . 81
5.4.1 Fatigue Stages . . . 81
5.4.2 Automatic Session . . . 84

5.5 Data visualization . . . 86
5.5.1 Mobile App . . . 86
5.5.2 Administrative Panel . . . 88

6 Tests and Validations **93**

6.1 Evaluation Metrics . . . 94
6.2 Preliminary Validation . . . 95
6.2.1 Transmission Test . . . 95
6.2.2 Security Analysis . . . 96
6.2.3 A First Experiment . . . 98
6.2.4 Validation of IMU Sensors . . . 99
6.3 Experimental Studies with Volunteers 1 . . . 106
6.3.1 Experimental Protocol . . . 107
6.3.2 Removal of Stimulation Artifacts in EMG Signals . . . 109
6.3.3 Maximum Voluntary Contraction (MVC) . . . 113
6.3.4 Knee Extension Movement Recognition . . . 115
6.3.5 Discussion Experiment 1 . . . 122
6.4 Experimental Studies with Volunteers 2 . . . 123
6.4.1 Experimental Protocol . . . 124
6.4.2 Automated Movement Recognition . . . 125
6.4.3 Fatigue Metrics Evaluation . . . 127
6.4.4 Muscle Fatigue Level Simulator . . . 130
6.4.5 Mobile Data vs. Cloud Data . . . 134
6.4.6 Discussion Experiment 2 . . . 137
6.5 Experimental Studies with Volunteers 3 . . . 138
6.5.1 Experimental Protocol . . . 139
6.5.2 Pre-Processing . . . 141
6.5.3 Movement Recognition: CDSS vs MoCap . . . 143
6.5.4 Comparison between Stimulation Modes . . . 149
6.5.5 Muscle Fatigue Evaluation . . . 154
6.5.6 Fatigue Level Simulator vs Self-Report Feedback . . . 158
6.5.7 Discussion Experiment 3 . . . 168

7 Conclusion **170**

7.1 Scientific Contributions 172

7.1.1 Journal Papers 172

7.1.2 Conference Papers 173

7.1.3 Doctoral Symposium 173

7.1.4 Extended Abstract in Conference 173

7.1.5 Co-authored Conference Papers 173

7.1.6 Talks and Demos 174

7.1.7 Article in Online Newspaper 174

7.2 Future Perspectives 174

List of Figures

1 Population growth in Portugal by age group (Ritchie et al., 2023). 1
2 DSRM Process Model (Peffers, 2008). 6
3 CRISP-DM methodology (Wirth and Hipp, 2000). 8
4 Muscle strength across the life course (Cruz-Jentoft et al., 2019). 10
5 The Kellgren and Lawrence Classification (Hayashi et al., 2016). 11
6 Schematic of biphasic electrostimulation pulses. Adapted (Lynch and Popovic, 2008). . 14
7 The genealogy of the DSS field, 1960–2010 (Arnott and Pervan, 2014). 16
8 The CDSS Components (Shoaip et al., 2019). 18
9 PRISMA 2020 flow diagram of the systematic review. Adapted from (Page et al., 2021). . 28
10 Annual Scientific Production. 29
11 Top 10 bigram terms over time. 30
12 Co-occurrence Network of bigram terms. 31
13 Reasoning methods of the selected articles. 40
14 The treatment scenario in the clinic. 44
15 The treatment scenario in patient's home. 45
16 System Architecture. 47
17 Representation of pseudonymization technique. 49
18 Signature and content verification process using asymmetric keys. 49
19 Entity-Relationship (ER) Model of the Management API Database. 50
20 NoSQL data model for the clinical service. 52
21 Wearable Device Design. 54
22 Wearable Device Components in PCB. 55
23 MVVM pattern applied to Android app. 57
24 Use Case Diagram for System Panel. 63

25 IMU sensor with the reference coordinate system. 65
26 (**a**) Frame representation relative to a reference. (**b**) Linear mapping of a frame to another. 65
27 Sensors with the angles representation. Adapted from (Olinski et al., 2017). 66
28 Data collected during knee extension exercise. 67
29 Classification of movement between the four phases. 68
30 Phases of contraction recognition interfaces. 69
31 Example of EMG sensor data clipping by recognized movement. The EMG sensor signal is displayed in blue and the knee angle is displayed in black. 72
32 Screens of the calibration process. 77
33 Sequence Diagram of the Commercial Stimulator. 78
34 Sequence Diagram of the Raising the Leg Stimulator. 79
35 Sequence Diagram of the Range of Angle Stimulator. 80
36 Muscle Fatigue Stages Simulator. 83
37 Automatic Session Form. 85
38 Automatic Session Adaptation Screens. 86
39 Calibration Overview Screen. 87
40 Real-time analysis screen. 88
41 Session Information Screen. 90
42 Clinical History Page - Part 1. 91
43 Clinical History Page - Part 2. 92
44 Packet exchange time between the wearable system and the mobile app. 96
45 Test treatment session on a volunteer without electrostimulation. (A) Subject's leg relaxed. (B) Subject's knee is fully extended. 98
46 Oscilloscope with stimulation pulses applied to the resistor. 99
47 Δ Time of IMU samples collected by the wearable system. 100
48 Wearable modules attached to the UR3 robot. 101
49 Wearable system raw data synchronized with UR3 data. 102
50 CF filter implemented in wearable embedded system. 105
51 Wearable system and mobile app recognizing the movement of a volunteer's leg. 106
52 Positioning of sensors and stimulator on the volunteer. 108
53 Example of EMG signal captured during the FES experiment. 109
54 Example of peak detection in the EMG signal. 110

55 Example of segment with identified stimulation artifact. 111
56 Example of EMG signal captured during the FES experiment filtered. 113
57 Example of segment with identified stimulation artifact filtred. 113
58 Mean muscle activity of subjects in mV. 114
59 Maximum Voluntary Contraction of subjects. 114
60 Mean muscle activity of subjects normalized by MVC. 115
61 Variation in Maximum Angle and Duration of Knee Extension Movement - Experiment 1. . 116
62 Cycles of Knee Extension Movement. 117
63 Muscle Activity in Knee Angle Ratio. 118
64 Comparison between the First and Third Test. 119
65 Comparison between the First and Last Movement. 119
66 Trajectory of Median Frequency and RMS during the First and Third tests. 121
67 Concatenated Trajectory of Median Frequency and RMS during Tests 1 and 3. 122
68 Variation in Maximum Angle and Duration of Knee Extension Movement - Experiment 2. . 125
69 Cycle of Knee Extension Movement - Exp 2. 126
70 Trend of the avgFreq metric during the session. 128
71 Trend of the medianFreq metric during the session. 128
72 Trend of the RMS metric during the session. 128
73 JASA Method apply to Experimental Test. 129
74 (A) Occurrence of Fatigue (B) Intensity of Occurrences by Configuration. 131
75 Fatigue Levels Achieved by Configuration. 132
76 Contraction number at first fatigue level achieved. 132
77 (A) Amount of Occurrence (B) Average Intensity of First and Last Level per Participant. . 133
78 (A) Contractin Number of Levels Change (B) Average Intensity per Level. 134
79 Comparison between systems of the $AvgFreq$ metric. 135
80 Comparison between systems of the $MedFreq$ metric. 135
81 Comparison between systems of the RMS metric. 135
82 MoCap equipment: Camera (A) and Body Makers (B). 138
83 Experimental Setup Showing the Positioning of Electrodes, Sensors, and Markers. 140
84 Pre-Processing Methodology. 141
85 OpenSim Model Scaling. 142
86 Variation in Maximum Angle and Duration of Knee Extension Movement - Experiment 3. . 144

87 Comparison of Maximum Angle Variation between CDSS and MoCap. 145
88 Comparison of Maximum Angle Variation between CDSS Adjusted and MoCap. 146
89 Kinematic Comparison of Movement between the systems. 147
90 Dynamic Comparison of Movement between the systems. 148
91 Knee angle at the start and end of stimulation modes.. 150
92 EMG signal during *Raising the Leg* stimulation. 151
93 EMG signal during *Range of Angle* stimulation. 151
94 Self-Reported Feedback of Experiment 3. 152
95 Stimulation Noise in the EMG signal. (A) *Raising the Leg* (B) *Range Of Angle*. 154
96 Muscle Activity in Both Legs - Experiment 3. 155
97 Muscle Activity Variation During Experimental Sessions in Both Legs - Experiment 3. . . 155
98 Trend of the Averange Frequency Metric - Experiment 3. 156
99 Trend of the Median Frequency Metric - Experiment 3. 156
100 Trend of the RMS Metric - Experiment 3. 157
101 Joint Amplitude and Spectrum Analysis (JASA) - Experiment 3. 157
102 Fatigue Occurrences by Configuration in Both Legs - Experiment 3. 158
103 Intensity of Occurrences by Configuration in Both Legs - Experiment 3. 159
104 Fatigue Levels Achieved by Configuration on the Left Leg - Experiment 3. 160
105 Fatigue Levels Achieved by Configuration on the Right Leg - Experiment 3. 160
106 Contraction Number at First Fatigue Level Achieved on the Left Leg - Experiment 3. . . . 161
107 Contraction Number at First Fatigue Level Achieved on the Right Leg - Experiment 3. . . 161
108 Amount of Fatigue Occurrences (A) and Intensity (B) by Subjects on the Left Leg. 162
109 Evolution of Fatigue Perception in the Self-Report on the Left Leg. 162
110 Amount of Fatigue Occurrences (A) and Intensity (B) by Subjects on the Right Leg. . . . 163
111 Evolution of Fatigue Perception in the Self-Report on the Right Leg. 164
112 Comparison of self-report fatigue with predicted level by subject. 166

List of Tables

1 Inclusion Search Terms. 24
2 Exclusion Search Terms. 25
3 Research Questions. 26
4 Inclusion Criteria. 27
5 Exclusion Criteria. 27
6 Identification of Selected Articles. 34
7 Data and Acquisition Tools Used in the Selected Studies. 38
8 Study participants by type. 41

9 Biofeedback data and packet volume. 59
10 Optimized Data Transmission Frequency. 59

11 Evaluation metrics of the applied filters in degrees. 104
12 Anthropometric data of the subjects - Experiment 1 107
13 Comparative Metrics between the First and Third Tests. 120
14 Anthropometric data of the subjects - Experiment 2. 124
15 Assessment metrics on fatigue metrics. 136
16 Anthropometric data of the subjects - Experiment 3. 139
17 Kinematic Evaluation Metrics Comparison. 147
18 Dynamic Evaluation Metrics Comparation. 148
19 Average Variation in Fatigue and Comfort Across Experimental Sessions. 153
20 Correlations between predicted and self-reported fatigue levels. 167

Chapter 1

Introduction

This chapter opens the dissertation, outlining its contents. Initially, the first section contextualizes the motivation behind the doctoral project. Subsequently, the second section explains the objectives and highlights their relevance in the research context. The third section details the research methodologies used in the study. Finally, the fourth section discusses the general structure of this document.

1.1 Motivation and Relevance

Over the last few decades, a substantial global increase in life expectancy has been recorded, particularly in regions such as Europe and Portugal. This positive trend is linked to advances in healthcare technology, improvements in living standards, and greater access to education. Notably, the demographic group of individuals aged 65 and above, constituting the elderly population, stands out as one of the fastest-growing segments, significantly impacting societal dynamics and the healthcare systems (Dattani et al., 2023).

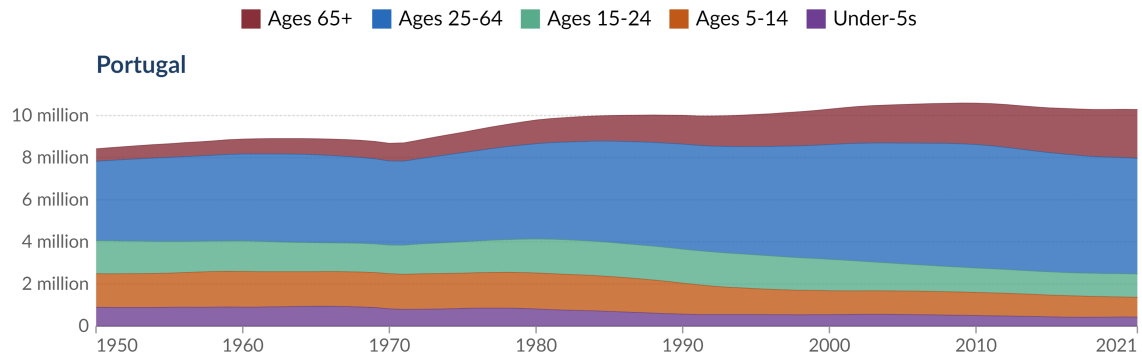


Figure 1: Population growth in Portugal by age group (Ritchie et al., 2023).

To understand the magnitude of population growth, Figure 1 illustrates population growth in Portugal divided by age groups. Comparing statistics from 1980 to 2020, it is possible to note that Portugal's elderly population grew from 1.12 million to 2.32 million, representing an increase of more than 100%.

Similarly, European populations are reflecting this growth at a proportional rate, worldwide this growth is even bigger, close to 200% for the same period (Ritchie et al., 2023).

As the proportion of older adults increases, the demand for primary and long-term health services also grows, especially those related to chronic conditions and age-related diseases. The gradual decline in functional capacity due to aging is natural progress common to all living beings, requiring constant care to preserve an active and dignified life (WHO, 2021). Thus, rehabilitation treatments face a critical accessibility problem that tends to get worse.

A Study was carried out by Cieza et al. (2020) to assess the demand for rehabilitation services worldwide and its impact on the healthcare system. The results obtained reveal that one in three people in the world, approximately 2.4 billion individuals, need these services. These estimates contradict the common belief that the need for rehabilitation is restricted to a limited number of people. This finding highlights the magnitude of the demand for rehabilitation services and emphasizes the importance of effective strategies to serve this considerable portion of the global population.

The concern about the delay in finding the necessary treatment is addressed by the World Health Organization (WHO) in their report on healthy aging for the decade between 2021 and 2030 (WHO, 2021). The report highlights the significance of improving functional capacity to promote more independent aging and suggests data-driven solutions to achieve scalable and accessible answers.

The traditional treatment for mobility rehabilitation is regular physical exercise, improving the performance of strength, endurance, balance, flexibility, and so on. However, regular training for the elderly can be expensive since some pathologies such as cardiovascular diseases and neuromuscular problems can make the execution of some exercises unfeasible, generating a need to attend specialized training centers or hire specialized agents (Chodzko-Zajko et al., 2009).

A solution positioned as an interesting and less expensive alternative to the traditional training methods could be home-based neuromuscular electrical stimulation (NMES), also known as Functional Electrical Stimulation (FES). NMES is a technique that artificially produces muscle contraction through the application of an electrical current with surface electrodes on the muscles. There is still no consensus on all reactions that the application of NMES provokes in the body and especially in the muscle. However, it is believed that training with NMES produces an increase in the muscle's capacity to generate force, triggering a series of benefits (Imoto et al., 2013).

NMES is generally applied to improve functional capacity, preservation and recovery of muscle mass, and muscle strengthening. A systematic review presented by Langeard et al. (2017) show that training with NMES is safe and has an efficiency similar to traditional training in the elderly. Furthermore, they

show that training with NMES can bring considerable benefits to the physiological state, improving gait and balance performance, especially in less active elderly people.

Despite this, the use of NMES as a training method for muscle rehabilitation in the elderly is considered recent. So far, there is no consensus on which configurations produce a more adequate rehabilitation. Several parameters have already been tested for the treatment, however, there is no evidence that only a certain set of parameters can trigger positive effects in the treatment. (Langeard et al., 2017). Maffiuletti (2010) reports that evidence suggests that the effectiveness of electrostimulation depends more on the patient's natural characteristics than on the adjustable parameters of NMES treatment.

In this context, the research area Health 4.0 can play an essential role in constructing treatments that consider individual particularities. Health 4.0 is a recent area that encompasses how health is managed and delivered, considering the latest technological advances that combine concepts derived from Industry 4.0, including the Internet of Things, Big Data, Machine Learning, and mobile apps (Bause et al., 2019).

Combining these elements provides the fundamental requirements to create patient-centered approaches that were not available before. The key that enables the design of innovative treatments is the data collected through sensors integrated into wearables or smart devices (Lou et al., 2020). Several sensors can acquire high-quality data that can be clinically relevant, for example, motion identification through the Inertial Measurement Unit sensor (IMU), heart rate measurement through the Electrocardiogram sensor, muscle contraction volume through the Electromyogram sensor (EMG), blood pressure through Oximeter sensor, among others (Jayaraman et al., 2020).

1.2 Research Objectives

This doctoral project aims to advance the principles of Health 4.0 by designing and developing a Clinical Decision Support System (CDSS) tailored for neuromuscular electrical stimulation (NMES) treatments in muscle rehabilitation for the elderly. The CDSS is conceived as an intelligent system that supports healthcare professionals in creating personalized rehabilitation plans that adapt to each patient's unique biological responses. Additionally, the system facilitates remote, home-based treatments through a wearable device, addressing the growing demand for scalable, accessible, and effective rehabilitation solutions to manage conditions such as sarcopenia and knee osteoarthritis in the aging population.

Research Question

How can a Clinical Decision Support System be designed to support remote rehabilitation with electrostimulation using a wearable device?

This main research question guides the investigation into how a CDSS can be developed to effectively support remote muscle rehabilitation by integrating real-time biofeedback data from NMES treatment sessions. The goal is to create a system capable of performing automated analyses of muscle behavior, providing personalized treatment that adjusts to the patient's condition over time. Moreover, the CDSS is expected to enhance communication between healthcare professionals and patients, ensuring a more integrated, data-driven, responsive rehabilitation process.

In order to address the central research question effectively, it is necessary to break it down into specific investigations that focus on critical elements of the CDSS design and functionality. Each research question targets a fundamental part of the system, contributing to a structured and comprehensive understanding of its development. These questions are crucial for guiding the design and implementation of the CDSS in a structured, evidence-driven approach that facilitates the achievement's replicability.

Specific Research Questions

1. How can real-time biofeedback from a wearable device be processed to monitor and assess muscle fatigue during remote rehabilitation accurately?

2. What methods can be implemented to securely store and transmit sensitive patient data within the system architecture?

3. How can electrostimulation treatments be dynamically adjusted in real-time based on biofeedback data during a treatment session?

Given on the research questions that pilot this PhD thesis, the doctoral project establishes four main objectives for overcoming the technological, clinical, and ethical challenges in developing the CDSS.

Objectives

- Design a System Architecture: Develop a system architecture that supports the integration of advanced algorithms such as machine learning and computational simulations within the context of muscle rehabilitation, ensuring the feasibility of remote treatments.

- Establish a Technological Interface: Create an interface that streamlines the rehabilitation process and enhances communication between patients and healthcare providers, promoting more efficient treatment monitoring and personalized feedback.
- Ensure Data Protection and Privacy: Implement robust mechanisms for secure storage and transmission of sensitive patient data that align with ethical and legal standards.
- Develop a Reasoning Method: Design a reasoning method capable of dynamically adjusting electrostimulation parameters based on real-time biofeedback.

In addition, the project commits to contribute to the WHO proposals for the decade of healthy aging in two scientific forms. The first refers to collaboration with innovative ways to collect, measure and analyze data on the health of the elderly. The second refers to lower the cost of new treatments and expand access, opting for alternatives that enable online communication.

1.3 Research methodology

This PhD work used two methodologies. Considering the nature of this research project, which involves the development of an Information System, the methodology adopted was Design Science Research, specifically Design Science Research Methodology for Information Systems (DSRM-IS).

Since it was also required to develop models and explore different types of data, a second methodology that fits better was applied. In this context the research was guided by the Standard Cross-Industry Process for Data Mining (CRISP-DM).

1.3.1 Design Science Research Methodology for IS

The DSRM-IS methodology consists of a set of principles, practices and procedures that must be followed to develop Information Systems and the necessary analytical perspectives to develop IS research. DSRM-IS is an iterative process that includes six main activities: Identify Problem and Motivate, Define objectives of a solution, Design and Development, Demonstration, Evaluation, Communication (Peffers, 2008). The DSRM-IS activities are presented in Figure 2.

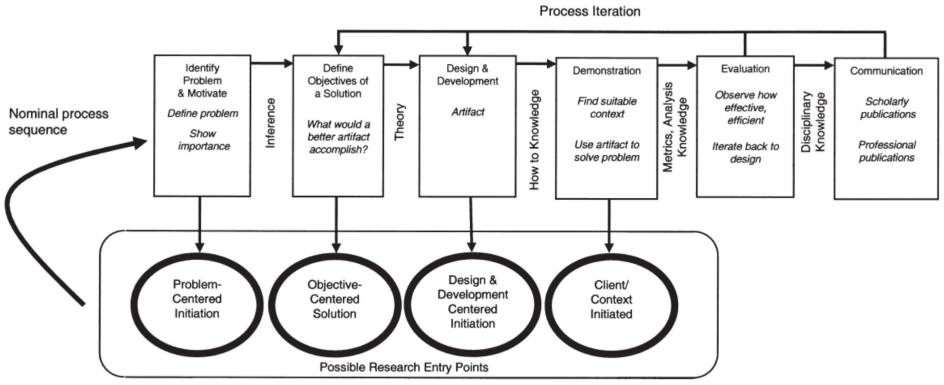


Figure 2: DSRM Process Model (Peffers, 2008).

Briefly, the competencies that must be performed in each activity are described below:

- **Identify Problem and Motivate:** The first activity consists of defining the specific research problem and justify the value of the solution presented.

- **Define objectives of a solution:** this activity aims to infer the solution objectives from the definition of the problem and the possible and attainable knowledge. Objectives can be quantitative or qualitative, as long as they allow reaching a solution to the identified problem.

- **Design and Development:** the third activity consists of creating the artifact. A design research artifact can be any designed object as long as it has the research contribution built into the design.

- **Demonstration:** In activity four it is necessary to demonstrate the use of the artifact solving at least the problem instances. The demonstration can be made in the form of experimentation, simulation, case study, proof, or other appropriate activity.

- **Evaluation:** In this activity, it is necessary to observe and measure how well the artifact supports a solution to the problem. For this, knowledge of relevant metrics and analysis techniques is required. At the end of this activity, it is required to decide whether to iterate back to activity 3 to try to improve the artifact's effectiveness.

- **Communication:** The last activity is related to the communication of the problem and its importance, the artifact, its usefulness and novelty, the rigor of its design and its effectiveness for researchers. For this project, the communication activity was carried out through the publication of research articles and the publication of the doctoral dissertation.

1.3.2 Cross-Industry Standard Process for Data Mining

The CRISP-DM methodology defines a hierarchical process model in terms for the execution of Machine Learning projects. This methodology can be described in four levels of abstraction: phase, generic task, specialized task and process instance. The purpose of CRISP-DM is to provide an overview of the life cycle of a project divided into 6 phases. The different phases are: business understanding, data understanding, data preparation, modeling, evaluating and deployment. This life cycle is an iterative process, where the outcome of the phase will determine the next step to be taken (Wirth and Hipp, 2000). Figure 3 illustrates the phases and links between the phases of the CRISP-DM methodology.

The competencies that must be performed in each phase are described below:

- **Business understanding:** The first phase is concerned with understanding the objectives and requirements from a business perspective. From the goals, a data mining problem and a preliminary project plan are defined.

- **Data understanding:** The second phase aims to know the data after an initial collection. It is intended that this phase can identify data quality problems, discover features and detect important subsets of the data. There is a close link with the first phase, as formulating the data mining problem requires at least some understanding of the available data.

- **Data preparation:** In this phase, all activities to build a final dataset are performed, including the selection of datasets, rows and attributes, as well as data transformation and cleansing. Thus, the output of this phase is the input set for the modeling tools.

- **Modeling:** The fourth phase consists of selecting and applying several modeling techniques to the data. There is a close link between the third phase as some data issues can be found during modeling and need to go back to data preparation.

- **Evaluating:** At this stage, it is expected that the project has some models that demonstrate high quality from the perspective of data analysis. The main objective is to evaluate using metrics that justify a solution in the business objectives defined in the first phase. At the end, a decision must be made about the implementation of the models.

- **Deployment:** The task assigned to the last phase of the CRISP methodology depends on the purpose for which the models were created. As an example, for a theoretical study it is preferable to create documentation or write an article. However in industry it may be more interesting to implement the model in production.

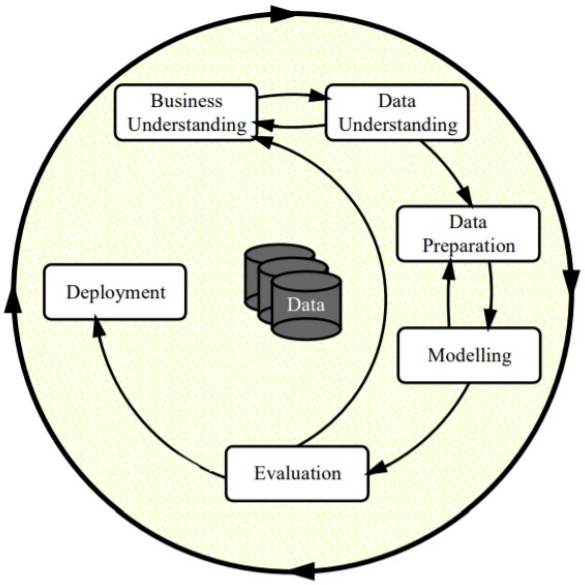


Figure 3: CRISP-DM methodology (Wirth and Hipp, 2000).

1.4 Document Structure

The structure of this dissertation was organized to guide the reader through all stages of the development, implementation, and validation of the CDSS for electrostimulation treatments in muscle rehabilitation named myHealth. After introducing the research concepts and objectives, Chapter 2 addresses aging-related pathologies that impact mobility, the use of electrostimulation as a rehabilitation tool, and clinical decision support systems. In Chapter 3, a Systematic Literature Review is conducted to identify the main trends and challenges in the development of CDSS for muscle rehabilitation with electrostimulation.

The subsequent chapters focus on the development and validation of the myHealth. Chapter 4 describes the design and prototyping of the CDSS such the system architecture and data protection measures. Chapter 5 details intelligent features implemented in myHealth such as movement recognition, muscle fatigue monitoring, and personalized stimulation modes. Chapter 6 presents the experimental studies conducted with volunteers to test and validate the CDSS, culminating in Chapter 7, where the main conclusions and future perspectives are discussed.

Chapter 2

Background

This chapter introduces the main concepts for understanding the project and common terms used in orthopedic medicine. The first section addresses the impact of aging on functional capacity, with a focus on conditions such as sarcopenia and knee osteoarthritis, which impair mobility in the elderly. The second section explores electrical stimulation as a rehabilitation tool, explaining its principles and applications in the treatment of muscular dysfunctions. The third section discusses the concept of decision support systems, addressing the main reasoning methods used in healthcare.

2.1 Aging and Functional Impairment

Aging is a natural and inevitable process that affects all human beings. As we age, a series of physical and physiological changes occur in our body, some of which can directly impact our functional impairment. Functional impairment refers to a decrease in an individual's ability to perform essential daily activities autonomously and effectively.

Several authors point out a series of factors that lead the elderly to lose part of their mobility. Such as, slowing down of metabolism causing a direct decrease in protein synthesis (Anisimova et al., 2020), accumulation of fat and changes in the type of muscle fiber (Evans and Lexell, 1995), decreased neural communication to the muscle (Manini et al., 2013), among others.

Sarcopenia is a condition often associated with aging, characterized by the progressive loss of muscle mass and strength, becoming more noticeable over the years. Muscle weakening compromises an individual's ability to perform tasks that require physical strength, such as lifting heavy objects, climbing stairs, and maintaining balance. Additionally, sarcopenia contributes to a decrease in bone density, increasing the risk of falls and fractures, significantly impacting functional autonomy (Cruz-Jentoft and Sayer, 2019).

In 2023, the prevalence of sarcopenia was estimated to affect 10% to 16% of the elderly population worldwide. Despite its relatively recent diagnosis, with the term being described only in 1980, the condition

was officially recognized as an independent entity with a code in the International Classification of Diseases (ICD-10) in 2016. Sarcopenia is associated with a high risk of various adverse health outcomes, including increased difficulty in postoperative recovery. Factors such as physical inactivity, malnutrition, smoking, excessive sleep duration, and diabetes can contribute to the early development of sarcopenia (Yuan and Larsson, 2023; Cruz-Jentoft and Sayer, 2019).

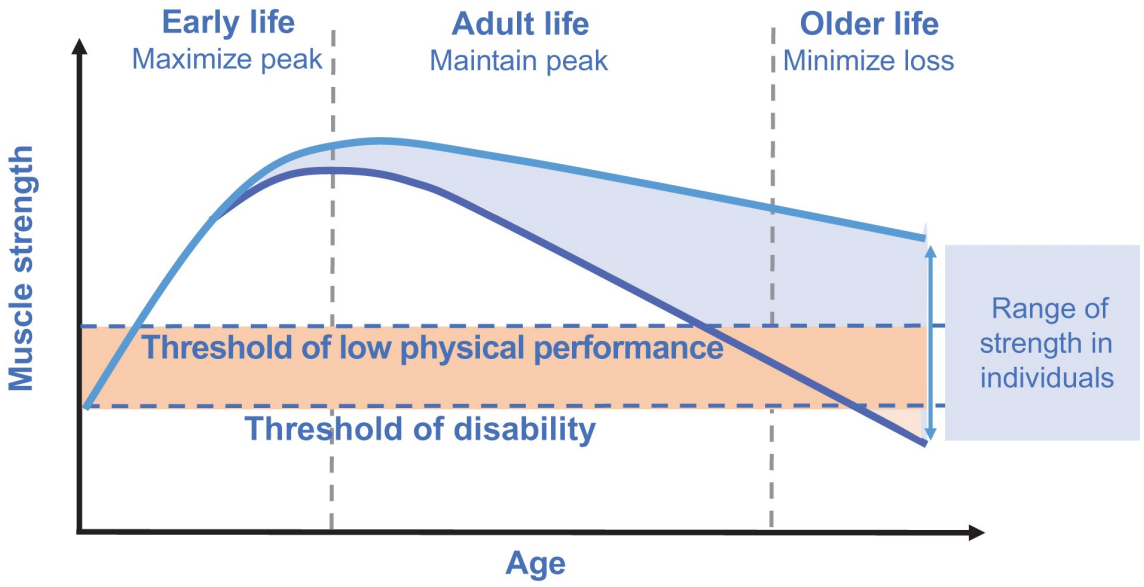


Figure 4: Muscle strength across the life course (Cruz-Jentoft et al., 2019).

Figure 4 illustrates muscle strength across the life course, highlighting the importance of maximizing muscle mass in youth and young adulthood, aiming to maintain muscle mass in middle age and minimize loss in older age. In the early stages of sarcopenia, an individual may be above the threshold for poor physical performance and most likely above the disability threshold. Genetic and lifestyle factors can accelerate muscle wasting and the progression to functional impairment and disability, but interventions such as nutrition and exercise training have been shown to slow or reverse these processes (Cruz-Jentoft et al., 2019).

Osteoarthritis (OA), the most common form of arthritis, is a degenerative joint disease caused by rupture and eventual loss of the cartilage that lines the bony extremities (Nelson and Jordan, 2015). This disease is directly related to aging and usually affects the knee, hip, spine, big toe, and hands. Estimates show that about 10% of men and 18% of women over 60 years of age have some kind of the OA, reinforcing its worldwide importance in public health (Nelson, 2018).

In particular, knee osteoarthritis (KOA) is the type of OA with the highest perceived prevalence. The most characteristic symptoms of KOA are usually changing in biomechanical behavior, such as joint pain, stiffness, cracking, and locking of the joints. These symptoms are usually noticed earlier because they

interfere in daily activities, especially abnormalities caused in gait (Zhang and Jordan, 2010).

The total set of factors that trigger the emergence and progression of KOA is under investigation. It is accepted that KOA is of multifactorial origin, that occurs in a slow process that typically takes 10 to 15 years. There are several correlations associated with modifiable and modifiable risk factors include family history, age, obesity, diabetes, synovitis, systemic inflammatory mediators, innate immunity, lower limb, joint integrity, mechanical forces, and cellular and biochemical processes. (Lespasio et al., 2017).

The KOA disease affects the three compartments of the knee joint, being medial, lateral and patellofemoral. It can be characterized by cartilage thinning and fibrillation with loss of joint space, osteophyte formation, subchondral bone sclerosis, subchondral cysts, and deformity. The pathophysiology of OA involves cartilage degradation, changes in the subchondral bone, synovium, ligaments, tendons, meniscus, muscle and nervous tissues (Nelson and Jordan, 2015).

The most common approach for confirming the KOA diagnosis is via radiographic images of the knee region. Kellgren and Lawrence (1957) formalized an escalation that takes into account a set of evidence that an X-ray needs to have to confirm the presence and stages of OA. This method is commonly adopted for its practicality and was accepted by the WHO in 1961.

The Kellgren and Lawrence scale (K-L) has five degrees, being divided between 0 for healthy individuals and 1 to 4 representing pathological stages from the mildest to the most critical. The K-L scale is also the most widely used method to examine OA in seven other joints, including the distal interphalangeal joint, metacarpophalangeal joint, first carpometacarpal joint, wrist, cervical spine, lumbar spine, and hips (Kohn et al., 2016).

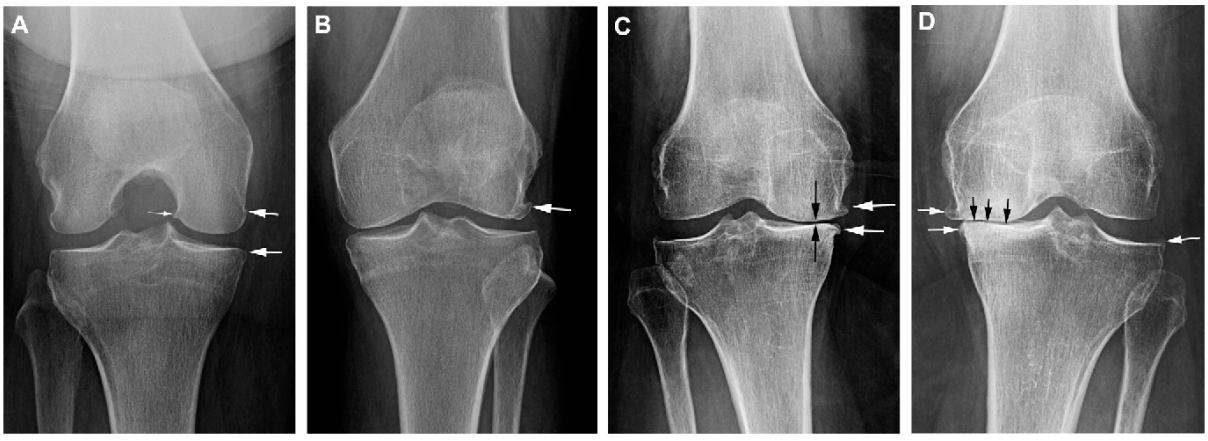


Figure 5: The Kellgren and Lawrence Classification (Hayashi et al., 2016).

Figure 5 shows the radiographs of the four pathological stages identified by the K-L scale. The main factors observed to perform the classification are marginal osteophytes and narrowing of the joint space

on radiography. In Figure 5A, the large arrows point to the minimal and ambiguous osteophytes on the medial margins of the joint. The small arrow indicated notch osteophytes in the center of the joint, which are not considered on the scale. In Figure 5B, it is possible to visualize the presence of at least one defined marginal osteophyte without evidence of joint space narrowing, this evidence justifying grade 2. Grade 3 in Figure 5C is characterized by signs of defined joint space narrowing and several marginal osteophytes. Figure 5D shows the last degree, in which it is possible to visualize the bone-bone contact and complete obliteration of the joint space in addition to the defined marginal osteophytes.

Both conditions, sarcopenia and knee osteoarthritis, highlight the direct influence of physical changes resulting from aging on functional impairment. Recognizing this reality is essential to implement preventive strategies, such as regular physical exercise, as well as seeking appropriate rehabilitation treatments. Early intervention proves to be even more beneficial, contributing not only to the preservation of functionality, but also to improving quality of life and promoting independence throughout the aging process.

2.2 Electrical Stimulation as a Rehabilitation Tool

Electrical stimulation is an innovative technique that has been increasingly recognized as an effective tool in the rehabilitation field. This approach uses controlled electrical currents to stimulate specific muscle groups, promoting muscle contraction and providing therapeutic benefits. The application of electrical stimulation as part of the rehabilitation process has gained prominence due to its ability to improve muscle strength, promote functional recovery and alleviate pain (Maffiuletti, 2010).

Electrical stimulation treatments can be found by many names, including Electrical muscle stimulation (EMS), neuromuscular electrical stimulation (NMES), functional electrical stimulation (FES), transcutaneous electrical nerve stimulation (TENS), Russian electrical stimulation, interferential current (IFC), pulsed electrical stimulation (PES), non-invasive interactive neurostimulation (NIN), among others (Zeng et al., 2015). Furthermore, the term Electrical Stimulation can also be described as Electrostimulation, usually when the focus is rehabilitation.

Each name refers to the effects the treatment is intended to achieve with electrostimulation, and helps to categorize the application settings and the parts of the body that will be stimulated. As an example, TENS treatments are usually applied for pain relief, while NMES treatment is generally recommended to retrain muscles after an injury, although both TENS and NMES treatments handle similar stimulation waveforms. In this work, the NMES termology is used since it has the characteristic of being more applied at home and appearing in the literature as an efficient and promising treatment for elderly (Langeard et al.,

2017), making it possible to find reviews on specific conditions such as sarcopenia (Nishida et al., 2016) and KOA (Imoto et al., 2013).

Treatment with NMES is normally used in four circumstances. The first concerns the preservation of muscle mass and function; The second refers to the recovery of muscle mass and function; The third is about improving muscle function; The last is related to preoperative strengthening. The first and second circumstances normally recommended when the patient is for prolonged periods of disuse or immobilization. NMES is also applied to healthy individuals such as elderly subjects, recreational athletes and competitive athletes usually looking for an improvement in muscle function (Imoto et al., 2013). According to Maffiuletti (2010) the NMES treatment programs were implemented in the following areas:

- **Cardiovascular medicine:** Patients with chronic or refractory heart failure, cardiac transplant, chronic obstructive pulmonary disease;
- **Orthopedic medicine:** Patients with anterior cruciate ligament reconstruction, bone fracture, knee osteoarthritis, rheumatoid arthritis, total knee arthroplasty, total hip arthroplasty, meniscectomy, patellofemoral pain;
- **Neurological medicine:** Patients following stroke, spinal cord injury, cerebral palsy;
- **General medicine:** patients with hemophilia, cancer and critically ill patients;
- **Geriatric medicine:** Healthy and unhealthy elderly subjects;
- **Space medicine:** Astronauts, simulated microgravity;
- **Sports medicine:** Healthy and injured athletes of individual and team sports.

Although electrostimulation is widely explored in several areas, there is no consensus on which NMES treatment settings produce greater efficacy. There is a considerable inter-individual variation in the response to NMES exercise, indicating that some intrinsic anatomical properties can determine the quality of the muscle's response to the application of current electricity to the skin. The suggested key to optimizing the effectiveness of NMES is the level of evoked strength in relation to maximum voluntary strength, also known as muscle tension. The aim is to manipulate the parameters of the electrostimulation in order to maximize muscle tension (Maffiuletti, 2010).

There are three main parameters for controlling electrical stimulation: frequency, intensity and pulse width. Frequency refers to the number of electrical pulse trains emitted per second, intensity refers to the

amplitude or strength of the pulses, and pulse width indicates the temporal duration of each pulse train (Lynch and Popovic, 2008).

Despite these fundamental parameters, there is a variety of studies and treatments that go further, modifying the shape of the wave used. Among these modifications are rectangular, triangular or even irregular wave configurations. Generally, the pulses are biphasic, consisting of a positive pulse followed by a negative pulse. However, there are variations, including monophasic (a single pulse) or three-phase (three pulses in sequence) configurations.

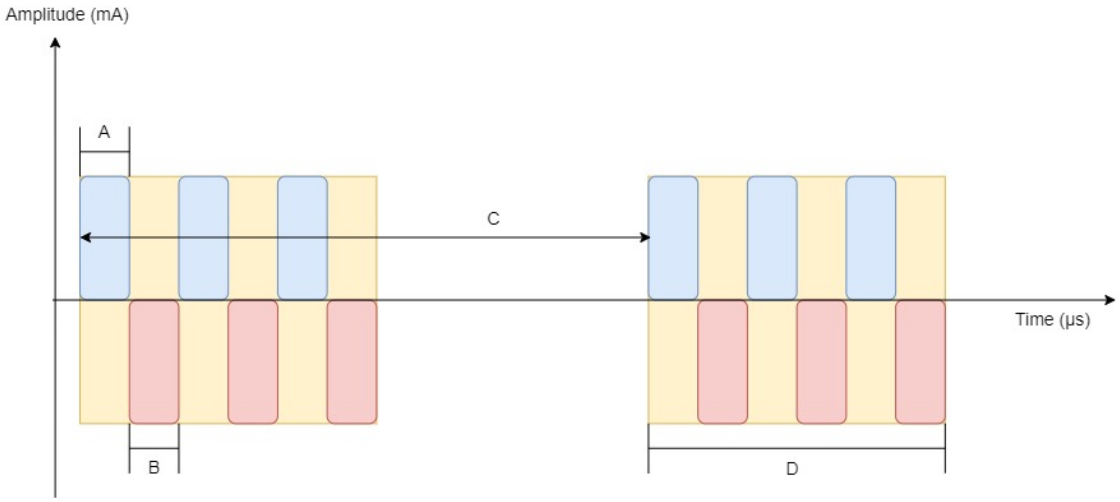


Figure 6: Schematic of biphasic electrostimulation pulses. Adapted (Lynch and Popovic, 2008).

Figure 6 visualizes these concepts schematically. The parameters A in Figure 6 represent the size of an individual pulse. Since the schematic is of a biphasic electrostimulation, the negative component is present. The negative component size is represented by parameter B, which generally has the same value as A. Parameter C describes the period, being the amount of time between the beginning of one pulse and the beginning of the next. The D parameter indicates the pulse width, representing how long the pulse train will remain active.

In a review presented by Langeard et al. (2017) of the functional effects that NMES has in the elderly, reports that electrical stimulation programs are highly inconsistent. The use of symmetrical rectangular pulses from 100 to 400 µs biphasic was the only common point of all the researched studies. The frequency ranged from 20 Hz to high levels close to 100 Hz, with adjustment of the tolerance level for each patient. In addition to the variation in stimulation characteristics, studies also show variations in the temporal composition of the treatment. The duration of treatment programs can vary from 4 to 16 weeks before reformulation. The number of weekly sessions also varies, from 2 to 4 times a week. Lastly, a single NMES treatment session can take 9 to 40 minutes to complete .

Despite this, several programs were successful in their purpose. Langeard reports any NMES training between 2 and 4 times a week for at least 4 weeks, with a frequency between 20 Hz and 70 Hz and with an intensity between 30 mA and 128 mA seems to be safe to trigger positive effects of NMES for muscle rehabilitation in the elderly. Furthermore, the use of NMES combined with voluntary training can increase the effectiveness of the treatment.

The review presented by Nishida et al. (2016) investigated the potential use of electrostimulation as an intervention for sarcopenia in the elderly. Although the review emphasizes the variability of the effects of NMES depending on different treatment protocol, including stimulation frequency and session duration, the literature indicates that the application of low frequency stimuli (less than 20 Hz), short sessions (less than 30 minutes) linked to fatigue management may have better results. Notably, protocols with higher frequencies (60 Hz) also demonstrated positive results in healthy elderly people, indicating an increase in the diameters of both type I and type II muscle fibers. Thus, it is noteworthy that the determination of the ideal parameters to treat sarcopenia in the elderly has not yet been definitively established, requiring additional clinical studies with outcome measures focused on improving muscle strength.

Imoto et al. (2013) performed a randomized clinical trial looking for evidence of the effectiveness of NMES in patients with KOA. Studies show that NMES is effective in improving pain, function and activities of daily living in patients with KOA. The treatment program administered ranged from 4 to 12 weeks in duration using a frequency of 25 to 50 Hz.

2.3 Decision Support System

Belonging to the field of information systems (IS), Decision Support Systems (DSS) are computer-based systems developed to assist in decision making. The term DSS started before the 1970s and its focus was to improve the management decision-making process and pay-off (Arnott and Pervan, 2005). Power (2002) defines DSS as *interactive computer-based systems that help people use communications, data, documents, knowledge and computer models to solve problems and make decisions* and agrees with Arnott and Pervan (2005) that refer to Alter (1980) as one of the pioneers in the DSS field.

Alter (1980) indicates that a DSS is identified through the following characteristics:

1. Specifically designed to facilitate decision-making processes;
2. Design to support, rather than automate decision-making;
3. Able to respond quickly to the changing needs of decision makers.

From the beginning, much of the theoretical study in DSS is focussed in understanding how the decision-making process takes place and how great managers make their decisions. In practice, the evolution of the DSS shows that the transformation of these theories into the effective use of DSS is a time-consuming process and only after other subfields (mainly Business Intelligence and business analytics) matured and were incorporated to solve major problems in DSS area, the topic began to expand (Arnott and Pervan, 2014).

Arnott and Pervan have been working for years looking to organize knowledge about DSS and define new questions about the discipline. Among their publications, a diagram of the DSS area genealogy was built from 1960 to 2000 (Arnott and Pervan, 2005) and updated until 2010 (Arnott and Pervan, 2014). Shown in Figure 7 , the purpose of this diagram is to understand how, and which fields of information technology (IT) have come together to create a new subfield in DSS area.

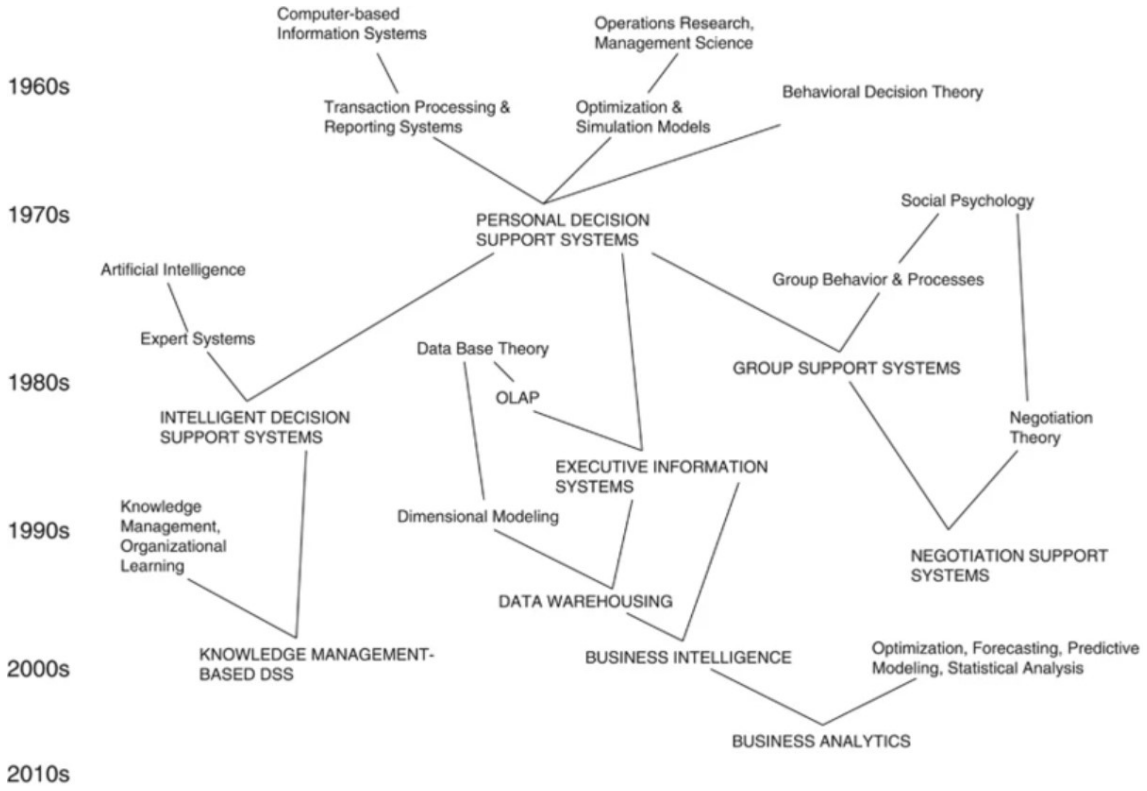


Figure 7: The genealogy of the DSS field, 1960–2010 (Arnott and Pervan, 2014).

In sequence, Arnott and Pervan (2008) indicate the most relevant subfields in the DSS, namely:

1. Personal Decision Support Systems (PDSS): Systems developed for one manager or a small group of managers focused on assisting their decision tasks.

2. Group Support Systems (GSS): DSS built to improve the efficiency of group work and communication.

3. Negotiation Support Systems (NSS): Systems that deal with the optimization of negotiations between opposing parties.

4. Intelligent Decision Support Systems (IDSS): the application of artificial intelligence techniques to decision support.

5. Knowledge Management-Based DSS (KMDSS): Systems that use the knowledge of individual and organizational memory to decision support.

6. Data Warehousing (DW): systems that provide the large-scale data infrastructure for decision support.

7. Enterprise Reporting and Analysis Systems: enterprise focused DSS including executive information systems (EIS), business intelligence (BI), and corporate performance management systems (CPM).

Since this PhD project is focused on building custom NMES treatments using data-driven, it is natural to focus on Intelligent DSS (IDSS), which involves DSS that incorporates Artificial Intelligence like machine learning techniques and modern optimizations. According to the genealogy shown in Figure 7, the doctoral work scope falls under Knowledge Management, which encompasses the objectives of analyzing data collected through various systems to generate knowledge and apply it to improve decisions.

2.3.1 Clinical Decision Support Systems

Clinical Decision Support Systems (CDSS) are tools designed to improve healthcare services by utilizing clinical knowledge, patient information, sensor data, and diagnostics. By providing knowledge that is intelligently filtered and presented at appropriate times, CDSS aims to improve health and healthcare. It supports clinical decision making, contributing to system efficiency, reducing errors and unnecessary expenses, and potentially improving patient well-being (Loya et al., 2014).

Since the inception of the term CDSS in 1970, a wide variety of tools and interventions, both automated and non-automated, have been introduced to improve clinical decision making. The suite of non-automated tools includes clinical guidance and digital resources, also known as an Electronic Health Record (EHR). This technological advance plays an essential role in the management of medical information, translating the traditional paper patient record into a digitalized version, providing substantial improvements in the efficiency of the healthcare system (Sutton et al., 2020).

Another category, known as basic or simple clinical decision support systems, cover systems focused on guiding attention and time management. Examples of these systems include laboratory information

systems (LISs) and pharmaceutical information systems (PISs) Wasylewicz and Scheepers-Hoeks (2019). These platforms issue alerts and suggest practical actions, such as recommending new medications or warnings about possible drug interactions.

Finally, the latest progress is seen in advanced CDSS, providing personalized recommendations for each patient taking into account their unique characteristics. These systems represent a notable advance in the field of medical diagnosis, being applied in extensive and intricate domains (Wasylewicz and Scheepers-Hoeks, 2019). CDSSs have been widely discussed in the literature, helping doctors choose appropriate treatments and identify pathologies. Currently, CDSS are already used in practice, such as the use of x-ray images to recognize cancer, increasing the accuracy of diagnosis and accelerating the recovery process.

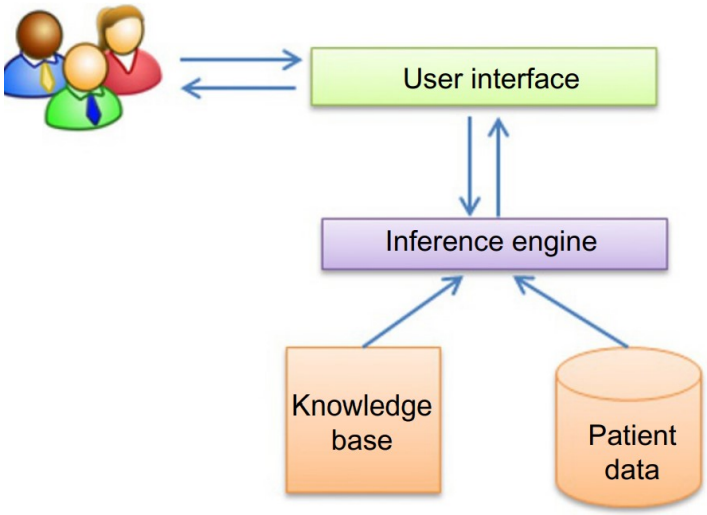


Figure 8: The CDSS Components (Shoaip et al., 2019).

Advanced CDSS typically consists of three essential components. The first component refers to storage strategies for clinical knowledge and health data. This component encompasses concerns about the protection of sensitive data, the availability of resources, interoperability, and among other responsibilities. The second component is the Inference Engine, where a certain deductive process is applied to transform the stored information into knowledge relevant to a specific decision-making process. The third component is the User Interface, which serves as a communication bridge between the knowledge generated and the users. CDSS typically embed a User Interface through mobile applications, desktop systems or websites, significantly influencing the acceptance and use of these tools.

The core of the CDSS lies in the Inference Engine, which employs reasoning methods. These reasoning methods provide powerful tools and techniques for manipulating knowledge, making inferences, and making decisions to effectively solve problems. The reasoning process in a medical diagnosis is complex, as it must consider several facts, including the patient's history, current symptoms, test results, therapies

received, and possible allergies (Shoaip et al., 2019).

The most common reasoning methods in the medical field include Rule-Based Reasoning (RBR), Case-Based Reasoning (CBR), Machine Learning-Based Reasoning (MLBR) and Model-Based Reasoning (MBR). Each of these methods offers distinct approaches to inferring clinical knowledge, from applying logical rules to learning from large clinical data sets. This diversity reflects the need to choose reasoning methods appropriate to different representations of knowledge and areas of application in medical practice.

According to Papadopoulos et al. (2022), reasoning methods can be found divided into two main categories. The first, "Knowledge-Based," includes approaches such as Work-flow driven, RBR and Probabilistic reasoning. The second category is "Non-Knowledge Based", involving different AI approaches such as Machine Learning (ML) algorithms, Artificial Neural Networks (NN), Genetic Algorithms (GA), Support Vector Machines (SVM), among others. Despite being labeled as "Non-Knowledge-Based", these methods do not imply the absence of the use of data. In reality, the term means that AI algorithms typically do not rely on pre-existing knowledge during processing.

2.3.2 Rule-Based Reasoning

Rule-Based Reasoning (RBR) is a method that uses logical rules to infer new information from existing facts. In the context of CDSS, the application of RBR allows the formal representation of medical knowledge, maintaining machine interpretability (Papadopoulos et al., 2022).

Rule-based systems are recognized for their agility in dealing with constantly changing circumstances and are commonly referred as the core of Expert Systems. These systems comprise a base of rules, usually organized into sets, and an inference engine that operates based on these rules. The representation of rules follows the $IF-THEN$ form, mathematically $A => B$, where A are the conditions (antecedent) leading to the actions C (consequent) (Velickovski, 2016).

A crucial feature is that although rules collaborate as part of the program, they must be stored as data to facilitate maintenance and enable scalability. Thus, rules generally reside in the "production memory" or "rule knowledge base" of a CDSS. The inference engine compares these rules with the "facts" (patient data) in the "working memory" and, when the conditions are met, the rules are triggered, being able to generate new facts, withdraw information, add an alert, or modify an existing state.

Several expert systems have already been presented in the literature, some of which are currently in the public domain and widely used, such as CLIPS [1] and Drools [2]

[1] https://clipsrules.net

[2] https://drools.org

. Although not specifically designed for medical data, they are widely used in CDSS applications. These tools, highlighted by stability and support from a vast community, support the development of expert systems and CDSSs (Papadopoulos et al., 2022).

RBR presents benefits such as modularity, ease of explanation, and similarity with human thinking and the cognitive process. However, it faces challenges when dealing with rule exceptions, lack of information, unexpected values in the data, and some tasks can be very specific to a condition or process, which makes it hard to parameter the actions (Shoaip et al., 2019).

2.3.3 Case-Based Reasoning

Case-Based Reasoning (CBR) emerges as an innovative approach to solving computational problems inspired by the human cognitive process. The fundamental premise of CBR lies in the reuse of solutions derived from past cases to address current challenges, providing an efficient and adaptive approach.

The benefits of CBR become evident in the continuous improvement of system performance, which becomes more effective by remembering and adapting previous solutions to similar problems. This method optimizes resolution time and contributes to continuous learning over time (Shen et al., 2015).

CBR operates through a cycle of four fundamental steps. Firstly, the retrieval of relevant past cases occurs, where case memory stores information about previous diagnoses and treatments. Then, the past solution is adapted to suit the current clinical situation, considering individual patient characteristics. Application of the adapted solution is followed by evaluation of results, forming the basis for continuous updating of the case memory. Finally, the last step is to decide whether the new case will be maintained or not (Verma, 2022). The main challenge in a CBR system is the similarity matching algorithm to extract from the CB the previous cases 'most similar' to the present one.

The CBR method integrates qualitative and quantitative aspects for storing and retrieving cases, resembling problem-solving through comparison with previous indexed cases. Semantic distances from different approaches, such as structural similarity algorithms and statistical learning, are generally used to obtain previous cases.

CBR stands out for its intuitive nature, lack of knowledge elicitation to create rules, and continuous learning through use. However, it presents challenges such as considerable storage space required and the large amount of processing time needed to find similar cases. The adaptation of the cases can also be a challenging process (Shoaip et al., 2019).

2.3.4 Model-Based Reasoning

Model-Based Reasoning (MBR) is a technique that employs computational models to simulate complex real-world systems. These models can be based on theoretical or empirical knowledge, and aim to accurately reproduce the real behavior of the chosen process. In the context of CDSS, MBR is generally used to create simulations to predict and diagnose medical conditions.

MBR is particularly effective in situations where a comprehensive understanding of the underlying mechanisms is essential. In the medical field, this involves creating models of physiological processes, disease progression, and treatment outcomes. These models enable CDSS to generate hypotheses, test scenarios, and provide insights that support clinical decision-making. For example, models of cardiovascular dynamics can simulate therapeutic interventions and predict patient outcomes (Shoaip et al., 2019).

A notable example of MBR in practice is the use of musculoskeletal models, such as OpenSim [3], to simulate human body dynamics. OpenSim is an open-source tool that allows the construction and analysis of musculoskeletal models of the human body. These models can simulate movements and dynamics in various situations, providing valuable insights for muscle rehabilitation (Delp et al., 2007a).

MBR supports continuous learning and adaptation. As new data is collected, the models can be updated to reflect the latest knowledge and trends, ensuring that the CDSS remains updated and effective. This adaptability is crucial in the medical field, where new treatments and discoveries are constantly emerging. However, building and maintaining these models requires high-quality data and can be complex and costly. Model validation is essential to ensure they accurately reflect real patient conditions (Papadopoulos et al., 2022).

2.3.5 Machine Learning-Based Reasoning

Machine learning-Based reasoning (MLBR) involves using machine learning algorithms to analyze large data sets and identify patterns useful in decision-making. Unlike traditional methods that rely on explicit programming, MLR uses algorithms that learn from data, identify patterns, and make decisions with less human intervention.

MLBR utilizes large datasets to train models that can predict outcomes, classify medical conditions, and suggest treatments based on historical data. This approach is particularly valuable in healthcare, where vast amounts of patient data, including EHR, medical images, and genomic data, can be harnessed to improve clinical decision-making (Sutton et al., 2020).

[3] https://simtk.org/projects/opensim

A significant advantage of MLBR is its ability to manage complex and non-linear relationships within the data. Machine learning models, such as neural networks (NN) and support vector machines (SVM), are proficient at capturing these intricate patterns, which might be challenging for traditional statistical methods. For example, deep learning algorithms have shown remarkable results in image recognition tasks, such as detecting abnormalities in radiographs and Magnetic Resonance Imaging (RMI) (Wasylewicz and Scheepers-Hoeks, 2019). An exemplary case is Enlitic [4], a company that develops CDSS specifically designed to analyze medical images like X-rays and MRI. Their AI-driven solutions assist radiologists by accurately detecting anomalies, thus speeding up diagnostic processes and enhancing clinical outcomes.

This approach also supports personalized medicine by considering individual patient characteristics and tailoring recommendations accordingly. This personalized approach enhances treatment efficacy and reduces the risk of adverse effects. However, obtaining and managing the extensive and diverse data required for effective MLBR poses a significant challenge (Papadopoulos et al., 2022).

[4] https://enlitic.com

Chapter 3

State of the Art

To understand the state of the art on CDSS for muscular rehabilitation of the lower limbs with electrical stimulation, an approach was adopted that integrates bibliometric analysis and systematic literature review. The bibliometric analysis offers an overview of research trends over time, while the systematic review focuses on providing a detailed assessment of the most recent and relevant studies in the field.

3.1 Methodology

The methodology used to develop the state of the art can be divided into two main stages. Initially, an iterative search process was carried out to identify keywords that should be included and excluded from the search query. At this stage, the R Studio tool and the Bibliometrix library (Aria and Cuccurullo, 2017) were used to analyze the meta information of the articles. In the second stage, it was applied the methodology developed by Kitchenham and Charters (2007) to create a Systematic Literature Review considering publications from the last 5 years, that is, from the beginning of 2019 to the end of 2023.

3.1.1 Keywords Identification

The proper identification of keywords is a crucial step in conducting a literature review, especially when dealing with a multidisciplinary subject such as the development of CDSS for muscular rehabilitation of the lower limbs with electrical stimulation. Nowadays online literary databases provide a set of tools that help create advanced searches, such as the use of Boolean logic and field restriction, but for some subjects it still common to find a huge number of studies unrelated to the main topic.

In our case, the high number of unrelated studies is mainly due to two factors. The first factor is related to the vast literature available on muscular rehabilitation treatments without mentioning the use of any system. The second factor is linked to the high applicability of electrical stimulation in the human body, not restricted only to the lower limbs. Furthermore, the term electrical stimulation can also be found

in other areas not linked to muscular rehabilitation. Therefore, it was necessary to carefully select the keywords to ensure greater efficiency and relevance of the included studies.

The process of identifying keywords began with the definition of three central concepts that must be present in studies: “System”, “Decision Support” and “Electrostimulation”. These concepts served as the basis for building the initial search query, called “Query_Inclusion”, comprising synonymous and equivalent terms to ensure comprehensive coverage. Table 1 provides a complete list of these terms.

ID	Concept	Query with Terms and Synonyms
QI_01	System	“system” OR “application” OR “app”
QI_02	Decision Support	“decision support” OR “intelligent decision” OR “decision making” OR “decision-making” OR “learning system” OR “data driven” OR “data-driven” OR “artificial intelligence” OR “machine learning” OR “based reasoning” OR “control system” OR “controller” OR “closed-loop” OR “closed loop”
QI_03	Electrostimulation	“electrostimulation” OR “electric stimulation” OR “electrical stimulation” OR “electrical muscle stimulation”

Table 1: Inclusion Search Terms.

Query_Inclusion: QI_01 **AND** *QI_02* **AND** *QI_03*

The searches were made in the PubMed, Web of Science and Scopus databases, considering all years available on the platforms until the end of 2023. The initial search results were analyzed using the R Studio tool through the bibliometrix library. The bibliométrix library allowed a detailed analysis of the keywords most frequently used by authors, in addition to providing other relevant information, such as the journals where the articles were published.

Through these analysis, a set of keywords and periodicals were observed that were not directly related to the scope of the research, which resulted in the inclusion of several non-pertinent articles. To address this issue, it was necessary to create a new query using the exclusion keywords with the “and not” condition, thus refining the search results and removing articles not aligned with the review theme.

This refinement process was iterative, carefully evaluating the selected keywords and their application in subsequent searches. Table 2 describes the concepts and search terms added to create Query_Exclusion, which includes all terms that have been removed.

ID	Concept	Terms and Synonyms
QE_1	Body Parts	“hand” OR “finger” OR “brain” OR “head” OR “heart” OR “chest” OR “torso” OR “arm” OR “shoulder” OR “elbow” OR “cells” OR “ankle” OR “trunk” OR “transcranial” OR “diaphragm” OR “lung” OR “pupil” OR “ganglion” OR “subcortical” OR “cortical” OR “cortex” OR “blood” OR “sacral” OR “urinary” OR “upper limb” OR “tactile”
QE_2	Treatments	“surgery” OR “cochlear implants” OR “dropped foot” OR “drop foot” OR “tremor”
QE_3	Other stimulator	“microstimulation” OR “electrotactile” OR “electrophysiology” OR “spinal cord stimulation” OR “microelectrode” OR “spinal cord stimulator”
QE_4	Not Human	“animal” OR “animals” OR “primate” OR “rats”
QE_5	Metal Construction	“ion” OR “iron” OR “energy efficiency” OR “energy consumption” OR “alumina” OR “aluminum” OR “carbon” OR “ultrasonic” OR “microstructure” OR “metal” OR “light metals”

Table 2: Exclusion Search Terms.

Query_Exclusion: QE_01 **OR** *QE_02* **OR** *QE_03* **OR** *QE_04* **OR** *QE_05*

Finally, Query_Final represents the optimized query used in the development of this state of the art.

Query_Final: Query_Inclusion **AND NOT** *Query_Exclusion*

This optimized query reduced the number of articles retrieved from the databases from 5300 to 1464, considering publications from 1980 until 2023 in the three databases. For the last five years, 2019-2023, the quantity decreased from 1343 to 371. This is an approximate 72% reduction in the number of articles, removing only terms that are not of interest.

3.1.2 Systematic Literature Review Approach

The systematic literature review performed to write the state of the art was conducted according to the Kitchenham and Charters (2007) methodology. This methodology divides the review process into three

phases: planning, execution and summary. In the planning phase, a detailed protocol was developed, defining research questions, inclusion and exclusion criteria.

In the execution phase, a comprehensive literature search was carried out, followed by the selection of relevant studies based on the established criteria. Finally, in the summary phase, data is extracted, synthesized and compared to generate the results of the review. The State of the Art through Systematic Review (StArt) tool (Fabbri et al., 2016) was used to assist in protocol management.

Planning

This systematic literature review aims to synthesize, elucidate and analyze decision support systems described in academic literature over the last five years. In particular, the focus is on systems developed to assist in the rehabilitation of lower limb muscles through electrical stimulation. Table 3 presents the six research questions (RQs) formulated to guide this study.

ID	Question
RQ_01	What are the main characteristics of system architecture?
RQ_02	What data is used and how is it acquired?
RQ_03	How is sensitive data protected?
RQ_04	What are the reasoning methods used in these systems?
RQ_05	How do systems modify electrical stimulation?
RQ_06	How were the systems validated?

Table 3: Research Questions.

The keywords defined in section 3.1.1 were then applied to the PubMed, Web of Science and Scopus databases, restricting the search to articles published between January 2019 and December 2023 inclusive. Using the tools available in online databases, a filter was applied to return only conference articles and journal articles. Additionally, survey articles were removed, ensuring that only primary studies were considered in the systematic review.

The articles selected from the referred databases were evaluated based on the criteria established in Tables 4 and 5. For an article to be accepted in the review, that is, to actually be fully read and have its information extracted, it is necessary to comply with all inclusion criteria and no exclusion criteria.

ID	Inclusion Criteria
IC_01	Studies published between 2019 until 2023 inclusive.
IC_02	Studies written in English.
IC_03	Studies that do not have a more recent version.

Table 4: Inclusion Criteria.

ID	Exclusion Criteria
EC_01	Studies that do not present the complete article or without access.
EC_02	Studies do not use electrical stimulation or only use computer simulation.
EC_03	Studies that do not apply electrical stimulation to the lower limbs.
EC_04	Studies that do not use computerized system.

Table 5: Exclusion Criteria.

Execution

In the execution phase, searches were carried out in the selected databases in accordance with the protocol established in the planning phase. The search results were exported to the StArt software, which allowed efficient management of articles throughout the different stages of the review, in addition to facilitating the removal of duplicate articles.

The flow of articles throughout the selection process, from initial screening to final inclusion in the review, was documented using the Preferred Reporting Items for Systematic Reviews and Meta-Analyses (PRISMA) Statement and depicted in the flow diagram shown in Figure 9.

The use of PRISMA in this study not only guarantees the transparency and quality of the review report but also contributes to the replicability of the study, allowing other researchers to repeat and validate the results presented in this systematic review (Page et al., 2021).

During the screening phase, the titles, abstracts, and author keywords of the articles were read to determine their relevance to the main topic. The purpose of this stage was to quickly exclude articles that had no connection to the main theme. As a result, 58 articles were selected for full reading.

Among the 58 selected articles, 29 met all inclusion criteria and did not meet any exclusion criteria, thus being considered for further information extraction.

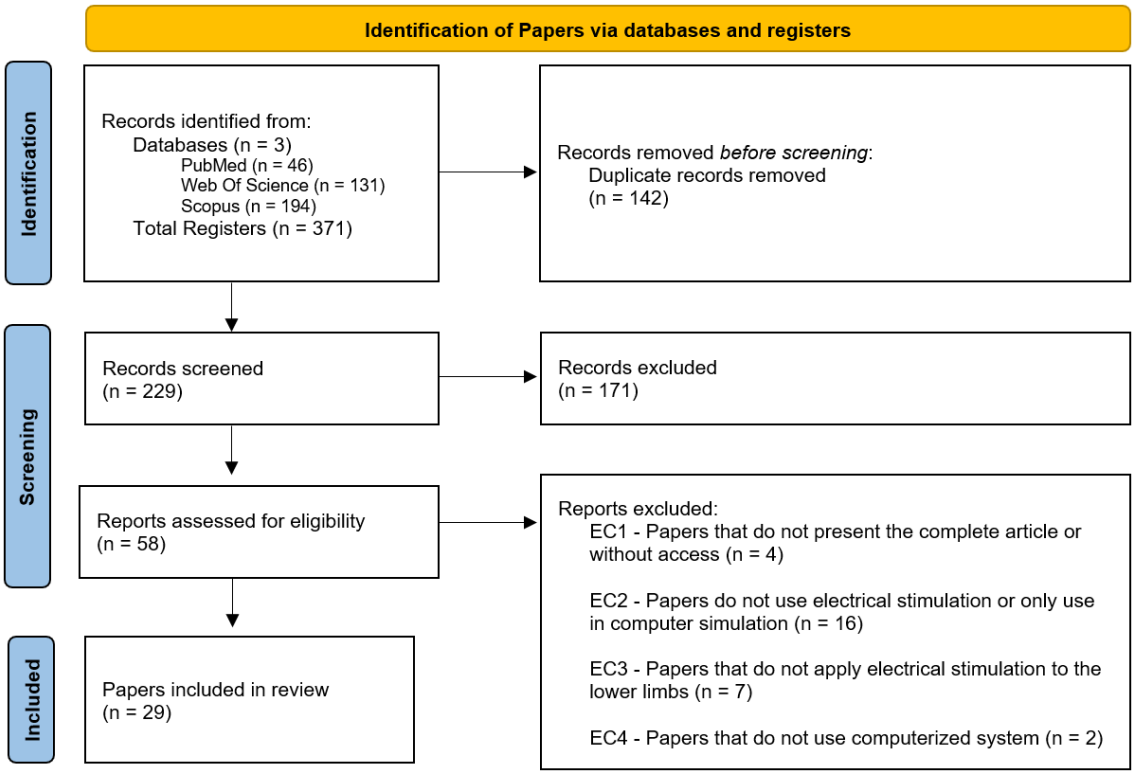


Figure 9: PRISMA 2020 flow diagram of the systematic review. Adapted from (Page et al., 2021).

The main reasons for excluding articles were the following: first, EC2, studies that did not effectively apply stimulation, such as studies that presented computer simulation of the use of electrical stimulation without presenting a real device or system architecture. The second most common reason for exclusion, EC3, was the lack of application of electrical stimulation to the quadriceps muscles, which was not aligned with the scope of the systematic review.

3.2 Research Trends Over Time

This section aims to provide a bibliometric analysis of the evolution of research in the area of CDSS for lower limb muscle rehabilitation with electrical stimulation. Understanding trends over time is crucial for the development of future technologies, allowing for an overview of what has been researched and current topics, as well as identifying obsolete terms or discontinued research lines.

For this bibliometric review, 1464 articles were collected from the PubMed, Web Of Science, and Scopus databases, covering the publication years from 1980 to 2023. Only one preprocessing operation was performed on this article collection to remove duplicates, resulting in a total of 1048 articles for analysis. The tools used to extract information were R Studio and the bibliometrix library, while Microsoft Excel was used for adjusting and designing the charts.

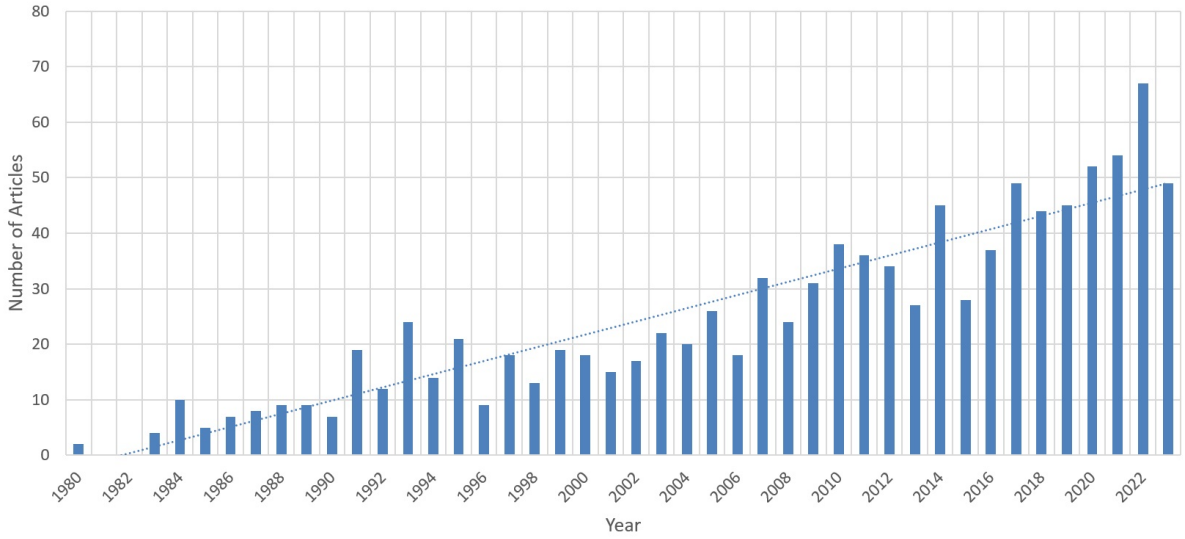


Figure 10: Annual Scientific Production.

The data series presented in Figure 10 reports scientific production over the years on the topic of the review. The number of publications remained relatively low from the early 1980s until the mid-1990s, with only a few articles published annually. However, from the late 1990s onwards, research activity increased significantly, with the number of publications steadily rising each year.

At least two turning points in the number of publications can be observed in Figure 10. The first occurred in 2007 when a minimum of 20 articles were published every subsequent year. The second turning point was 2016, when the minimum number of publications doubled to 40 articles per year. This upward trend peaked in early 2020, with a remarkable 67 publications in 2022, highlighting the exponential growth and maturation of the field. Additionally, the consistent presence of publications over the years indicates sustained interest and investment in research related to CDSS for muscular rehabilitation with electrical stimulation. This growth underscores the relevance of the topic in the scientific community.

The second analysis conducted involved extracting bigrams from the abstracts of the articles. This technique, applied through natural language processing algorithms, identifies pairs of words frequently occurring together in texts, providing valuable insights into the main themes and concepts addressed in scientific literature.

During the bigram extraction process, irrelevant terms such as “results demonstrate” or “error system” were removed, as they do not contribute to understanding the research topics. Additionally, terms related to electrostimulation were excluded, as all studies use this technique as part of their intervention. The aim was to highlight secondary terms associated with electrostimulation, providing a deeper insight into the concepts and themes addressed in research on CDSS for muscle rehabilitation.

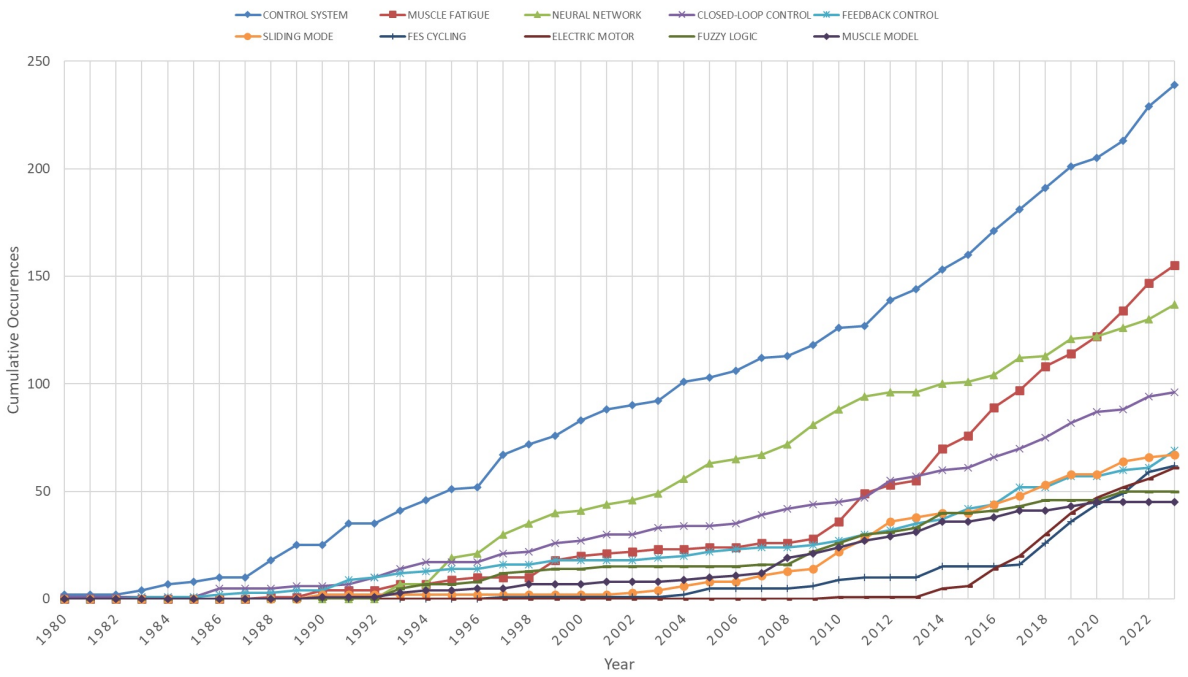


Figure 11: Top 10 bigram terms over time.

The analysis of the bigrams presented in Figure 11 revealed interesting patterns in the evolution of the most frequent terms over time. The term “control system” emerges as the main and most consistent term over the years, with the first publications dating back to the early 1980s and a continuous presence until the present day. This suggests that researchers have consistently sought to control movement since the beginning of investigations.

Secondly, “muscle fatigue” stands out, especially from 2010 onwards, indicating a growing interest in this complex topic. This rise suggests an evolution in researchers’ understanding over time, expanding the scope of investigations to consider not only movement control but also the effects of muscle fatigue in this context. This shift in focus is supported by the evolution of the term “muscle model”, which follows a similar but less intense trend.

The third most used term, “neural network”, demonstrates a constant rise over the years, with periods of stagnation interspersed. This pattern suggests computational challenges that may limit the effective use of neural networks at certain times, highlighting the need for continued development in this area.

Other notable terms include “FES Cycling” and “ELECTRIC MOTOR”, which show a similar increase in frequency and are correlated. This indicates that research on muscular rehabilitation with electrical stimulation, using bicycles and exoskeletons, began to gain prominence in 2015 and continues to be one of the main research topics today.

Continuing with the analysis of the bigrams extracted from the abstracts, a Co-occurrence network

graph was generated. This graph was constructed based on the terms that co-occurred most frequently in the abstracts, revealing the relationships between the terms and identifying significant thematic groupings.

The Louvain algorithm was applied to identify clusters, with the number of nodes set to 100 to ensure a comprehensive analysis. This algorithm utilizes a hierarchical clustering method that recursively combines communities into a single node and performs modularity clustering on condensed graphs. The goal is to maximize a modularity score for each community.

Modularity quantifies the quality of the assignment of nodes to communities. It assesses how densely connected the nodes are within a community compared to how connected they would be in a random network. This results in groups of terms that co-occur more frequently and are more strongly interconnected, with no overlap Lu et al. (2015).

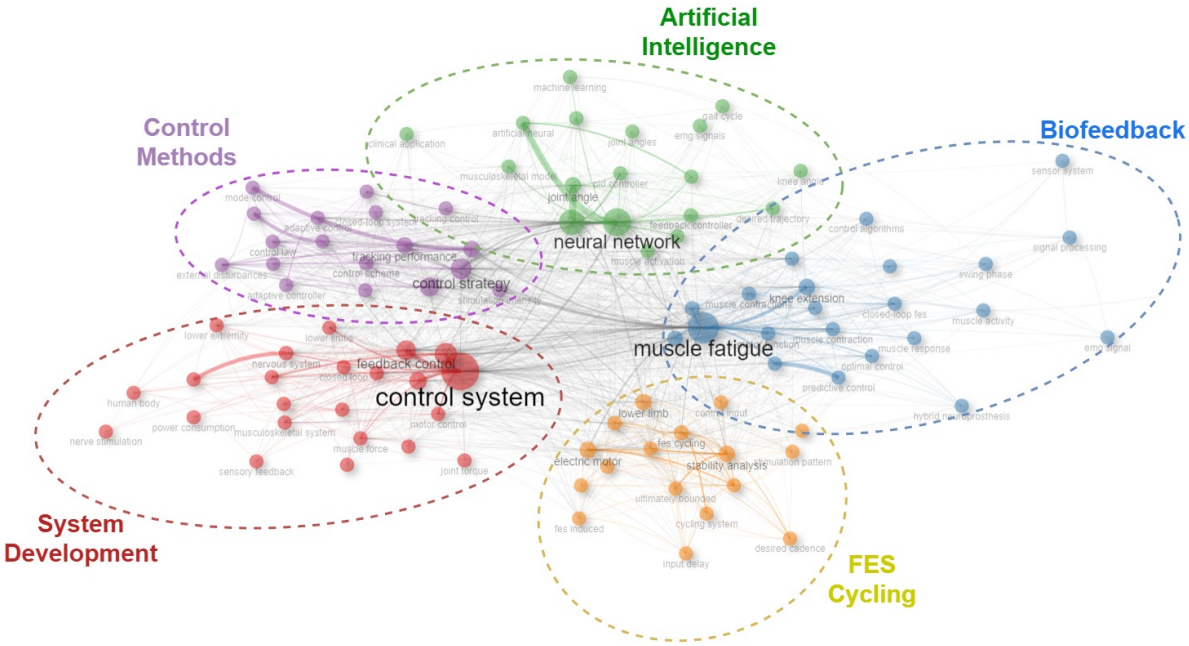


Figure 12: Co-occurrence Network of bigram terms.

Five distinct clusters were identified, as illustrated in Figure 12, each representing a specific branch of study applied to systems with electrical stimulation for lower limbs rehabilitation. The central theme of each cluster was determined empirically based on the related terms included in the cluster.

- **System Development:** This cluster is centered around terms related to the development of control and stimulus systems. Includes words such as “control system”, “stimulation parameters”, “closed loop”, “stimulation patterns”, “motor control”, “power consumption”. This suggests a focus on creating and improving systems for controlling and administering electrical stimulation.

- **Control Method:** Set related to strategies and control methods to parameterize electrical stimulation given a certain objective. It includes terms such as “control strategy”, “control scheme”, “adaptive control”, “control law”, “sliding mode” and “tracking performance”. This indicates a concern with the development of adaptive and robust control techniques to optimize the effectiveness of electrical stimulation.

- **Artificial Intelligence:** This cluster focuses on the use of artificial intelligence in research related to muscle rehabilitation with electrical stimulation. It includes terms such as “neural network”, “machine learning”, “artificial neural”, “musculoskeletal model”, and “clinical application”. This suggests a growing trend of using machine learning algorithms and advanced computational models to improve muscle rehabilitation approaches.

- **Biofeedback:** This group is related to the physiological response and monitoring of biological signals during the muscular rehabilitation process. Relevant terms include “muscle fatigue,” “muscle contraction,” “muscle model,” “signal processing,” “real time,” “muscle activity,” and “EMG signal.” These terms reflect the interest in understanding muscle fatigue and muscle activity during treatment.

- **FES Cycling:** This cluster focuses on research exploring the use of electrical stimulation using bicycles and exoskeletons. Includes terms such as “fes cycling”, “electric motor”, “tracking error”, “stability analysis”, “cadence tracking”, “desired cadence”, “cycling system” and “hybrid system”. This cluster collaborates with the idea that this topic is increasingly on the agenda and can bring relevant benefits to muscular rehabilitation.

Analyzing bigram terms and identifying clusters provides information about the main topics surrounding this Ph.D. research topic and how they relate to each other. The clusters highlight different aspects of research, from the development of control systems and their methods to the application of artificial intelligence and the use of biofeedback. The intersection between these clusters suggests promising opportunities for interdisciplinary research and the integration of innovative approaches.

Finally, this bibliometric analysis provides a comprehensive overview of the leading research trends in CDSS for lower limb muscle rehabilitation through electrical stimulation. This detailed understanding of trends over time can guide future investigations and contribute to the continuous advancement of the area, allowing the identification of knowledge gaps and opportunities for innovation.

3.3 Systematic Literature Review

This section presents an analysis of the 29 selected articles, following the previously described systematic review methodology (see Figure 9), covering the period from 2019 to 2023 inclusive. As said above, the search was to find articles describing decision support systems developed to assist physicians in electrostimulation treatment. However, none of the analyzed articles actually presented a decision support system. Instead, all selected articles describe electrostimulation control systems for lower limb rehabilitation, without the effective participation of the physician during treatment or monitoring of the patient's clinical progress throughout the sessions.

The selected articles mainly address three main themes: 17 focused on FES Cycling, 8 on Exoskeleton and 4 on Knee Control. Regarding the type of publication, 8 are from conferences and 21 are journal articles. The corresponding authors come from various countries, with the United States leading with 12 articles, followed by Brazil with 3. Italy, France, Iran and China contributed 2 articles each, while Japan, Turkey, Malaysia, Serbia, Germany and the United Kingdom contributed with 1 article each. This detailed information is available in Table 6, along with the references and authors of the articles.

ID	Author (Year)	Aim	Country	Type
A1	Watanabe and Tadano (2019)	FES Cycling	Japan	Conference
A2	Obuz et al. (2019)	Exoskeleton	Turkey	Journal
A3	Estay et al. (2019)	FES Cycling	USA	Conference
A4	Ghanbari et al. (2019)	FES Cycling	USA	Journal
A5	Rahim et al. (2019)	Exoskeleton	Malaysia	Conference
A6	Cerone et al. (2019)	FES Cycling	Italy	Conference
A7	Sijobert et al. (2019)	FES Cycling	France	Journal
A8	Duenas et al. (2020)	FES Cycling	USA	Journal
A9	Bao et al. (2020)	Exoskeleton	USA	Journal
A10	Teodoro et al. (2020)	FES Cycling	Brazil	Journal
A11	Ricarte et al. (2020)	FES Cycling	Brazil	Conference
A12	Zhang et al. (2020b)	Knee Control	China	Journal

A13	Zhang et al. (2020a)	Knee Control	China	Conference
A14	Arcolezi et al. (2021)	Knee Control	France	Journal
A15	Isaly et al. (2021)	FES Cycling	USA	Journal
A16	Cousin et al. (2021)	FES Cycling	USA	Journal
A17	Aldrich and Cousin (2021)	FES Cycling	USA	Journal
A18	Molazadeh et al. (2021)	Exoskeleton	USA	Journal
A19	Rouse et al. (2021)	FES Cycling	USA	Journal
A20	Allen et al. (2022)	FES Cycling	USA	Journal
A21	Chang et al. (2022)	Exoskeleton	USA	Journal
A22	Nekoukar (2021)	Knee Control	Iran	Journal
A23	Jafari and Erfanian (2022)	FES Cycling	Iran	Journal
A24	Coelho-Magalhães et al. (2022)	FES Cycling	Brazil	Journal
A25	Popović-Maneski and Mateo (2022)	FES Cycling	Serbia	Journal
A26	Lyu et al. (2023)	Exoskeleton	Germany	Journal
A27	Wannawas and Faisal (2023)	FES Cycling	England	Conference
A28	Sun et al. (2023)	Exoskeleton	USA	Journal
A29	Ferrari et al. (2023)	Exoskeleton	Italy	Conference

Table 6: Identification of Selected Articles.

FES-Cycling

FES-Cycling is a therapeutic approach that combines the use of stationary bicycles with electrical stimulation of the muscles of the lower limbs. Generally, the quadriceps, hamstrings and gluteal muscle groups are stimulated in a coordinated sequence to generate a positive crank cycle. This method presents improvements in the cardiorespiratory, neuromuscular and skeletal system, such as increased muscle mass, improved blood circulation and reduced bone loss. However, these improvements may be mitigated due to the possibility of accelerated fatigue or physical exhaustion (van der Scheer et al., 2021).

Generally, bicycles or tricycles have a motor that also assists the movement, allowing patients with

little or no capacity for voluntary movement in their legs to perform the exercise. This practice is carried out indoors, generally in a stationary system with a focus on rehabilitation, however, it is currently possible to find competitions that use this system and demonstrate new technologies, such as the Bike Race - Cybathlon [1].

The main challenge of FES-Cycling is to coordinate electrical stimulation with the bicycle motor to maintain an effective and comfortable cadence for the patient without excessive fatigue. This synchronization is often done through complex mathematical models and the use of sensors to monitor cadence and adjust the electrical stimulus and motor accordingly. In the United States, the group led by researcher Warren Dixon was responsible for all 8 publications on FES-Cycling that were selected for this systematic review. The work of this group has contributed significantly to the advancement of knowledge about FES-Cycling and its potential in lower limb rehabilitation.

Exoskeleton

Exoskeletons represent an important innovation in the area of rehabilitation, designed to help people with motor disabilities regain mobility and independence. These devices consist of external mechanical structures equipped with motors, sensors and control systems, designed to be worn around the joints of the human body, providing support and assistance during movement. Its main objective is to offer additional help to people with physical disabilities, such as spinal cord injuries, strokes or musculoskeletal disorders (Anaya et al., 2018).

The selected studies address an exoskeleton model that incorporates the application of electrical stimulation to muscles to aid movement. This technique, also known as hybrid exoskeletons or FES exoskeletons, aims to provide a more effective, safe and robust rehabilitation therapy. It compensates for the lack of strength in muscles stimulated with the motor to produce movement, similar to FES-cycling.

Hybrid exoskeletons for lower limb rehabilitation generally have motors in the hip and knee joints, focusing on movements such as lifting the leg while sitting in a chair, getting up from a chair or walking. However, as in the case of FES-cycling, the biggest challenge is coordinating the stimulator and the motors together to produce the necessary movement, without causing excessive fatigue or discomfort to the patient. For more complex movements, such as walking, the challenge can be even greater, requiring a more sophisticated control system.

[1] https://cybathlon.ethz.ch/en/event/disciplines/fes

Knee Control

Knee controllers represent a simpler approach compared to other rehabilitation technologies such as FES Cycling and exoskeletons. In this approach, no motors are used, only FES stimulation is used to control the knee joint. Generally, electrical stimulation is applied only to the quadriceps, aiming at the movement of lifting the leg. Thus, the system needs to calculate the stimulation parameters to perform the movement, aiming to increase the range of movement or sustain repetitions without excessive fatigue.

In addition to offering a more traditional rehabilitation solution, knee control can be seen as a proof of concept for other applications, such as exoskeletons. This simplified approach allows the implementation of new technologies in a basic version, which can then be scaled to more advanced applications. An example is the addition of electromyography sensors to monitor muscle fatigue in real-time.

3.3.1 RQ_01: What are the main characteristics of the system architecture?

Most of the reviewed studies do not provide a precise description of the adopted system architecture, mentioning multiple devices and systems without clearly explaining their interactions. Instead, they typically mention a series of devices connected by cables to a computer, where processing is performed primarily in MATLAB/Simulink or in-house developed software, with few additional details. These devices range from encoders to measure bicycle cadence, power meters and acquisition boards, especially in studies related to FES-cycling. Furthermore, it is notable that the most commonly used stimulation machine was the Hasomed RehaStim.

However, three studies stand out for proposing systems that are not limited to cable connectivity and present a more unified approach.

Study A6 proposes a modular systems architecture composed of two sets of wireless modules. One module is responsible for signal acquisition, while the other represents a stimulator machine. These modules communicate via WiFi to a multiplatform software developed with the Qt framework in C++. While this approach allows flexibility as the modules can be apply to multiple regions, it also brings with it significant technological challenges for the control system.

Study A11 describes a modular architecture based on the Robot Operating System (ROS), representing a more structured approach compared to other studies. The modular part of the architecture allows the acquisition of signals and the use of different types of sensors. In the case analyzed, it was implemented with an IMU motion sensor. The rest of the architecture consists of a portable computer and a stimulator,

both connected by cables.

Study A24 deserves attention as it provides a more detailed description of its system architecture. Using an electronic board, this study establishes communication with an Android mobile application via Bluetooth. However, it remains unclear how the data is subsequently transferred for offline processing. Additionally, the study incorporates a power meter that transmits data via Bluetooth to a computer, but without details about its complete integration into the overall system.

In summary, while most studies do not provide a detailed description of the system architectures used, there is a trend towards wired connectivity to a computer for data processing, with some mention of wireless communication for data transmission. Moreover, the lack of details on how colleted data is stored offline and integrated into the global system remains a common gap in the studies reviewed.

3.3.2 RQ_02: What data is used and how is it acquired?

A diverse set of sensors and tools were used in the selected articles to collect crucial data for controlling electrostimulation. In some cases additional data for validation were also collected that were not used in the control. Table 7 seeks to summarize the information found.

ID	Data Used	Acquisition Tools
A1	Crank angle (EMG data were used to defined stimulation patterns in previously study)	2 IMUs sensors
A2	Knee angle	Encoder
A3	Crank angle, velocity and acceleration and power	Encoder and power meter
A4	Crank angle, velocity and acceleration and power	Encoder and power meter
A5	Knee angle (for validation only)	Cameras
A6	Knee angle	Electronic goniometer
A7	Thigh angle	2 IMU sensors
A8	Crank angle, velocity and acceleration and power	Encoder and power meter
A9	Knee angle	Encoder
A10	Crank angle, velocity and acceleration	Electronic goniometer and IMU sensor
A11	Crank angle	1 IMU sensor

A12	Knee angle	Electronic goniometer
A13	Ankle and knee angle and rectus femoris EMG	Angle sensor and myoeletronic sensor
A14	Knee angle	Electronic goniometer and IMU sensor
A15	Crank angle, velocity and acceleration and power	Encoder and power meter
A16	Crank angle, velocity and acceleration and power	Encoder and power meter
A17	Crank angle, velocity and acceleration and power	Encoder and power meter
A18	Knee and hip angle	2 Encoders
A19	Crank angle, velocity and acceleration and power	Encoder and power meter
A20	Crank angle, velocity and acceleration and power	Encoder and power meter
A21	Knee and hip angle, leg force and angular displacement	2 Encoders, force sensor and treadmill
A22	Knee angle	2 IMUs sensors
A23	Crank angle	Encoder
A24	Crank angle, velocity and acceleration and power	Encoder and power meter
A25	Crank angle	Encoder
A26	Body motion capture, motor torque	Torque sensor and cameras
A27	Crank angle	Encoder
A28	Knee angle, force, motor torque	Encoder, dynamometer and torque sensor
A29	Motor torque, knee angle, rectus femoris EMG	Encoder and EMG sensor

Table 7: Data and Acquisition Tools Used in the Selected Studies.

As can be seen from Table 7, most studies rely on joint angles to guide electrostimulation control, with the knee joint being the most common among them, although the thigh, ankle, and hip angles were also found to be used. For FES-Cycling studies, except for articles A6 and A7, all studies use crank angle. It can also be observed that all studies were using some type of joint angle.

Given that the majority of studies focus on FES-Cycling and employ crank angle, the most common acquisition tool is the encoder, which also measures bike speed and acceleration. Second, it is noticeable

that IMU sensors are increasingly gaining space in this research area, as well as electronic goniometers, which can be seen as prototypes of IMUs in this use case. This is due to the fact that many of these IMU sensors, despite having accelerometers and gyroscopes inside, are used to convert their data into angles, a function fulfilled with precision by electronic goniometers.

Finally, EMG sensors were also seen, which are important for assessing muscle activity and are related to fatigue. However, only 2 articles use this data, both collecting from the rectus femoris muscle.

3.3.3 RQ_03: How is sensitive data protected?

None of the selected studies addressed or at least commented on data storage or sensitive data protection, revealing a significant and critical gap in the field of research. Even the articles that mention the use of offline data for training machine learning algorithms do not discuss details on how this data is stored or made available, leaving an important question unanswered.

This lack of attention to data security highlights the immaturity of systems focused on stimulation control in terms of infrastructure and system architecture. It also suggests a lack of interoperability between these systems and a very low commercial availability. These issues are crucial not only for academic research but also for the practical implementation of these technologies in clinical environments.

3.3.4 RQ_04: What are the reasoning methods used in these systems?

As previously mentioned, the selected studies do not explicitly describe a decision support system but rather control systems for stimulation. However, each system incorporates a type of reasoning method to adjust stimulation parameters, although these methods are not explicitly described using these terms. Figure 13 presents a chart quantifying the reasoning methods found.

The majority of the selected articles utilize the model-based method as their reasoning method, employing mathematical models to simulate scenario behavior and determine the necessary stimulation parameters to maintain movement as planned. This method is typically applied in a closed-loop control system, where encoder and power meter data are used to feed the model.

Six studies employed the rule-based reasoning method to control stimulation. This method is simpler than others, typically activating and deactivating stimulation based on a variable or set of variables. A simple example is controlling the timing of muscle stimulation activation and deactivation based on predefined crank angles in FES-cycling.

The remaining six studies utilized machine learning algorithms to control stimulation. Some studies used these algorithms only to activate and deactivate stimulation, without controlling parameters such

as intensity, pulse width, and frequency. However, in a more sophisticated manner, machine learning algorithms seek to identify more subtle patterns of activation. This reasoning method is still new in the research field and has ample room for future development.

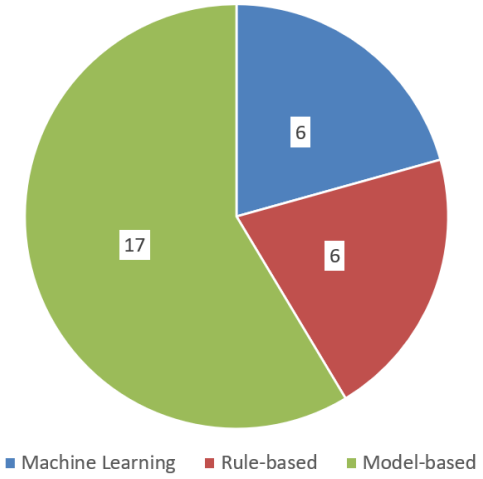


Figure 13: Reasoning methods of the selected articles.

3.3.5 RQ_05: How do systems modify electrical stimulation?

The studies reviewed demonstrate a variety of approaches to modifying stimulation parameters. The majority of studies focused on adjusting a single parameter, with 22 of them varying only one. Specifically, 16 of these studies chose to vary the pulse width, while 6 opted to vary the intensity, which refers to the pulse's amplitude. It's worth noting that in some articles, the term "intensity" was also used to describe the total applied force, as exemplified by "intensity was altered by both pulse width and pulse amplitude".

Three studies stood out for modifying more than one parameter. Studies A24 and A29 simultaneously altered two parameters in their control systems: pulse width and intensity. Only one study, A22, was notable for varying all three parameters, including frequency. This particular study questioned the fact that most articles modified only pulse width and aimed to demonstrate the feasibility and effectiveness of the control system by using all three parameters.

Finally, four studies (A5, A6, A7 and A27) showed no variation or did not make clear how the parameters were modified. In these cases, the control system generally activated and deactivated the stimulation with predefined fixed values.

3.3.6 RQ_06: How were the systems validated?

The validation of systems is a crucial step in the development of new technologies, as it provides a means of measuring the effectiveness and safety of these systems before their clinical implementation. Upon analyzing the selected articles, a total of 137 subjects who participated in the studies were identified, with 40 of them having neurological conditions, primarily total lower limb paralysis. Table 8 illustrates the quantity of subjects grouped by type. It is interesting to note that, despite there being more than double the number of studies on FES-Cycling compared to Knee Control, both have a similar quantity of participants with neurological conditions involved in the studies.

Subjects	**FES Cycling**	**Exoskeleton**	**Knee Control**	**Total**
Healthy	61	15	21	97
Neurological Conditions	18	7	15	40
Total	79	22	36	137

Table 8: Study participants by type.

Each type of study had a similar maximum number of participants. Study A2, involving exoskeletons, tested its system on 10 healthy participants and 3 with neurological conditions, recording the highest number of participants among the studies analyzed. Meanwhile, study A22, focused on knee control, evaluated the system's performance on 10 participants with neurological conditions, and study A29, on FES-Cycling, tested it with 10 healthy participants. The remaining studies typically involved an average of 4 healthy participants and at least 1 with neurological conditions in their validations.

The variation in the number of participants reflects the challenging limitations for validating innovative rehabilitation systems. In total, 6 studies used a single participant, A3, A27, A11, A6 and A7, all with a healthy participant, with the exception of study A24, which included a participant with a neurological condition. These validations can offer valuable insights into the initial viability of the system, but demonstrate a long development path ahead.

3.4 Conclusions

This chapter presented the state of the art, derived from a rigorous methodology composed of two parts. The studies extracted from the three databases - PubMed, Web of Science, Scopus - aimed to develop

systems to improve muscular rehabilitation treatment of the lower limbs through electrical stimulation. The first part of this review focused on carrying out a bibliometric analysis of articles extracted from 1980 to 2023. Meanwhile, the second part involved a systematic review, aiming to address six main questions and provide detailed information on the current development of systems in this field . For this second part, a more recent period was considered, from 2019 to 2023.

The bibliometric review demonstrated how search terms were interconnected over the years, revealing current trends in the most relevant topics. From the review, stand out the increase in the number of publications on the topic, indicating a growing scientific interest. The most prominent topics were categorized into four distinct groups.

The first highlights the consistent focus from the beginning on developing systems that adapt stimulation to control a specific joint. The second concerns to biofeedback, a topic that is increasingly being discussed, probably because it is more viable than years ago. Likewise, the application of artificial intelligence is showing a significant increase. Finally, it was noticeable in the bibliometric analysis that there is a big scientific interest in FES-Cycling for rehabilitation of the lower limbs.

The systematic literature review was conducted to understand the proximity of the systems presented by the selected articles to decision support systems. One of the main results highlighted that the term "decision support" is still in its early stages for systems adopting lower limb electrostimulation. No system explicitly describes a decision support system, and no article addressed how data is stored or how sensitive data is managed. The system architecture presented, when mentioned, are generally simple, without cloud connectivity or interoperability.

However, several reviewed studies were able to control electrostimulation through complex models and validate with patients with neurological conditions, demonstrating maturity in the scientific process for clinical validation. Furthermore, current studies applying machine learning algorithms to control stimulation were found, although some studies only turn stimulation on and off without changing parameters, demonstrating the application of new technologies with future development prospects.

Finally and in what concerns the Ph.D. work here reported, it is possible to say that the CDSS with the objective of helping physicians to construct treatments with electrical stimulation for rehabilitation of the lower limbs is a recent topic, worthwhile to be explored, with little material in the area of information systems. Moreover, there is a broad and consolidated scientific foundation on joint control and parameter adaptation strategies to improve lower limb rehabilitation.

Chapter 4

myHealth System

The proposed system, myHealth, aims to revolutionize the way muscle rehabilitation with electrostimulation treatment is conducted, offering an innovative and technologically advanced solution that combines the efficiency of electrical stimulation with the practicality of telehealth. By enabling treatment sessions to be carried out both in clinical settings and in the comfort of the patient's home, myHealth seeks to increase the accessibility, convenience, and efficiency of the rehabilitation process. This system requires careful design considerations to ensure a user-friendly and efficient experience for patients and healthcare professionals.

This chapter presents the myHealth system in two main parts: the proposal and the prototyping. The first part, Proposal, covers the design aspects, including treatment scenarios, system architecture, sensitive data protection, and database modeling. The second part, Prototyping, details the implementation aspects such as cloud infrastructure, the wearable system, the mobile application, the communication between the systems, and the system panel. Each section provides an in-depth look at the components and processes involved in realizing this comprehensive CDSS for electrostimulation treatments.

myHealth system was developed as a technological proof of concept, highlighting the integration of advanced technologies and user-centered design. This system aims to demonstrate how modern solutions can enhance the effectiveness and accessibility of muscle rehabilitation treatments, offering a robust platform for future research and development in healthcare.

4.1 Design

4.1.1 Treatment Scenarios

The description of treatment scenarios is crucial for identifying the requirements of the decision support system. These scenarios allow us to understand the specific needs of both patients and healthcare professionals, and how the system can effectively address them. Furthermore, providing a detailed overview

of the scenarios has helped guide the development of the system, establishing a clear roadmap for the implementation of necessary functionalities.

Based on this analysis, two distinct scenarios have been developed to the application of the proposed treatment. One of the goals is to reduce the frequency of medical appointments, although regular in-person meetings with specialized professionals are essential in the initial stages, to ensure effective adaptation of the system. The first scenario outlines the recommended actions for conducting a treatment session in the clinic, as illustrated in the Figure 14.

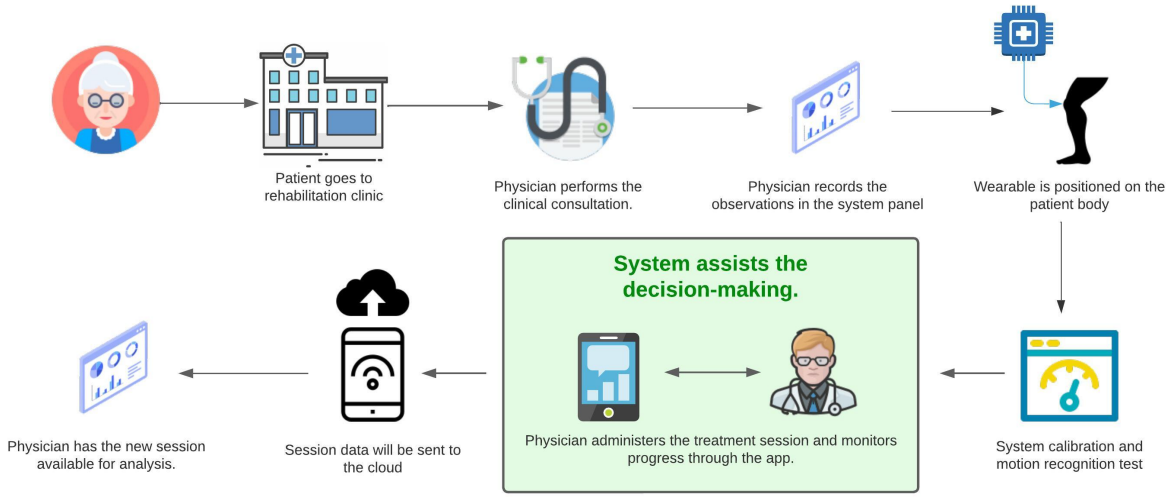


Figure 14: The treatment scenario in the clinic.

The beginning of the treatment scenario in the clinic resembles conventional treatment, but with the difference that all observations and notes are recorded in a specialized administrative panel. This panel provides a centralized and efficient interface for detailed monitoring of the patient's progress. The session then progresses to the use of electrical stimulation for muscle rehabilitation. At this point, the stimulation device is replaced by the wearable device.

In a comfortable and safe environment, the physician carefully places the wearable device on the patient, ensuring that sensors and electrodes are correctly positioned. The wearable device is controlled via a mobile application. Upon activation, initial tests are conducted to verify the system's conditions and perform a personalized calibration according to the treatment environment. This ensures that the wearable device is optimized and ready for the electrostimulation session.

Using the mobile app, the physician can manage the entire treatment session with the support of an intelligent system. In addition to being able to configure standard electrical stimulation parameters, the application also allows the selection of personalized stimulation modes and provides real-time biofeedback

information, such as the progression of metrics related to muscle fatigue.

At the end of the session, the physician can save all the data collected from the sensors and the stimulation parameters. These data can be accessed through the administrative panel, where an intelligent system processes the information to generate detailed insights into the patient's physical condition. These insights enable continuous adaptation and personalization of the treatment, aiming for more effective rehabilitation tailored to the patient's specific needs.

After the completion of the monitored sessions at the clinic, the treatment advances to the next scenario, which is conducted in the patient's home, as depicted in Figure 15. In this scenario, the physician uses the administrative panel to create a new treatment session, specifying the necessary parameters for electrostimulation. The patient is then notified about the new session and the scheduled date for it.

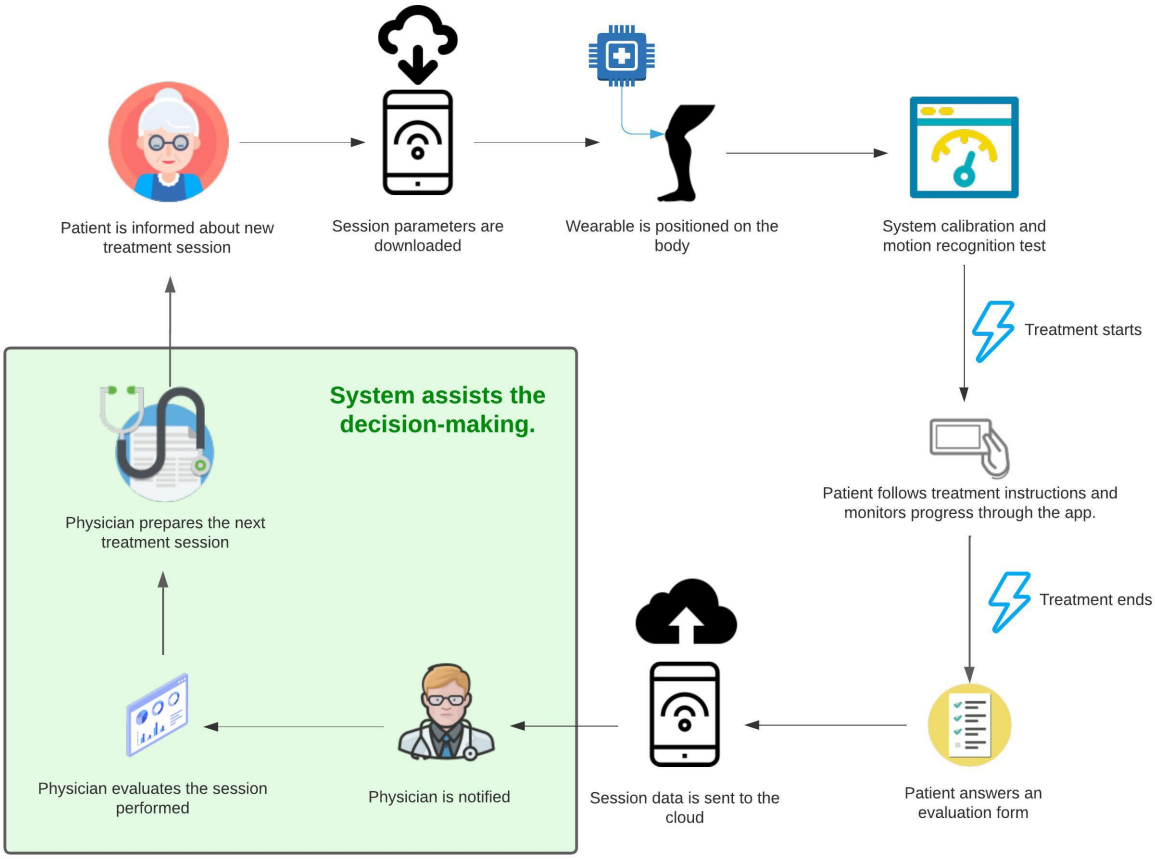


Figure 15: The treatment scenario in patient's home.

At the appointed time, the patient accesses the mobile application and selects the session to be initiated. With this, the parameters defined by the physician are downloaded to the device. The patient then places the wearable device according to the instructions received during the clinical sessions and the guidelines provided by the physician. Once the wearable device is turned on, calibration tests are

performed, ensuring the device is optimized for the treatment environment.

The mobile app will guide the patient through a user-friendly interface, offering instructions and session progress information. The application will replicate the stimulation mode performed in the clinic and will also allow dynamic adjustments during the session. If the system detects changes in muscle fatigue metrics that exceed the limits established by the doctor, the app will automatically adjust the treatment.

At the end of the session, the patient will complete a brief questionnaire about the experience and their physical condition. All collected data, including sensor information, stimulation parameters, and questionnaire responses, will be uploaded to the cloud. The physician is immediately notified that the session has been completed.

This approach allows the physician to access biofeedback data online, enabling he or she to assess the patient's response to treatment and create a detailed evaluation report. If necessary, the physician can modify the session settings and schedule a new session for the patient. This continuous treatment cycle repeats until the rehabilitation process is fully completed.

4.1.2 System Architecture

The proposed system architecture for muscular rehabilitation treatments using electrical stimulation was designed to incorporate the technological advances of health 4.0. This includes the use of microservices, cloud computing, internet of things, mobile applications, among others. This approach aims to offer a comprehensive and effective solution, capable of meeting the requirements described in the treatment scenarios. A detailed overview of systems that inspired this design and the initial implementation is provided in the article (Franco et al., 2022b).

It is important to emphasize that the information to be stored is highly confidential. In addition to personal information, such as the names and addresses of system users, health-related data such as active diseases, clinical observations, and more will also be managed and processed. To ensure the security of this sensitive data, a strategy has been developed to adhere to best practices for data protection, segmenting stored data and mitigating potential cyberattacks.

The proposed system is based on a three-layer architecture, using the smartphone as an intermediary device. Despite this, we split the interior of the secure cloud layer into two layers, making it possible to consider this architecture as four layers. This division guarantees that only the components that need external communication are available with public IP. Components that need to be more secure, such as databases and the logging service, are separated and only available on the private network. The system architecture shown in Figure 16 has seven main components. The characteristics and functions of each

component are as follows:

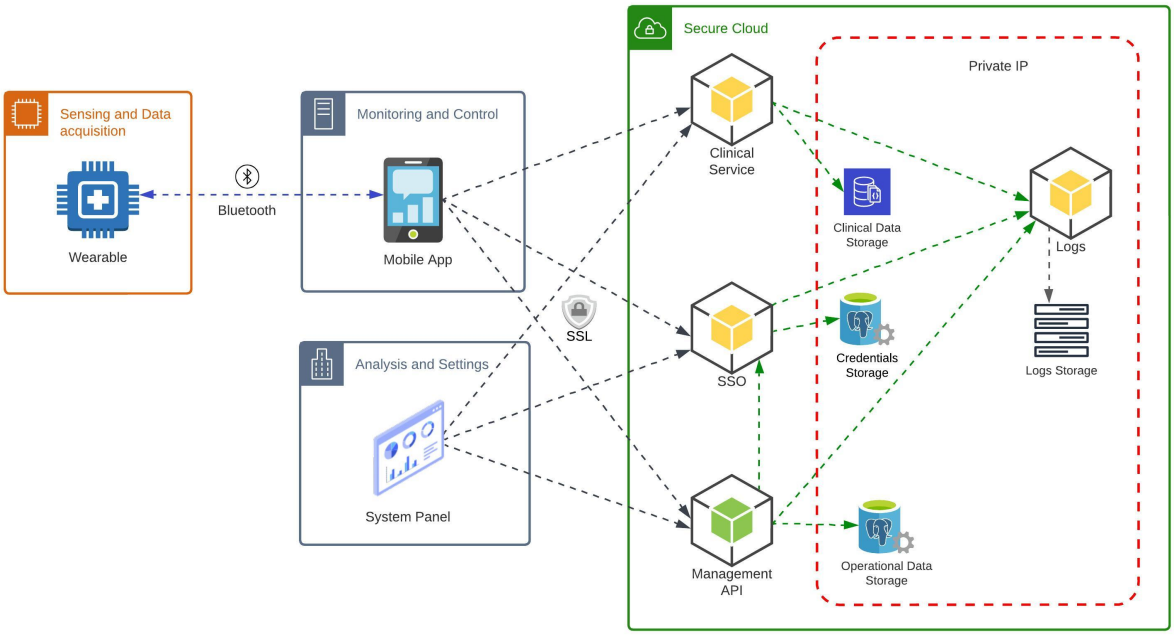


Figure 16: System Architecture.

Wearable Device: Component that includes a system, sensors for biofeedback data acquisition and the electrical stimulator. This component is the actuator device that perform the remote rehabilitation and communicate with mobile app.

Mobile Application: Intermediate application between the wearable device and the cloud. Its main functions will be: receive the stimulation protocol from the cloud and providing it to the wearable device; organize the data received by the treatment session and send it to the cloud; provide and collect the patient information.

System Panel: Administrative panel for professionals to manage patients and treatments. On this website, the physician will be able to visualize and adapt the treatment plan. In addition, it will be possible to view the biofeedback acquired by the wearable device and respond to messages from patients.

Clinical Service: Service that stores and processes the clinical data of patients. This information are: patient characteristics and medical history, clinical reports and biofeedback collected by wearable device during sessions.

Management API: A module capable of managing and providing the necessary resources for the operation of the mobile app and the administrative panel. For example, managing patients, professionals, messages, equipment, and others.

Single Sign-On (SSO): Component responsible for generating the access and refresh tokens. The

purpose of SSO is to provide a single point of authentication within the architecture, thus ensuring that access of the multiple services is secure and transparent.

Log Service: Component required to maintain log integrity across the entire architecture. The intent is that all components provide logs periodically for this service, creating a unique auditable and secure access point.

The communication between the components is varied, depending on their purpose within the architecture. To optimize battery life, the wearable device communicates with the mobile app via Bluetooth Low Energy. Meanwhile, interactions between the secure cloud, the mobile app, and the system panel adhere to the HTTP protocol with Secure Sockets Layer (SSL) certificate and JSON Web Token (JWT). The Clinical Service, SSO, and Management API systems communicate with the Log Service also using HTTP with SSL, but with public and private key authentication.

4.1.3 Sensitive Data Protection

The architecture is based on micro services. This approach enables data to be split and stored in different parts according to the operational needs of each service. Thus, the patients' personal data, such as addresses, phone numbers, responsible doctor, among others, are stored under the Management API. The clinical data, such as treatment plans, recommended treatments, disease history, diagnoses, among others, are stored in the Clinical Service.

To maintain data privacy, the identifiers of each entity must be different in each database. This ensures that if both database systems are hacked, the attacker would not be able to link which diagnosis belongs to which patient, minimizing the impact.

To maintain the data relationships between the systems, the pseudonymization technique was applied. This technique allows the identity of subjects to be hidden from any outsourced services by assigning pseudo-identifiers. Thus, the third-party services are not able to relate the pseudonyms to the real identifications, so they do not recognize the author of the data provided. If a client application needs to recognize the identity of the data, a grant of access is requested. If the request is accepted, the triggered services return the data that can be queried by the client app that requested it (as can be seen in Figure 17).

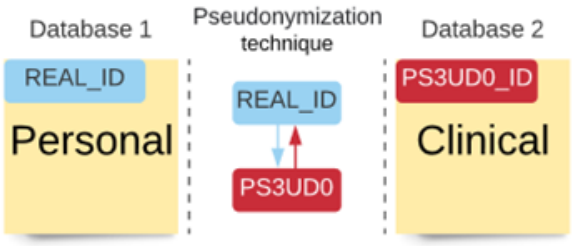


Figure 17: Representation of pseudonymization technique.

To ensure the integrity of requests JSON Web Signature (JWS) was used during communication. Each service was configured with asymmetric keys and has access to public keys of other services. In this way, the data in a message is signed by a sending service using its private key, so other services can verify the information using the public key of the sending service. Figure 18 represents a simplified process of signing and checking content using asymmetric keys.

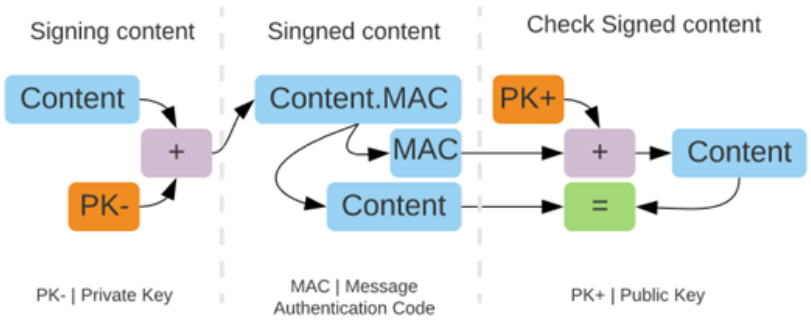


Figure 18: Signature and content verification process using asymmetric keys.

Using signed messages prevent repudiation of services. The public key can be used to reveal the real sender of a message, and modifications during transmission (integrity). All micro services have a specific key, and the check process only works with the correct public key. The trust of information is established when the generator of a message is recognized as an internal service.

The relationship of the Clinical Service and the Management API can be understood as outsourced services to each other. Thus, when a mobile app wants to access either of the two services, it must send in the header of each request the access token provided by SSO service. Inside this token, three main pieces of information will be stored, the role the user belongs to, and two encrypted packets. The first packet is encrypted by the public key of the Clinical Service with the pseudo-anonymized identifier for the Clinical Service. The second packet follows the same logic but encrypted and pseudo anonymized for the Management API.

When a request is made, each service can open the packet with its private keys and search in their data

for information that correlates with the sent identifiers. This ensures that the only ones who could discover the relationship between the two databases are the owners of the information, that is, the ones who should really have access. In his Master's work, developed in conjunction with this doctoral project, (Silva, 2021) has explored the information security and scalability approaches to be used in this architecture.

4.1.4 Database Modeling

To maximize the efficiency of each module of the system architecture, different Database Management Systems (DBMS) were employed. Taking into account the distinct characteristics of the stored data, Postgres[1] (SQL) was chosen for the Management API database and the Single Sign-On (SSO) service, while MongoDB [2](NoSQL) was selected for the Clinical Service database.

To ensure system interoperability, a set of elements was adapted by adding attributes and modifying nomenclature to facilitate the exchange of information with systems that follow the HL7 FHIR[3] health data exchange standard. HL7 FHIR (Fast Healthcare Interoperability Resources) is a crucial standard that promotes efficient clinical data integration between different systems, modernizing healthcare processes.

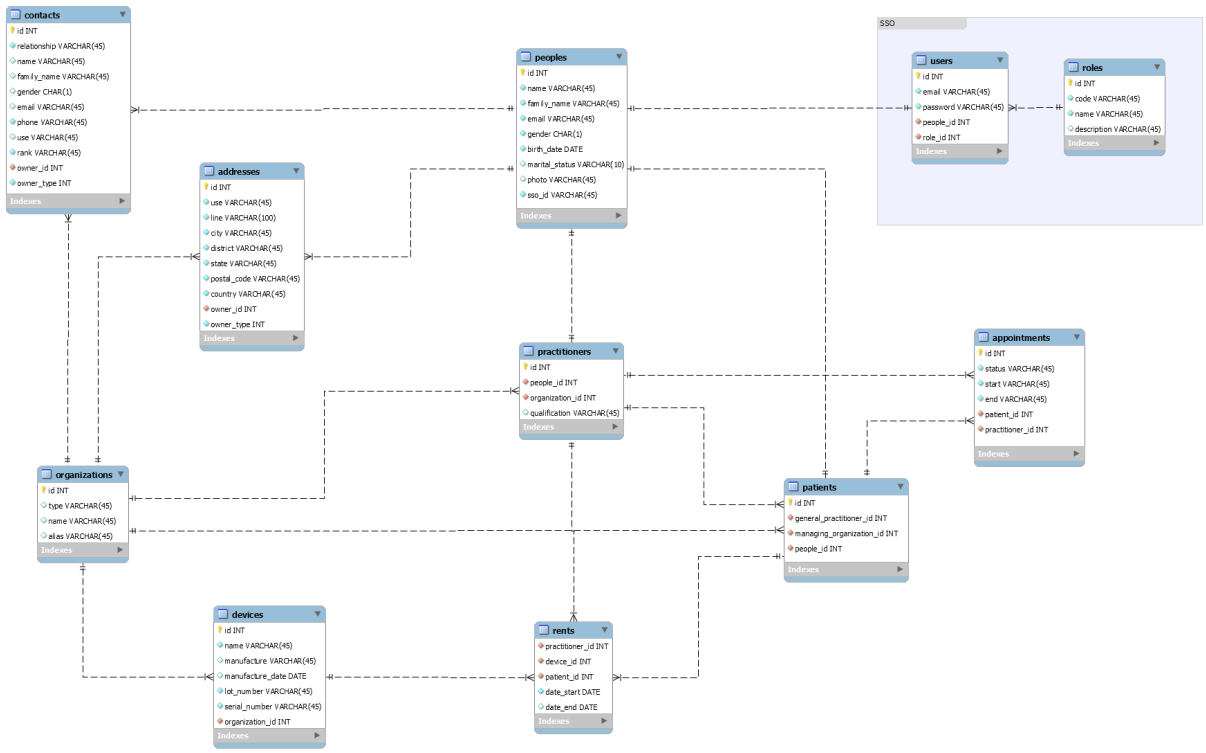


Figure 19: Entity-Relationship (ER) Model of the Management API Database.

1 https://postgresql.org

2 https://mongodb.com

3 https://fhir.org

Figure 19 illustrates the entity-relationship model used to design the necessary data structure for the Management API. This database was set up to handle personal data, including information on practitioners, patients, appointments, and rental devices. The Entity `People` was created to aggregate related attributes, serving as the primary entity in the hierarchy. Each record in the Entity `People` must have an SSO_ID to link the user to the SSO service and may have multiple addresses and contacts.

Entity `Appointment` store the status, start time, and end time, and can include information about the location. However, they do not store data related to the pathology being treated. Although it has not yet been implemented, the system is also designed to support the borrowing of wearable devices, with the expectation that these devices may come in different versions.

The NoSQL data model required for the functioning of the clinical service is depicted in Figure 20. This model stores data related to patient health and applied treatments. Since MongoDB supports embedded documents, the database consists in only four main collections: `Conditions, Observations, Care-Plans and Sessions`. The another "collections" that appear in Figure 20 are embedded documents of the four main collections mentioned above.

The collection `Conditions` pertains to specific illnesses and their initial stages. The collection `Observations` stores updated information on the patient's condition, with a new observation document generated for each appointment.

The collection `Sessions` collection, the most complex in the data model, is responsible for storing stimulation parameters, biofeedback data, and calibration data, among other information. Additionally, there is a contractions document that records metrics related to muscle fatigue during treatment sessions, which are calculated by the mobile app. All raw sensor data is stored compressed in binary form.

For home-based treatment sessions, a care-plan document needs to be generated, specifying the start date and objectives. In the data model, home sessions extend the standard clinic sessions by incorporating additional information and features giving rise to the `Care-Plans` collection. The design includes an intelligent rules system that adapts sessions in real-time. The automatic session settings document stores triggers for stimulation adjustments proposed by the physician, ensuring personalized and responsive treatment.

This approach ensures that the system can handle with the complexity and sensitivity of patients' health data, offering a secure, efficient, and scalable data model for muscle rehabilitation treatments. The final database model was repeatedly refactored throughout the development process to incorporate new technologies.

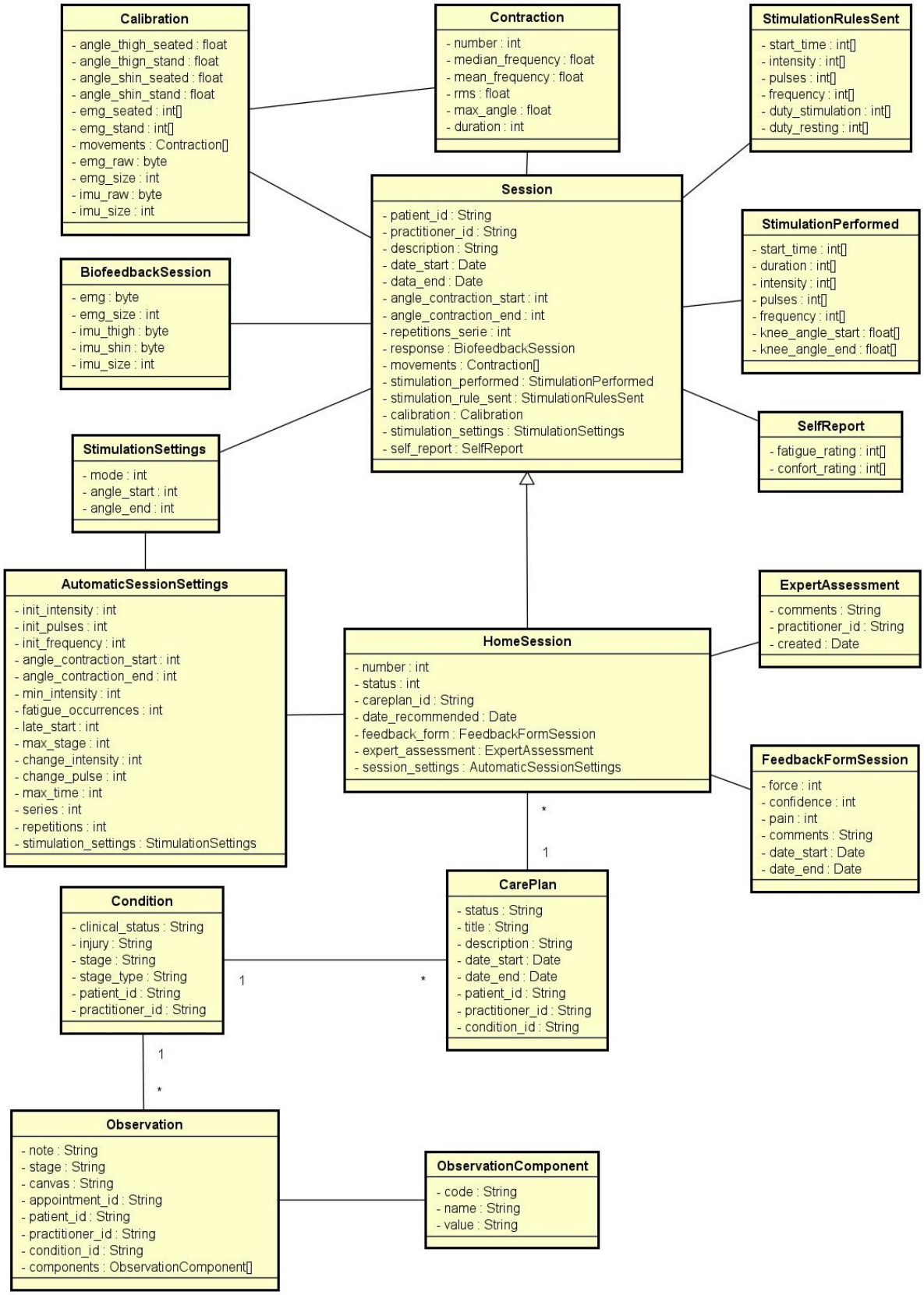


Figure 20: NoSQL data model for the clinical service.

4.2 Prototyping

4.2.1 Cloud Infrastructure

The cloud infrastructure developed distributed the components of the system architecture across seven virtual machines (VMs) based on Ubuntu Server 20, hosted within the Research Centre in Digitalization and Intelligent Robotics (CeDRI) cluster at the Instituto Politécnico de Bragança (IPB) building. Out of the seven VMs, only three have IPs on the public network, each dedicated to a different module of the system being Clinical Service, Management API, and SSO.

The Clinical Service and Management API were developed from scratch using Python[4] programming language and Flask[5] framework, recognized for its flexibility and ease of implementation. Both services were designed following the Model-View-Controller (MVC) design pattern (Trygve, 2003), ensuring clear separation of concerns for enhanced maintainability and scalability. Furthermore, the service endpoints were documented using Swagger[6], a tool that offers interactive and dynamic documentation of APIs, simplifying understanding and used by developers for standardizing inputs and outputs.

For providing the SSO service, the open-source solution Keycloak[7] was adopted. Installed via Docker[8], this choice offers a user-friendly interface for implementing secure and complex authentication strategies, such as two-factor authentication and OAuth v2[9].

The remaining four VMs were allocated in an internal network, allowing access only to the three services with public IPs. Thus, one VM was for the MongoDB database, and two were for the Postgres database to supply Management API and SSO. The last VM is destined to Logs service and its database were installed on the same VM, as this module does not require a public IP. This configuration aims to enhance the security of access for each component of the infrastructure.

4.2.2 Wearable Device

Supported by the Portugal 2020 program and international partnerships, the NanoStim project[10] united a consortium focused on advancing remote rehabilitation. The team included six Portuguese organizations: Instituto Politécnico de Bragança, Universidade do Minho, NATG, INOVA+, Impetus, and TeandM, and the

4 https://www.python.org

5 https://flask.palletsprojects.com

6 https://swagger.io

7 https://www.keycloak.org

8 https://docker.com

9 https://oauth.net/2

10 https://nanostim.pt

University of Texas, USA. In this document, the term *wearable device* refers primarily to the hardware component developed during the NanoStim project. The term *wearable system* is used to refer to the system running inside the *wearable device* that is part of the proposed system architecture.

Figure 21 illustrates the design of the wearable device, which integrates essential components chosen for their low cost and ability to provide effective muscle rehabilitation treatment.

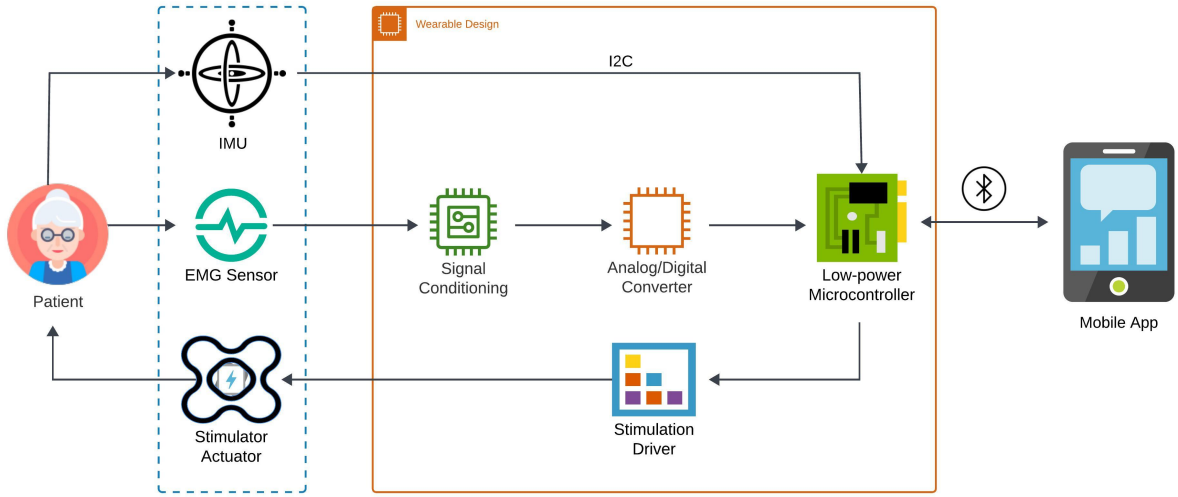


Figure 21: Wearable Device Design.

The primary component is the low-cost microcontroller, a small computer on a single chip that integrates a processor, memory, and peripherals. This microcontroller manages all the sensors and communicates with the mobile application. The ESP32 microcontroller, specifically the WROOM-32E[11] version, known for its versatility, cost-effectiveness, and built-in Wi-Fi and Bluetooth features, was utilized. The ESP32 is ideal for wearable devices and IoT applications due to its low power consumption, support for multiple communication interfaces, and efficient processing capabilities, such as Bluetooth Low Energy v4.2[12]. Its key specifications include a dual-core 32-bit Tensilica Xtensa LX6 CPU operating at up to 240 MHz, 448 KB of SRAM, 520 KB of ROM, and peripheral interfaces with a 12-bit ADC.

The wearable device includes two types of sensors: Electromyography (EMG) sensors and Inertial Measurement Unit (IMU) sensors. The EMG sensor measures the electrical activity of muscles through electrodes positioned on the skin. The measured electrical activity is returned as an analog signal with a frequency band of interest between 0 and 500 Hz, which is then converted to digital by the microcontroller. The signal conditioning circuit, essential for processing EMG signals, was developed from scratch and more

[11] https://www.espressif.com/en/products/socs/esp32

[12] https://www.bluetooth.com/specifications/specs/core-specification-amended-4-2

details can be found in article (Sestrem. et al., 2022).

IMU sensors measure acceleration and rotation across multiple axes, typically consisting of a 3-axis accelerometer and a 3-axis gyroscope, known as a 6-axis IMU. The accelerometer measures linear acceleration, while the gyroscope measures angular velocity. In the field of rehabilitation, this data is generally used to monitor movements and orientations in three-dimensional space. The MPU-6050[13] IMU sensor was chosen for its reliability and efficiency in I2C communication[14].

An essential component in the proposed application is the electrical stimulation circuit, which generates electrical impulses to stimulate nerves controlling the muscles, promoting contractions and movements. This component is the actuator for restoring or improving muscle function in patients with injuries or diseases in our context. The stimulation circuit was also developed from scratch and a Master's thesis (Gonçalves, 2023) was developed testing various low-cost components to replicate the electrical stimulation of commercial devices.

All mentioned components are integrated into a Printed Circuit Board (PCB), as illustrated in Figure 22. The PCB is enclosed within a 3D-printed case with dimensions of 10 cm (length) × 12.5 cm (width) × 3.5 cm (height), excluding the USB cable. This case also houses the system's battery, which provides an operational life of approximately 6 hours per charge. The portable design allows the wearable device to be conveniently charged via USB and easily used in various environments. Additionally, the total cost of production for each unit remains below 100 euros, making it a cost-effective solution.



Figure 22: Wearable Device Components in PCB.

[13] https://invensense.tdk.com/wp-content/uploads/2015/02/MPU-6000-Datasheet1.pdf

[14] https://docs.arduino.cc/learn/communication/wire

The combination of selected components seeks to offer precise monitoring and coordinated stimulation during rehabilitation sessions simultaneously, providing innovative benefits for muscular rehabilitation.

NanoStim project ended in July 2023, with a live demonstration held at University of Minho in which all partners showcased their achievements to to enhance the project outcomes.

4.2.3 Mobile Application

The mobile application is the main piece within the system architecture aiming to provide a technological and user-friendly interface for using the wearable device and managing muscular rehabilitation treatment. The implementation of the app was guided by principles aimed at modularity, maintainability, and efficiency. The application, developed in Kotlin[15] using Android Studio[16], was designed for devices with a minimum version of Android 5.0 Lollipop[17]. The architecture adopted was the Single Activity Architecture[18], combined with the Model-View-ViewModel (MVVM)[19] pattern and dependency injection using Hilt[20].

The Single Activity Architecture centralizes navigation and simplifies the lifecycle management of user interface components. In this pattern, a single activity (the MainActivity) acts as a container for all fragments, each representing a specific screen or functionality. Centralizing navigation allows for more efficient management of screen transitions and facilitates the reuse of interface components, promoting greater modularity and reducing the consumption of smartphone resources.

To separate business logic from the user interface and improve testability, the MVVM pattern was adopted. This pattern organizes the application into three main components: Model, View, and ViewModel. The Model layer contains data logic and business rules, communicating with local and remote data sources such as SQLite databases and REST APIs. The View is responsible for presenting data to the user, observing changes in the data provided by the ViewModel, and updating the user interface as necessary. The ViewModel acts as an intermediary between Model and View, managing the data for the user interface and containing presentation logic, while using LiveData to observe data changes and notify the View.

The Figure 23 illustrates the interaction between the main components of the application using the MVVM pattern. The user interacts with the user interface through fragments, which are hosted by a single activity. The fragment inflates XML layouts that define the visual components, meaning it converts the XML-based description of the UI elements into actual objects that can be displayed and interacted with.

[15] https://kotlinlang.org

[16] https://developer.android.com/studio

[17] https://android.com/versions/lollipop-5-0

[18] https://developer.android.com/topic/architecture

[19] https://learn.microsoft.com/en-us/dotnet/architecture/maui/mvvm

[20] https://dagger.dev/hilt

The fragment binds to the ViewModel, which fetches or updates the data in the Model. The Model abstracts the data access logic through repositories, which fetch data from network sources and local storage.

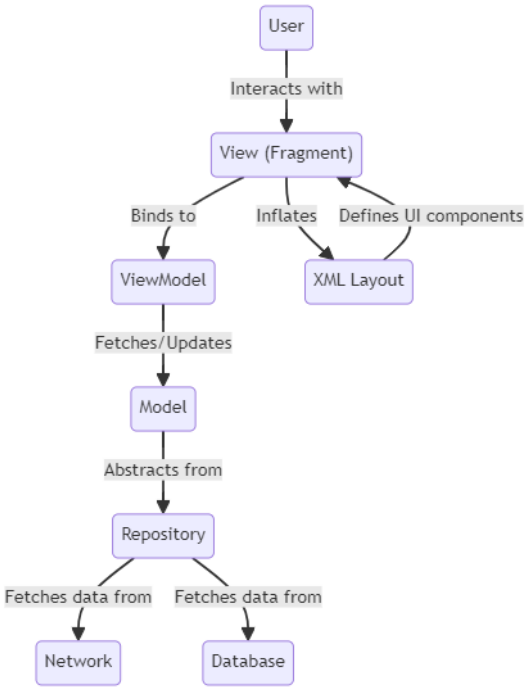


Figure 23: MVVM pattern applied to Android app.

As illustrated in Figure 23, the user interacts with the user interface, which reuse fragments. The fragment inflates the XML layouts, defining the visual components. The UI binds to the ViewModel, which fetches or updates data in the Model. The Model abstracts data access logic through repositories, which obtain data from network sources and local storage. The ViewModel acts as an intermediary between the Model and the View, managing data for the user interface and using LiveData to observe data changes and notify the View.

To efficiently manage dependencies and promote a decoupled design, Hilt, a dependency injection library for Android, was used. Hilt automates the creation and injection of dependencies, reducing the need for repetitive code and facilitating maintenance.

For data management, the library Retrofit[21] was used for HTTPS communication with the cloud, ensuring secure and efficient data transmission. Raw sensor data collected during the treatment is stored in local files. This approach is adopted due to the nature of the data being time series and the large volume of data generated by sensors, making files the best option for temporary storage. At the end of the treatment, the data is sent to the cloud and the files are cleared, ensuring that the mobile device maintains adequate storage space.

[21] https://square.github.io/retrofit

Lastly, it was necessary to implement asynchronous operations and manage multiple threads during rehabilitation treatment. For this purpose, Kotlin's Coroutines library[22] was used. Coroutines allow tasks to run without blocking, providing a responsive user interface and improving application performance. This implementation was necessary especially to guarantee the processing of biofeedback data, updating of interfaces, and sending of stimulation parameters simultaneously.

4.2.4 Communication Between the Wearable System and the Mobile App

The communication between the wearable system and the mobile app is essential for the functionality of the decision support system, enabling the operation of the actuator device for muscle rehabilitation treatment. This process is based on the Bluetooth Low Energy (BLE) protocol, where the wearable system acts as the server and the mobile app as the client.

Communication Protocol

In the BLE communication protocol, characteristics are the basic units of data exchanged between devices. Each characteristic has a UUID (Universal Unique Identifier) and is used for reading or writing information. The Receive Characteristics (Rx) to transmit data from the wearable system to the mobile app. Each type of data collected by the wearable system corresponds to a specific characteristic:

Rx: EMG Sensor Data: Each data packet collected by the EMG sensor consists of 2-byte integers, with a maximum value of 65535. However, the ADC (Analog-to-Digital Converter) of the ESP32 used has a maximum resolution of 12 bits, resulting in a maximum reading of 4095. The data collection frequency is 1000 Hz, according to the Nyquist theorem, which requires sampling at least twice the maximum frequency of interest to accurately capture the signal.

Rx: IMU Sensor Data: The data collected by the two IMU sensors is sampled at 100 Hz, and each packet is a combination of three float values. These three values represent the angle of the IMU sensor on the shin, the angle of the IMU sensor on the thigh, and the sampling time difference between the last collection and the current collection. Each float value is stored in 4 bytes, being 1 byte for the sign, 2 bytes for the integer value, and 1 byte for the mantissa, totaling 12 bytes per IMU reading.

Rx: Battery Level: The battery level data is represented by 1 byte, with a maximum value of 100, indicating the percentage of the battery level. The data collection frequency is 1 Hz and is immediately sent to the mobile app; this data is not stored.

Rx: Performed Stimulation Parameters: The packets responsible for sending the performed

[22] https://kotlinlang.org/docs/coroutines-guide.html

stimulation parameters consist of seven float values, each stored in 3 bytes, with 2 bytes for the integer value and 1 byte for the mantissa, totaling 21 bytes per packet. The data collection frequency varies as the stimulation is performed. These values include: 1. Start time, 2. Duration, 3. Intensity, 4. Pulse width, 5. Frequency, 6. Knee angle at the start of the stimulation, 7. Knee angle at the end of the stimulation.

Table 9 summarizes the data transmitted by each reading characteristic. The BLE version supported by ESP32 used in this system allows a maximum length of an Attribute Protocol (ATT) packet of 517 bytes, also known as Maximum Transmission Unit (MTU).

Characteristic	**Sampling (Hz)**	**Data Size (bytes)**	**Maximum Packet Payload**
EMG	1000	2	250
IMU	100	12	42
Performed Stimulation	As performed	21	24
Battery Level	1	1	500

Table 9: Biofeedback data and packet volume.

The data transmission frequency does not match the data sampling frequency. This is due to the fact that transmission is optimized considering the user experience. This implies that although IMU data is collected at a lower frequency, it is sent at a higher frequency to provide immediate feedback to the user, updating the measured knee angle value 10 times per second. Table 10 summarizes the transmission parameters used during treatment:

Characteristic	**Transmission Frequency**	**Transmission Delay**
EMG	4 Hz	250 ms
IMU	10 Hz	100 ms
Performed Stimulation	20 collected	20 collected
Battery	1 Hz	1000 ms

Table 10: Optimized Data Transmission Frequency.

The Transmit Characteristics (Tx) enables the mobile app to send data to the wearable system, which is essential for controlling the device's operation during rehabilitation treatment. In the developed system, there are two key transmit characteristics:

Tx: Control Commands: The mobile application controls the wearable system through commands

sent in JSON format. The commands allow management of the treatment, the type and parameters of stimulation and the transmission of biofeedback data. The list below describes the nine implemented commands:

1. Start: Initiates the treatment process. This command requires specifying the stimulator mode, which can be one of the following:
    1.1 Without Stimulation
    1.2 Commercial Stimulator
    1.3 Leg Elevator
    1.4 Angle Range
2. Stop: Terminates the current treatment.
3. Pause: Pauses the ongoing treatment.
4. Continue: Resumes the paused treatment.
5. IMU Deviation Calibration: Calculates and stores the IMU sensor deviation in the wearable's ROM memory.
6. Enable data transmission: Configures the data transmission settings, with the following options:
    6.1 Start Transmission
    6.2 Stop Transmission
    6.3 Transmission Test
7. Set IMU Human Deviation: Sets the deviation of the positioned IMU sensors on the subject. This command requires specifying the deviation angles for both the thigh and the shin.
8. Set Minimum Angle for Contraction Recognition: Defines the minimum knee angle required to recognize a muscle contraction.
9. Set Angle Range for Stimulation: Defines the range of angles for stimulation. This command requires two parameters: the start angle and the end angle.

Tx: Stimulation Parameters: This characteristic is used to configure the intensity and frequency of the stimulator. Also transmitted in JSON format, there are five parameters: Intensity, Pulse Width, Frequency, Stimulation Duty Cycle and Rest Duty Cycle. All stimulation parameters sent to the wearable system are saved by the mobile app, along with the time elapsed since the start of treatment.

Pairing Process and Transmission Test

The pairing process is initiated by the mobile app establishing the BLE connection and performing the "handshake." Immediately after, the MTU is configured to 517 bytes. Subsequently, the mobile app registers to receive notifications from the Rx characteristics. If the registration attempt fails, the app waits 500 ms before retrying.

Once all Rx characteristics are configured, the mobile app starts the data transmission and reception test. It resets the reception counters and sends the command 6.3 to the wearable system. If the wearable system correctly receives the command, it begins a special data transmission. This transmission involves sending 20 packets of the maximum packet payload with the maximum scale value through the four characteristics every 100 ms, totaling 2 seconds of testing. If all test values are completely according to the expected, the app considers the pairing successful.

If at least one value is incorrect or no packets are received, the mobile app disconnects from the wearable system. As a result, the wearable system restarts automatically, as it is designed to reset fully upon disconnection. This ensures a clean state for the device, but it requires the pairing process to be restarted from the beginning.

4.2.5 System Panel

This section describes the front-end system developed using the Angular framework[23] and programmed in TypeScript[24], designed to manage users and CDSS treatments. This system was developed using a pattern similar to MVC, with the addition of services and data binding to facilitate communication between components and the data layer.

The system panel has two user roles: administrator and physician. Each role has specific permissions and accesses different system functionalities, as detailed below.

Administrator: The administrator has the ability to manage all organizations in the system, as well as the physicians associated with these organizations. Organizations are institutions that can use the system,

[23] https://angular.dev

[24] https://www.typescriptlang.org

such as research institutions, clinics and hospitals. The main features available to the administrator are:

1. Manage Organizations: The administrator can create, edit and delete organizations. To register an organization it is necessary to provide the address and contact details of someone responsible for the institution.

2. Manage Physicians: The administrator can add, edit, and remove physicians by associating them with specific organizations. The physician's registration includes credentials, qualifications, contact and address.

Physician: The physician is responsible for managing patients, appointments and care plans. The functionalities available to the physician includes managing:

1. Patients: Register and maintain patient information, including personal data, credentials, contact and address.

2. Appointments: Schedule, edit, and cancel appointments, allowing efficient management of the appointment calendar.

    2.1 Observations: Add observations and notes to appointments, recording important information about the patient's condition and treatment progress.

3. Medical Records: Maintain patients' medical records, including:

    3.1 Pathologies: Record and update patient pathologies, documenting relevant medical conditions.

    3.2 Treatment Plans: Define and monitor treatment plans, specifying therapeutic goals and methods to be used.

    3.3 Treatment Sessions: Record and track sessions performed, including viewing biofeedback data recorded by the wearable system, recording an automatic treatment session and simulating fatigue levels based on a previously performed session.

The Use Case diagram in Figure 24 describes in detail the interactions of the actors, enhancing the actions each role can perform. Before accessing these functionalities, users must first log in using a SSO system with OAuth 2.0 authentication, ensuring secure access to the system.

The development of the web-based administrative panel enhances user convenience, allowing access to the system at any time and from any location. This approach provides flexibility and facilitates the

efficient and accessible management of treatments and clinical research. Additionally, the management of sessions enables detailed analysis of the biofeedback data collected by the wearable system, as well as the applied stimulation parameters, offering valuable insights for monitoring and optimizing treatments.

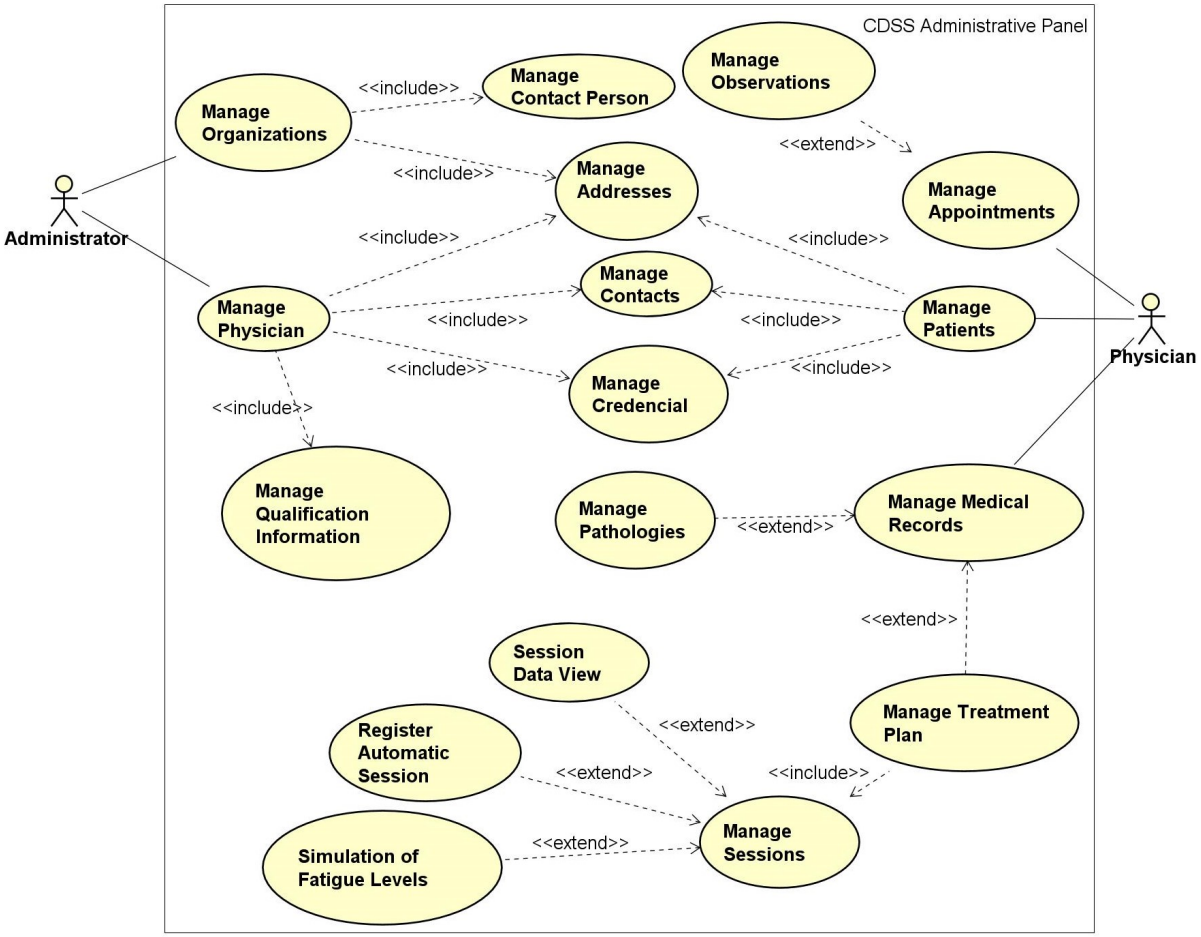


Figure 24: Use Case Diagram for System Panel.

Chapter 5

Intelligent Features for Treatment Customization

In this chapter, five essential features are presented that form the foundation of a CDSS designed to make muscle rehabilitation treatments more responsive to biofeedback data collected from patients during electrostimulation sessions. These features not only enhance the informatization of the treatment but also significantly improve response time, making the system more intelligent and adaptable compared to traditional rehabilitation treatments using conventional actuators.

The five features can be divided into three main categories. The first category encompasses movement recognition and fatigue parameterization, describing the methods used to transform raw data into valuable information about the physiological state of the muscle under treatment. The second category focuses on the implemented electrostimulation treatment modes and how they can be adapted based on biofeedback. Finally, the last section outlines the utilities developed to enhance the healthcare professional's experience when using the CDSS.

5.1 Movement Recognition

Understanding the movements performed by the patient during treatment sessions is crucial for optimizing rehabilitation protocols. Initially, the NanoStim project planned to use a single EMG sensor to extract the parameters related to muscle state and effort. However, this approach may be limited, as with just the EMG signal, it would be challenging to differentiate the amplitude of movements, making it difficult to assess the effectiveness of the treatment over time.

To address this limitation, a research was conducted to identify the most suitable sensors and data processing methods needed to accurately capture leg movements during treatment. A literature review on biomechanical approaches for classifying knee osteoarthritis Franco et al. (2021) highlighted the extensive use of IMU sensors. These sensors are often used to measure the angle of the knee joint through two IMU sensors, one attached to the thigh and the other to the shin.

Guided by these findings, the decision was made to integrate two IMU sensors into the wearable system to monitor the knee joint angle in real time. Therefore, this session describes how raw data extracted from IMU sensors is used to recognize and classify movements performed during rehabilitation treatment.

5.1.1 Mathematical Model

The mathematical model used to compute knee angle of the subject is based on the theory of multibody system dynamics, as presented by (Olinski et al., 2017). In this approach, the orientation of a body in space is given by the orientation of a local frame attached to the body with respect to a reference coordinate system as illustrated in Figure 25.

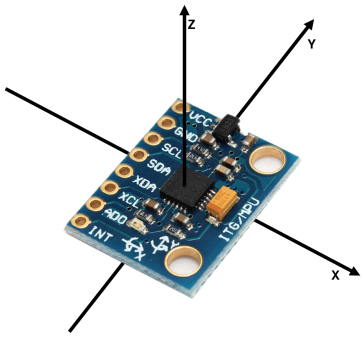


Figure 25: IMU sensor with the reference coordinate system.

Considering the particular case in which the orientation changes occur in a specific plane, as presented in Figure 26a, the mapping of frames with respect to a reference frame can be represented by a single rotation from a reference to another (Figure 26b).

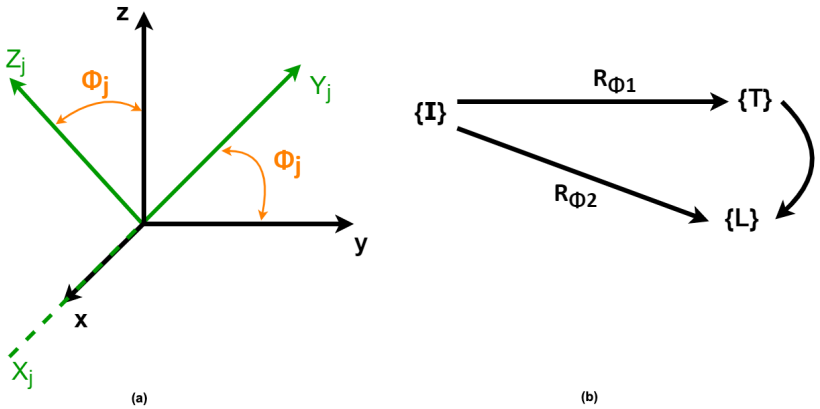


Figure 26: (**a**) Frame representation relative to a reference. (**b**) Linear mapping of a frame to another.

To map a frame worth in respect to another in the case of rotations in the YZ-plane of an angle Φ_j around the x-axis, as presented in Figure 26, the Euler angles are determined by applying the linear mapping successively from rotation matrices ($R_{\Phi 1}$ and $R_{\Phi 2}$) in each of these spaces. The rotation matrix is given by Equation (5.1), where $j = 1$ or $j = 2$:

$$R_j = \begin{bmatrix} 1 & 0 & 0 \\ 0 & cos(\Phi_j) & -sen(\Phi_j) \\ 0 & sen(\Phi_j) & cos(\Phi_j). \end{bmatrix} \tag{5.1}$$

Considering the sagittal plane as the plane of reference for the movements, once the abduction/adduction angles are neglected (Figure 27), the orientation of the leg's frame and the thigh's frame, both concerning the inertial coordinate system, are represented as rotations in the referred plane.

When the monitored movement occurs in the sagittal plane, the knee angle is given by the difference between the thigh and leg angles $\Phi_{knee} = \Phi_2 - \Phi_1$.

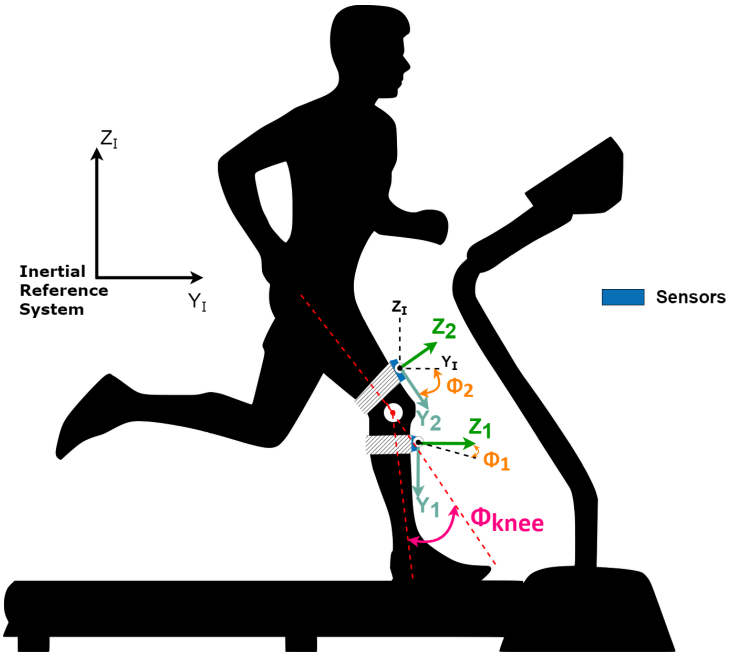


Figure 27: Sensors with the angles representation. Adapted from (Olinski et al., 2017).

IMU data is measured relative to the inertial coordinate system. By attaching an IMU to both the thigh and the shin, their respective orientations can be determined in relation to the inertial system. The difference in these orientations provides the knee angle. This method allows for accurate and continuous monitoring of knee movements, ensuring precise data for rehabilitation purposes.

5.1.2 Knee Extension Exercise

The knee extension exercise is fundamental in muscle rehabilitation, especially for the quadriceps muscle group. This exercise involves extending the knee joint and activating the quadriceps femoris, the largest muscle group in the thigh. Strengthening the quadriceps is essential for maintaining knee joint stability and promoting proper gait patterns (McGinty et al., 2000).

To perform the knee extension exercise, the patient sits in a chair or on a knee extension machine with knees bent at a 90-degree angle and feet flat on the floor or footrests. The exercise begins by extending the knees and raising the legs until they are parallel to the floor or fully extended. The movement is completed when the patient's leg returns to the starting position. Figure 28 illustrates the data collected by the biofeedback system during a knee extension exercise.

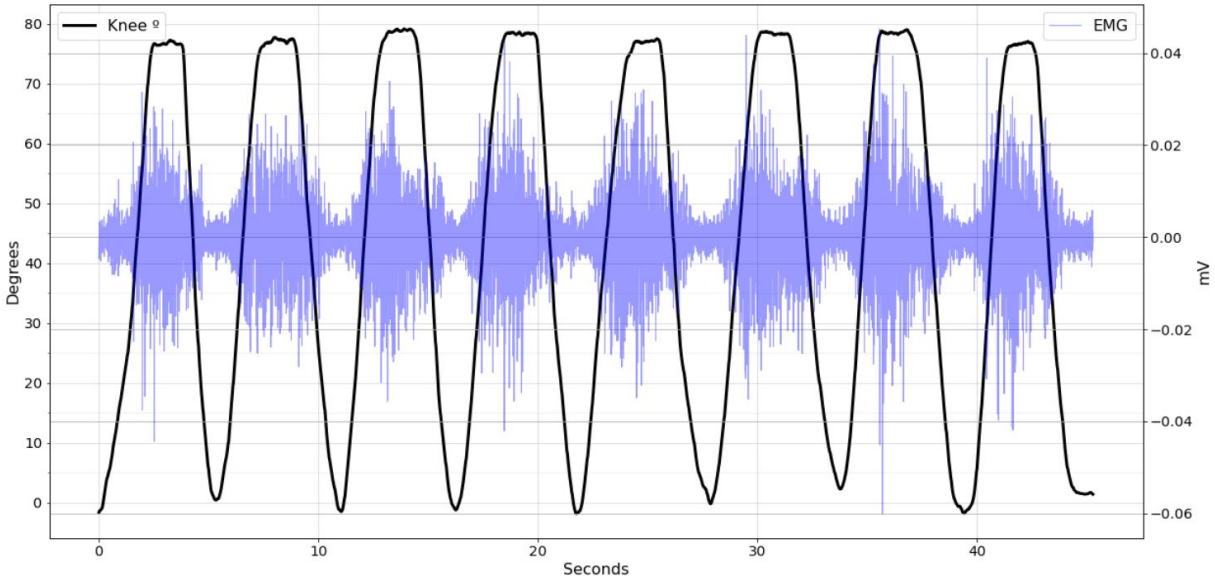


Figure 28: Data collected during knee extension exercise.

The knee angle illustrated in Figure 28 passes through several parabolas with the concavity facing upwards, representing each time the knee extension movement was performed. It is also possible to visualize the EMG signal synchronized with the movement, with an increase in the signal amplitude when the leg begins to rise and a decline in amplitude when the leg begins to descend, representing the muscle activation required by the vastus medialis muscle to perform the movement.

In this method, the knee extension movement was segmented into four distinct phases, systematically defined by two threshold lines. The first threshold line determines the minimum angle the knee angle must go through to be considered the start of the leg rise. The value for the first threshold was determined as 20°. The second threshold line represents the minimum angle the knee angle must go through for

the knee extension movement to be considered sufficient. The physician should adjust this value for each patient since the full knee extension range can be reduced in a muscle rehabilitation context. However, in this study, it was defined as 60°.

From the threshold lines, the four phases are determined from the following intervals: The first phase represents the upward movement, starting with values above the first threshold and ending at the second threshold; for example, the leg left 20° and reached 60°. The second phase is when the movement is already considered sufficient. It can be categorized when the knee angle is above the value of the second threshold, that is, values above 60°. The third phase represents the downward movement of the leg, which can only happen if phase 1 and phase 2 have occurred previously. It can be categorized as descending when the values are between the first and second threshold, equal to phase 1. Finally, phase 4 represents the leg at rest, classified when the knee angle values are below the first threshold, for example, values below 20°.

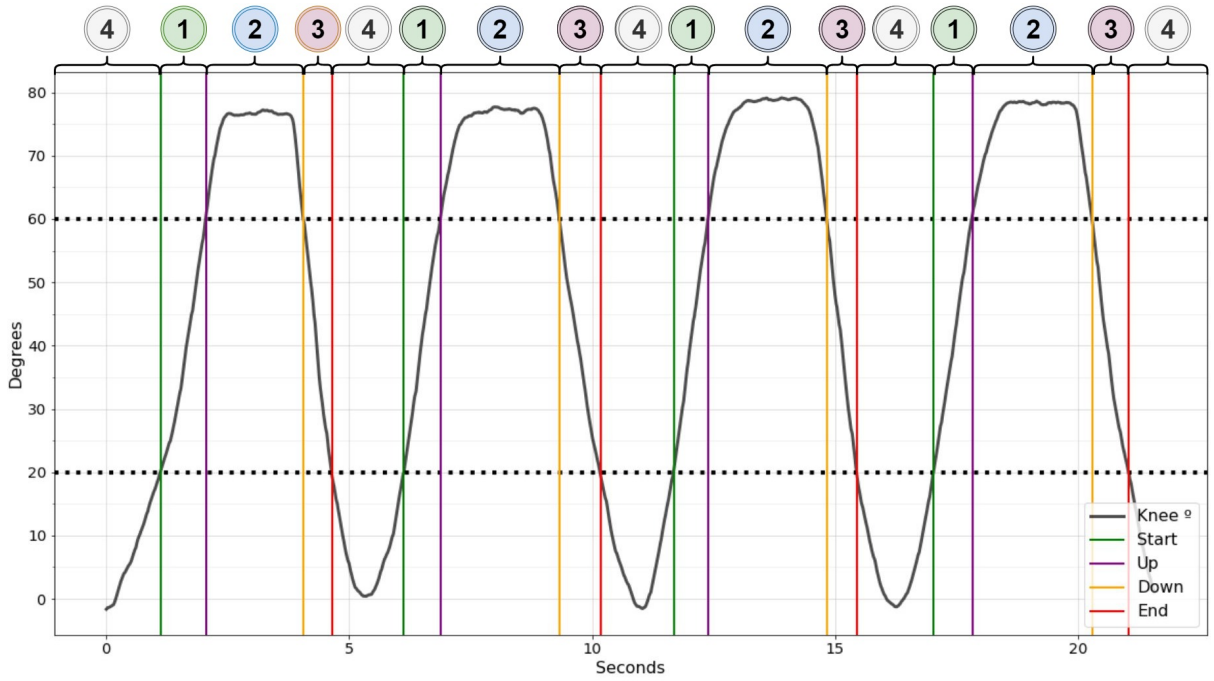


Figure 29: Classification of movement between the four phases.

In this way, as the mobile application receives the knee angle data, the current state of movement is classified based on this system of rules, as illustrated in Figure 29. Similar to a state machine, it is considered that the subject managed to perform the knee extension movement correctly once when the four phases were performed in sequence. When the sequence is complete, and the movement is considered correct, it is considered in this study that the subject performed a contraction. Thus, it is possible to visualize four recognized contractions in Figure 29.

The EMG signal used to analyze each contraction in this system is obtained by cutting the corresponding EMG signal between phases 1, 2, and 3 of the knee extension movement, excluding phase 4. This cutting method focuses on capturing only the most significant part movement, omitting the rest time between contractions. The decision to exclude phase 4 is based on the understanding that this phase, characterized by leg rest, contains less representative information for analysis. Additionally, it is likely to introduce positioning noise and prolonged periods with minimal muscle activity, which can impair the accuracy of the analysis.

When the knee extension movement fails to go through all four phases, it is classified as incorrect contraction. For example, the subject started to lift the leg, failed to reach the second threshold, and returned to the resting position, keeping phases 2 and 3 missing. In these cases, the corresponding EMG signal is disregarded for analysis.

Algorithm 1 materializes the described method responsible for updating the movement of the knee extension phase. This code runs continuously in the background during rehabilitation treatment in the wearable system and the mobile app.

In order to provide a user-friendly interface, a screen in the mobile application was developed to supply real-time visualization of knee angle movement. The screen updates at a frequency of 10 times per second, aligning with the data transmission rate of the wearable system. This dynamic interface allows users to continuously monitor knee extension movements as they occur.

The interface displays the current phase of contractions, the description of the current angle, and the total number of contractions recognized. Additionally, the physicians can easily adjust the minimum angle limit using user-friendly buttons on the screen, as depicted in Figure 30. This functionality aims to improve the adaptation of the rehabilitation process to the needs of each patient with accurate and updated information for the physician.

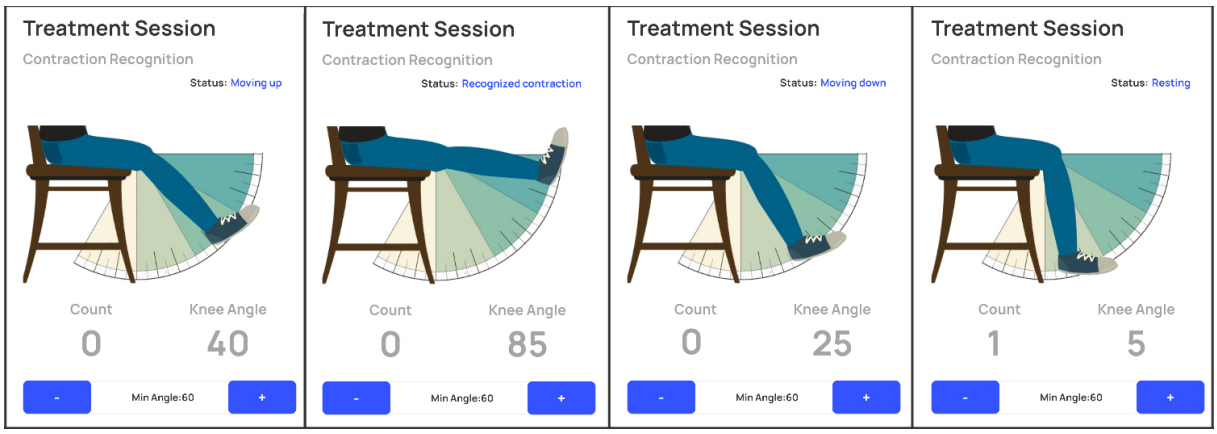


Figure 30: Phases of contraction recognition interfaces.

Algorithm 1 Knee Extension Movement Recognition Algorithm

```
kneeExtensionPhase ← "resting"
angleStartContraction ← 20
angleRecognizeContraction ← 60
currentContractionStatus ← False
while isRecognitionActive do
    angleKnee ← updateKneeAngle()
    if angleKnee > 0 then
        if angleKnee < angleStartContraction then
            if kneeExtensionPhase == "moving down" then      # Contraction Recognize
                processContraction()
            else                                             # Reset without contraction
                kneeExtensionPhase ← "resting"
                currentContractionStatus ← False
            end if
        else if currentContractionStatus == False then       # Start Contraction
            currentContractionStatus ← True
            kneeExtensionPhase ← "moving up"
        else if angleKnee > angleRecognizeContraction then # Recognition Angle Achieved
            kneeExtensionPhase ← "up"
        else if kneeExtensionPhase == "up" then              # Below the achieved recognition angle
            kneeExtensionPhase ← "moving down"
        end if
    end if
    delay(10)
end while
```

5.2 Muscle Fatigue Monitor

Monitoring muscle fatigue is crucial for muscle rehabilitation treatments, allowing physician to adjust treatment protocols and prevent overexertion or injury. Muscle fatigue is the inability of a muscle to generate or sustain a given level of force, leading to decreased performance, increased risk of injury, and delayed recovery (Enoka and Duchateau, 2008). By monitoring muscle fatigue, physician can assess patient progress, determine if the current treatment plan is effective, and adjust treatment intensity and frequency according to the patient's muscle response.

In muscle rehabilitation treatments, patients usually perform exercises targeting specific muscles, such as the knee extension exercise, which focuses on recovering quadriceps muscle, especially the vastus medialis and vastus lateralis. These exercises are usually repeated several times, and the intensity and duration can gradually increase over time, leading to muscle fatigue (Hassanlouei et al., 2012).

In traditional clinical settings, physician closely monitor patients and adjust exercises as needed. However, in remote rehabilitation, this level of interaction is more difficult, despite advances in remote rehabilitation, making it crucial to have a system that can monitor muscle fatigue in real-time during a treatment session.

5.2.1 Fatigue Metrics

The vastus medialis muscle is one of the thigh muscles responsible for extending the knee. When this muscle is healthy, more stability is generated in the knee, avoiding inappropriate movements. However, with aging, the vastus medialis can become weaker, resulting in decreased knee stability and an increased risk of injury (Moznuzzaman et al., 2021). Figure 31 shows an example of data from the EMG sensor positioned in the vastus medialis muscle and applied the method to recognize knee extension movement.

This section describes the operations performed on EMG signal clipped to calculate three relevant metrics in the context of muscle fatigue. Two metrics are related to the signal spectrum: the average and median frequencies. These metrics provide information about the frequency characteristics of the EMG signal and can indicate changes in muscle fiber activation. Specifically, a shift in activation from fast-twitch (type 2) fibers to slow-twitch (type 1) fibers indicate muscle fatigue. This shift is reflected in the signal spectrum by a leftward skew of the mean and median frequencies, resulting in lower frequency values (Cifrek et al., 2009).

In addition, Root Mean Square (RMS) is calculated to quantify the amplitude of the EMG signal. The RMS value indicates the level of muscle activation. Higher RMS values correspond to greater muscle

activation, while lower values indicate less muscle activation. Monitoring RMS over time makes it possible to assess changes in muscle activation levels, which can help evaluate muscle fatigue (Cifrek et al., 2009).

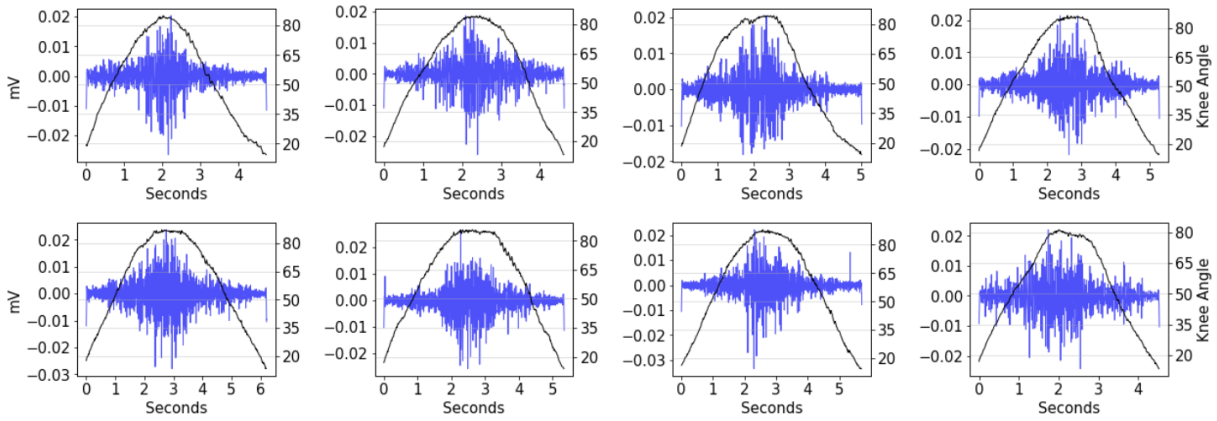


Figure 31: Example of EMG sensor data clipping by recognized movement. The EMG sensor signal is displayed in blue and the knee angle is displayed in black.

The EMG surface electrodes analogically capture the difference in electrical potential generated by the motor units activated at that moment. This analog signal is then transformed into a digital signal with 12 bits of resolution, producing an integer vector that discretely represents the sum of the motor unit electrical activity recorded. Since the frequency is set at 1KHz, the size vector corresponds to the duration of the contraction in 1ms.

To restrict the signal frequency between the most relevant range, a low-pass filter and a high-pass filter are applied. The low pass filter will attenuate frequencies above a cutoff frequency of 500 Hz, allowing only the lowest frequency components to pass through. On the other hand, the high pass filter will attenuate frequencies below a cutoff frequency of 20 Hz, allowing only the highest frequency components pass through (Potvin and Brown, 2004).

In this study, Welch's method (Welch, 1967) was applied to estimate the Power Spectral Density (PSD) of the EMG signal, which is required for calculating the average frequency (avgFreq) and median frequency (MedFreq). This method divides the signal into overlapping segments with a hop size determined by the overlap factor, which must be between 0 and 1. The periodogram of each segment is computed using the Fast Fourier Transform (FFT) algorithm. Thus, the PSD estimate using the Welch method is obtained by averaging the periodograms from all segments.

Transform the Signal to Millivolts

The EMG signal is transformed from raw to millivolts (mV) using Equation 5.2.

$$signalEMG_t = \frac{signalRAW_t - 2048}{4096} \tag{5.2}$$

where $signalRAW_t$ represents the raw EMG signal at time t, and 2048 and 4096 correspond to the values that scale the signal to the 12-bit resolution.

Compute the Segments

The window size M for each segment was determined as 1024 elements. This choice ensures an appropriate balance between frequency resolution and computational efficiency. Given an EMG signal sampling frequency of 1000Hz, the resulting frequency resolution is approximately 0.97Hz.

An overlap factor parameter α was defined as 0.1 to minimize potential spectral leakage. Each segment will overlap the previous segment by 10% of its length. The overlap helps capture transient information and improves the overall accuracy of the PSD estimate.

The number of segments L was computed based on Equation 5.3.

$$L = \left\lfloor \frac{N - M}{M * (1 - \alpha)} + 1 \right\rfloor \tag{5.3}$$

where N is the length of the $signalEMG$.

The vector S of size L can be defined as a collection of segments from the $signalEMG$, denoted as $S_i = signalEMG[a_i : b_i]$, where a_i and b_i represent the initial and final indices used to extract the segment from $signalEMG$.

The vector S can be constructed using Equation 5.4 as follows:

$$\begin{aligned} a_i &= (i - 1) * (M - \beta * M) \\ b_i &= a_i + M - 1 \end{aligned} \tag{5.4}$$

Apply Hanning window

This study employs a Hanning window in signal processing to mitigate the effects of spectral leakage and reduce aliasing (Jwo et al., 2021). The equation to create the Hanning window is defined as:

$$W_n = 0.5 - 0.5 \cos\left(\frac{2\pi n}{M - 1}\right), \quad n = 0, 1, 2, ..., M - 1 \tag{5.5}$$

where n represents the index, and M is the length of the window.

The windowed signal E is a vector of segments obtained by element-wise multiplication of the vector S with the Hanning window as W. The definition of each segment is expressed by Equation 5.6.

$$E_{ij} = W_{ij} * S_{ij} \qquad \begin{matrix} i = 0, 1, 2, ..., L-1 \\ j = 0, 1, 2, ..., M-1 \end{matrix} \tag{5.6}$$

where i represents the segment index, and j is the window index.

Compute the PSD Estimated

The Fast Fourier Transform (FFT) algorithm is applied to each signal segment to compute the PSD estimate. The result of the FFT algorithm is a complex-valued spectrum that includes both positive and negative frequencies.

In this way, only the positive frequencies are considered in the subsequent analysis to extract meaningful information and avoid redundancy. Thus, the frequency vector is constructed by taking the positive frequencies from the FFT result.

The frequency vector consists of evenly spaced frequency values ranging from 0 Hz to the Nyquist frequency, which is half the sampling frequency. Thus, to match the response of the FFT algorithm applied to E, the length of the frequency vector is equal to half the window size, defined as V.

Each point in the frequency vector represents a specific frequency component of the signal. The frequency values in the vector can be computed using Equation 5.7:

$$F_k = \frac{k}{M} * f_s \qquad k = 0, 1, 2, ..., V-1 \tag{5.7}$$

where k represents index of the frequency vector F, and f_s represents the sampling frequency.

The periodogram of the segments is computed using the FFT algorithm according to Equation 5.8.

$$\begin{aligned} X_i &= FFT(E_i) \qquad i = 0, 1, 2, ..., L-1 \\ P_{ik} &= \frac{|X_{ik}|^2}{M} \qquad k = 0, 1, 2, ..., V-1 \end{aligned} \tag{5.8}$$

where X_i represents the result obtained from each segment E_i using the FFT algorithm, and k denotes the index of corresponding frequency. Thus, the averaged PSD estimate of the entire $signalEMG$ defined as T, is then computed using Equation 5.9:

$$T_k = \frac{1}{L} * \sum_{i=0}^{L-1} P_{ik} \tag{5.9}$$

Average Frequency Computation

The average frequency $AvgFreq$ is computed by weighting the frequency values by their corresponding PSD values and calculating their average. Thus, Equation 5.10 is the one required to obtain this value:

$$\text{AvgFreq} = \frac{\sum_{k=0}^{V-1} F_k * T_k}{\sum_{k=0}^{V-1} T_k} \tag{5.10}$$

Median Frequency Computation

In order to calculate $MedFreq$, it is necessary to create the cumulative power vector of the estimated PSD. These values are obtained by summing the values of T cumulatively. The cumulative potency C_k and the total potency CT are obtained from Equation 5.11 and 5.12.

$$C_k = \sum_{i=0}^{K-1} T_i \qquad k = 0, 1, 2, ..., V-1 \tag{5.11}$$

$$CT = \sum_{k=0}^{V-1} C_k \tag{5.12}$$

The $MedFreq$ is the frequency value at which the cumulative power equals half of CT. It is determined by finding the frequency bin F_k that satisfies the conditions in Equation 5.13:

$$C_k \geq \frac{CT}{2} \quad \text{and} \quad C_{k+1} < \frac{CT}{2} \tag{5.13}$$

where C_k represents the cumulative power at frequency bin F_k.

Root Mean Square Computation

The RMS value is calculated by taking the square root of the mean of the squared values of the signal samples. Let $signalEMG$ represent the signal obtained in step 1. The RMS value is calculated according to Equation 5.14.

$$RMS = \sqrt{\frac{1}{N} \sum_{n=1}^{N} signalEMG(n)^2} \tag{5.14}$$

where N represents the length of the $signalEMG$.

By following these steps, it becomes feasible to calculate the three metrics ($AvgFreq$, $MedFreq$, RMS) employed in this system to evaluate muscle fatigue. All steps were developed from scratch within the mobile app except for the FFT algorithm. The FFT algorithm utilized in the app was imported from the

Apache Math3 library in the Kotlin language. The library Scipy Signal of Python language was used for the data processed in the cloud.

5.2.2 Normalization and Calibration

This section emphasizes the importance of normalizing the EMG data within the context of fatigue monitoring. Ensuring reliable and consistent measurements is crucial for accurately assessing muscle fatigue levels. The EMG signal exhibits inherent variability in signal amplitude due to factors like electrode positioning and individual physiological characteristics. Consequently, comparing EMG data between sessions and subjects becomes challenging without appropriate normalization (Halaki and Ginn, 2012).

In order to address this challenge, a calibration method composed of a sequence of steps has been developed to establish a baseline reference for subsequent measurements. The reference values obtained in calibration will be used to transform the fatigue metrics into a percentage scale relative to each individual's initial state. This normalization approach establishes a standardized metric for evaluating muscle fatigue, enabling meaningful comparisons and accurate monitoring of fatigue.

The most usual method in comparative EMG signal studies is to apply normalization based on the maximum contraction volume. This method involves determining the greatest amplitude of the EMG signal generated during the performance of contractions by applying all possible forces (Sousa and Tavares, 2012). However, this approach often requires assistance from a physician or specialized equipment, making it impractical for implementation in home settings, which is one of our goals.

Instead, an alternative method will be utilized, involving the average of three contractions performed without any associated weight. These contractions represent the baseline level of electrical muscle activity considered natural or normal during the knee extension movement. The sequence of steps for calibration comprises six intuitive screens within the mobile app, divided into three main processing steps. The terminology "Initial Evaluation" is used instead of "Calibration" to improve the user experience, as illustrated in Figure 32.

This process was designed for use in a clinical setting, where the physician can correctly position the EMG sensors on the patient's muscle. However, for sessions conducted at home, there is a challenge in ensuring that the patient can correctly place the sensors without professional assistance. In such cases, a wearable or method that adapts to the patient's anatomy and is easy to handle would be necessary. The first and third steps would remain unchanged for home use, but the second step, which involves the precise placement of the sensors, would need to be adapted to address the challenge of ensuring accurate sensor placement.

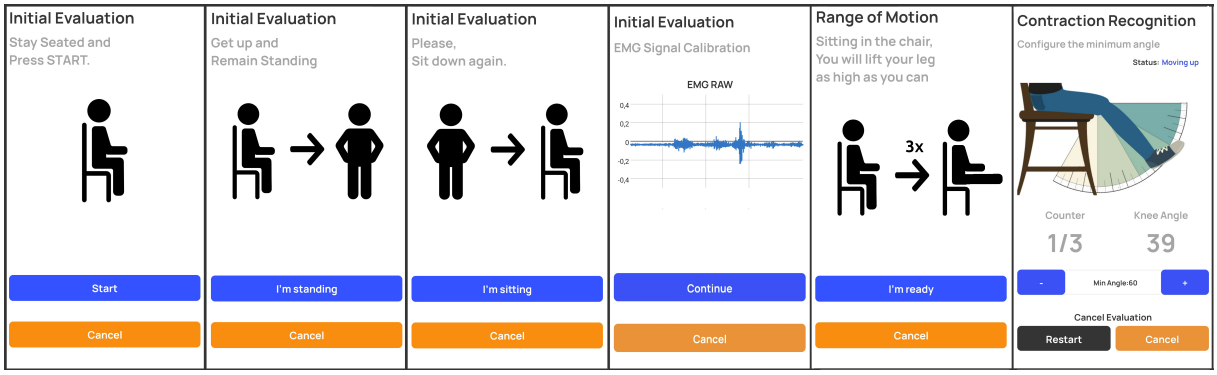


Figure 32: Screens of the calibration process.

IMU sensors position evaluation: The first screen of instructions directs the patient to sit comfortably in a chair, establishing the starting point for the calibration process. The second instruction screen guides the patient to stand up and remain standing. The third screen of instructions asks the patient to sit down again. During these steps, the mobile app saves the thigh and shin angle from the IMU sensors and records one second of raw EMG data again. With this, it is possible to understand the knee angle's initial position, which is not usually perpendicular and minimize the positioning error of the IMU sensors.

EMG sensor position evaluation: The fourth calibration screen is designed to assess whether the EMG signal is being correctly acquired. In this step, the physician will ask the patient to move their leg and will analyze the graph to check for muscle activity. The purpose of this screen is not to analyze the signal in detail, but rather to verify sensor positioning and detect any noise. If the displayed signal does not clearly show muscle activity during the patient's movement, the physician must reposition the EMG sensors and restart the calibration process.

Contractions: The fifth instruction screen provides information on how to perform a knee contraction and extension movement. The sixth screen aims to test the automatic recognition of the knee extension movement and capture the average signal from the EMG sensor. In this interface, the physician can define the minimum angle to recognize a contraction, a functionality shown in the previous section.

With each contraction, the mobile app calculates the metrics related to fatigue and at the end the average between the three contractions is saved to serve as a basis for normalization. Furthermore, the app also saves all the raw data from this calibration process to enable fine analysis later.

5.3 Stimulation Modes

One of the intelligent features of the CDSS for electrostimulation treatments is the ability to utilize diverse stimulation modes. These modes are essential for adapting the treatment to the specific needs

of patients, providing greater management capabilities and responsiveness to real-time movement. This section describes three distinct stimulation modes, detailing their general and specific parameters, as well as practical implementation via the wearable system and mobile application.

All stimulation modes share three main parameters common to muscle stimulators: intensity, pulse width, and frequency, as detailed in Section 2.2. In addition to these, each mode has specific parameters to manage its unique characteristics.

5.3.1 Commercial Stimulator

The first mode replicates the functionality of the traditional commercial stimulator. In this mode, the stimulator operates in a cyclical pattern, where it is activated for a predetermined period and then deactivated for another period. This cyclical pattern is usually described as a duty cycle ratio, such as 1:2, meaning one second with the stimulator active and two seconds inactive.

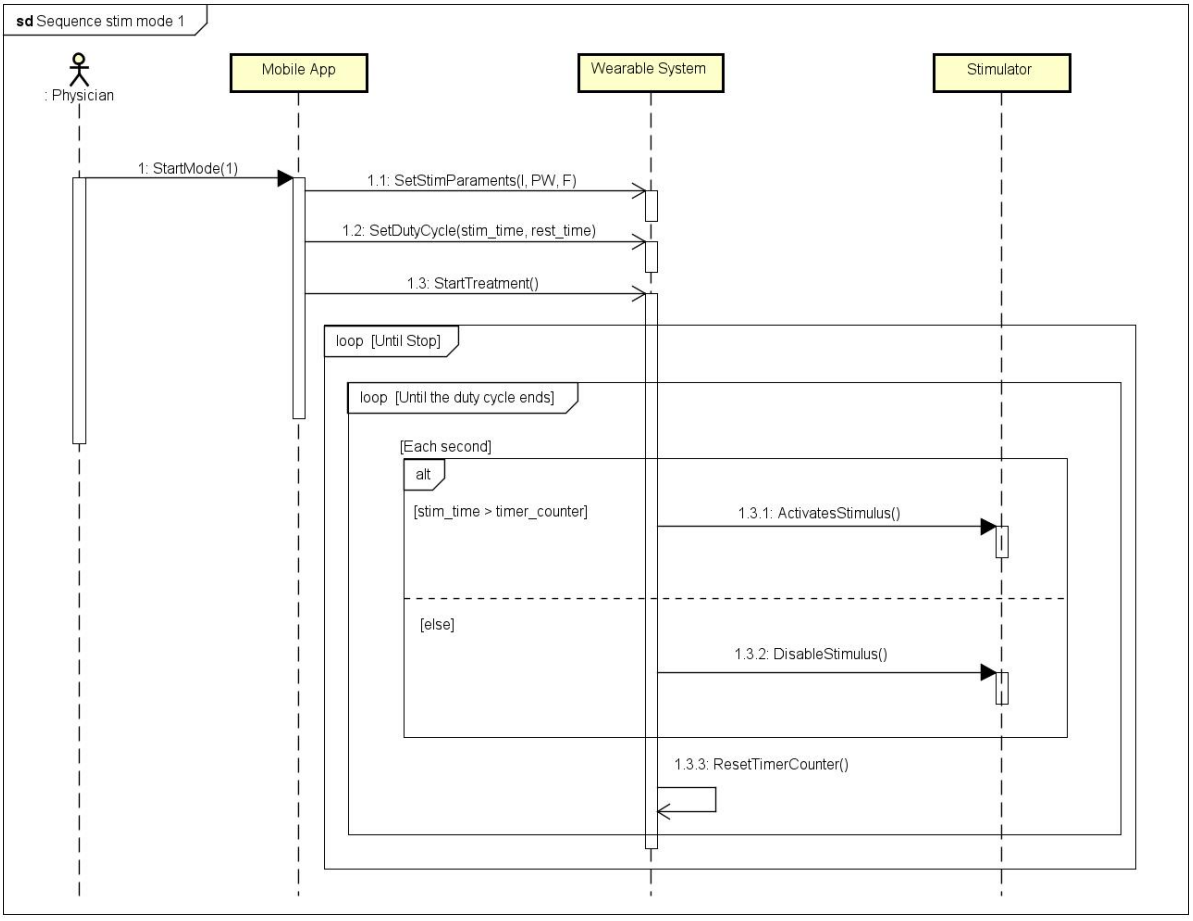


Figure 33: Sequence Diagram of the Commercial Stimulator.

Figure 33 shows the sequence diagram of the integration of the mode 1 in CDSS. The physician

initiates mode 1 on the mobile application, configures the stimulation default parameters, defines the duty cycle parameters, and starts the treatment. At this stage, the wearable system starts two loops: the first manages the overall treatment time, while the second controls the duty cycle. The second loop runs with a period equal to the total duration of the stimulation and rest phases combined. During each iteration of this loop, the system checks the current time within the cycle and adjusts the stimulation accordingly, ensuring that the activation and rest intervals follow the predefined parameters.

5.3.2 Raising the Leg Stimulator

The second mode introduces a more dynamic approach to muscle stimulation. In this mode, the stimulator is activated only when the leg is in phase one (moving upward) of the knee extension movement. This ensures that the electrical stimulation is synchronized with the active muscle contraction phase, providing support precisely when the muscle is working most intensively. This method can help improve muscle coordination and reduce the risk of fatigue by optimizing the timing of stimulation.

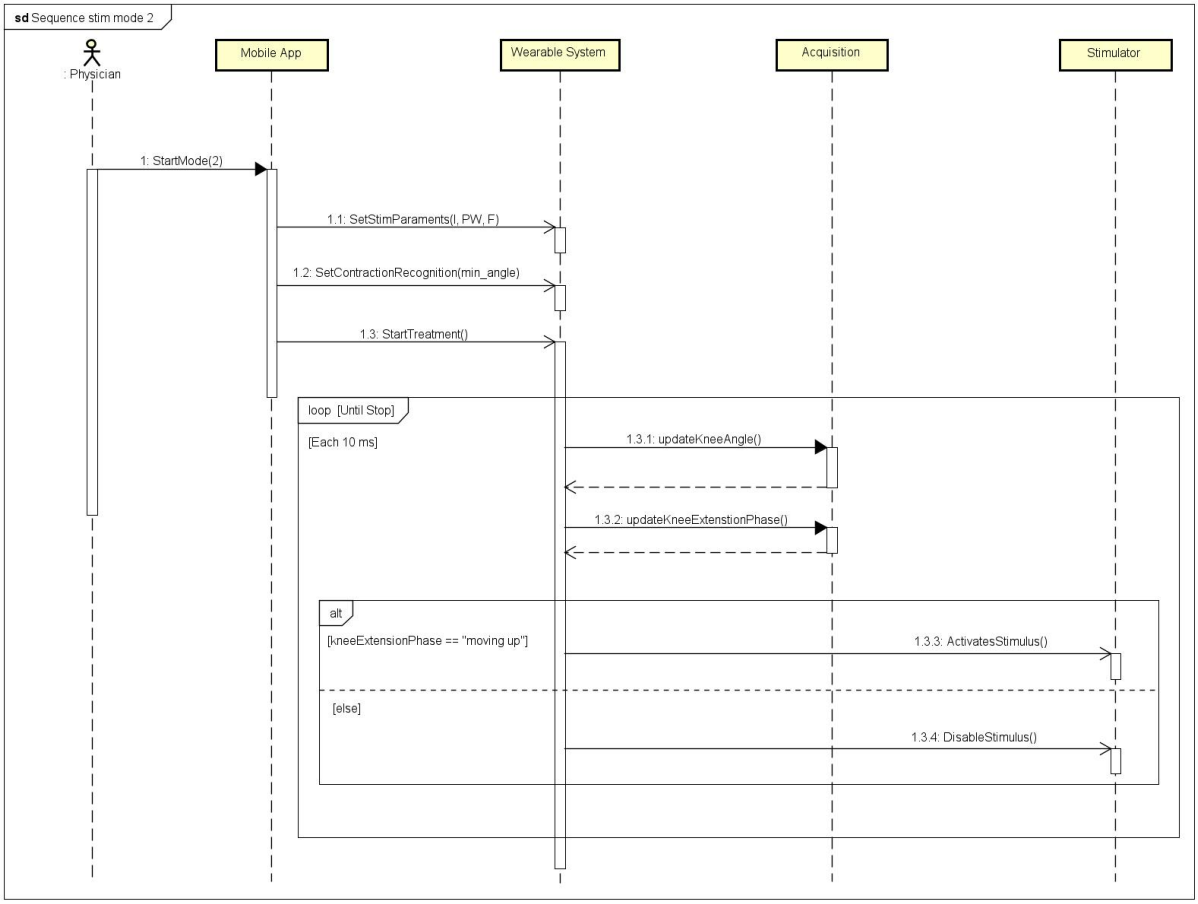


Figure 34: Sequence Diagram of the Raising the Leg Stimulator.

Figure 34 presents the sequence diagram for the second mode. The physician initiates mode 2 on the

mobile application, configures the standard stimulation parameters, sets the limit angle to recognize the knee extension movement, and starts the treatment. In this mode, during each iteration of the treatment cycle, the contraction phase is updated according to Algorithm 1. Next, it is checked whether the movement phase corresponds to the active phase of stimulation.

5.3.3 Range of Angle Stimulator

The third mode aims at a more specific customization, allowing the physician to select a specific range of knee angles during which the stimulator should be activated. This targeted approach ensures that the muscle receives stimulation during the moment of greatest activation, providing assistance in sustaining the movement. Furthermore, this stimulation mode is more adaptable to patients' muscle activations, which may differ from the expected pattern for knee extension movement.

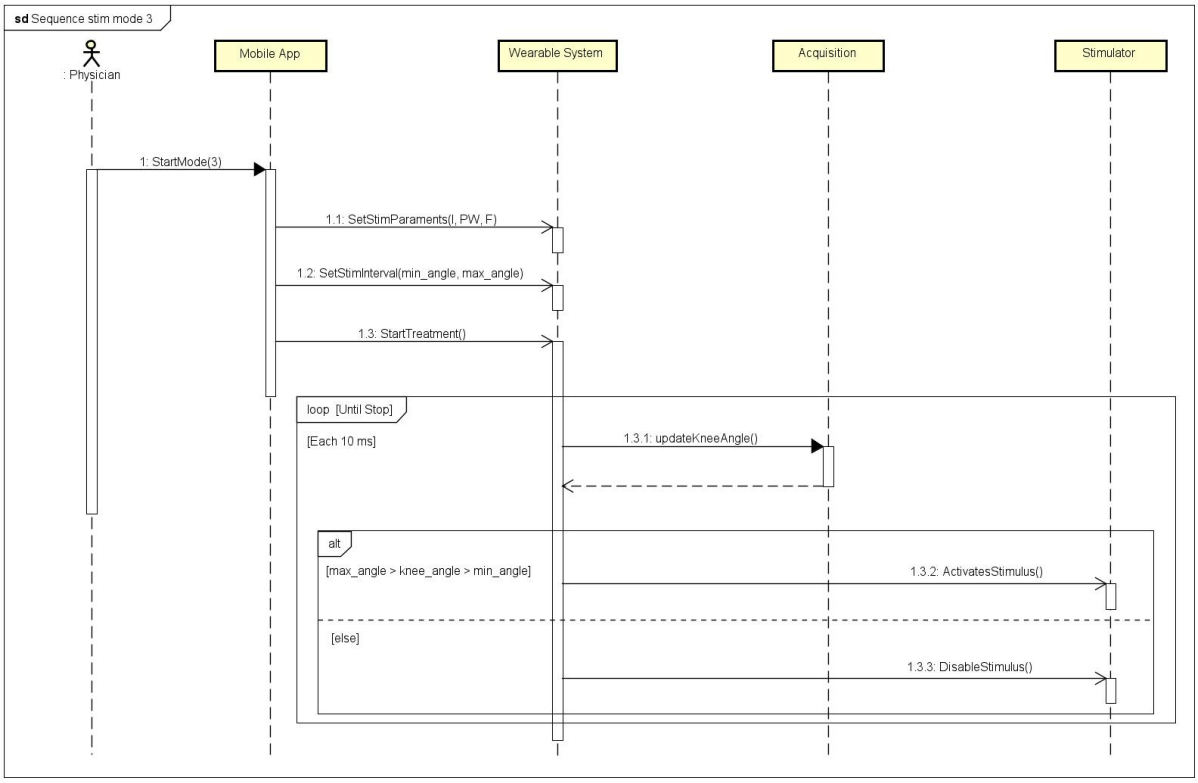


Figure 35: Sequence Diagram of the Range of Angle Stimulator.

Figure 35 illustrates the sequence diagram for the range of angle stimulation mode. The physician starts mode 3 in the mobile application, configures the standard stimulation parameters, defines the range of angles, that is, the minimum angle to start stimulation and the maximum to stop stimulation, and starts the treatment. Every 10 ms, the wearable system updates the knee angle and checks whether it is within the defined range. If the knee angle is within the range, the stimulus is activated; otherwise, it is disabled.

5.4 Rule-based Stimulation

One of the key intelligent features investigated in this thesis for treatment customization is rule-based stimulation. This approach enables the adjustment of electrostimulation parameters in response to muscle fatigue by utilizing real-time biofeedback. It also allows physicians to interpret the patient's muscle response during the session, which is not commonly possible in traditional clinical physiotherapy settings. This interaction allows for the parametrization and customization of treatment according to the individual characteristics of each patient.

Rule-Based Reasoning (RBR) systems are a well-established approach in CDSS, as discussed in the background section. The implementation of this system was motivated by two main factors. First, the ease of interpretation of rule-based methods by physicians results in a shorter learning curve compared to more complex methods. Advanced techniques can cause problems or lead to inadequate treatments if physician are not fully familiar with them. Therefore, the simplicity of RBR ensures that physicians can adopt and use the system with confidence.

Second, creating consistent datasets for applying more complex methods is a significant challenge. Obtaining large volumes of consistent, high-quality data is especially difficult in projects that started from scratch, as it requires multiple initial validations and ethics committee approvals. The need for robust data limits the effectiveness of artificial intelligence-based approaches, making RBR a practical and efficient alternative.

5.4.1 Fatigue Stages

The rule-based system developed for the CDSS relies on the definition of fatigue stages as one of its key operational mechanisms. These fatigue stages are determined using metrics related to muscular fatigue, being Root Mean Square and Median Frequency, calculated for each contraction performed by the patient. To interpret these metrics and identify fatigue occurrences, the CDSS uses the Joint Analysis of Spectrum and Amplitude (JASA) method, widely used in the literature to differentiate between normal and fatigued muscle responses during exercise.

The JASA method was originally proposed to distinguish the effects of muscle fatigue from variations in muscle strength through the simultaneous analysis of changes in the frequency spectrum and the amplitude of the EMG signal. Studies like Luttmann et al. (2000), Conforto et al. (2014) and Dufaug et al. (2020) help to validated the effectiveness of JASA in assessing changes in muscle behavior, especially in activities involving repetitive or prolonged efforts.

JASA is effective in graphically representing the relationship between Median Frequency, which reflects the conduction velocity of muscle fibers, and RMS, which indicates signal amplitude and is associated with muscle strength. When observed on a Cartesian plane, these two metrics allow the categorization of muscle state into four main physiological scenarios:

Q1: An increase in RMS and a shift in MDF to the right, suggesting an increase in muscle strength.

Q2: A decrease in RMS and a shift in MDF to the right, indicating fatigue recovery.

Q3: A decrease in RMS and a shift in MDF to the left, indicating a reduction in muscle strength.

Q4: An increase in RMS and a shift in MDF to the left, characterizing muscle fatigue.

This approach has been widely validated, and studies have shown a strong correlation between the drop in frequency of the EMG signal and the increase in amplitude as markers of fatigue. The JASA method effectively identifies the point at which the muscle begins to show signs of fatigue, allowing treatments, such as electrostimulation, to be adjusted based on the patient's muscle condition.

In simple terms, a fatigue occurrence is interpreted when the muscle needs to generate more force to perform a task but does so less efficiently by using slower fibers. This pattern is identified when there is a simultaneous increase in RMS (indicating greater muscle effort) and a drop in MDF (indicating the use of slower fibers). The CDSS calculates these metrics for each contraction, and when both conditions are met, the system identifies a fatigue occurrence.

In addition to detecting these occurrences, the CDSS evaluates the intensity of each fatigue event. This intensity is calculated using the Euclidean norm equation $\sqrt{x^2 + y^2}$, where x is the percentage increase in RMS and y is the percentage decrease in MDF. This allows the system not only to detect fatigue but also to quantify its severity, distinguishing between mild and intense episodes.

Control Parameters

The rule-based system of the CDSS uses three main parameters to define the progression of fatigue stages:

Late Start (S): Defines the number of initial contractions that are ignored when monitoring fatigue occurrences, eliminating events related to the muscle's initial adaptation to the exercise.

Fatigue Occurrences (F): Specifies the number of fatigue occurrences required for the system to register a change in stage, adjusting the treatment sensitivity according to fatigue progression.

Minimum Intensity (M): Determines the minimum intensity a fatigue occurrence must reach to be considered valid, ensuring that only significant events are accounted for.

These parameters allow the physician to customize the treatment according to the patient's muscle response. When a fatigue stage is reached, the system can trigger specific rules that adjust electrostimu-

lation parameters as needed.

To facilitate the adjustment of these parameters and provide a clinical validation tool, a fatigue stage simulator was developed and integrated into the CDSS administrative panel. This simulator allows physician to test different combinations of S, F, and M and visualize how the system responds to the patient's muscular fatigue progression. This feature is particularly useful for optimizing treatment and ensuring the system appropriately responds to the needs of each patient.

Figure 36 demonstrates the simulator in a test session with 100 contractions. This tool provides a clear visualization of fatigue stage progression, helping physicians precisely and optimally adjust the parameters to increase treatment effectiveness.

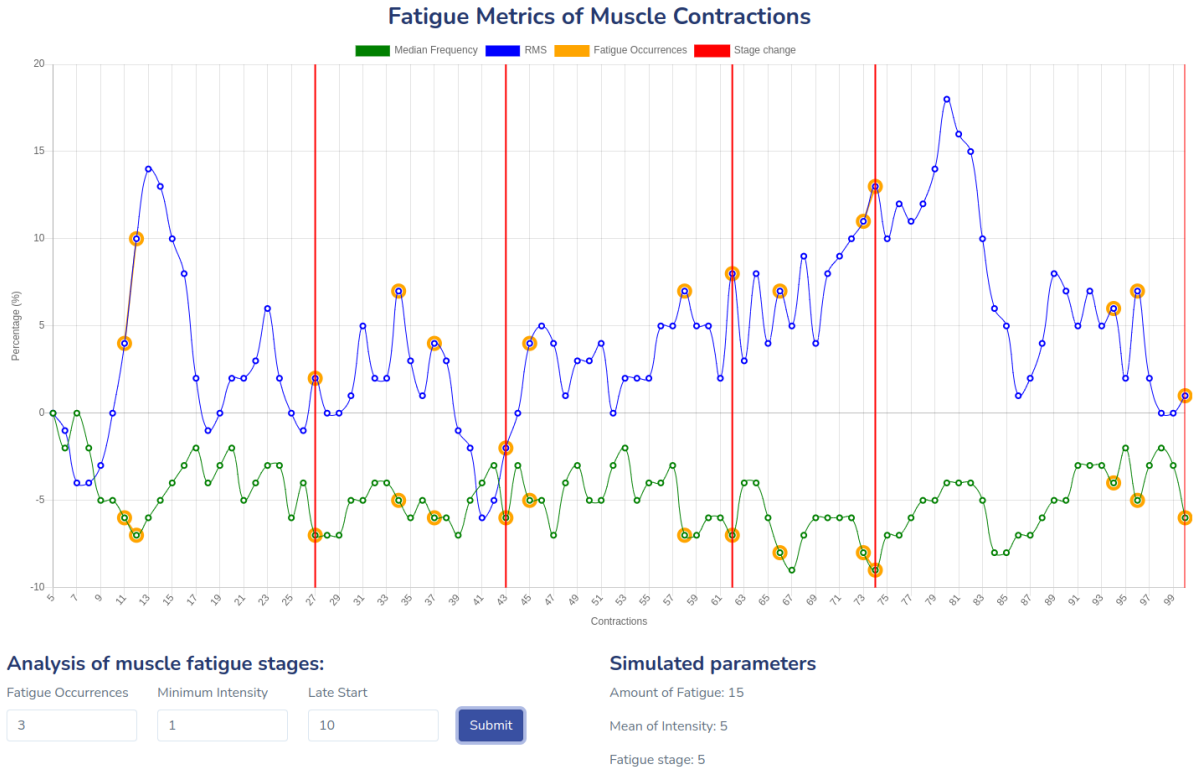


Figure 36: Muscle Fatigue Stages Simulator.

As shown in Figure 36, the trajectory of the fatigue metrics does not follow a linear pattern, presenting oscillations throughout the test session. These variations reflect the dynamic nature of muscle activity and fluctuations in the effort required to perform the movement. In this example, the fatigue occurrence parameter was configured to detect three occurrences to trigger a stage change, with a minimum intensity of 1 and the late start set to 10, ensuring that the count of occurrences only begins after the tenth contraction, avoiding influences from the initial phase of muscle adaptation.

The orange points in Figure 36 represent contractions identified by the CDSS as fatigue occurrences,

signaling moments when there was an increase in RMS and a decrease in MDF, both with intensities above 1, according to the defined parameters. In this example, the participant experienced 15 fatigue occurrences throughout the session, and since the occurrence parameter was set to 3, the system recognized 5 fatigue stages. This indicates that the clinician would have five opportunities to adjust the stimulation parameters, such as pulse width and stimulation intensity, as muscle fatigue progresses.

5.4.2 Automatic Session

To differentiate sessions conducted in the clinic and manually adjusted by the physician from pre-programmed sessions using the rule-based system, the terminology of assisted sessions and automatic sessions was established. As described in the proposed treatment scenario, initial treatment sessions are conducted in the clinic to familiarize both the physician and the patient with the new treatment and devices. Additionally, these sessions aim to create an initial baseline of the patient's muscle response.

With the initial data collected, the fatigue stage simulator is used to analyze muscle responses and determine the optimal values that allow for coherent stage transitions as personally assessed by the physician. Once the fatigue parameters are adjusted, the physician can register an automatic session. In these sessions, the stimulation parameters are automatically adjusted by the system when a fatigue stage change occurs, as defined by the rules.

Figure 37 shows the form that needs to be filled out to create an automatic session. Initially, the form requests the treatment plan, the recommended date, and a session description. Next, the physician can adjust the initial stimulation parameters, including standard parameters and those specific to the stimulation mode. After that, it is possible to adjust the adaptive parameters of the patient's fatigue stage, such as the number of fatigue occurrences, minimum intensity, late start, and the minimum angle for contraction recognition. Subsequently, the physician must define how much to increase the intensity and pulse width at each fatigue stage change.

Finally, the stop session parameters are defined, which include the maximum stage archived, the total duration of the session, and the maximum number of contractions. The primary objective is to complete all the contractions planned by the physician before one of the other two stop conditions is reached. However, if there is an indication of excessive fatigue, it is expected that one of the other two conditions will be activated.

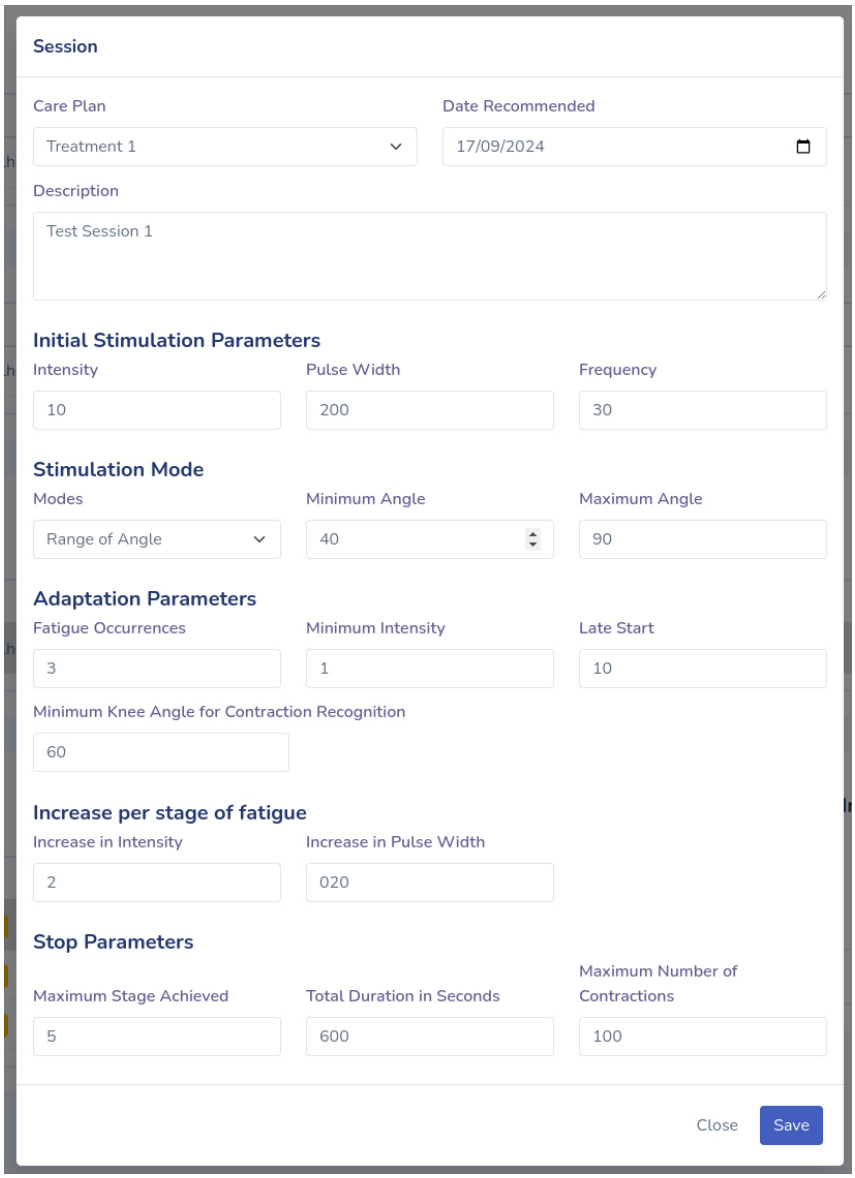


Figure 37: Automatic Session Form.

Figure 38 displays the main interfaces of the treatment session with the rule-based system activated. As shown in the first screen, there is an indication of the fatigue stage as 0, representing the initial state of the session. When the subject reaches the first fatigue stage, the second screen appears, requesting the patient's permission to increase the stimulation intensity as previously set by the physician. Following this, the treatment interface is updated with the new fatigue stage, and the session continues.

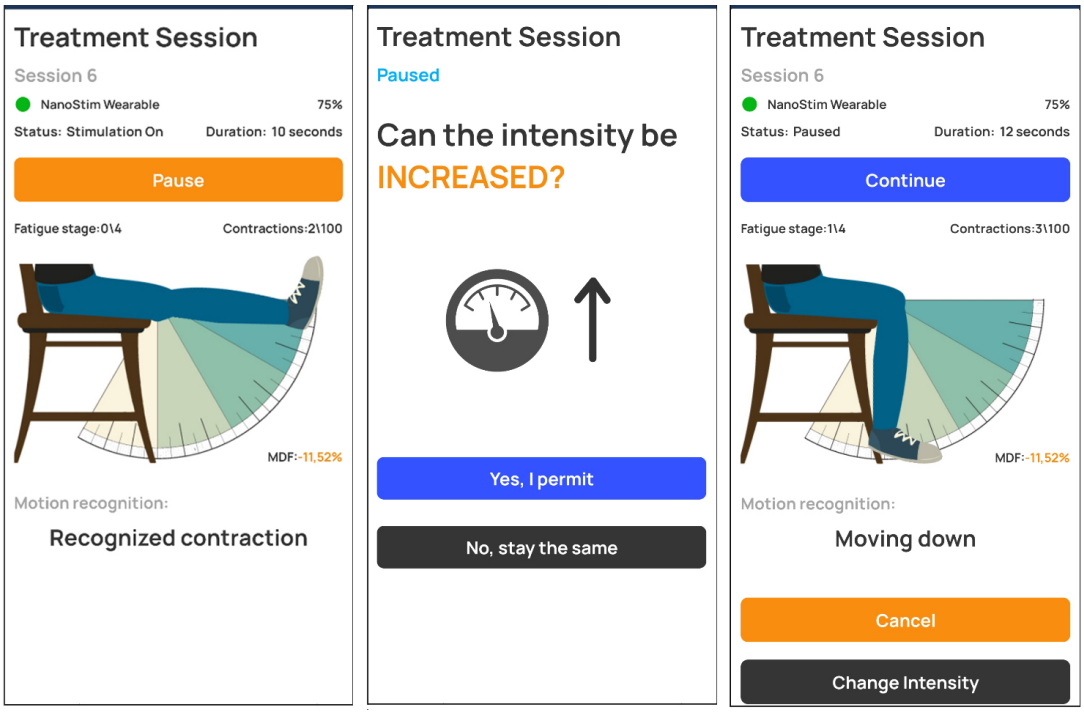


Figure 38: Automatic Session Adaptation Screens.

5.5 Data visualization

Data visualization plays a fundamental role in the CDSS, converting complex data sets into comprehensible and actionable information. In muscle rehabilitation, real-time visualization helps physicians monitor progress, adjust parameters, and ensure the accuracy of the administered treatment. In addition to providing specialized analysis, these visual tools are designed to enhance the interaction between the system and its users, making the rehabilitation process more transparent and manageable.

The final section of this chapter explores the data visualization components implemented in the CDSS. In addition to the interfaces already described in previous sections, four more interfaces have been implemented, two in the mobile application and two in the administrative panel. These interfaces aim to facilitate physician' decision-making by transforming captured biofeedback into interpretative and intuitive visual components.

5.5.1 Mobile App

Two main screens were developed in the mobile application that ensure accurate capture of biofeedback data and help the physician understand the muscle response in real time.

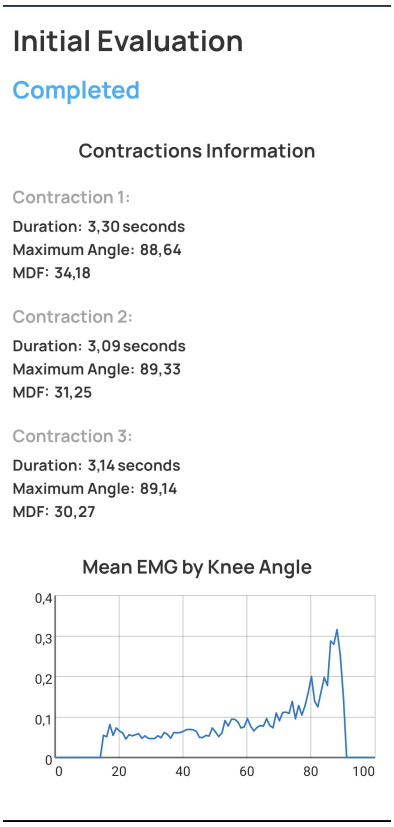


Figure 39: Calibration Overview Screen.

The calibration overview screen, as shown in Figure 39, displays the results of a successful calibration performed with the myHealth System. This screen presents processed data for the three contractions recognized during the calibration phase. The data, including the maximum angle reached, the median frequency value calculated in Hz, and the duration of each contraction, are not just numbers. They are practical tools that can be used to compare with previous treatment sessions and check for progress in the patient's range of motion.

A chart showing the average volume of the EMG signal captured during the three contractions is presented at the end of the interface. This chart allows for analyzing the knee angles at which the muscle shows greater activation during the knee extension movement. In this way, this chart is significant for two stimulation modes: the raising the leg stimulator and the range of angles stimulator, which rely on the angle to activate the stimulation. Thus, besides ensuring that the electrodes are well-positioned and capturing the correct muscle activity, it also enables a more precise adjustment of the stimulation, considering the patient's current response.

The second data visualization interface of the mobile app is illustrated in Figure 40. This interface provides a real-time analysis of the contractions recognized during the treatment session. Each time a contraction occurs, the mobile app calculates metrics related to muscle fatigue and updates the graphs.

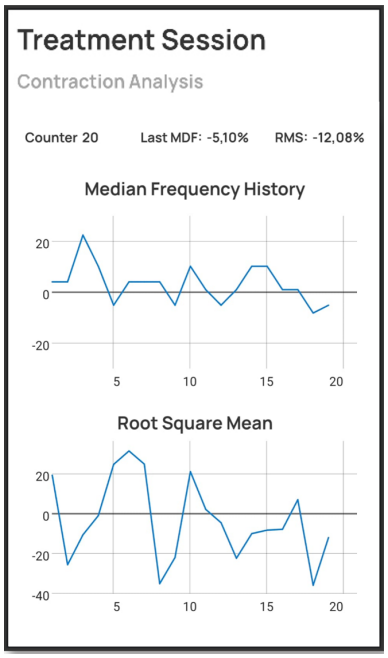


Figure 40: Real-time analysis screen.

The values presented in the graphs are normalized by the calibration and are the same values used by the rule-based system to adjust the stimulation.

The ability to track the trajectory of metrics related to muscle fatigue during the knee extension movement allows for rapid intervention by the physician if any irregularities are detected. When available in clinical environments, this type of information is typically processed after the session has ended. In addition to the information displayed in Figure 40, the raw EMG signal is also shown, enabling the healthcare professional to replace or reposition the electrodes if any displacement occurs during the session.

5.5.2 Administrative Panel

In the administrative panel, two primary interfaces were developed to support physicians' decision-making and facilitate the management of muscle rehabilitation treatments with electrostimulation.

Figure 41 shows the web page designed to provide a detailed report of the assisted session conducted with the wearable system. At the top of the page, the patient's personal information and the session's schedule are presented. Additionally, there is a button to download raw EMG sensor data in `.h5` format[1] for more in-depth analysis. The `.h5` format was chosen because it is compatible with other signal acquisition equipment, such as Bitalino[2]. Moreover, many signal processing software, like OpenSignals[3], accept the

1 https://docs.fileformat.com/misc/h5

2 https://www.pluxbiosignals.com/pages/bitalino

3 https://www.pluxbiosignals.com/pages/opensignals

`.h5` medical data format, facilitating interoperability and further analysis.

The first chart on this interface displays the trajectory of the patient's knee angle movement recognized by the system during the session. This chart indicates the moments when the stimulator was activated and deactivated, represented by green and red dots, respectively. For instance, in the example shown in Figure 41, the "raising the leg" stimulation mode was activated, with activations starting around a 15-degree angle and deactivations occurring around 60 degrees. The vertical orange line marks when the physician adjusted the stimulation parameters via the mobile application.

Below the chart, a table presents the values of the stimulation parameters that were adjusted during the session, providing a comprehensive history of the rehabilitation performed. The second visual component of this interface is the fatigue levels simulator, illustrated in Figure 36. This tool enables the simulation of different scenarios and displays the trajectory of the MDF metric throughout the session.

This detailed visualization allows the physician to better understand the patient's response to the treatment, facilitating more informed future adjustments. The ability to review and analyze these post-session data is essential for the continuous optimization of the treatment plan.

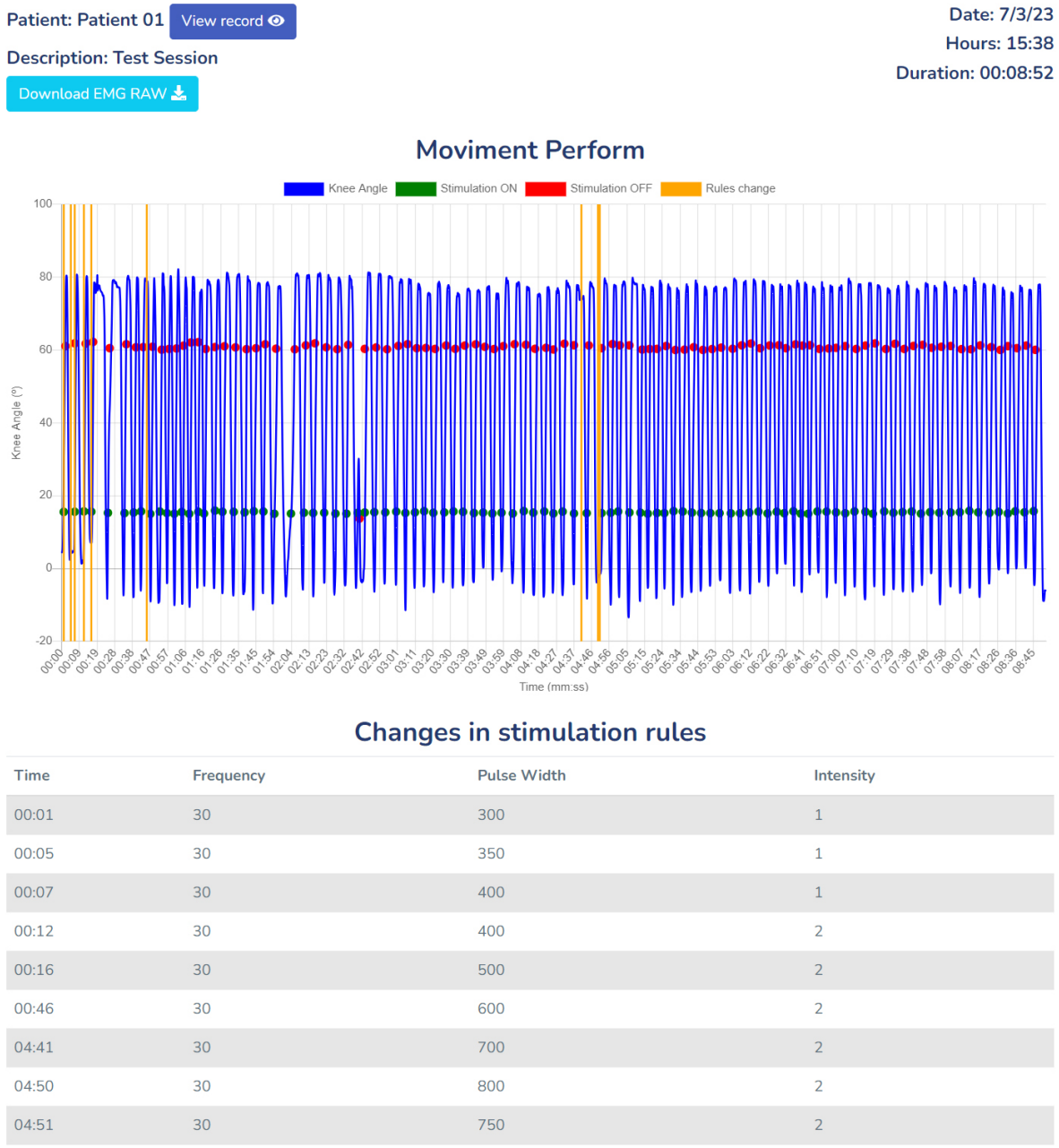


Figure 41: Session Information Screen.

The second web page developed for data visualization is the clinical history page, as shown in Figure 42. This interface provides a view of the patient's medical record and rehabilitation sessions.

Initially, personal information such as age, emergency contacts, and the patient's address are presented. The first section of the medical record offers a management system for appointments and their scheduling. It is possible to record observations for each appointment, including quantitative notes and free-text annotations. Additionally, an interactive chart allows the addition of markers on the body to indicate the position and type of injury.

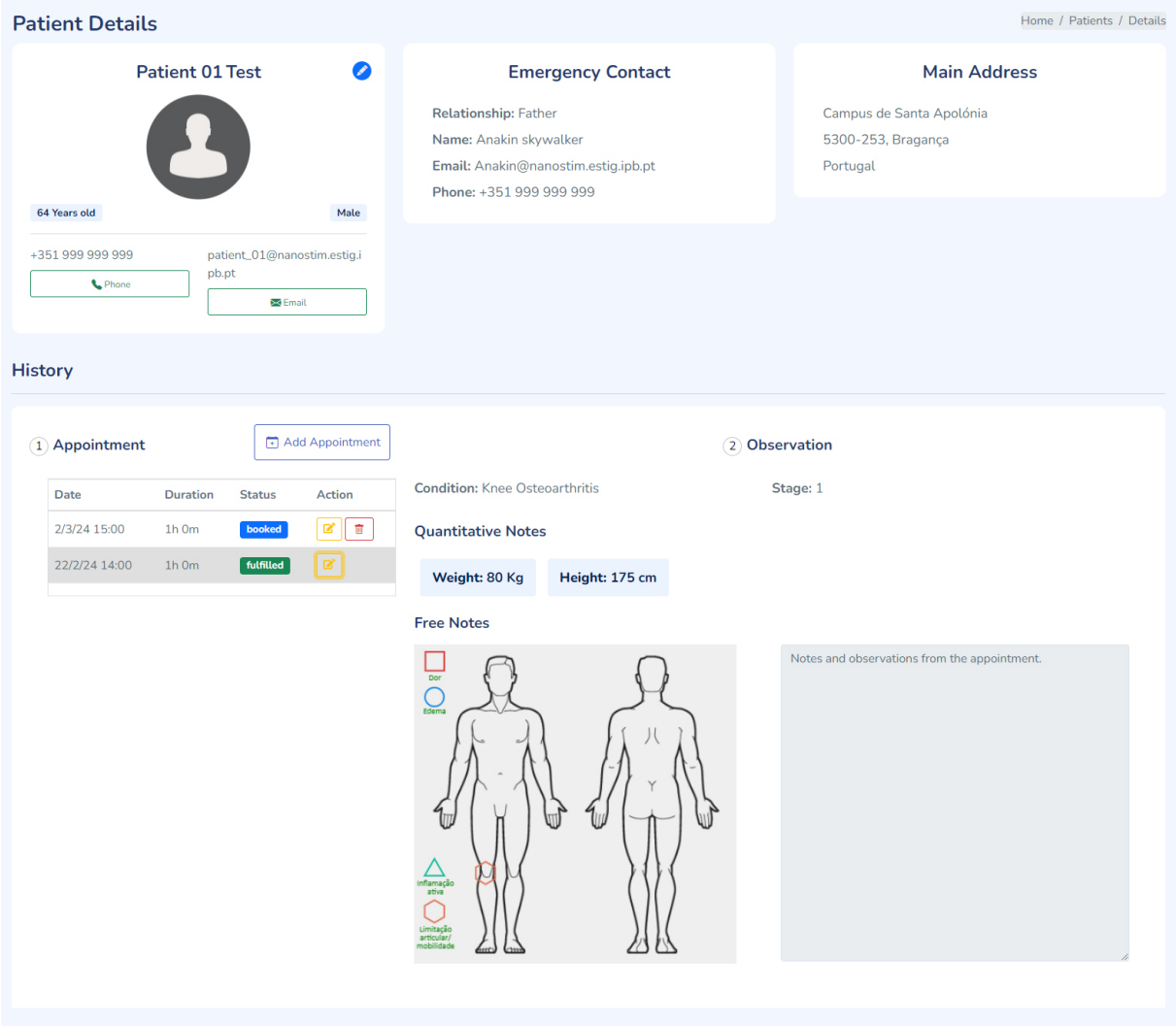


Figure 42: Clinical History Page - Part 1.

The continuation of the clinical history page, illustrated in Figure 43, enables detailed management of conditions and treatments. Automatic sessions can be added once an injury and treatment are registered, as described in the previous section. These automatic sessions can have three different states: "To Do," indicating that the session is available at the patient's home; "To Review," when biofeedback data is sent after the patient completes the session; and "Completed," when the physician evaluates the patient's performance and adds a final note, completing the cycle scenario described in section 4.1.1

This detailed record gives the physician comprehensive information on all stages of the muscle rehabilitation treatment, with a history of the patient's progress. Both the data visualization interfaces in the mobile application and the administrative panel play a crucial role in personalizing and enhancing muscle rehabilitation treatment with electrostimulation. These methods aim to improve the patient experience and increase physician' confidence in using advanced technologies.

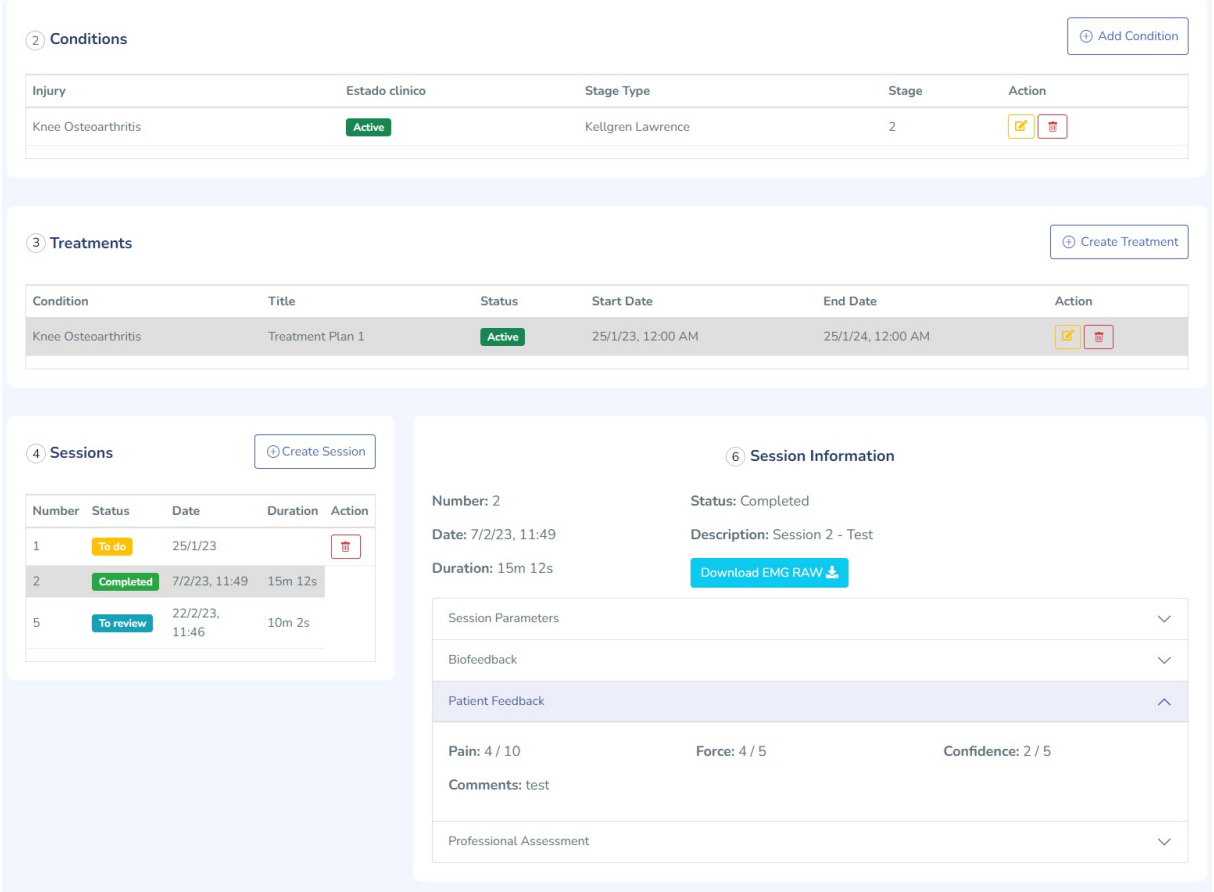


Figure 43: Clinical History Page - Part 2.

Chapter 6

Tests and Validations

The validation of a CDSS is an essential step to ensure the efficacy and safety of its application in healthcare environments. In the context of muscle rehabilitation with electrostimulation, the need for scientific precision and ethical compliance is even more pronounced, given the direct impact on the health and well-being of patients. This chapter describes the tests and validations conducted to evaluate the CDSS developed in this doctoral thesis, highlighting the system's evolution and the results obtained in experimental scenarios.

Implementing a CDSS that assists physicians in personalizing treatments with electrical stimulation requires a robust and systematic approach. The tests conducted aim to validate the intelligent features of the system and ensure that the CDSS can effectively manage a muscle rehabilitation treatment with continuous interaction between the healthcare professional and the patient.

During the development of the CDSS, three ethical approvals were submitted and granted: two by the ethics committee of the Instituto Politécnico de Bragança (Portugal) and one by the Universitat Politècnica de Catalunya (Spain). Each approval allowed the execution of specific tests that contributed to the incremental evolution of the system, ensuring compliance with rigorous ethical standards and the safety of participants. These approvals reflected a commitment to scientific integrity and ethical responsibility throughout all phases of the research.

The objectives of this chapter are multifaceted. Firstly, comparative studies will be presented that demonstrate the precision and reliability of the CDSS in relation to similar technologies. The primary focus is the description of three experimental tests with volunteers, which helped validate the system and provided results that contributed to the continuous implementation of the CDSS. Each set of results helped to refine and develop more robust test protocols for subsequent tests. Finally, a comprehensive discussion of the results will offer a detailed interpretation of the data, identifying trends and areas for future improvements.

This chapter not only aims to answer the research questions of this doctoral thesis but also highlights the potential of the CDSS to transform the practice of muscle rehabilitation with electrostimulation, aligning

with the objectives of promoting personalized treatments. Through a rigorous methodology and detailed empirical validations, it is intended to demonstrate that the developed CDSS is an innovative and valuable tool for physicians and patients, significantly contributing to the advancement of muscle rehabilitation with electrostimulation.

This chapter is divided into five main sections. The first section outlines the evaluation Metrics used during the development and testing phases. The second section describes the preliminary validation procedures, including hardware verification, security analysis and preliminary sessions. The subsequent sections present the experimental studies, each addressing a different validation of the system. The first experimental study examines the quality and synchronization of the data acquisition and process EMG signals with stimulation artifacts generated by commercial device. The second study focuses on real-time muscle fatigue monitoring and analyzes the system's ability to process data during treatment sessions. The final study provides an in-depth analysis of the CDSS's accuracy by utilizing a gold-standard motion capture system, comparing different stimulation modes, and examining the statistical correlation between the fatigue perceived by participants and the levels of fatigue predicted by the CDSS.

6.1 Evaluation Metrics

To evaluate the performance of the developed CDSS, three key metrics were employed: Mean Absolute Error (MAE), Mean Squared Error (MSE), and Root Mean Squared Error (RMSE). In our context, these metrics will be applied to comparative analysis between the CDSS with other systems and methodologies, such as comparing real-time processing done by the mobile app with processing done on a computer using raw data.

To elucidate these evaluation metrics, consider two data sets we aim to analyze for similarity: the data points vector from the CDSS (A) and the data points vector from a comparable technology (F). If all elements of vector A are subtracted from vector F, the resulting error vector E represents the discrepancies between the two data sets. An ideal system would yield an error vector with a sum of zero, indicating no error.

The MAE metric is calculated as the average of the absolute errors, disregarding the error signs. This means that errors above and below the actual value are treated equally. MAE provides a straightforward interpretation of the average magnitude of the errors, making it a useful metric for general error analysis. The equation for MAE is given by:

$$MAE = \frac{1}{n}\sum_{t=1}^{n}|A_t - F_t| \tag{6.1}$$

The MSE metric is the average of the squared differences between the actual and system output values. By squaring the errors, this metric places a larger penalty on larger errors, thus highlighting significant discrepancies more effectively than MAE. The MSE is calculated using the following equation:

$$MSE = \frac{1}{n}\sum_{t=1}^{n}(A_t - F_t)^2 \tag{6.2}$$

The RMSE metric is the square root of the MSE, providing an error metric in the same units as the original data, which makes it more interpretable. RMSE is particularly sensitive to large errors (outliers) and thus is a robust measure of the system's performance. The equation for RMSE is:

$$RMSE = \sqrt{\frac{1}{n}\sum_{t=1}^{n}(A_t - F_t)^2} = \sqrt{MSE} \tag{6.3}$$

6.2 Preliminary Validation

This section covers the initial experiments and fundamental validations conducted to ensure the functionality and robustness of the proposed system. These steps were essential early in the development process to ensure that the system operates as expected and meets the rigorous safety and efficiency standards required in clinical settings.

Preliminary testing includes a variety of analyses, such as data transmission tests, safety analysis, initial hardware and software tests, and validation of the IMU sensors. The primary goal was to establish a solid foundation for subsequent development. Each of these subsections provides a detailed overview of the methods and results obtained, demonstrating how each component of the system was tested.

6.2.1 Transmission Test

Initially, the first prototyping of the presented system included the implementation of all components described in the system architecture, albeit with basic functionalities such as user and session registration. Before hardware implementation, the capability of the ESP32 microcontroller was tested to handle EMG sensor acquisition, manage stimulation and parameter changes, and communicate via BLE with the mobile app simultaneously. Additionally, the system's ability to manage a treatment session, including starting, pausing, canceling, and saving data to the cloud, was verified.

The first test simulated a treatment lasting 1 minute, with stimulation parameter changes sent every 8 seconds. To verify the reception of EMG sensor data, a data packet was sent every 200 ms from the wearable system to the mobile app with simulated data. More details about this test and pertinent discussions at the beginning of the system's development were presented in the article (Franco et al., 2022b).

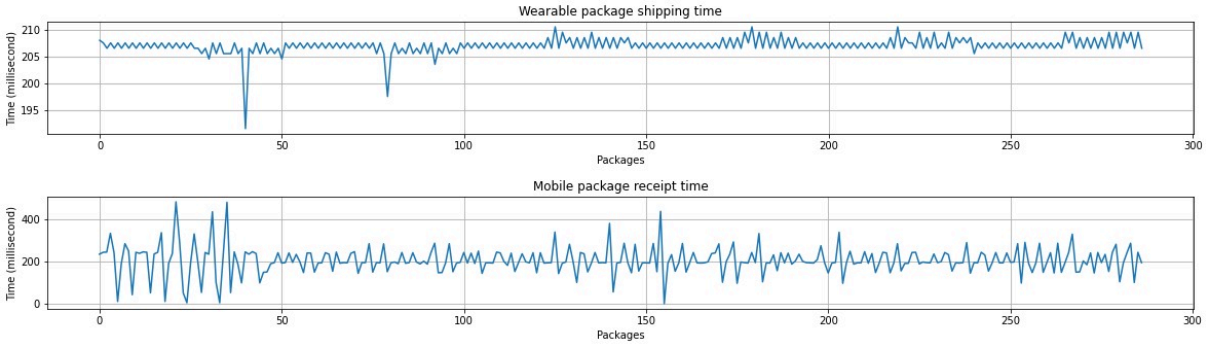


Figure 44: Packet exchange time between the wearable system and the mobile app.

As shown in Figure 44, the low-cost, low-power ESP32 microcontroller proved capable of efficiently maintaining both the processing of electrostimulation and data transmission. The analysis of packet exchange times showed that the average packet transmission time is 206 ms, indicating an average delay of only 6 ms to assemble each processed packet. This result suggests that the additional latency introduced by data transmission is minimal and does not significantly affect the system's operation. The ability to perform multiple functions simultaneously without noticeable performance degradation is a promising indicator of the proposed system and the chosen hardware.

6.2.2 Security Analysis

To ensure the integrity, privacy, and availability of clinical data managed by the CDSS, a master's thesis was developed in conjunction with this doctoral thesis within the NanoStim project (Silva, 2021). This thesis was motivated by the need for scientific rigor in validating the protection of sensitive data in clinical environments. The main strategies for protecting sensitive data implemented in the CDSS were covered in Section 4.1.3. This subsection describes the key tests conducted and their conclusions as detailed in Silva (2021)p, elucidating the robustness of the presented system architecture.

The security analysis comprised three main components: availability testing, functional testing, and threat modeling. To simulate a realistic scenario for the system's usage, the CDSS implementation used for security analysis included Kubernetes for container orchestration, ClusterControl for database man-

agement, and HAProxy as a load balancer. This setup aimed to ensure automated failover, ease of maintenance, scalability, and auditability of the architecture.

The first test, availability testing, aimed to evaluate the CDSS's behavior when one of its services fails and measure the response time until the system stabilizes again. The results showed that the Management API and Clinical Service took 2 to 4 seconds to become available again, while the SSO service with Keycloak took about 50 seconds to reestablish. Using Kubernetes, ClusterControl, and HAProxy minimizes availability issues, as redundancy ensures the system remains available even if a service or database is removed, with only a brief reduction in processing power.

The functional test aimed to validate the communication strategies between the system's components and the CDSS behavior under peak request loads on each of the APIs, preventing Distributed Denial of Service (DDoS) attacks. For this, endpoints from each service (Management API, Clinical Service, and SSO) were selected for testing. Each endpoint involved a specific routine to promote authentication and the exchange of pseudo-anonymized information. A Python script was used to simulate the information flow, repeatedly sending requests to identify if the server's resource usage increased. The number of requests incremented by 100, up to a maximum of 3500 simultaneous requests. The results showed no significant changes in the average response time, remaining consistent across all request levels.

Finally, STRIDE threat modeling was conducted. This analysis describes potential threats, understands their causes, and creates mitigation strategies. STRIDE modeling addresses aspects such as spoofing, tampering, repudiation, information disclosure, denial of service, and elevation of privileges. The analysis revealed that all system assets could be targeted, indicating a broad attack surface. The assets in insecure environments, such as the mobile app, web administrative panel, and wearable device, are potential entry points for attacks. Identifying and reducing the likelihood of these threats is essential for enhancing CDSS security. Establishing robust methods for recognizing services, devices, users, and information complicates the malicious exploitation of CDSS functionalities, positively impacting privacy.

The security analysis conducted supports the thesis that it is possible to create a CDSS that handles sensitive data. The described strategies, along with the test results, demonstrate the ability to ensure data protection in a CDSS that collects sensor data through a wearable system. Additionally, the implementation used in the tests with Kubernetes, ClusterControl, and HAProxy software demonstrates the CDSS's capability in a more realistic environment, with scalability and redundancy.

6.2.3 A First Experiment

The first prototype of the hardware for the wearable system developed in the NanoStim project was assembled on a breadboard, connecting the components of the ESP32 Dev Kit microcontroller, a commercial signal acquisition board (EBZ-AD8233), and a custom-made electrical stimulation circuit. This initial prototype was described in (Sestrem. et al., 2022), which explores in greater detail the electronic components included in the wearable system and the EMG signal acquisition test with wet and dry electrodes.

With this hardware, it was possible to implement a first version of the mobile application, described in (Franco et al., 2022a). This version of the application included all the activity flows described in the treatment scenarios, including receiving stimulation parameters registered in the cloud by the physician, a treatment screen that displayed the acquired EMG sensor signal in real-time, and a self-report feedback interface after the completion of the treatment session.

To validate this version of the application, a test treatment session was configured through the administrative panel, lasting 1 minute and varying the stimulation configurations. The test session was conducted with four healthy volunteers, with the EMG sensor positioned on the *vastus medialis muscle* with the help of a physician. When the test session began, the volunteer, seated on a bench, lifted their leg five times in one minute without being stimulated.

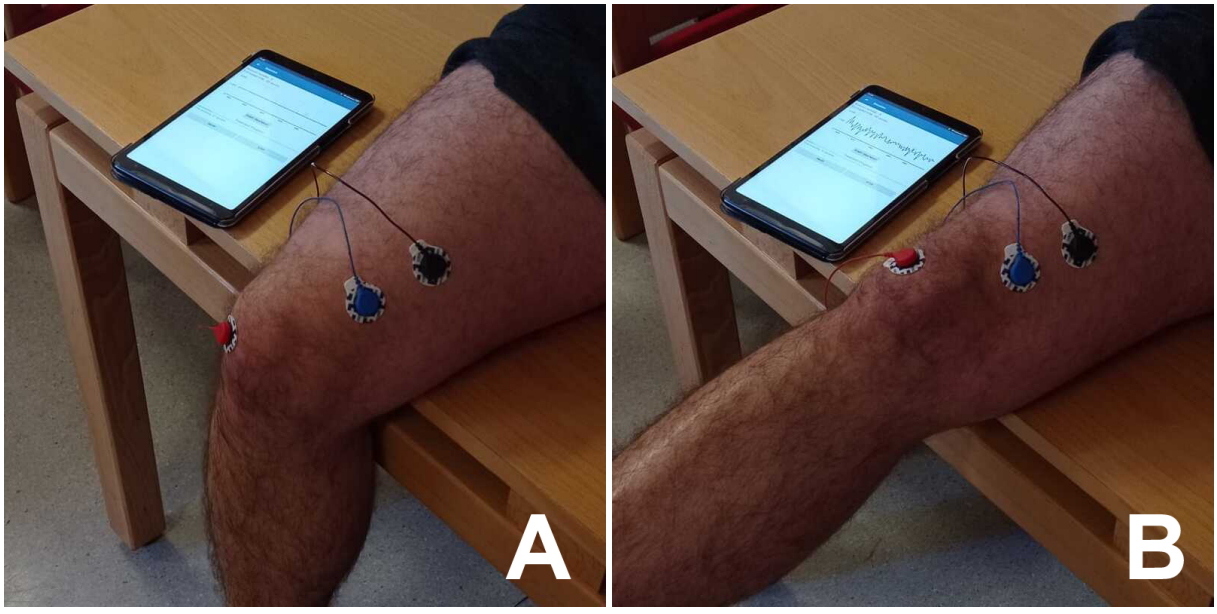


Figure 45: Test treatment session on a volunteer without electrostimulation. (A) Subject's leg relaxed. (B) Subject's knee is fully extended.

The test conducted to validate that the application can follow the necessary steps for NMES muscle rehabilitation treatment, as illustrated in Figure 45. In Figure 45A, the volunteer's leg is relaxed, repre-

senting the rest period. At this moment, muscle activity is low, resulting in a slight alteration in the EMG signal displayed by the application. When the volunteer lifts their leg, a voluntary muscle contraction is generated. Therefore, in Figure 45B, it is possible to see how the EMG signal displayed by the application significantly changed its wave amplitude.

To verify if the NMES configurations were being transmitted correctly, a resistor was placed at the NMES actuator output of the wearable system to simulate human skin. A multimeter was connected to this load to verify the current value as well as an oscilloscope to measure the frequency and waveform, as shown in Figure 46. The signal indicated by the devices followed the parameters provided by the mobile application, confirming the accuracy of the transmission of the stimulation configurations.

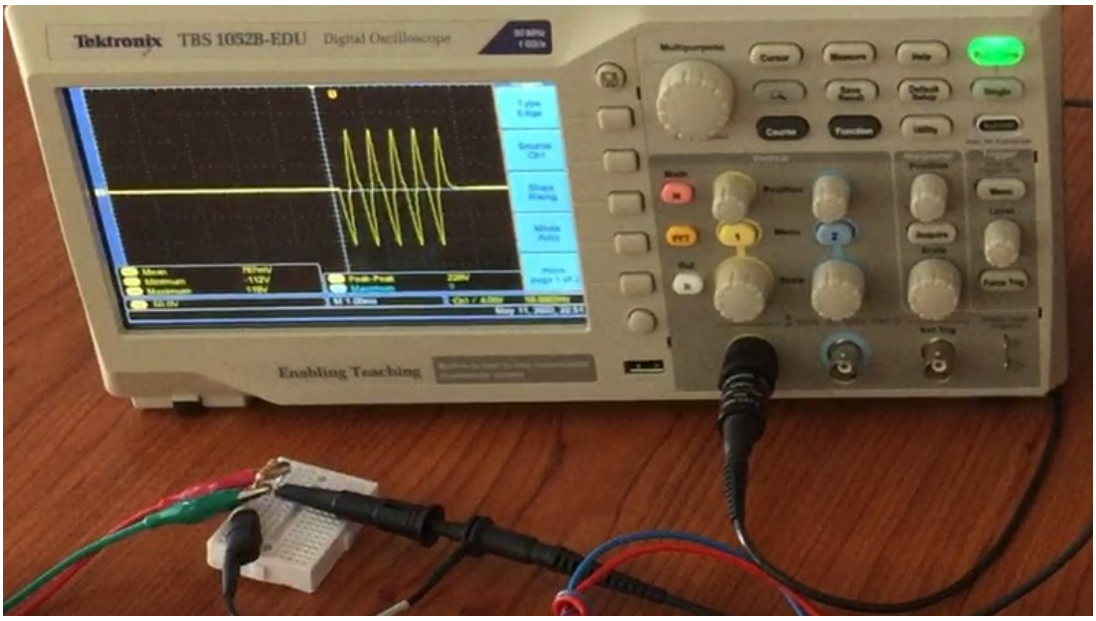


Figure 46: Oscilloscope with stimulation pulses applied to the resistor.

6.2.4 Validation of IMU Sensors

Following the implementations, the next step was to validate the IMU sensors. For this, the study described in (Franco et al., 2022c) was conducted. In this study, a new wearable system was created, composed of two identical modules. Each module included an ESP32, an MPU-6050 IMU sensor, and a battery, all soldered onto a perforated board and housed in a 3D-printed case. The case was designed to be placed on the thigh and shin, and hold by an elastic band. The purpose of this study was threefold.

The first purpose was to verify that the ESP32 could handle two additional tasks: reading from two IMU sensors using I2C communication and sending the data via BLE. The second purpose was to validate the mathematical model presented in Section 5.1.1 for knee angle recognition and the real-time update

of the mobile app interface. The third purpose was the characterization and comparison of low-cost computational filters to improve the accuracy of the IMU sensor to measure angles.

Computational Power Problem

The ESP32 is an MCU with sufficient computational power to acquire sensor data at high frequencies, as the clock of a standard model, such as the ESP32-WROOM-32D, exceeds 150 MHz. However, due to the number of simultaneous tasks, it was observed that the time between each sample from the IMU sensor varied. To address this, the IMU modules were programmed to execute a software replicating the treatment protocol, with the addition of a dedicated thread designed to collect a IMU sample every 8 ms. This setup ideally results in a sampling frequency of 125 Hz.

However, due to the shared processing power with other tasks, the collected data showed acquisition frequencies of 99–100 Hz. Additionally, the average time interval between each sample was 9.8 ms, with some peaks above 24 ms. The graph in Figure 47 shows the time difference between each sample collected by the wearable system in a sample acquisition.

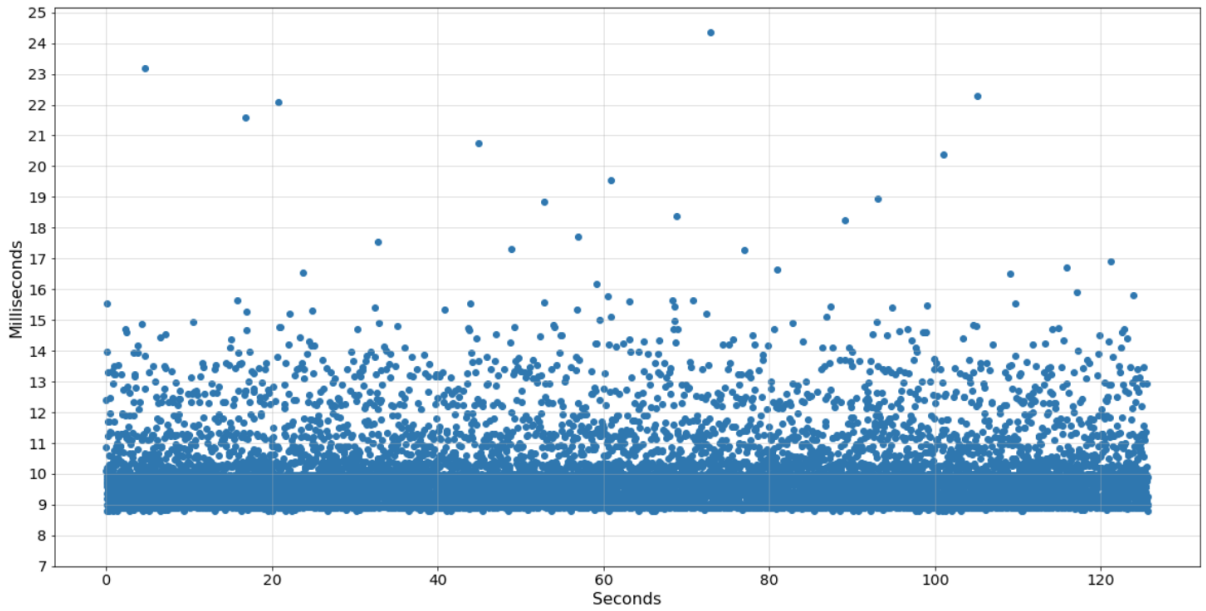


Figure 47: Δ Time of IMU samples collected by the wearable system.

In contrast, the reading of the EMG sensor does not experience these delays. This is because the EMG sensor reading is executed through an interrupt function, triggered precisely every 1 ms. This level of precision cannot be achieved with the IMU sensors because their communication occurs via I2C. On the ESP32 MPU, it is not possible to collect data from the I2C interface within an interrupt function. As a

result, the IMU reading thread competes with other threads, such as data transmission via BLE, leading to the delays observed in Figure 47.

IMUs Sensor Validation Scenario

To investigate the performance of IMU sensors for knee angle recognition, the UR3 robotic arm was used. The UR3 collaborative industrial robot from Universal Robotics[1] is suitable for assembly and screwdriver activities, usually positioned on the top of benches. This robotic arm was chosen for two main reasons: firstly, the availability of the robot in the laboratory where the research was carried out; secondly, due to the fact that the UR3 has a certificate validating the precision of the joint's movements. Thus, it is possible to configure the UR3 to perform a given movement with a minimum error in trajectories, making the validation more cohesive.

Each wearable module was attached with clothing elastics to different parts in one of the joints of the UR3 robot, representing the knee joint, as illustrated in Figure 48.

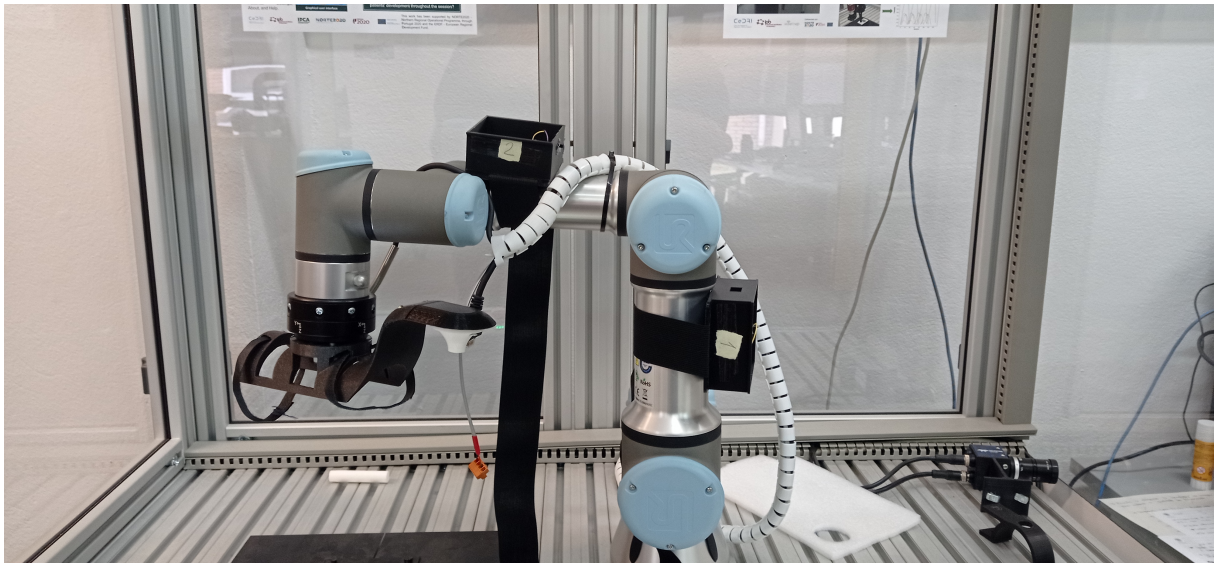


Figure 48: Wearable modules attached to the UR3 robot.

The UR3 robot can be programmed to follow a sequence of positions determined by the joint angle. Thus, for all tests performed, the robot was programmed to move the selected joint in the following positions repeatedly: $[0°, 90°, 75°, 90°, 60°, 45°]$. Each time the joint reached one of the chosen angles, the UR3 remained static for two seconds before moving to the next position.

To compare the movement performed by the UR3 robot with the wearable system, a Python application

[1] https://universal-robots.com/products/ur3-robot

was developed to communicate with the UR3 via Wi-Fi and collect the angle of the chosen joint. It is important to note that the UR3 updates the register that stores the joint angle at a frequency of 30 Hz. To align with the amount of data generated by the wearable system, the sampling frequency of the software was set to 100 Hz, allowing for a higher density of comparable data.

To analyze the data acquired by the wearable system, a treatment session without stimulation was recorded for each test performed. The acquired data were stored in a MongoDB database, from where they could be imported into a Jupyter Notebook for analysis before implementing the knee angle recognition feature in the mobile app. In the end, two time-series arrays were generated for each test, containing the angles recorded by the UR3 and the wearable system.

The tests consisted of powering both systems and acquiring data continuously for 100 seconds. This procedure was repeated several times to verify the consistency of the acquired data, and no significant differences were found between the runs. The results presented in this section represent a snapshot of the movement performed by the systems three times during one of the acquisitions.

Although both systems were configured with the same sampling frequency, it was not possible to automatically synchronize data acquisition from both systems simultaneously. Therefore, manual synchronization of the data was necessary. Figure 49 shows the raw data from the wearable system synchronized with the data acquired by the UR3 robot.

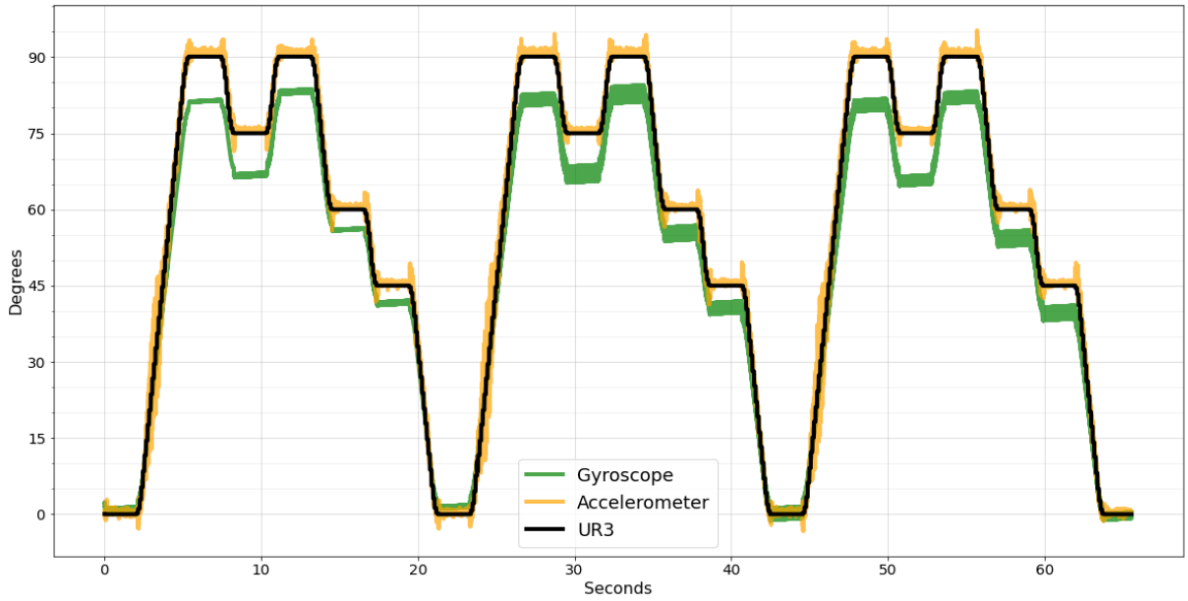


Figure 49: Wearable system raw data synchronized with UR3 data.

As can be seen in Figure 49, both sensors, gyroscope, and accelerometer can reproduce the movement performed by the UR3, but they are inaccurate. As the accelerometer can better measure slow

movements, the error is small during continuous movements, as shown in Figure 49 in the range of motion from 0° to 90°. However, when the UR3 stops, the accelerometer takes time to stabilize, generating noise peaks.

Contrarily, the gyroscope can better measure sudden speed changes, presenting less noise. However, in continuous movements, a small error is accumulated in every sample, resulting in a significant difference compared to the desired degree at the end of the movement.

Comparing the two sensors using the evaluation metrics, the gyroscope has a considerably worse result than the accelerometer. For the MAE metric, the accelerometer has a value of 1.27 and the gyroscope 5.37, four times higher. For the RMSE, the accelerometer has 2.09 and the gyroscope 6.18, three times higher. Lastly, the MSE of the accelerometer is 4.38, and for the gyroscope it is 38.27, eight times higher.

Filters with Algorithmic Complexity $\mathcal{O}(1)$

Within the area of Signal Processing, several filters have been studied to improve the accuracy of IMU sensors. As commented in the literature review of the article Franco et al. (2022c), the implementation of filters such as Kalman and Madgwick can considerably reduce errors in the measurement of joint angles. However, the implementation of the best filters requires a very high computational cost, which is a resource often limited in embedded systems.

The Big O notation is one of the most used notations to describe the computational cost of a given algorithm. This notation takes into account the size of the input and counts the number of instructions used to execute a given sequence of code. For example, for an algorithm that calculates whether the given input is even or odd, only one instruction will be used, resulting in an algorithmic complexity of $\mathcal{O}(1)$. For an algorithm that needs to traverse a vector of size n, the algorithmic complexity is $\mathcal{O}(n)$, since at least n instructions will be executed to complete the task (Chivers et al., 2015).

The algorithm complexity presented by Valade et al. (2017) for the Kalman filter is $\mathcal{O}(10n^3)$; for the extended Kalman filter, it is $\mathcal{O}(4n^3)$. A study on the algorithmic complexity of the Madgwick filter was not found, but as calculations with matrices were used, the algorithmic complexity was to be at least $\mathcal{O}(n)$. Furthermore, these algorithms require memory resources to store the intermediate matrices needed in every calculation, that is not also abundant in embedded systems.

Given this scenario, three filters with lower computational cost and algorithmic complexity of $\mathcal{O}(1)$ were tested to determine the best one for implementation in the wearable embedded system. The filters tested were: *Simple Moving Average* (SMA), *Exponential Moving Average* (EMA), and *Complementary Filter* (CF) for the accelerometer and gyroscope.

For each algorithm, parameters were adjusted to achieve the best possible results. Table 11 presents the evaluation metrics calculated for the raw data of the wearable system and after applying the three filters SMA, EMA, and CF.

Table 11: Evaluation metrics of the applied filters in degrees.

	ACC	**GYRO**	**CF (α = 0.76)**	**SMA (w = 6)**	**EMA (α = 0.3)**
Min	0.0001	0.0078	0.0003	0.0002	0.0016
Max	15.5530	12.6619	6.4770	7.7324	7.6490
MAE	1.2795	5.3728	0.8775	0.9070	0.9225
RMSE	2.0922	6.1867	1.1173	1.1645	1.1942
MSE	4.3806	38.2753	1.2484	1.3560	1.4262
Improved ACC RMSE			46.59%	44.34%	42.92%
Improved ACC MSE			71.5%	69.04%	67.44%

As seen in Table 11, the three filters applied improved the wearable system's raw data error in more than 42% of the RMSE and 67% of the MSE. The MAE metrics of all filters were below 1 degree. The CF filter obtained the best result among the filters, but with a slight difference of 4% over the EMA filter and only 2% over the SMA in RMSE and MSE. Despite this, the same test was performed more than once, and the CF filter always obtained better results than the other filters.

Thus, the CF filter was selected to be implemented in the wearable embedded system. With this optimization the mobile app will only receive the angles already processed, reducing the amount of information needed to be transmitted.

Figure 50 shows the movement recognized by the wearable system with the CF filter already implemented. Analyzing the new data, it was noticed that the performance of the CF filter was even better, resulting in 0.6 degrees on MAE, 1.0058 on MSE, meaning a 77% improvement, and 1.0029 on RMSE, meaning a 52% improvement.

It was possible due to the improved resolution of the worked data. As previously, the raw data were sent to the mobile app; the maximum that the mantissa could reach was 255 since only one byte was reserved. Once the calculation is performed within the embedded system, it is possible to declare variables with greater precision to perform the calculation, such as the double type, representing a mantissa of up to 15 decimal places.

The systems were applied in a real-world environment to validate the implementation of the IMU sensors. Five healthy volunteers were recruited to perform a test performing the knee extension movement. In this test, each volunteer remained seated on a bench and was requested to lift their leg five times for one minute, keeping their leg raised for approximately 4 s each time in the maximum muscle contraction.

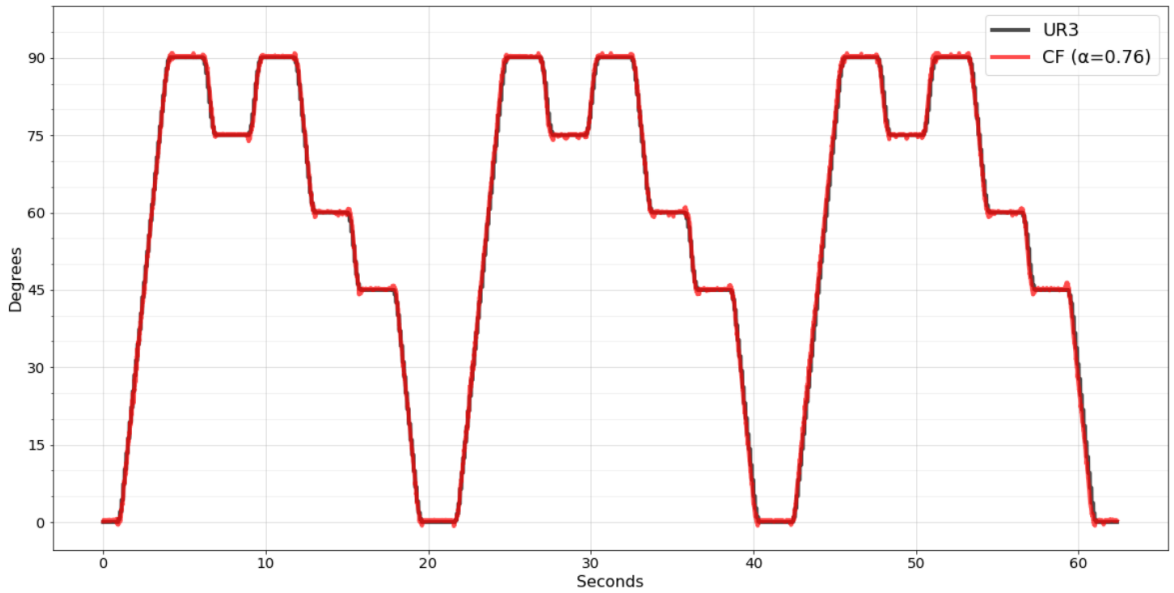


Figure 50: CF filter implemented in wearable embedded system.

Figure 51 shows the volunteer's knee angle being recognized by the mobile app through the IMU sensors of the wearable system developed. As planned, the app successfully recognized the volunteer's knee angle. However, it was noted that one more adjustment would need to be made. As can be seen in Figure 51, the wearable module positioned on the volunteer's thigh does not remain precisely parallel to the thigh bone. Thus, it generates an angular deviation that varies between each person due to the unique anatomy of the leg muscle.

Fortunately, this angular deviation tends to be constant and the same during all treatment sessions, varying only by person. Thus, this value can be added and validated by the physician during the first treatment sessions, which are expected to be performed in the clinic and accompanied by the physician. With all the hardware components and techniques tested, the next validation tests will be conducted with volunteers, assessing the system's performance in more realistic scenarios.



Figure 51: Wearable system and mobile app recognizing the movement of a volunteer's leg.

6.3 Experimental Studies with Volunteers 1

An experimental study with volunteers is a research approach where individuals are recruited to participate in a predefined protocol. The experimental protocol details the activities that participants must perform, the data to be collected, and the analysis methods to be employed. These studies are conducted on scheduled days, with volunteers who have agreed to participate and signed an informed consent form. These studies must be conducted following the guidelines of the Declaration of Helsinki and under an approved ethical committee, ensuring that all procedures meet established ethical and safety requirements.

The results described in this section are from the first and only volunteer test conducted during the NanoStim project. This study was approved by the Ethics Committee of the Polytechnic Institute of Bragança (protocol code 77/2022, approved on March 9, 2022). This experimental study did not include the use of the stimulator from the NanoStim wearable system as it was still in the initial development phase. Instead, a commercial stimulation device was used to apply the electrostimulation.

6.3.1 Experimental Protocol

Fifteen healthy volunteers, consisting of researchers and students from the academic and social circle with no history of muscular or joint problems, were recruited for this study. All participants were informed about the study's objectives and signed an informed consent form. The experimental protocol was divided into three main tests: two repetitions of knee extension exercises and one maximum volume task. Each test and its sequence were designed to evaluate different muscular responses from the volunteers.

The first and third tests of the experimental protocol were identical. The volunteers were instructed to perform the knee extension exercise 15 times, divided into three sets of 5 repetitions each. During the second set, from the 5th to the 10th contraction, the volunteer was stimulated using a commercial device. The stimulation involved applying the minimum intensity and pulse width parameters capable of generating a visible contraction in the vastus medialis muscle, with a frequency set at 1 Hz. The volunteer was instructed to complete each set of exercises within one minute, with a minimum of 3 seconds of holding the leg at maximum amplitude. To achieve this goal, an instructor was present next to the volunteer to indicate when the volunteer should lower or raise the leg.

The second test of the protocol included the Sit-to-Stand (STS) test, which evaluates the strength and endurance of the leg muscles. This test was divided into two specific tests. In the first test, named the 5 Times Sit-to-Stand Test (5STS), the volunteers were instructed to stand up from a chair and sit down five consecutive times as quickly as possible. This test aimed to assess muscle strength and the ability to perform rapid, repetitive movements. In the second test, named the 30-Second Sit-to-Stand Test (30STS), the volunteers were instructed to stand up and sit down as many times as possible within 30 seconds. This test aimed to evaluate muscle endurance and the capacity to sustain intense physical activity over a long period.

The third test of the protocol was a repetition of the first test. The volunteers again performed the knee extension exercise 15 times, divided into three sets of 5 repetitions, under the same conditions. Table 12 shows the average and standard deviation of participants' anthropometric data.

Table 12: Anthropometric data of the subjects - Experiment 1

Sex	**Amount**	**Age**	**IMC**
M	8	26.8 ± 1.9	25.5 ± 3.0
F	7	27.0 ± 1.5	23.1 ± 4.5

For each volunteer, the entire set of three tests took approximately 15 to 20 minutes, excluding the

time required for positioning sensors and electrodes. On average, volunteers took about 3 to 5 minutes to complete tests 1 and 3 and an additional 2 to 3 minutes for test 2. Volunteers rested for 2 minutes between tests, with the option to take longer breaks if needed.

The positioning of the wearable system components on the vastus medialis muscle in the human leg model is demonstrated in Figure 52. One of the EMG electrodes is placed on the knee bone to function as a reference, while the other two EMG electrodes and FES electrodes are positioned on the top of the targeted muscle. The motion sensors, on the other hand, can be positioned at any height on the thigh and shin while facing the front of the body.

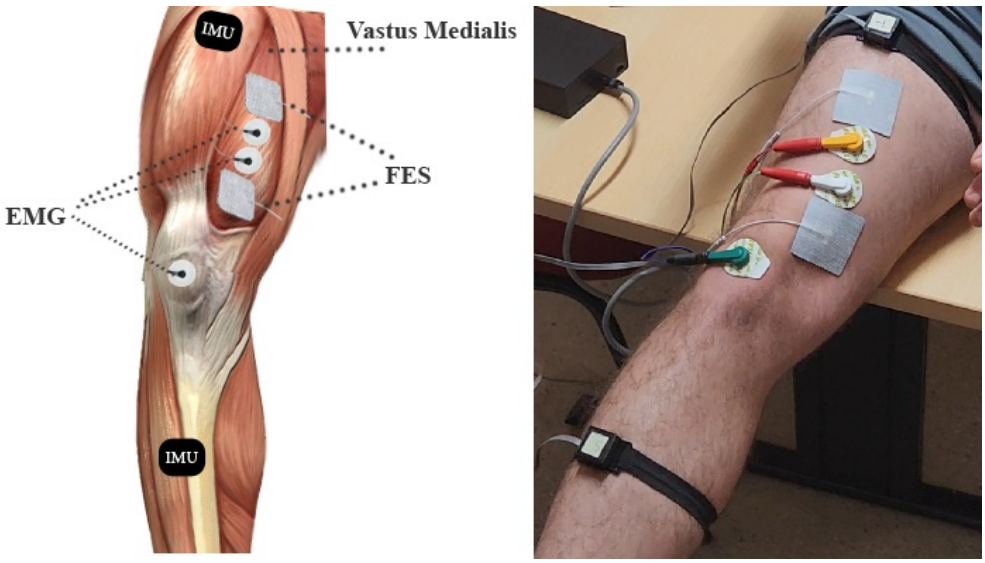


Figure 52: Positioning of sensors and stimulator on the volunteer.

Experimental Objectives

The central goal of this study was to evaluate the system's ability to simultaneously recognize and analyze EMG signals and knee movement angles in healthy volunteers. The CDSS only included raw data acquisition and transmission to the cloud at this stage without implementing intelligent functionalities in the mobile application and wearable system. This study had three main objectives.

The first objective was to examine the interference of FES with the EMG signal. This experiment was the first time EMG signals were processed together with FES, and the main concern was determining the impact of FES on EMG signal quality. The analysis presented aims to identify the interference caused by stimulation and investigate a method to mitigate this interference.

The second objective was to address the difficulty in normalizing the EMG signal, a well-known issue due to the variability in replicating the amplitude results of the acquired signal. EMG signal normalization is

typically performed using Maximum Voluntary Contraction (MVC). However, conducting an MVC test in the home treatment scenarios as proposed will not be feasible. Therefore, a maximum effort test was included to observe the difference between this signal and normal contractions. The goal was to understand this relationship better and to establish a methodology to normalize EMG signals under varied effort conditions without needing an MVC test.

Finally, the third objective was to investigate changes in the EMG signals between the first and third tests. The initial hypothesis was that there would be noticeable differences between the signals from the two tests, indicating possible muscle adaptation or fatigue throughout repetitive exercises.

6.3.2 Removal of Stimulation Artifacts in EMG Signals

EMG signals from electrically stimulated muscles can be contaminated by stimulation artifacts, which complicate the analysis of the volitional component of the signal. After a stimulation pulse, the recording captured by the EMG sensor begins with the stimulation artifact, a peak that lasts from less than a millisecond to a few milliseconds. This peak is followed by an excitation curve known as the M-wave, formed by the synchronous muscle action potentials (MAP) of all motor units activated by the stimulation pulse. The remainder of the EMG signal until the next stimulation pulse is considered the voluntary response of the muscle during the task performed by the individual (Sousa et al., 2018).

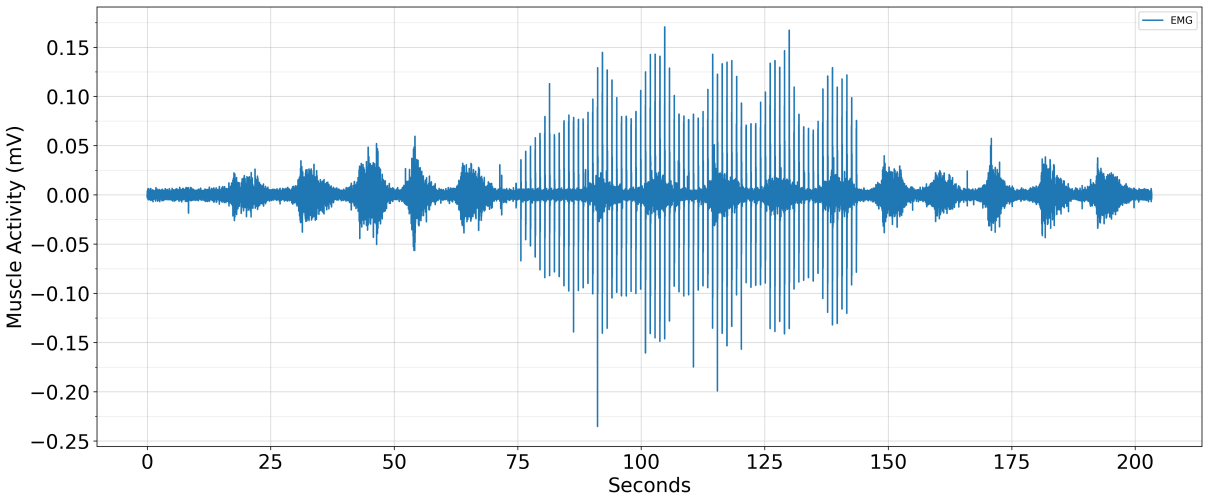


Figure 53: Example of EMG signal captured during the FES experiment.

In Figure 53, an example of a signal acquired from Test 1 is shown, illustrating an EMG signal captured during the experiment with FES. Each increase in muscle activity corresponds to performing a repetition of the knee extension exercise. When the stimulation is activated, around the middle of the presented signal,

various clearly visible peaks can be observed, indicating the stimulation artifacts.

Despite these peaks, the voluntary muscle response can also be seen occurring over the stimulation artifacts. When the stimulation is turned off, the peaks disappear, and the signal returns to normal activity, free from the interference of the artifacts. This section describes the methodology applied to remove these artifacts, resulting in clean, filtered EMG signals suitable for subsequent analysis.

The first step was to calculate the exact period between the stimulation pulses. Given that the commercial device was set to 1 Hz, the expected interval between pulses was 1000 ms. To confirm this, the signal from tests 1 and 2 was cropped to a segment that definitely contained stimulation for all participants, specifically from seconds 100 to 130.

Next, the $find\_peaks$ function from the SciPy library was used to detect peaks in the rectified EMG signal. These peaks were defined as values exceeding the signal's mean plus three times the standard deviation. With this, the average time between the peaks was calculated, and the median interval among all participants was determined, defining the time interval between each stimulation pulse. The result was an interval of 970.33 ms, diverging from the expected value. Figure 54 shows an example of the rectified EMG signal with its identified peaks, as described.

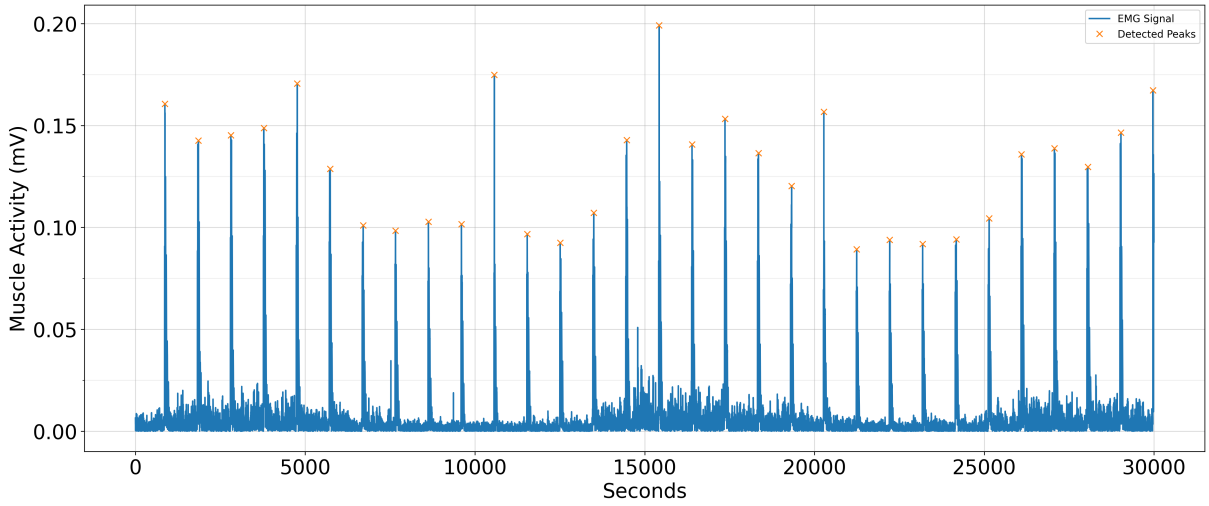


Figure 54: Example of peak detection in the EMG signal.

Artifact Segmentation

The logic for identifying the stimulation segment is based on the frequency of occurrence of the stimulation pulses. Knowing this frequency, the first step is to determine the start of the stimulation window. To achieve this, an algorithm was developed to segment the inter-pulse intervals (IPIs).

The algorithm works by analyzing two consecutive windows of data. For each window, the index with

the lowest value within that window is found. If the difference between these indices is less than a threshold of 30 points, it indicates that stimulation has likely started, as the minimum points are very close, signaling the presence of a stimulation artifact. To confirm that stimulation has indeed started, the next five windows are tested. If the difference between the indices remains below the threshold, the vector index indicating the start of stimulation is identified.

To segment the windows, the index is moved back 50 points to ensure a safety margin, and segmentation is performed every 970 points. Segmentation of the artifacts stops when the difference between the minimum indices of the windows exceeds the threshold.

After identifying the start of stimulation, the next step is to separate the stimulation artifact, the M wave, and the voluntary signal. The start of the artifact is defined as 30 points before the local minimum within the first 70 points of the window. Next, within the following 200 points of the vector, it is calculated where the signal crosses zero (i.e., shifts from negative to positive or from positive to negative). The first zero-crossing point is defined as the end of the stimulation artifact. The M wave is defined as the segment between the end of the stimulation artifact and the fourth subsequent zero-crossing point.

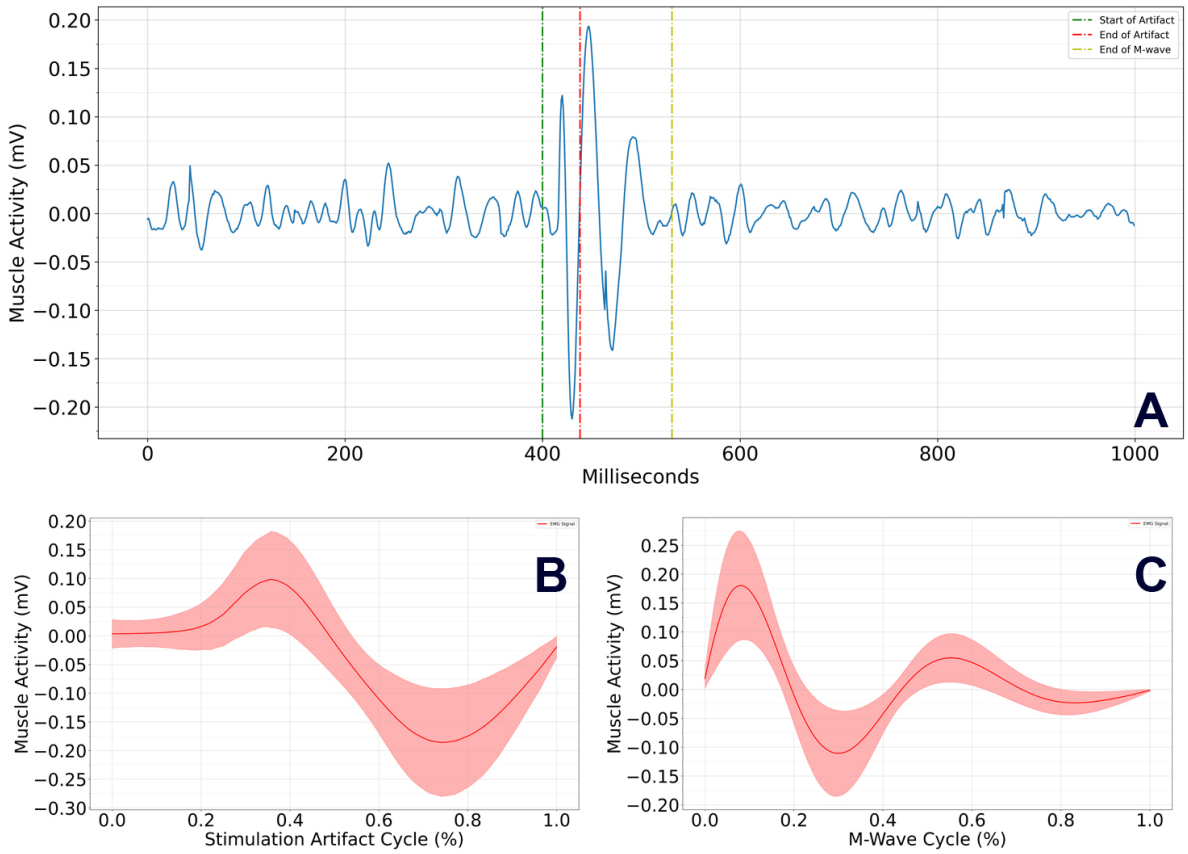


Figure 55: Example of segment with identified stimulation artifact.

In Figure 55A, an example of an IPI is shown with the marking of the start and end of the artifact and the M wave. Figures 55B and 55C display, respectively, the average and standard deviation of the artifacts and M waves of all experiment participants. The average time for the stimulation artifacts and M wave among participants was 160 ms out of 970 possible, corresponding to about 16% of the IPI. This segment of the signal needs to be filtered to achieve a clean EMG signal that closely represents the participant's true response.

Cubic Interpolation Filter

To ensure the continuity of the EMG signals and remove stimulation artifacts, a filter based on cubic interpolation of the data adjacent to the artifact segments was applied. Cubic interpolation is a mathematical technique used to estimate new data points within the range of a discrete set of known data points. Unlike linear interpolation, which connects adjacent points with straight lines, cubic interpolation uses third-degree polynomials to connect the points, resulting in a smooth curve that passes through the original data points.

Cubic interpolation is preferred in many applications because, unlike linear interpolation, it not only guarantees the continuity of the interpolated function but also the continuity of its first and second derivatives. This makes cubic interpolation especially useful for biological signals, such as EMG, where maintaining the signal's properties is particularly important.

To apply the filter to each identified artifact segment, the total size of the segment, or the number of points occupied by the artifact, is determined. Then, a set of data points equal to the size of the artifact is selected before and after the artifact. These segments are used to construct the cubic interpolation function. The 'CubicSpline' function from the SciPy library is used to generate the interpolation.

The cubic interpolation function is applied to the interval corresponding to the artifact segment, generating an interpolated segment that replaces the artifact in the original signal. This procedure ensures that the transition between the real data and the interpolated data is smooth and continuous, maintaining the integrity of the EMG signal.

In Figure 56, an example of an EMG signal after the application of the filter can be seen. Note that this is the same signal shown in Figure 53, but with the stimulation artifacts removed. Figure 57 shows an example of a segment with the stimulation artifact and the respective filtered signal. It can be observed that the application of the cubic interpolation filter effectively removed the stimulation artifacts, resulting in a clean and continuous signal.

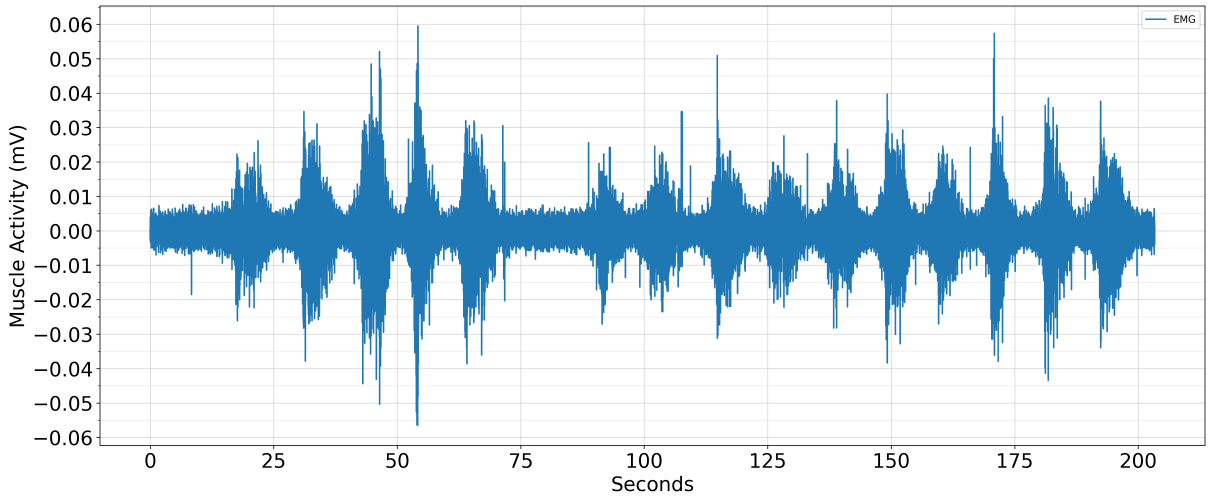


Figure 56: Example of EMG signal captured during the FES experiment filtered.

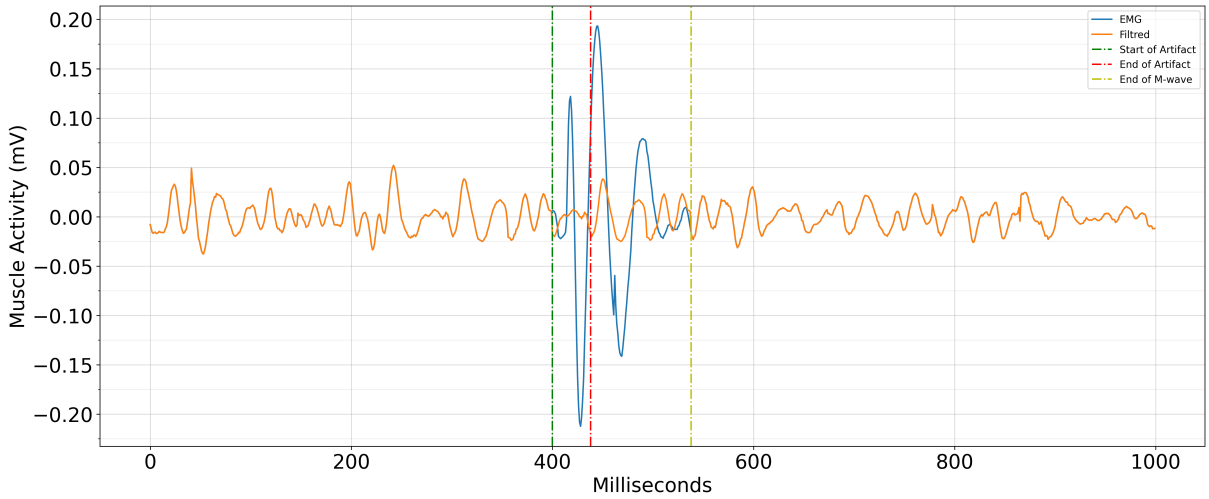


Figure 57: Example of segment with identified stimulation artifact filtred.

6.3.3 Maximum Voluntary Contraction (MVC)

MVC is a crucial concept in electromyography studies, used to measure the most significant force that a muscle or muscle group can generate during voluntary contraction. Practically, MVC serves as a reference point for normalizing EMG signals, allowing muscle activities to be expressed as a percentage of the individual's maximum effort. This normalization enables clear comparisons between subjects and experimental conditions, as it accounts for the inherent variations in absolute muscle strength across subjects.

In Figure 58, the average muscle activity of each subject during the first test is displayed in millivolts (mV). The visual analysis suggests that most volunteers exhibited similar muscle activation levels, with

some notable variations in three subjects. This observation implies that the subjects exercised comparable effort during the test.

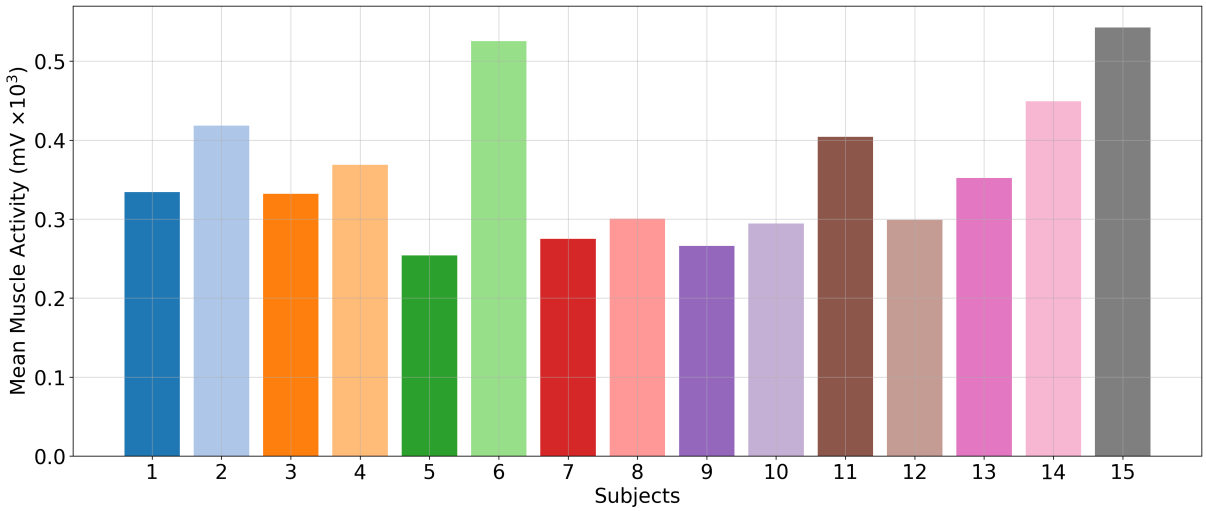


Figure 58: Mean muscle activity of subjects in mV.

For a proper normalization of the data, EMG signals collected during the second test (STS test) were used to identify the maximum muscle activity during a dynamic task. The final 15 seconds of the test were selected based on the assumption that subjects had performed their maximum effort during this period.

The extracted EMG signals were processed in four steps: (1) rectification of the signal, (2) smoothing using a moving average window of size 300, (3) identification of the peak amplitude, and (4) calculation of the average of 20 adjacent points around the identified peak. The results of this process are shown in Figure 59, which presents the MVC values of each subject.

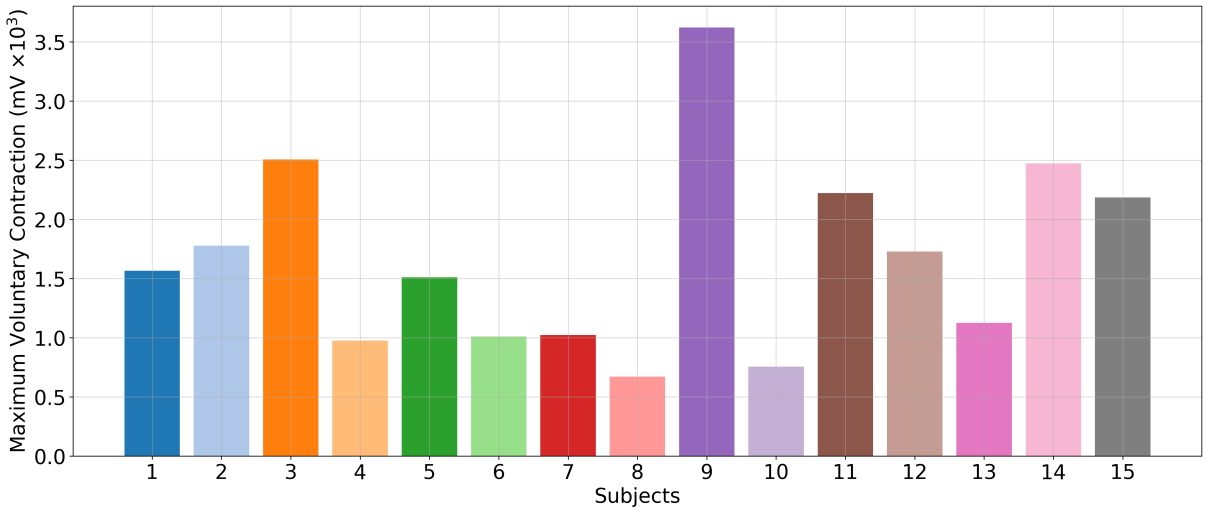


Figure 59: Maximum Voluntary Contraction of subjects.

Following the MVC calculation, all subjects' EMG data were normalized, expressing muscle activity as a percentage of the MVC, as illustrated in Figure 60.

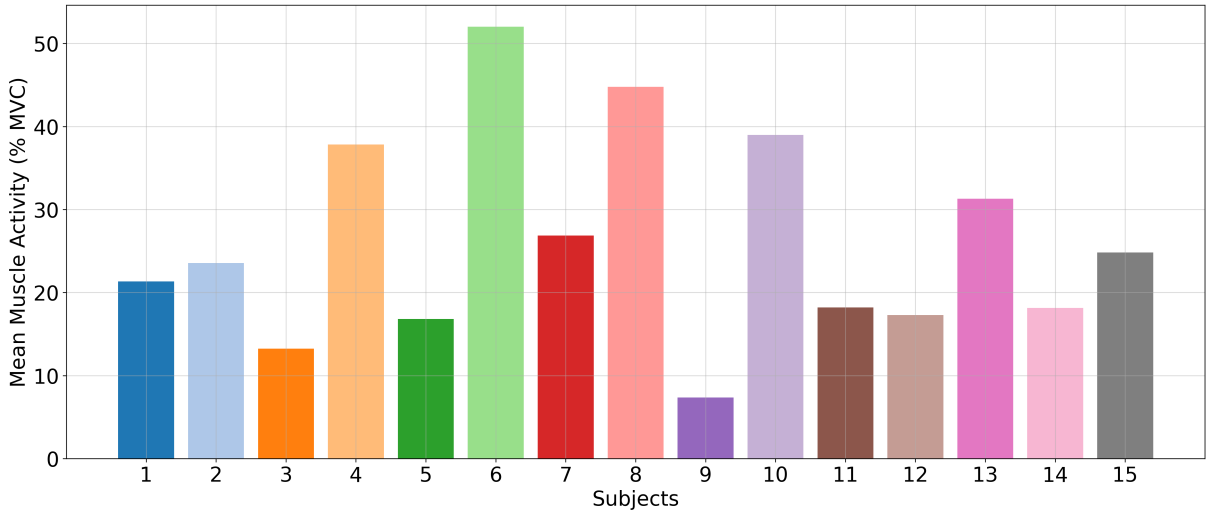


Figure 60: Mean muscle activity of subjects normalized by MVC.

A comparison between Figure 58 and Figure 60 highlights the normalization value. In Figure 58, muscle activation values appear relatively similar across subjects; meanwhile, in Figure 60, a bigger variability is observed, with some subjects using up to 40% of their total muscle capacity, while others utilized less than 10%. This indicates that some subjects had more ease in performing the movement than others, or in other words, some subjects needed to demand more of their vastus medialis muscle to perform the same task compared to other subjects.

It is important to emphasize that the mean muscle activation normalized by the MVC is a weak indicator of the subjects' muscle fatigue. Although it is possible to assess the percentage of muscle required to perform the movement, it is not possible to say how much longer the subject would be able to maintain the movement with the same percentage of muscle use. It is possible that some subjects, despite having high mean muscle activation values, can sustain the movement longer than a subject with a lower average. This happens because our muscles have varied intrinsic characteristics, such as fiber type, body fat, and muscle volume, which influence the muscle's ability to sustain the movement for a longer or shorter time, which would more accurately indicate muscle fatigue.

6.3.4 Knee Extension Movement Recognition

With the EMG signals properly processed and normalized, the next step in the experimental study was to apply the knee extension movement recognition algorithm, as described in Section 5.1. This phase of the

study was crucial for validating the effectiveness of the developed algorithm in accurately identifying and segmenting the movements performed by the volunteers using real data collected during the experimental sessions. The main goal was to verify whether the proposed method could precisely recognize movement cycles, an essential task for the CDSS's effective application in clinical environments.

The recognition algorithm was then applied to the data from all participants, resulting in 15 recognized movements in the first test and 15 more in the third test, as expected for each participant. The first investigation on this topic focused on the variation in the maximum angle achieved and the duration of each contraction.

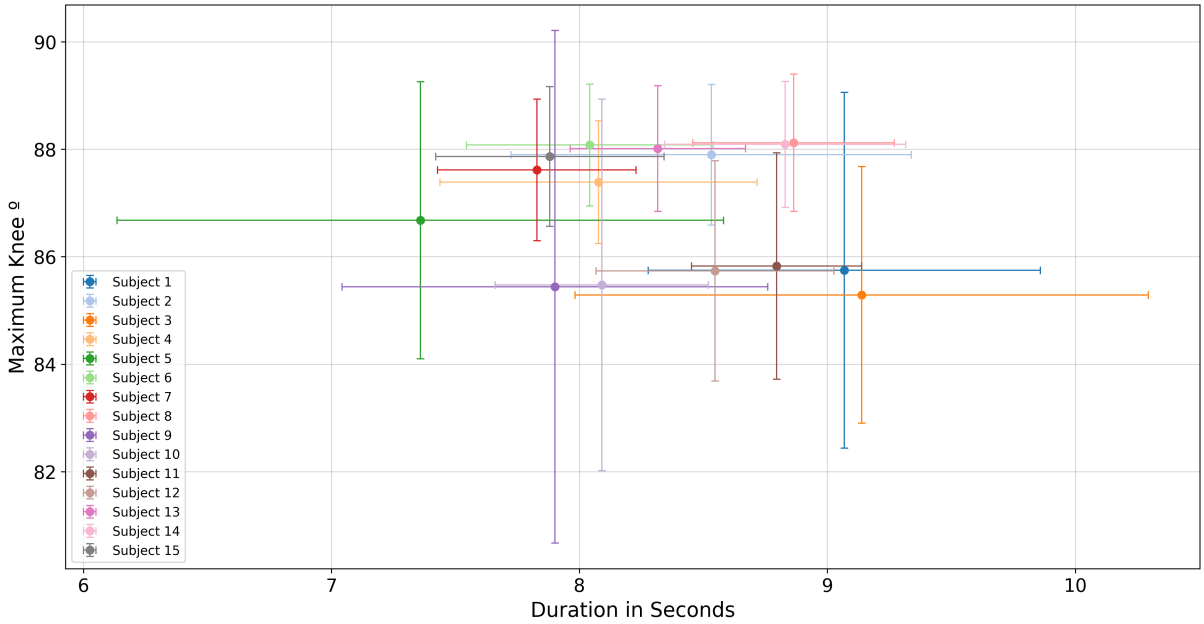


Figure 61: Variation in Maximum Angle and Duration of Knee Extension Movement - Experiment 1.

The chart in Figure 61 indicated that there was a variation in the duration of contractions recognized among the volunteers, with an average of approximately 8 seconds per contraction. Most subjects completed the movement by taking 1 second to raise the leg, maintaining the leg at the maximum position for 6 seconds, and taking 1 second to lower the leg.

However, the most notable observation was that all subjects displayed a maximum angle exceeding 90 degrees, which is anatomically improbable. This angular deviation was attributed to the imprecise positioning of the IMU modules, which had already been identified in preliminary studies. The confirmation of this deviation in this experimental study suggested the need for a system calibration process before each session to reduce angular error and ensure a more accurate representation of knee movement. A normalization process was performed to correct the knee angle collected in this experimental study, adjusting the maximum value of each test to 90 degrees, respecting human anatomical limits.

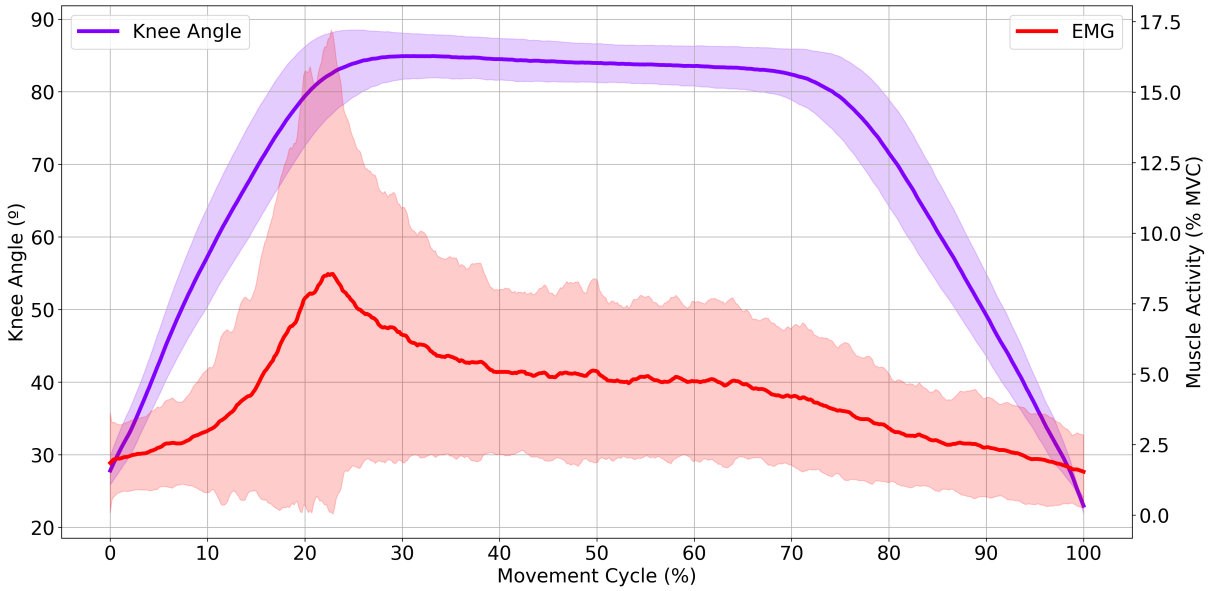


Figure 62: Cycles of Knee Extension Movement.

Figure 62 presents the mean and standard deviation of the recognized contractions, with the cropped knee angle and the EMG signal. The data were interpolated so that the duration of the movement cycle was transformed into a percentage of the total cycle, allowing for comparisons disregarding differences in contraction duration. The chart in Figure 62 evidence that the algorithm worked as expected since the data from the IMU and EMG sensors were synchronized. If the algorithm had segmented the movements incorrectly, disorganized peaks would be expected in the EMG signal. The chart shows an increase in muscle activity at the beginning of the movement, specifically during leg elevation, followed by a stable activation level during the holding phase and a gradual decrease during the descent phase.

The analysis of the results indicates slight variation in knee angle during the movements performed by the volunteers, suggesting that the movements were carried out consistently. However, muscle activity showed more significant variation among participants, indicating that some individuals needed to exert more muscle force to complete the movement compared to others. In some cases, muscle activity was up to twice as high in certain individuals.

For a more detailed analysis of muscle activity during knee extension movement, the EMG signal data were transformed into a ratio of the knee angle for each contraction. The mean and standard deviation of these ratios were then calculated, generating the chart shown in Figure 63.

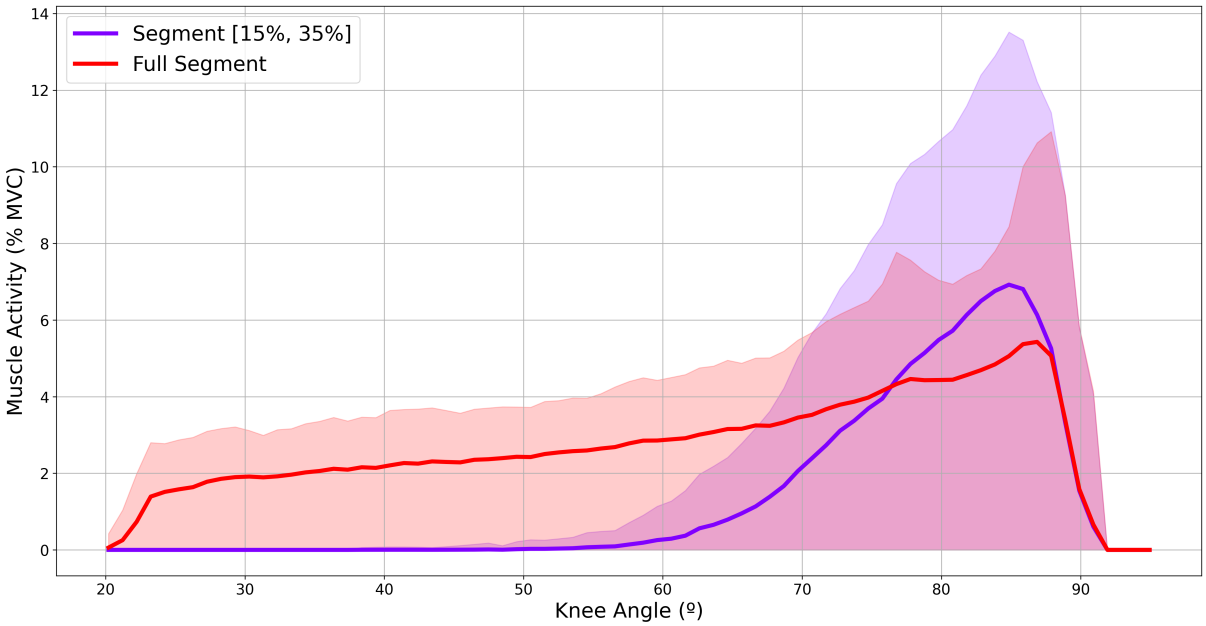


Figure 63: Muscle Activity in Knee Angle Ratio.

The analysis reveals that the volunteers' muscle activity gradually increased as the knee angle increased, reaching its peak in the last 20 degrees of extension. This result suggests that the vastus medialis muscle remains highly active during the initial phase of the movement, playing a crucial role in the full extension of the knee. However, muscle activity during the holding phase was less intense, indicating that muscle effort is significantly higher in the early stages of the movement.

In order to obtain a more precise representation of this hypothesis, a line in Figure 63 was added to evidence the muscle activity of a specific part of the movement cycle, being between 15% and 35% of the total cycle, where the peak of activity was observed in Figure 63. The chart revealed that muscle activity during this period was considerably higher than during the holding phase, reinforcing the importance of the vastus medialis muscle in the last 20 degrees of the knee extension movement.

First Test vs Third Test

Following the objectives, a comparative analysis was conducted between the data obtained in the first and third tests, with the primary goal of identifying and quantifying possible differences between the two assessment moments. This allowed the identification of signs of muscle fatigue or changes in movement execution over time.

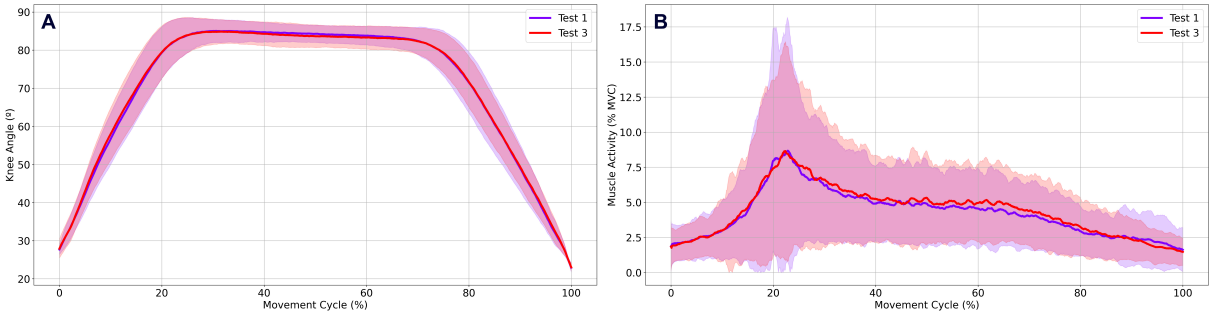


Figure 64: Comparison between the First and Third Test.

Figure 64 presents a graphical comparison between the movements recognized in the first and third tests. In Figure 64A, the graph shows the trajectory of the knee angle for both tests, while part B presents the muscle activity. As seen in Figure 64A, the movement recognized in both tests is quite similar, indicating that the volunteers consistently performed the knee extension movement. However, it can be observed that, in the third test, the knee angle during the sustaining phase is slightly lower compared to the first test. This suggests that the subjects had some difficulty maintaining the maximum angle as the muscles became more fatigued.

In Figure 64B, which illustrates the muscle activity, a more noticeable difference between the two tests is observed. The muscle activity in the third test is visibly higher compared to the first test, indicating that the volunteers' muscles had to work harder to perform the movement in the last repetition. This increase in muscle activity may be indicative of accumulated fatigue throughout the exercises, requiring additional effort from the muscles to complete the knee extension movement.

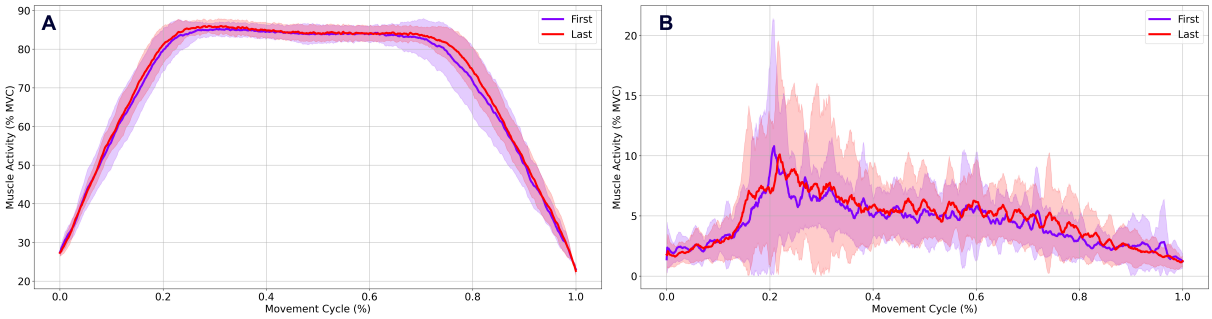


Figure 65: Comparison between the First and Last Movement.

A second analysis was conducted to investigate this difference further, presented in Figure 65. In this analysis, the first and last movements performed throughout the entire experimental session were selected. In Figure 65A, it is observed that there was no significant difference in the sustaining phase

between the first and last movements. However, there is a slight discrepancy during the leg-lowering phase, where the knee angle in the first movement is slightly lower.

The most significant difference, however, is observed in Figure 65B, where the muscle activity of the last movement remains elevated throughout nearly the entire movement cycle, indicating that the muscles were more fatigued and required more effort to perform the same task. This difference in muscle activity between the first and last movements reinforces the hypothesis that there was an accumulation of fatigue over the exercise protocol, making the movement more challenging for the volunteers as the experiment progressed.

Finally, Table 13 presents a quantitative comparison of the performance metrics between the first and third tests, as well as between the first and last movements. The evaluated metrics include the maximum value, MAE, standard deviation, and MSE.

Table 13: Comparative Metrics between the First and Third Tests.

	Max	**MAE**	**STD**	**MSE**
Test 1 vs Test 3: EMG	0.76	0.25	0.16	0.09
First vs Last: EMG	3.53	0.61	0.53	0.66
Test 1 vs Test 3: Knee °	1.39	0.39	0.30	0.25
First vs Last: Knee °	3.32	0.88	0.75	1.35

The data analysis in Table 13 corroborates the observations made in the graphs. All metrics increased when comparing the first and last movements, emphasizing the maximum value of muscle activity, which was more than four times higher in the last movement. The MSE, in particular, stood out as a sensitive metric to this difference, presenting a value of 0.09 in the comparison between the first and third tests but increasing to 0.66 in the comparison between the first and last movements. These results highlight a considerable discrepancy between the two moments, supporting the interpretation of muscle fatigue at the end of the exercise protocol.

Fatigue Assessment

This section analyzed metrics related to muscle fatigue, specifically the Median Frequency (MDF) and Root Mean Square (RMS). As observed in the previous results, participants exhibited signs of fatigue throughout the experiment, particularly when comparing the beginning and the end of the experimental session. This analysis aims to assess how these metrics behaved throughout the tests, seeking for more apparent

evidence of muscle fatigue.

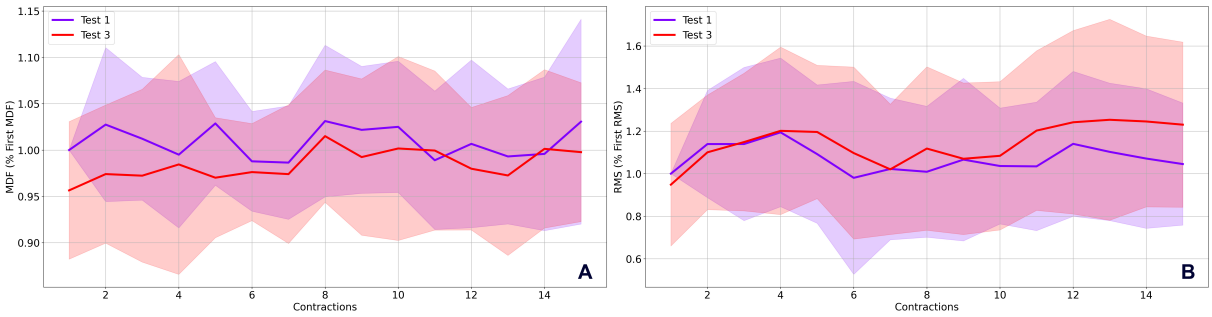


Figure 66: Trajectory of Median Frequency and RMS during the First and Third tests.

Figure 66 presents the trajectory of the MDF and RMS metrics in tests 1 and 3. In Figure 66A, the behavior of the MDF metric is shown, which tends to decrease when muscle fatigue occurs, as discussed in Chapter 5. As expected, the MDF showed a slight reduction throughout the experiment, suggesting the onset of muscle fatigue. Comparing the two tests, it can be seen that the MDF in test 3 was consistently lower than in test 1, indicating that the participants' muscles were more fatigued as the experiment progressed.

In Figure 66B, the behavior of the RMS metric is analyzed. When fatigue is present, the expected behavior of the RMS is a gradual increase, followed by a threshold point and, subsequently, a decrease. The graph shows a gradual increase in RMS throughout the experiment, with higher values in test 3 compared to test 1, suggesting that the muscles required more effort as the session progressed. However, the expected threshold point, followed by a gradual decline in RMS, was not clearly identified. This may indicate that while there were signs of fatigue, the participants did not reach an extreme level of muscle exhaustion that would result in a decline in strength.

Although the average MDF and RMS data behaved as expected, the analysis also revealed a significantly high standard deviation. This suggests a large variability in the participants' response to the exercise. While some participants showed clear signs of muscle fatigue, others completed the protocol relatively easily. This varied behavior underscores the need for individualized analysis to understand each volunteer's muscle response better.

In order to deepen this analysis and observe more clearly the trajectory of the metrics over time, Figure 67 was constructed, showing the concatenated MDF and RMS metrics for tests 1 and 3. Figure 67A demonstrates a more pronounced decline in MDF, confirming the trend of decreasing EMG frequency signals as fatigue progresses. Similarly, Figure 67B shows a more expressive increase in RMS, indicating that muscle activation was more intense during the later movements compared to the beginning of the

experiment.

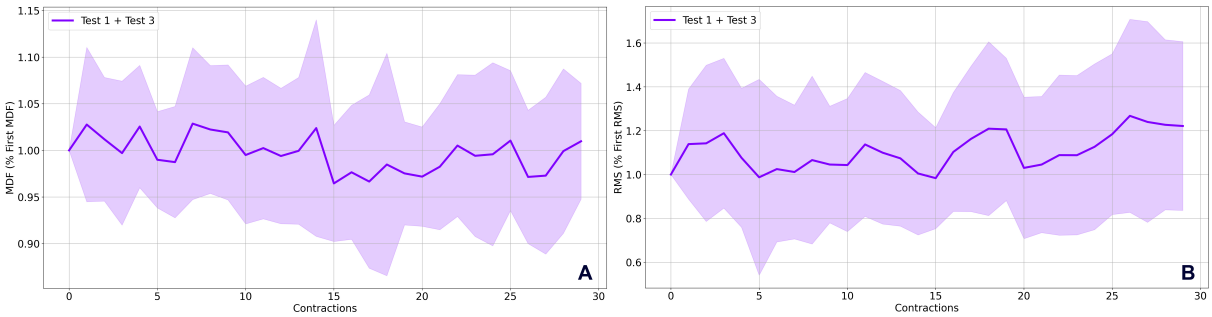


Figure 67: Concatenated Trajectory of Median Frequency and RMS during Tests 1 and 3.

These analyses reinforce the presence of muscle fatigue in several participants throughout the experimental protocol. The reduction in MDF and the increase in RMS indicate that muscle effort became more pronounced as the experiment continued, particularly in test 3. Although the results were heterogeneous among participants, the metrics demonstrate the ability to identify trends in fatigue, offering a more detailed overview of muscle behavior during prolonged exercise.

These findings also suggest that the use of metrics such as MDF and RMS can be a valuable tool for monitoring muscle fatigue in rehabilitation and training protocols, allowing for precise adjustments in exercise sessions to optimize performance and prevent muscle overload.

6.3.5 Discussion Experiment 1

The first experimental study developed in this doctoral thesis provided a series of promising indications regarding the effectiveness of the CDSS. This experiment marked the first time the CDSS was tested with a group of participants using a FES commercial device. This makes the study more realistic and closer to expected clinical conditions, as well as increasing its scientific rigor by involving multiple subjects.

One of the key issues addressed was the removal of stimulation artifacts present in the EMG signal. This process is essential to ensure that the signal can be used accurately in the analysis of metrics related to muscle fatigue. The method of segmenting the artifacts, followed by cubic interpolation, proved effective in cleaning the signal without altering its properties. The use of interpolation based on the segments adjacent to the artifacts, instead of traditional filters, allowed for a more faithful cleaning, maintaining the integrity of the original signal. This results are consistent with another studies, such as Hambly et al. (2024), that used same logic to segment the artifacts but applied different filtering techniques.

The analysis of maximum voluntary contraction was presented, along with its application for normal-

izing EMG data. Normalization is a crucial tool for the correct interpretation of the participants' muscle activity during the exercises. By applying MVC, it was possible to observe a wide variation in the muscle effort of the volunteers, with some using up to 50% of their maximum capacity. Without this normalization, such significant differences would not have been visible, as demonstrated in Figures 58 and 60.

The movement recognition phase was also essential in validating the CDSS's ability to collect and synchronize data effectively. The correct segmentation of movement cycles, performed by Algorithm 1, demonstrated that the system can accurately identify the knee extension cycle of the participants. This was key to comparing the EMG signals recorded in the first and third tests, highlighting the CDSS's ability to reliably monitor muscle performance.

The comparison between the EMG signals from the first and third tests revealed progressive muscle fatigue in the volunteers. In the third test, there was an increase in muscle activity and greater variability in the data, indicating that the muscles required more effort to perform the movement. These results underscore the CDSS's ability to monitor changes in muscle condition during exercise, providing valuable information on the behavior of muscle fatigue.

However, some limitations of the study should be noted. The stimulation was performed using a commercial FES device, which may not reflect the expected behavior of the wearable system developed in the NanoStim project. Furthermore, the average duration of the contractions was eight seconds per cycle, a relatively long time designed to allow for a more detailed analysis of muscle behavior. However, for future studies and in more realistic clinical contexts, shorter contraction times are expected to be adopted, better aligning with rehabilitation practices.

6.4 Experimental Studies with Volunteers 2

Based on the scientific advances achieved in the first experimental study, a real-time fatigue monitoring method for the CDSS was developed, as detailed in Sections 5.1 and 5.2 of this PhD dissertation. To evaluate the performance and effectiveness of this proposed method, a second experimental study was conceived. The results presented in this section are part of the article (Franco et al., 2024a), published in the International Journal of Online and Biomedical Engineering.

The experimental sessions were conducted under the supervision of a physician and were approved by the Ethics Committee of the Polytechnic Institute of Bragança (IPB), Portugal, under protocol number 504143.

6.4.1 Experimental Protocol

Ten healthy volunteers, composed of researchers and students, with no history of muscular or joint problems, were recruited for this study. All participants were informed about the study's objectives and signed an informed consent form.

Under the guidance of a physician, electrodes were precisely positioned on the vastus medialis muscle of each participant, ensuring a 2 cm separation between them. It is important to note that in this study, electrical stimulation was not applied, as the focus was exclusively on the acquisition and analysis of EMG signals. Therefore, stimulation electrodes were not placed on the volunteer.

The exercise protocol consisted of performing the knee extension exercise with 50 contractions. In order to ensure the standardization of the exercise, the subjects were asked to spend two seconds in each phase of the contraction, being two seconds to lift, two seconds sustaining the raised leg, and ending with a downward movement of two seconds, aiming to result in an average duration of six seconds

The study sample consisted of five men and five women, all researchers from IPB. Only one male participant did not engage in regular physical activity, while the others reported attending the gym at least four times a week, with leg exercises at least once a week. Table 14 shows the mean and standard deviation of the participants' anthropometric data.

Table 14: Anthropometric data of the subjects - Experiment 2.

Sex	**Age**	**IMC**	**Gym**
M	27.0 ± 3.3	24.0 ± 2.7	$4x \pm 2.3$
F	27.4 ± 2.2	24.8 ± 3.6	$5x \pm 0.4$

Generally, the testing sessions lasted around 10 to 15 minutes, with half of this time spent on positioning the equipment on the subject and the other half actually performing the 50 contractions. No subject reported difficulty in performing the exercise, and overall, no significant fatigue was reported.

Experimental objectives

This study was designed with two main objectives. The first was to evaluate the CDSS's ability to monitor muscle fatigue in real time during a continuous exercise protocol. The proposed method aimed to identify muscle fatigue patterns throughout the 50 contractions, allowing for a detailed analysis of physiological variations and muscle endurance over time.

The second objective was to compare the muscle fatigue values calculated by the mobile application in real time with the raw data processed later in the cloud. This comparison is crucial for assessing the accuracy of real-time processing, identifying possible discrepancies or technical challenges in data transmission. Additionally, this analysis provides valuable insights into the system's reliability in remote use environments, where real-time processing is essential for successful treatment.

6.4.2 Automated Movement Recognition

During the experiment, participants had the mobile app in front of them, which was responsible for monitoring and counting the knee extension contractions performed. As each contraction was recognized by the real-time algorithm, the app automatically incremented a counter that tracked progress until the required 50 contractions were completed. This visual feedback allowed participants to follow the number of contractions throughout the experiment.

After the experimental session, the raw data collected was analyzed to validate the effectiveness of the movement recognition algorithm. From this analysis, it was found that the algorithm successfully identified all contractions performed by the participants. There were no segments of raw data left unclassified in terms of the movement phase, highlighting the precision of the proposed method in segmenting and categorizing the different stages of the knee extension movement.

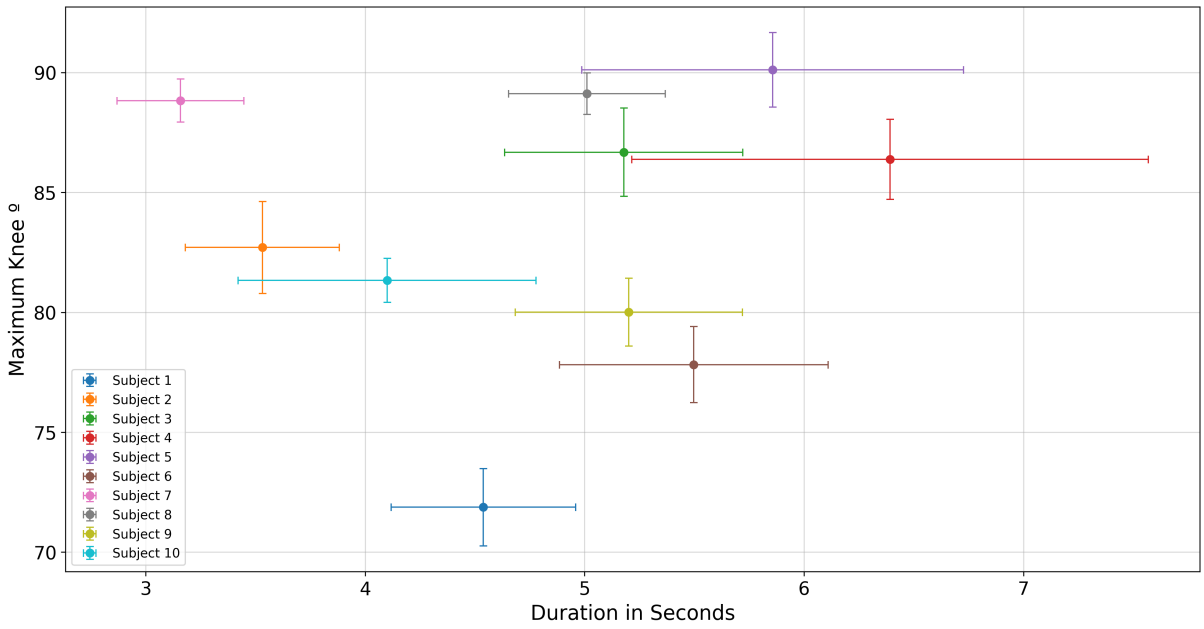


Figure 68: Variation in Maximum Angle and Duration of Knee Extension Movement - Experiment 2.

The graph in Figure 68 displays the subject's knee angle during each of the contractions that were recognized by the developed system. As can be seen, there was variation in the duration of contractions

between subjects, with an approximate average of 5 seconds for each contraction, with an average of 1 seconds to raise the leg, 3 second remaining at the top and 1 seconds on the way down.

The maximum angle reached was 83° on average across all subjects. It was also noted that the majority of subjects increased the maximum angle reached with each contraction, resulting in the maximum peak between contractions 30 and 40.

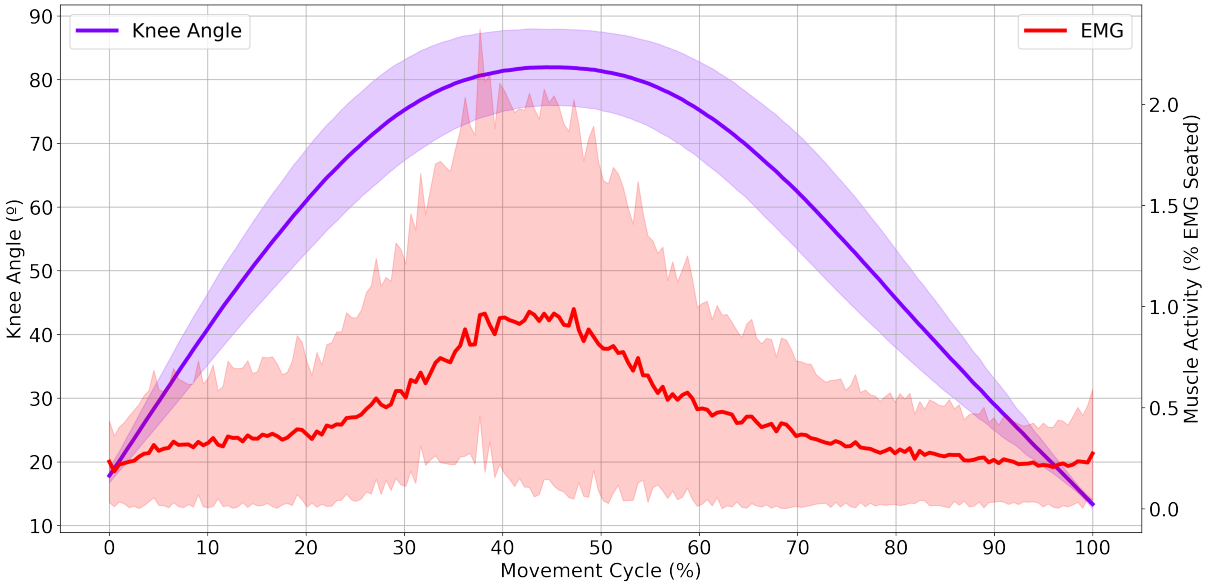


Figure 69: Cycle of Knee Extension Movement - Exp 2.

Similar to the first experimental study, the graph in Figure 69 presents the average and standard deviation of the segments from the EMG signal and knee angle, both normalized to the complete movement cycle. The data analysis shows that the signals are well synchronized, as expected, demonstrating the accuracy of the movement recognition algorithm. However, a notable difference compared to the first study is the timing of the peak muscle activity. In the second experimental study, this peak occurs closer to the middle of the contraction cycle.

This variation can be explained by the difference in the average duration of contractions between the two studies. In the first experimental study, the contractions lasted an average of 8 seconds, with 6 seconds dedicated to the holding phase. In contrast, in the second study, the holding phase was reduced to an average of 2 seconds, resulting in a redistribution of muscle activity throughout the movement cycle. This change was intentional in the protocol to replicate a contraction more similar to what is typically performed in rehabilitation clinics.

6.4.3 Fatigue Metrics Evaluation

This section presents a statistical analysis of three metrics related to muscle fatigue: AvgFreq, MedFreq, and RMS. These metrics were obtained from the EMG signal derived from the segment identified by recognizing contractions based on knee angle and subsequently calculated as described in section 4.2.

The calibration process described converts these metrics into percentages relative to the initial state of the test, which is crucial for monitoring the session's progression. However, to compare across multiple subjects, the data still needs to be standardized due to variations in EMG signal strength. Thus, the data were normalized as standard deviations from the mean.

Additionally, due to some failures in reading the EMG signal from the wearable system, it was necessary to remove up to 3 contractions from some subjects. Consequently, the reported values represent a moving average with a window size of five across 45 contractions. For subjects without signal discrepancies, the initial 5 data points were excluded. This methodology offers insights into the trend of metric values throughout the session.

Figure 70 and Figure 71 illustrate the trends of metrics related to signal frequency, AvgFreq and MedFreq for each subject, and the average trend among the entire group. The average trend decreases as contractions progress. This decline in frequency indicates a decrease in muscle fiber conduction velocity, which is consistent with the expected physiological response to fatigue. As the participant becomes fatigued, the muscle's ability to generate force decreases, resulting in a slower conduction velocity of the muscle fiber, shifting the signal power spectrum to lower frequencies Cifrek et al. (2009).

In some cases, there was a constancy or even an increase in the AvgFreq and MedFreq metrics until the half of the session. This can be understood as a period of adaptation to the movement that the subject went through. These results demonstrate similarities with those presented in Liu et al. (2019), where the median frequency went through several waves with a negative slope until the end of the exercise.

In contrast to the frequency metrics, the average trend of the RMS metric illustrated in Figure 72 does not exhibit a sharp decrease. In general, the predominant behavior was an increase until halfway through the session and then a decrease. This observation suggests that the subject added strength until halfway through the session, potentially adapting to the movement and compensating for the onset of fatigue. Afterward, there are two most likely possibilities: The first is that the RMS decreases, indicating fatigue with a lack of ability to generate more force to sustain the movement, as demonstrated by the authors in Shaw et al. (2020). The second option is when the RMS stabilizes or increases, indicating that the subject calmly endured the exercise until the end.

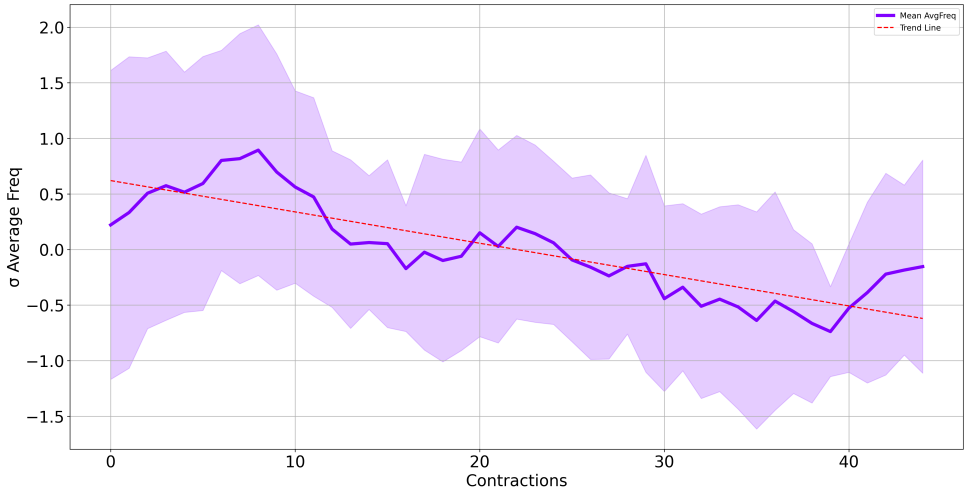


Figure 70: Trend of the avgFreq metric during the session.

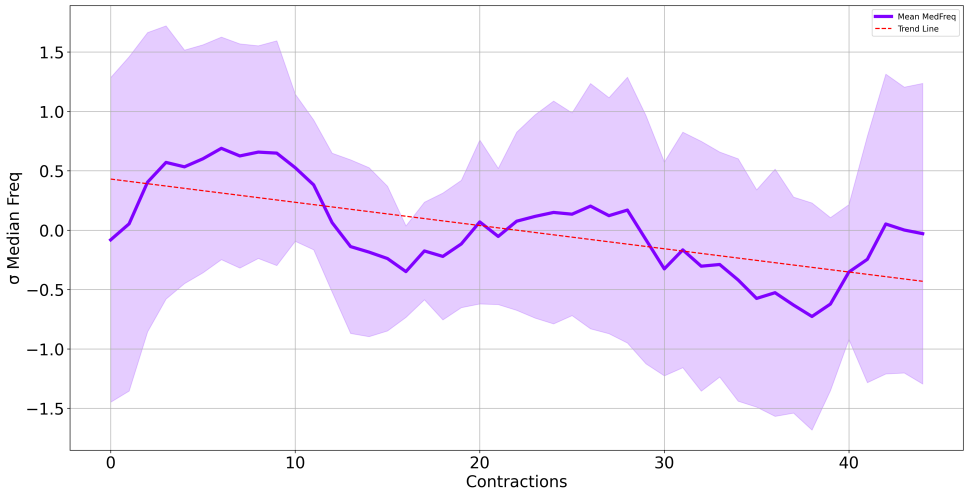


Figure 71: Trend of the medianFreq metric during the session.

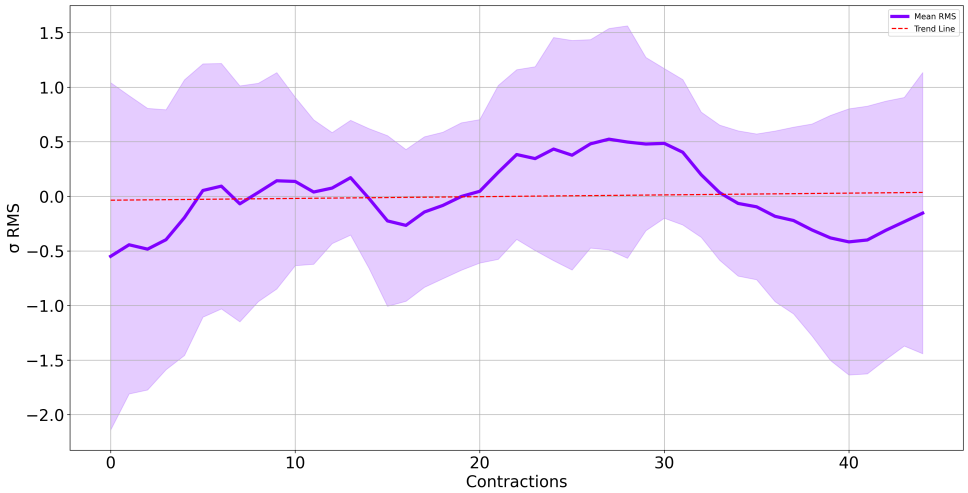


Figure 72: Trend of the RMS metric during the session.

The Joint Analysis of Spectrum and Amplitude (JASA) is a method that seeks to understand muscular responses by simultaneously considering the MedFreq and RMS metrics in a Cartesian plane. The JASA method aims to distinguish the changes observed in the EMG signal between the effects of muscle fatigue and variations in muscle force that occurred during exercise (Luttmann et al., 2000). These quadrants of the Cartesian plane represent different physiological scenarios: the increase in RMS and the displacement of MedFreq to the right indicate a possible increase in muscular force (Q1); the decrease in RMS and the displacement of MedFreq to the left suggest a probable reduction in muscular force (Q3); the increase in RMS and the shift of MedFreq to the left indicate muscle fatigue (Q4); the decrease in RMS and the shift of MedFreq to the right indicate recovery from previous fatigue (Q2).

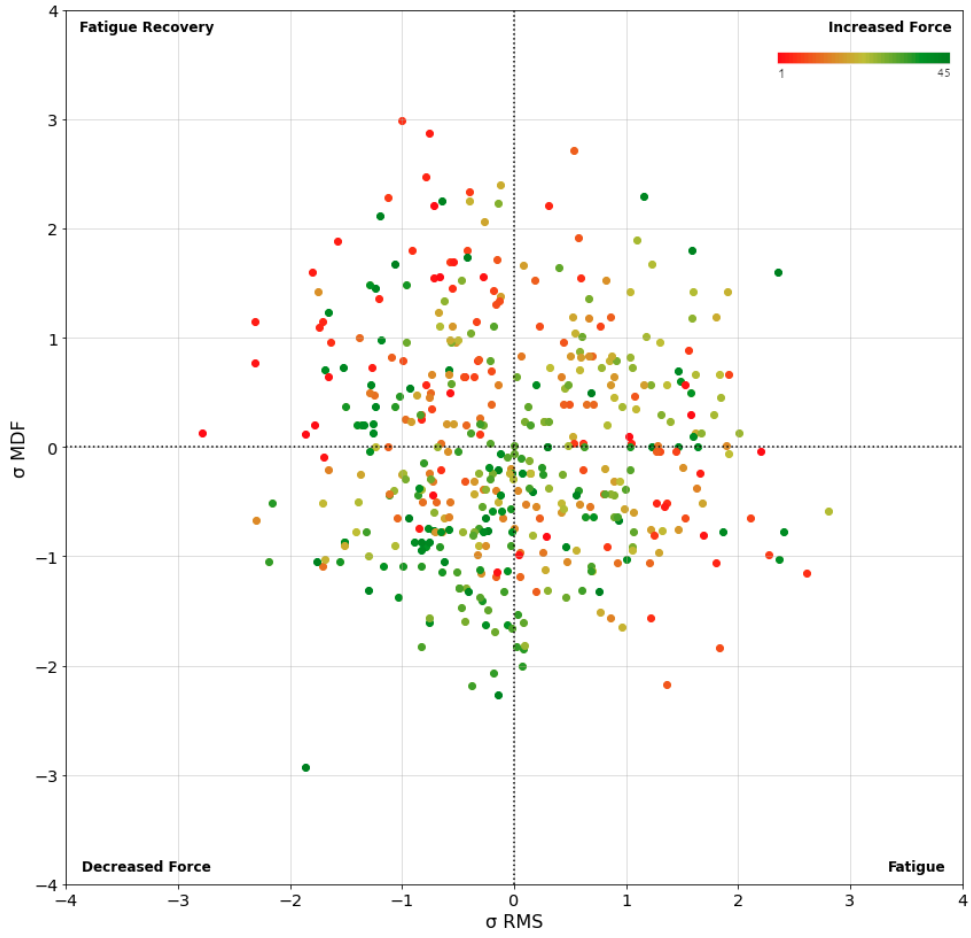


Figure 73: JASA Method apply to Experimental Test.

Figure 73 illustrates the application of the JASA method to the contractions recognized of the entire group. The dots were colored in a gradient from red to green, indicating the first contractions as redder to the last ones as greener. Thus, it is possible to see that despite the varied start, the average progression of the muscular response during the session was a decrease in force and some cases of fatigue.

This is an expected muscular response for healthy subjects who practice physical activity regularly.

Contributing again to an interpretation that there was some challenge at the beginning of the session to adapt to the movement, and then there was a control of force until the end of the session.

Using the chosen fatigue metrics allows a comprehensive assessment of muscle fatigue. While frequency metrics reflect physiological changes associated with fatigue, RMS provides information about participant exertion levels. The integration of these metrics improves the understanding of the progression of fatigue and facilitates the identification of different stages of muscle fatigue, as exemplified using the JASA method. Furthermore, other parameters related to muscle fatigue extracted from the EMG sensor can be used, as described by Cifrek et al. (2009), once the data has been properly cut and processed with motion recognition by the IMUs.

It is essential to emphasize that the interpretation of these findings must be the responsibility of the physician, who has the necessary knowledge about the patient's pathology. It is essential to recognize that different pathologies may present different fatigue behaviors compared to healthy individuals. Therefore, the physician plays a crucial role in analyzing these metrics and making informed decisions based on understanding the patient's condition.

6.4.4 Muscle Fatigue Level Simulator

The final analysis conducted with the data from the second experimental study focused on the behavior of the muscle fatigue level simulator, applied to the fatigue metrics calculated by the CDSS. This subsection aims to exemplify how the adjustable parameters of the simulator can influence the characterization of each participant's fatigue, allowing the stimulation treatment to be tailored according to the real-time biofeedback collected.

As previously explained in Section 5.4 of this document, the fatigue level simulator has three main parameters that determine its adaptability. The first parameter, referred to as S, represents the number of contractions after which the simulator begins to operate, helping to exclude fatigue episodes caused by initial muscle adaptation to the exercise. The second parameter, F, indicates the number of fatigue occurrences required to trigger a change in fatigue level. Lastly, the third parameter, M, corresponds to the minimum intensity that a fatigue occurrence must reach to be considered valid.

To demonstrate the simulator's flexibility, different sets of values were tested for each of these parameters: $S = [5, 10, 20]$, $M = [1, 2, 3]$, and $F = [2, 3, 4]$. These parameter combinations resulted in 27 different configurations, which were applied individually to each participant's session, generating the results of this section.

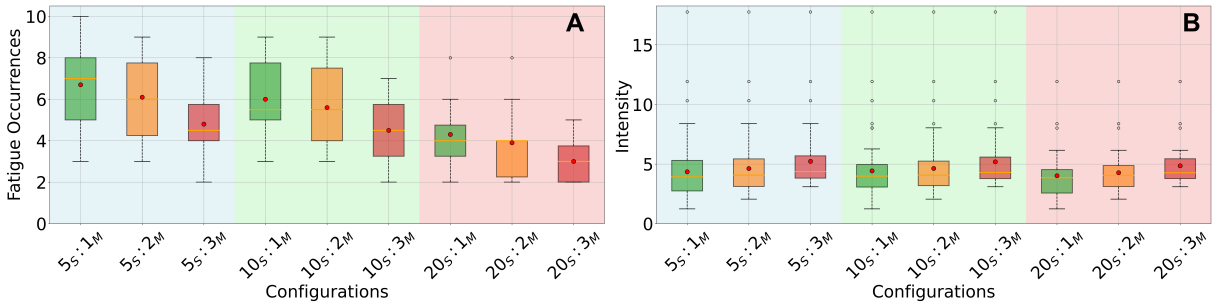


Figure 74: (A) Occurrence of Fatigue (B) Intensity of Occurrences by Configuration.

Figure 74A presents a box plot showing the number of fatigue occurrences when varying the S and M parameters. It is evident that the average number of fatigue occurrences among participants significantly decreased as the minimum intensity (M) increased, with $M = 3$ showing the fewest occurrences. The variation of the S parameter revealed little change when starting the monitoring after the 5th or 10th contraction. However, when the simulator began operating after the 20th contraction, both the average number of fatigue occurrences and the standard deviation decreased substantially.

Figure 74B shows the average intensity of the recorded fatigue occurrences for each configuration, with variations in the S and M parameters. As expected, the average intensities of the contractions increased as the minimum threshold (M) was raised, excluding lower-intensity values and pushing the average upward. Additionally, some fatigue occurrences were identified as outliers because their values were significantly above the norm. It is noted that these contractions with greater intensity predominantly occurred later in the session since only one of the outliner occurrences was filtered when the $S = 20$ configuration was applied.

Following the analysis, a comparison was made between the average levels of fatigue recorded by the CDSS, considering different numbers of occurrences required for a level change. The final level reached is a crucial metric in the CDSS's rule-based method, as it indicates how often can the physician adjust the parameters of the electrostimulation treatment during a session.

As shown in Figure 75, participants experienced a range of zero to five fatigue levels, depending on the simulator parameters. For configurations that required only two occurrences of fatigue, at least one level change occurred for all participants, with the average being around three level changes. In contrast, when four occurrences were required for a level change, some participants did not reach the first fatigue level. In the last scenario, most participants did not reach level 1, and only a few managed to do so.

In order to complement Figure 75, Figure 76 shows the repetition at which the first level change occurred in each configuration. It can be seen that configurations requiring two occurrences of fatigue led to relatively early level changes in the session, with most participants reaching the first level between

contractions 20 and 30, except for configurations with a late start defined at contraction 20.

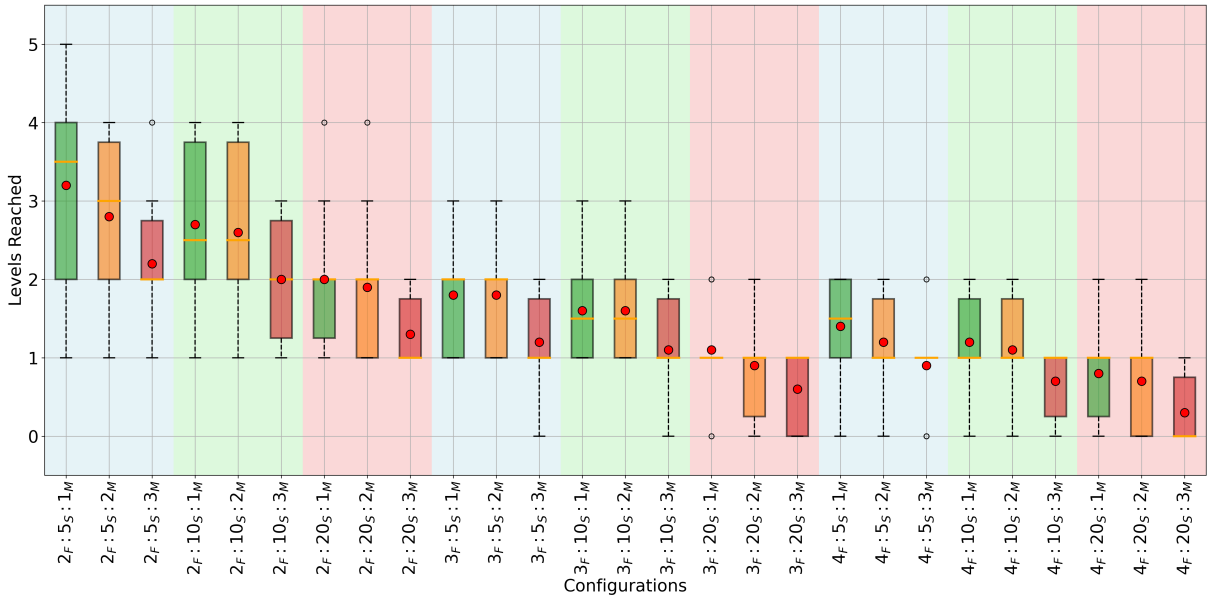


Figure 75: Fatigue Levels Achieved by Configuration.

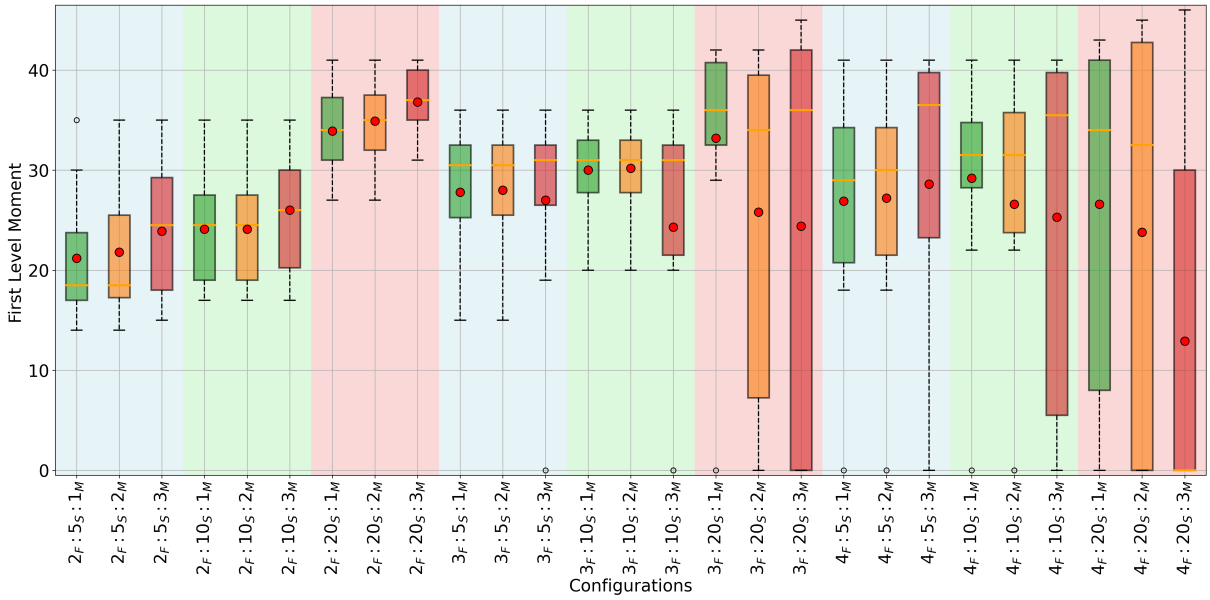


Figure 76: Contraction number at first fatigue level achieved.

The configurations that most accurately captured the participants' muscle responses during the experiment 2 sessions were those using the parameters $F = 3$, $S = 10$, and $M = 1$. This configuration considers a higher number of fatigue occurrences than $M = 2$, with all participants reaching at least one level, and for most, this level occurred around contraction 30.

Additionally, the hypothesis developed in the previous subsection suggests that, while participants experienced some level of fatigue, especially at the beginning of the session, they did not feel excessively

fatigued. Therefore, fatigue levels between one and three are expected to be normal for healthy individuals performing this type of exercise. This information provides valuable data for the physician to make informed adjustments to the treatment according to the expected effects.

Subjects Fatigue Evaluation

To further analyze the results, the chosen configuration for the subsequent data was $F = 3$, $S = 10$, and $M = 1$ of the fatigue level simulator, as it presented an optimal balance between sensitivity to muscle effort and the ability to track participants' fatigue progression throughout the experiment.

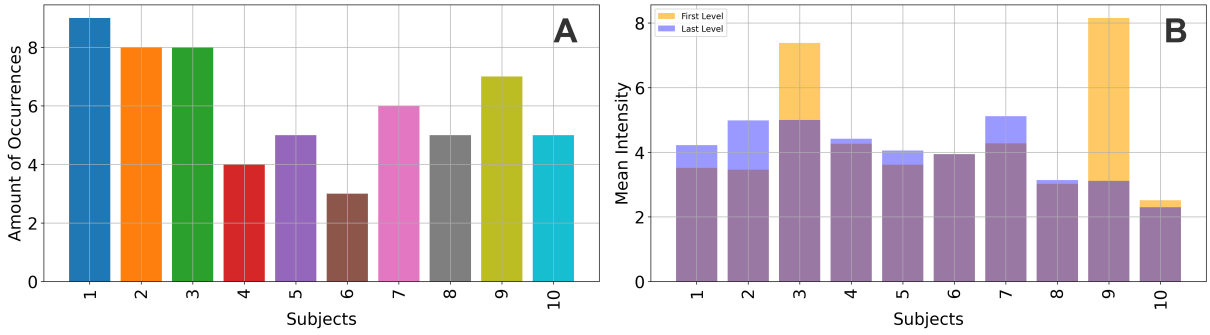


Figure 77: (A) Amount of Occurrence (B) Average Intensity of First and Last Level per Participant.

Figure 77A illustrates the number of fatigue occurrences for each subject during the session of experimental study 2. It is noted that participants exhibited a varied number of fatigue occurrences, supporting the hypothesis that only some subjects felt more fatigued. Three subjects recorded eight or more occurrences, while, on the other hand, subjects 4 and 6 had only 4 and 3 occurrences, respectively. This indicates that these subjects were better prepared for the exercise.

In Figure 77B, the average intensity of the first and last fatigue levels reached by the participants is compared. It is observed that, for three subjects, the initial intensities were higher than the final ones, highlighting greater difficulty in adapting to the exercise. Additionally, subjects 7 and 2 showed the largest increases in average intensity and also had high numbers of fatigue occurrences. For the defined configurations, the simulator indicated that subjects 2, 3, and 7 experienced more difficulty performing the exercise.

Finally, Figure 78 aims to clarify at what point during the experimental session the fatigue levels were reached on average and their respective intensities. As previously noted, for most participants, the first fatigue level was reached around the 30th repetition, which is more than halfway through the proposed exercise. The second and third levels, on average, were reached during the last 10 repetitions. The intensity between the fatigue levels was quite similar, although for level 2, a greater variation was observed

compared to level 1.

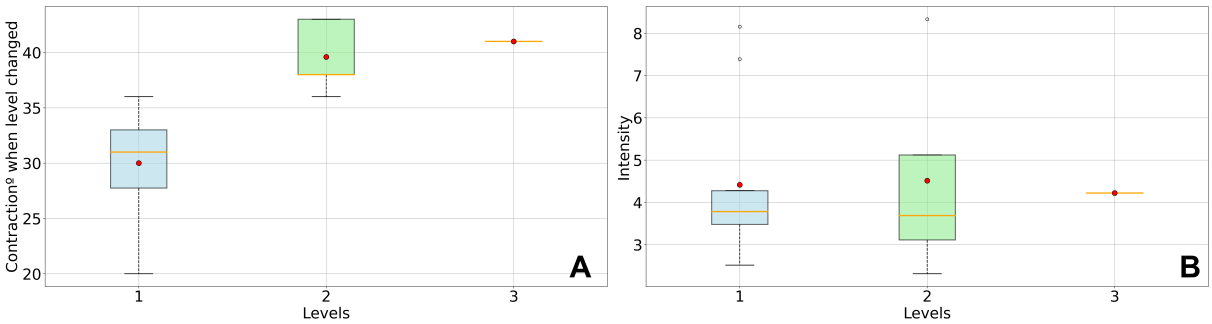


Figure 78: (A) Contractin Number of Levels Change (B) Average Intensity per Level.

6.4.5 Mobile Data vs. Cloud Data

In order to evaluate the consistency and accuracy of the Fatigue Monitoring Method in real-time, this section compares the data processed in the mobile app with the data processed on the computer from the raw data. With this, it is possible to obtain information about the performance and reliability of data processing algorithms.

Two metrics were used to perform the comparative analysis between the systems, namely: Mean Absolute Error (MAE) and Mean Mean Square Error (RMSE). These metrics seek to parameterize the difference between the data obtained in each system, interpreted as our error.

Figures 79, 80 and 81 present comparative charts showing the average error between real-time processing performed by the mobile application and cloud processing for calculating fatigue metrics for all subjects. These charts also provide insights into the average post-application error resulting from the implementation of a moving average with a window size of 5, as previously discussed. The vertical lines associated with each data point in the charts represent the standard deviation calculated across all subjects, allowing a deeper understanding of the data distribution.

From these charts, it is evident that the metrics related to frequency (AvgFreq and MedFreq) had more errors than the RMS metric. The most plausible explanation for the divergence between the systems lies in the calculations related to the transformation of the signal in the frequency spectrum and not in how the sensor data is cut and synchronized. Otherwise, the RMS metric would also present average errors similar to AvgFreq and MedFreq. Also, these calculations were one of the few parts within the mobile system that was not programmed from scratch, especially the Fourier Transform Algorithm. Given the use of different programming languages in implementing the method, variations such as differing variable precision may contribute to this effect.

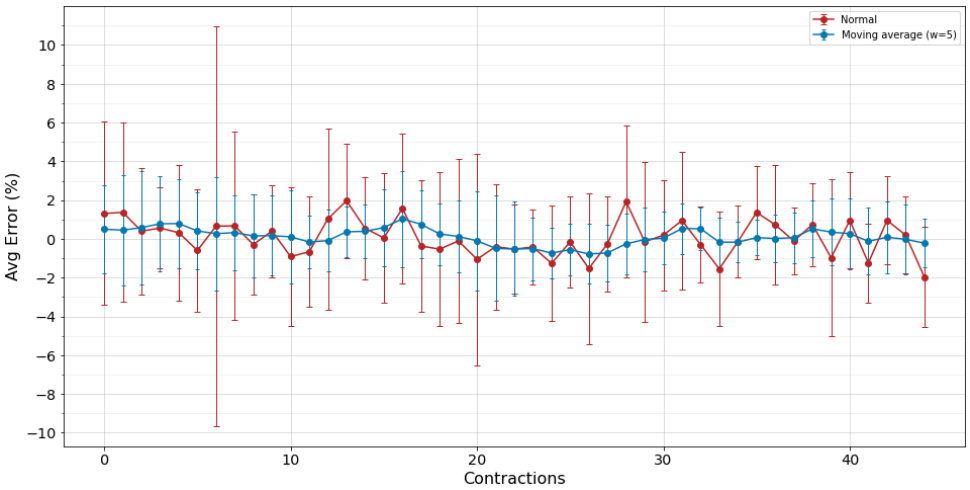


Figure 79: Comparison between systems of the $AvgFreq$ metric.

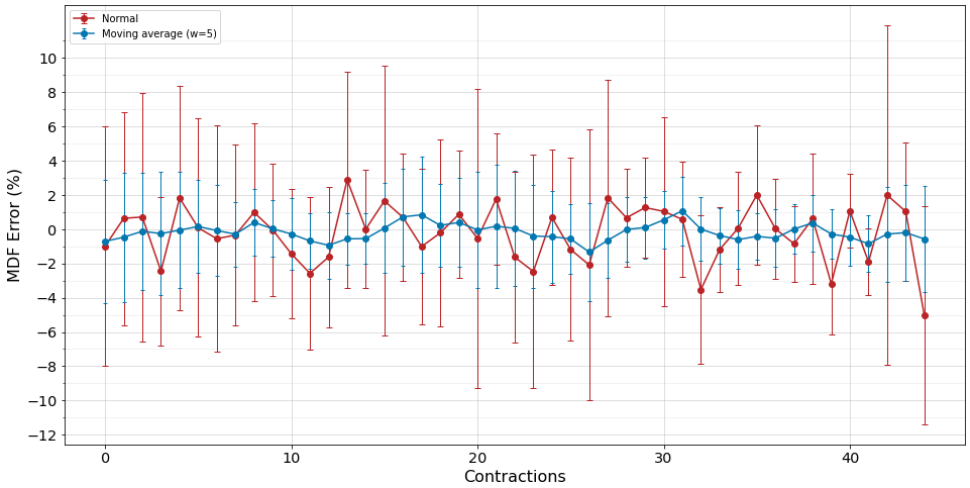


Figure 80: Comparison between systems of the $MedFreq$ metric.

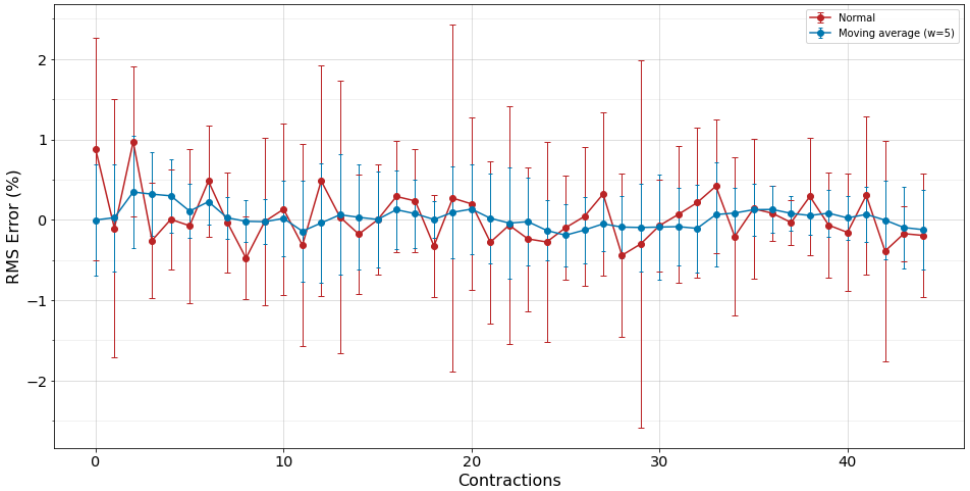


Figure 81: Comparison between systems of the RMS metric.

While the standard deviation may appear relatively high in some instances, the application of the moving average substantially reduces the values. This demonstrates that there are some points with significant errors that can be suppressed by neighboring data, making the average error low. Furthermore, the emphasis of this system lies in monitoring the oscillation trajectories of metrics associated with muscle fatigue, thereby introducing linearity through aggregated values by the moving average.

Table 15 illustrates the assessment metrics on the fatigue metrics.

Table 15: Assessment metrics on fatigue metrics.

Metric	**Max**	**MAE**	**RMSE**
AvgFreq	10.36 ± 6.35	2.61 ± 0.95	3.41 ± 1.38
AvgFreq MA	4.15 ± 1.34	1.46 ± 0.63	1.78 ± 0.71
MedFreq	16.67 ± 4.58	3.5 ± 0.77	5.35 ± 1.16
MedFreq MA	5.90 ± 1.53	1.96 ± 0.33	2.48 ± 0.45
RMS	2.72 ± 1.8	0.69 ± 0.4	0.93 ± 0.55
RMS MA	1.00 ± 0.54	0.34 ± 0.2	0.43 ± 0.25

Table 15 puts into numbers through the assessment metrics the difference in the application of the moving average with a window of size 5. The values of the frequency metrics AvgFreq and MedFreq have similar mean errors and standard deviations each other, with the AvgFreq metric having the best precision. The RMS metric has a MAE of less than 1%; this indicates that the mobile system could execute the proposed method in real-time, similar to the late processing of the raw data in Python.

The application of the moving average managed to improve the MAE metric, reducing the average error by more than 40% and the standard deviation by 50%. The RMSE metric also has similar improvements to the MAE metric. However, in particular, the maximum has the most significant error reduction when applying the moving average, approximately 60% of improvement.

In summary, the mobile application has successfully implemented the real-time fatigue monitoring method with some variations. The metric with the highest accuracy in real-time processing was RMS, while the metric with the highest deviation was MedFreq. Applying the moving average provided considerably smaller errors and could make the system more efficient in monitoring muscle fatigue during knee extension exercises. The mobile app could closely track the trajectory of data processed in the cloud, providing similar insights to the physician in real-time via the app.

6.4.6 Discussion Experiment 2

The second experimental study aimed to demonstrate the effectiveness of the CDSS in a treatment scenario closer to a real clinical setting, compared to experiment 1. In this context, participants followed the instructions provided by the mobile app, which recognized knee extension movements and calculated muscle fatigue metrics in real-time, providing immediate feedback on the subjects' muscle performance to the physician.

The calculation of these fatigue metrics was crucial as it provided detailed information about muscle behavior during the treatment session. This feature allows physicians to assess the patient's fatigue levels and adjust the treatment according to individual needs, which is essential for personalized rehabilitation processes. The development of a simple and intuitive interface in the mobile app also proved to be critical in facilitating professionals' interaction with the system, reducing operational complexity, and making the use of CDSS accessible even to those less familiar with advanced technology. During the experiment, physicians reported ease in conducting sessions, highlighting the practicality of the system.

The knee extension exercise was chosen because it is a traditional exercise in the treatment of muscle rehabilitation using electrostimulation. However, it is possible to expand the interpretation of the method to other muscles and any movement. For this, it will be necessary to know the limits to classify the phases of the chosen movement to cut and normalize the EMG signal precisely. This makes the CDSS highly flexible and promising for broader application in different rehabilitation contexts.

Although real-time processing showed some discrepancies in fatigue metrics compared to cloud-processed data, the app was able to track the trajectory of these metrics satisfactorily. This real-time monitoring capability represents a significant advancement in muscle rehabilitation treatments, as it allows for immediate interventions during the session, enabling adjustments to the electrostimulation program based on the observed muscle fatigue levels.

The results presented by the fatigue level simulator also proved promising. The simulator's flexibility, adjustable through configurable parameters, allowed for the identification of individual variations among participants, with some reaching higher fatigue levels while others showed fewer occurrences. This type of personalization is crucial in rehabilitation programs, as it provides a more targeted and efficient approach, adapting the treatment to each patient's physical condition and muscle responses.

However, some limitations should be considered. In both the first and second studies, exercises were performed only with the participants' right leg, which, in most cases, is the dominant leg. This could have influenced the results, as the dominant leg tends to show fewer signs of fatigue. Additionally, while the initial calibration of the IMU sensors was conducted correctly, some maximum angle values measured

during the experiment fell below expectations. Although there was improvement compared to the results from the previous experiment, there are still indications that sensor positioning may be prone to deviations, requiring future adjustments to increase measurement accuracy.

6.5 Experimental Studies with Volunteers 3

The last experimental study conducted as part of this doctoral project took place at the Biomechanical Engineering Lab (BIOMEC) of the Universitat Politècnica de Catalunya, Spain. The choice of this location was motivated by two factors.

The first factor was the availability of the optoelectronic motion capture (MoCap) equipment, which is considered the gold standard in movement analysis (Walmsley et al., 2018). The commercial MoCap system used was the OptiTrack V100:R2 from NaturalPoint Inc. This equipment is composed of infrared cameras that track the markers placed on specific anatomical landmarks of a subject. The markers are plastic balls, with a diameter of the order of one centimeter and covered with a reflector material. Figure 82 illustrate the equipment used in the experiment.

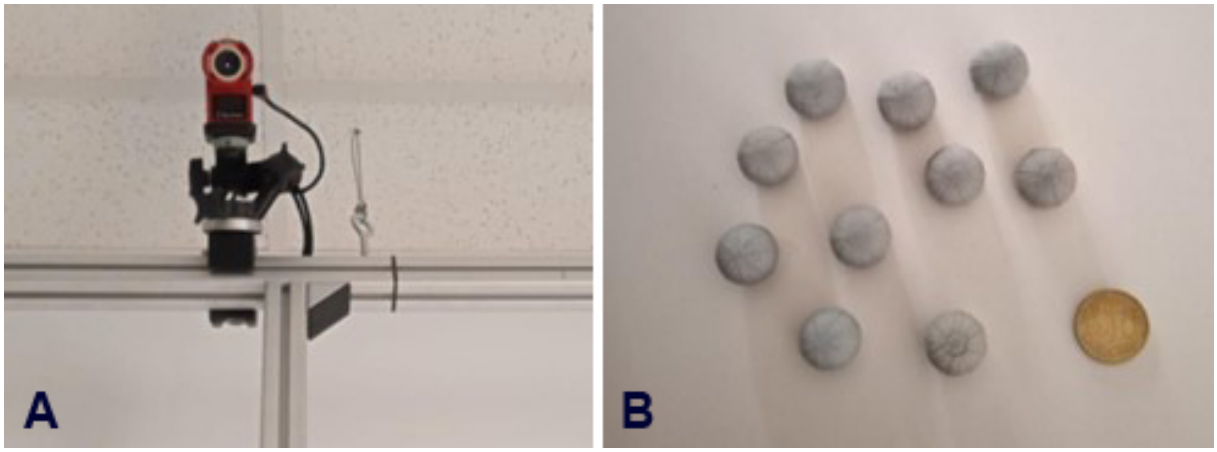


Figure 82: MoCap equipment: Camera (A) and Body Makers (B).

The second factor was the opportunity to explore musculoskeletal simulations using the OpenSim tool, applying the data collected and processed by the CDSS. The research group at BIOMEC, which assisted the experimental study, is specialized in muscle rehabilitation simulations and studies involving electrostimulation, providing an ideal scientific environment for this experiment.

The experimental sessions were conducted under the supervision of two researchers and were approved by the Ethics Committee of the Universitat Politècnica de Catalunya, Spain, under protocol number 2024-004.

6.5.1 Experimental Protocol

Five healthy volunteers, all students from the academic community with no history of muscular or joint problems, were recruited for this study. All participants were fully informed about the study's objectives and provided written informed consent. Table 16 presents the average and standard deviation of the participants' anthropometric data.

Table 16: Anthropometric data of the subjects - Experiment 3.

Sex	**Amount**	**Age**	**IMC**
M	3	24.3 ± 0.9	27.5 ± 3.9
F	2	21.5 ± 0.5	25.2 ± 5.0

For this experiment, in addition to the electrodes and sensors of the wearable system, 21 body markers were placed on the participants for camera tracking. The complete setup, including the positioning of the electrodes, sensors, and markers, can be seen in Figure 83. As observed, the electrodes were placed close to each other due to the relatively small size of the vastus medialis muscle. However, the electrode of the EMG sensor has a smaller diameter than it appears in the Figure 83, with most of the surrounding area composed of adhesive to fix it to the skin. Thus, the distance between the inner part of the electrodes was approximately 2 cm.

The experimental session proposed in this study was considerably more extensive and complex compared to the previous two experiments, encompassing four sets of tasks that involved electrical stimulation and were conducted for the first time on both legs. The first task performed by the participants was the extraction of the static Maximum Voluntary Contraction (MVC). For this purpose, an investigator held the participant's leg using a commercial microFET®2 dynamometer from Hoggan Scientific LLC. With only the CDSS activated, a session was recorded while the participant, seated in a chair, exerted maximum force for at least 3 seconds.

The second, third, and fourth tasks consisted of knee extension exercises under varying conditions. In the second task, the participant performed the exercise 60 times, divided into 6 sets of 10 repetitions, without any stimulation. In the third task, the participant performed the exercise 30 times, divided into 3 sets of 10 repetitions, with the stimulator set to the *Raising the Leg* mode, activated between 15° and 60° during the leg's upward phase. In the fourth task, similar to the third, the participant performed the knee extension exercise 30 times, divided into 3 sets of 10 repetitions, but in this task, the stimulator was set to the *Range of Angle* mode, activated from 60° to the maximum angle. After completing the four tasks

with the right leg, the entire protocol was repeated for the left leg.



Figure 83: Experimental Setup Showing the Positioning of Electrodes, Sensors, and Markers.

Except for the first task, which did not involve the knee extension movement, at the end of each completed set (10 repetitions), the participant answered a brief questionnaire on the mobile app consisting of two quantitative questions using the Visual Analog Scale (0 to 10) about perceived comfort and fatigue. To avoid biases in the results, the order of tasks 3 and 4 was alternated for the left leg. For each participant, the experimental session took approximately 1.5 to 2 hours to complete, including the setup time and the execution of the protocol on both legs.

Experimental Objectives

This experiment has four primary objectives, aiming to deepen the analysis and validation of the CDSS in more complex and realistic scenarios, as well as explore its potential in advanced simulations. The main focus is on comparing established technologies and investigating new possibilities for application in the field of muscle rehabilitation.

The first objective is to conduct a comparative analysis between the CDSS and MoCap to evaluate the effectiveness of the CDSS in capturing the kinematics of the lower body, both with and without the application of electrical stimulation. Until this stage of development, the IMU sensors of the CDSS had only been tested against the UR3 robotic arm under laboratory conditions, which significantly differ from

real-world usage scenarios. By utilizing MoCap, a gold standard in motion capture, this study seeks to obtain more precise and reliable data, providing robust validation for the CDSS.

The second objective is to compare the *Raising the Leg* and *Range of Angle* stimulation modes integrated into the CDSS, which differ from conventional stimulation techniques. Although previous tests with stimulation equipment from the NanoStim project have been conducted, as described by Gonçalves (2023), this is the first experiment where the CDSS utilizes stimulation modes developed explicitly for this system, offering a unique opportunity to assess their effectiveness.

The third objective is to examine muscle fatigue, as previous experiments did. However, in this study, participants also provided subjective feedback on their perception of fatigue during the exercise, allowing for a combined analysis of objective and subjective metrics, which enriches the understanding of the effects of the exercise protocol.

Finally, the fourth objective is to perform simulations using musculoskeletal models in the OpenSim tool based on real data collected from different participants. The motivation behind this objective is to explore the feasibility of creating personalized simulations for each subject using the information acquired by the CDSS. With its ability to simulate a wide range of human muscle movements, OpenSim offers a promising means to optimize future muscle rehabilitation treatments.

6.5.2 Pre-Processing

The data acquired was processed using a series of steps to ensure accuracy and synchronization between the different data collection systems before the comparative analyses. Figure 84 presents a block diagram that illustrates the methodology used in data pre-processing.

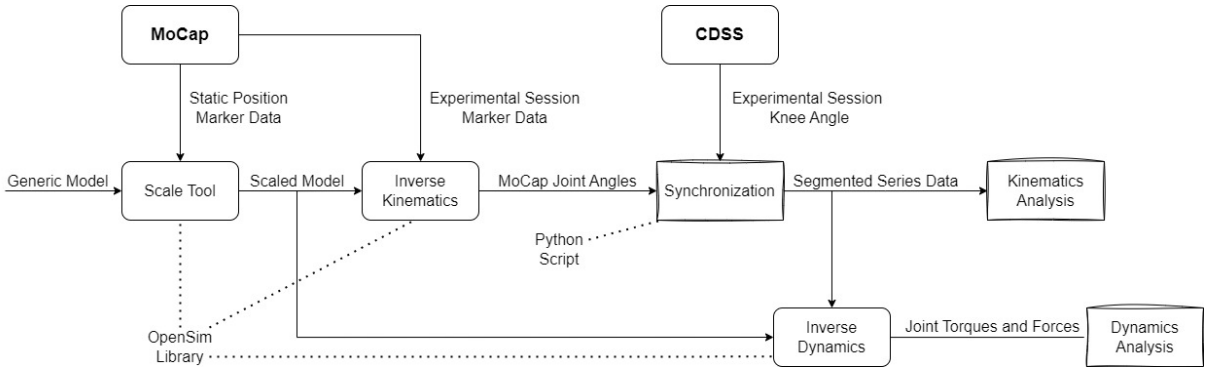


Figure 84: Pre-Processing Methodology.

OpenSim Tool

OpenSim is a powerful open-source software platform used for modeling, simulating, and analyzing musculoskeletal systems. This tool allows the creation of personalized musculoskeletal models that can simulate human movement and calculate the forces and moments exerted by joints and muscles during various physical activities. OpenSim is widely recognized and used in biomechanical and rehabilitation studies because it offers a robust interface for integrating experimental data with detailed anatomical models, enabling precise and personalized analyses (Delp et al., 2007b).

The first step in processing the data was to scale a musculoskeletal model for each participant using the Scale algorithm from the OpenSim tool. This algorithm adjusts a generic model to the individual dimensions of the subjects, based on marker data collected while the participant remained standing for 5 seconds, also known as static position. In this experiment, the generic model used was the Rajagopal2016 Model described by Catelli et al. (2019), which was modified by adding 21 body markers. Figure 85 shows an example of the scaled model generated by the Scale algorithm for one of the participants.

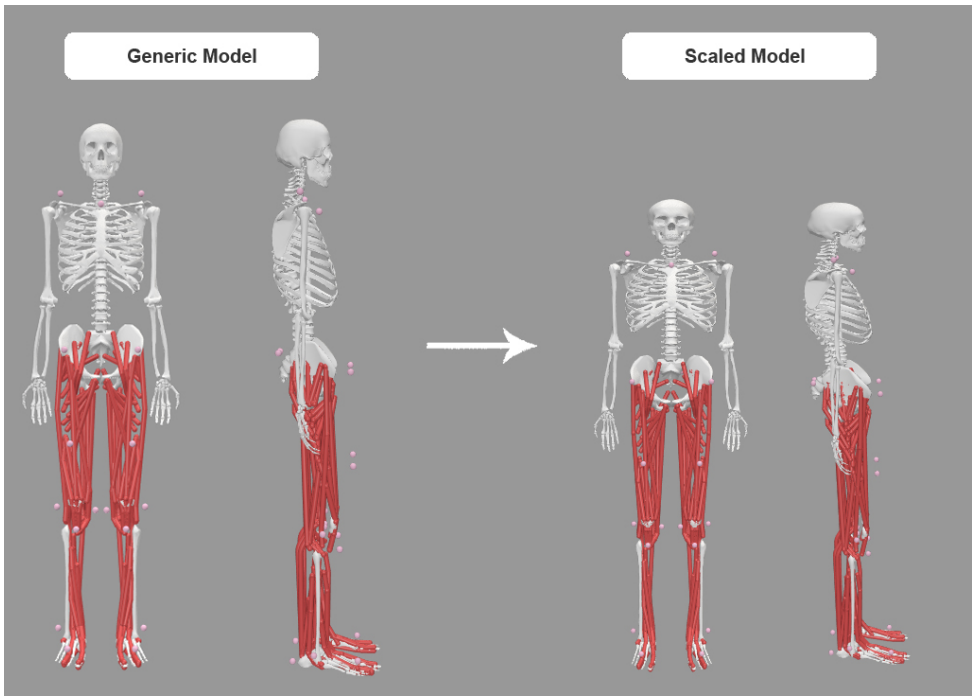


Figure 85: OpenSim Model Scaling.

With the musculoskeletal model properly adjusted, the next step involved applying the Inverse Kinematics algorithm, also available in OpenSim. This algorithm performs a computational calculations using the personalized musculoskeletal model to replicate the trajectory of the markers captured by the MoCap system. This calculations results in a file containing the angular trajectory of all the model's joints through-

out the experimental session. This pre-processing step was unnecessary for the CDSS data, as they were already stored directly as knee angles.

Synchronization

To facilitate synchronization between the two data collection systems, the participants were instructed to tap the floor lightly with their foot three times at the start of data collection. This simple procedure allowed for the manual identification of the corresponding data intervals for these three events in each sample. Subsequently, the *find_peaks* algorithm from the $scipy.signal$ library was used to identify potential synchronization points in the data from both systems.

Due to differences in the sampling frequencies of the systems (100 Hz for the MoCap and approximately 98 Hz for the CDSS), it was necessary to adjust the data to a common frequency of 100 Hz through interpolation. All identified synchronization points were tested, and the point that showed the smallest mean difference between the systems was selected as the synchronization point. From this point, the data was segmented by cycles of repetitions of the knee extension movement. From these segments, a series containing ten movements was defined.

After synchronization, each series of movements captured by the CDSS and MoCap systems was exported to separate files in .mot format, compatible with OpenSim, containing only the corresponding knee angle of the sample. The recognized movement was then analyzed based on this processed data.

An additional step was necessary to analyze the muscular dynamics of the participants during the experiment. Using OpenSim, the Inverse Dynamics algorithm was applied. This algorithm performs a computational simulation that calculates the moments (torques) generated in the joints during the experimental session using the personalized musculoskeletal model and the knee angle data.

6.5.3 Movement Recognition: CDSS vs MoCap

With the data properly processed and synchronized, this section presents a comparative analysis of the kinematics and dynamics obtained by the MoCap system and the CDSS of the participants under the experimental protocol.

Figure 86 illustrates the variation in the duration and maximum angle of contractions recognized by the CDSS for both legs of the participants. It is observed that the average duration of the contractions was approximately 2.5 seconds, with some contractions lasting less than 2 seconds. This shorter duration is due to the fact that the subjects performed the movement continuously, with approximately 1 second for the ascent and 1 second for the descent, without holding the leg at the maximum angle for a prolonged

period, as was done in previous experimental studies.

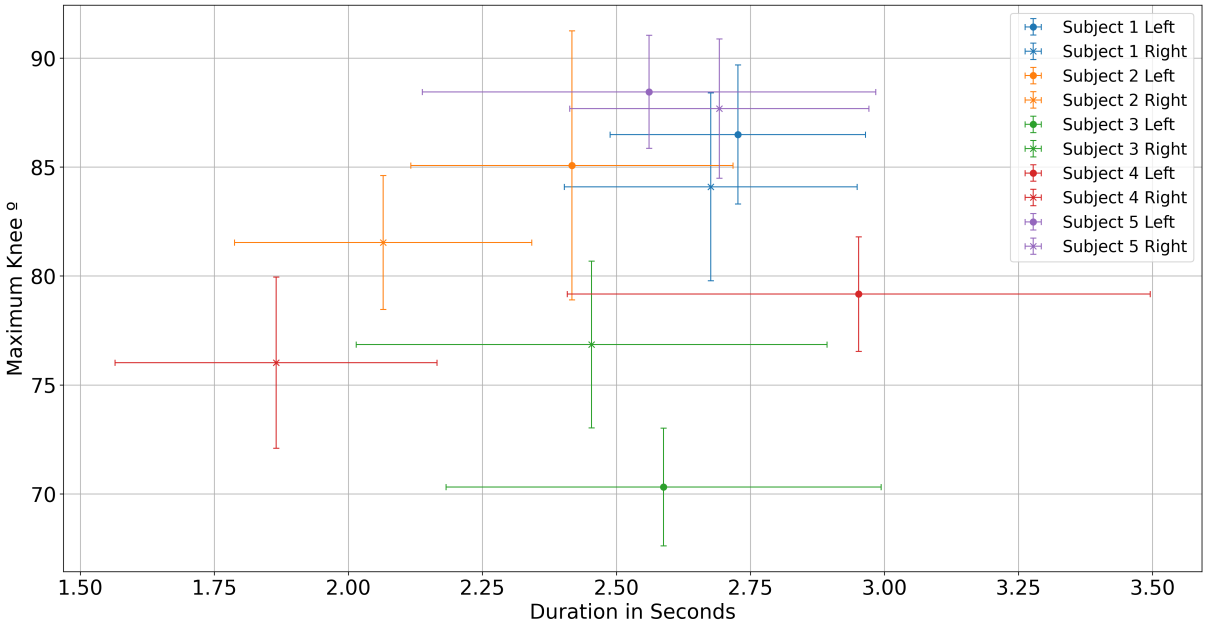


Figure 86: Variation in Maximum Angle and Duration of Knee Extension Movement - Experiment 3.

Regarding the maximum angle achieved, the average across all participants was 82°, with some sessions recording values below 75°. This observation motivated the first comparison between the CDSS and MoCap systems, focusing on the maximum angles recognized, as the issue of sensor IMU positioning deviation was already known. Even after initial calibration, there was still the possibility of differences in the maximum values recorded. Figure 87 presents a box plot of this comparison between the two systems.

As shown in Figure 87, the CDSS displayed a significant disparity compared to the MoCap in obtaining the maximum angle. The average maximum angle recorded by the MoCap was 88.8°, a value very close to the 90°, which is considered the natural limit for this joint in healthy individuals. This difference between the systems indicates the need for an additional adjustment in the CDSS beyond the initial calibration. This adjustment involves defining a reference value for the maximum angle of each participant, which should be clinically measured and regularly updated in the system.

The maximum angle adjustment algorithm was developed with the purpose of minimizing, in real-time, errors caused by slight changes in the positions of IMU sensors. As described in Algorithm 2, a reference value is used, which in this case is defined as 90°, along with calibration data to calculate a scale factor. This scale factor is obtained by subtracting the reference value from the maximum angle recorded during the three calibration contractions.

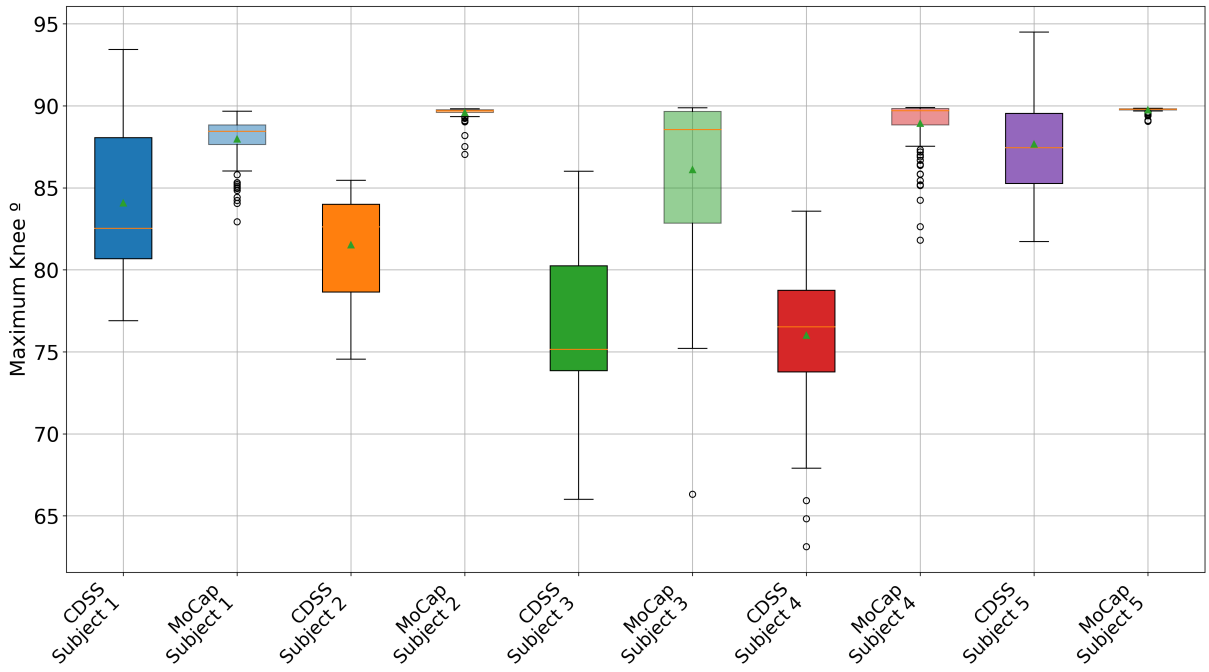


Figure 87: Comparison of Maximum Angle Variation between CDSS and MoCap.

Next, Algorithm 1 was applied to recognize the knee extension movement in the experimental session data. This algorithm returns the start and end points of each contraction within the knee angle vector. With this information, the maximum angle of the contraction is calculated, and two conditions are checked to identify any significant disparity compared to the previously recorded maximum angle. The first condition checks if the angle is 8 degrees lower than the maximum obtained during calibration. The second condition checks if the knee angle is 2 degrees higher than the value established by the physician as the maximum possible. If either of these conditions is true, the scale factor should be recalculated, assuming that there was a repositioning of the IMU sensors.

After applying Algorithm 2, the maximum mean CDSS value was adjusted to 88.1°, significantly closer to the 88.8° recorded by MoCap. The data adjusted will be presented later in this document as "Adjusted CDSS" as well as the new variations of maximum angle illustrated in Figure 88.

As can be observed, the application of Algorithm 2 resulted in the maximum averages for all subjects being adjusted to below 90°, similar to MoCap. Although some points indicate values of 92°, which was the upper limit for the calculation, we understand that an upper range of at least 2° is necessary to account for the natural increase in maximum angle or small reading errors that low-cost sensors, such as IMUs, might present. The standard deviation of the data decreased considerably compared to the unadjusted CDSS data, indicating that the lower adjustment threshold of -8° was also crucial.

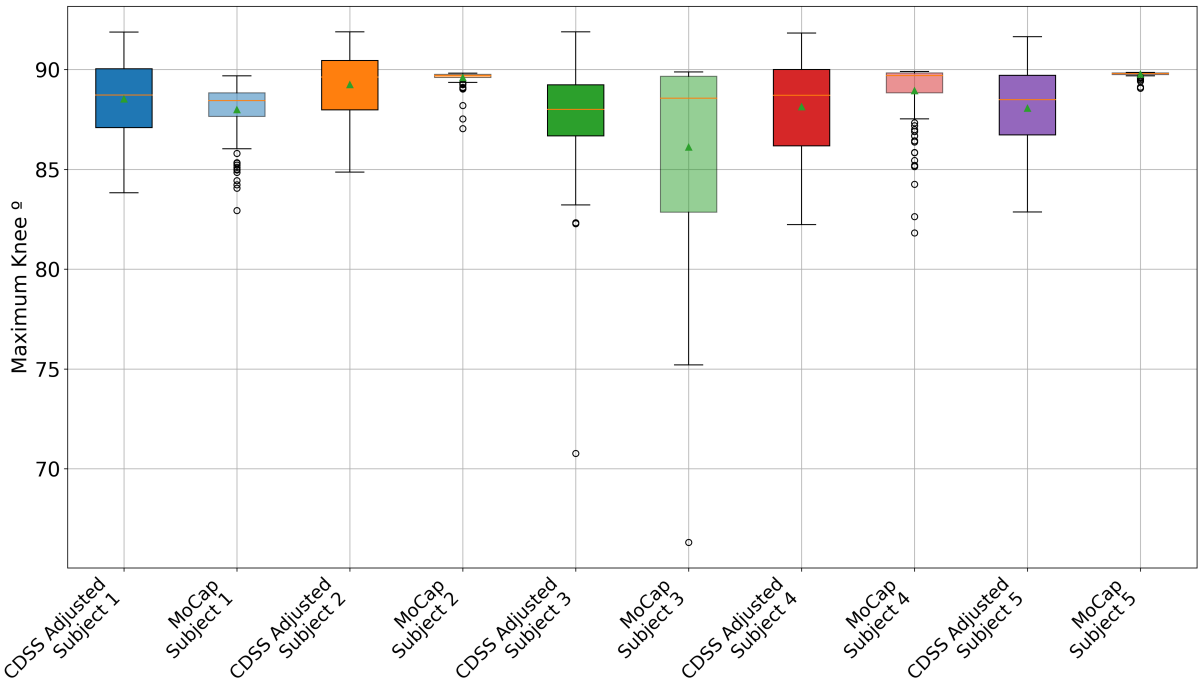


Figure 88: Comparison of Maximum Angle Variation between CDSS Adjusted and MoCap.

Algorithm 2 Knee Angle Adjustment Algorithm.

```
subject_max_angle ← 90
wearable_max_angle ← calibration_max_angle
scale_factor ← subject_max_angle - wearable_max_angle
session_data ← experimental_session_data
contractions ← movement_recognition(session_data)
adjusted_index ← contractions[0][0]                    # Start of the first contraction
session_data_adjusted = session_data[adjusted_index : ] + scale_factor
for (contraction_start, contraction_end) in contractions do
    contraction_max ← max(session_data[contraction_start : contraction_end])
    if abs(wearable_max_angle - contraction_max) > 8 OR
        (contraction_max + scale_factor) > (subject_max_angle + 2) then
        wearable_max_angle ← contraction_max
        scale_factor ← subject_max_angle - wearable_max_angle
    end if
    session_data_adjusted += session_data[adjusted_index : contraction_end] + scale_factor
    adjusted_index = contraction_end
end for
session_data_adjusted += session_data[adjusted_index:] + scale_factor
```

Kinematics

Figure 89 compares the kinematics of the knee extension movement, normalized by the movement cycle for both legs in all tasks of the experiment. The analysis shows that the movement recognized by the system is very similar, allowing for a clear identification of the phases of the knee extension movement. Additionally, it is observed that the standard deviation of the left leg data was smaller, suggesting that the movement was more uniform in this leg compared to the right.

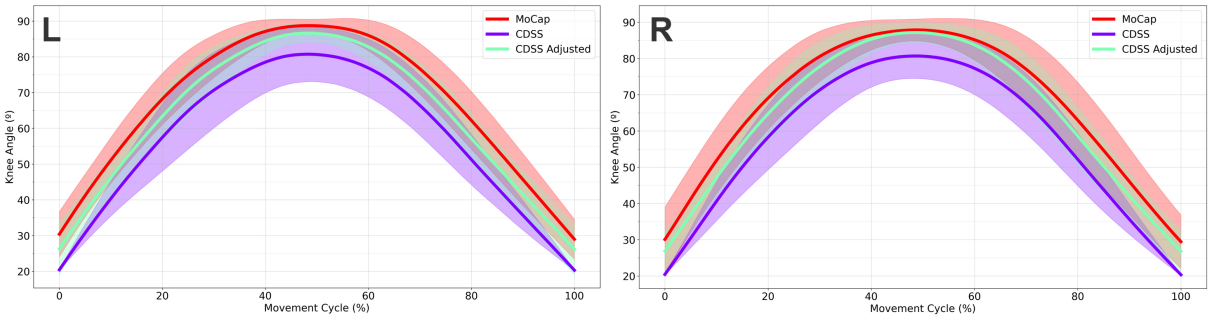


Figure 89: Kinematic Comparison of Movement between the systems.

CDSS Adjusted data shows a significant improvement in the accuracy of the knee angle scale, bringing the CDSS results closer to those of the MoCap. For the left leg, the corrected data presented a greater alignment with the MoCap throughout the entire movement cycle, while for the right leg, the most significant differences occurred at the beginning of the movement, with a convergence of values at the end.

In order to promote a quantitative analysis of the kinematics obtained between the systems, Table 17 presents the evaluation metrics.

Table 17: Kinematic Evaluation Metrics Comparison.

	Max	**MAE**	**STD**	**RMSE**	**MSE**
CDSS vs Mocap - Left	10.95	9.73	0.93	9.77	95.60
CDSS Adjusted vs MoCap - Left	5.06	3.84	0.93	3.95	15.63
CDSS vs Mocap - Right	11.25	9.42	1.37	9.52	90.70
CDSS Adjusted vs MoCap - Right	4.78	2.95	1.37	3.26	10.62

Table 17 reveals that CDSS Adjusted significantly reduced errors compared to the original CDSS. The maximum error value for the left leg decreased from 10.95° to 5.06°, and the MAE decreased from 9.73° to 3.84°. The RMSE also showed a significant reduction, dropping from 9.77° to 3.95°. Similar results

were observed for the right leg, confirming that the scaling adjustment effectively improved the accuracy of the angles recognized by the CDSS.

Dynamics

The dynamic analysis of the movement was performed using the results of Inverse Dynamics algorithm from OpenSim tool, which calculated the joint moments in Mili Newton based on the kinematic data. Figure 90 presents the trajectory of the knee moment, normalized by the movement cycle, considering all tasks of Experiment 3.

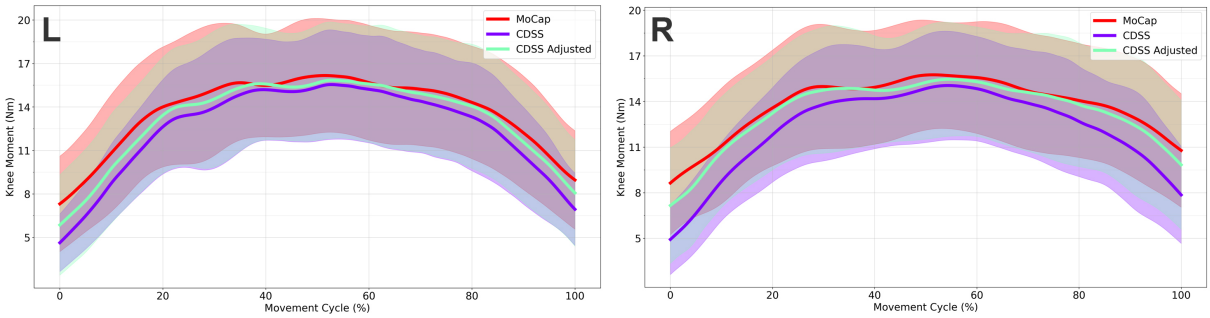


Figure 90: Dynamic Comparison of Movement between the systems.

The results indicate that both systems, CDSS and MoCap, produced similar trajectories for the knee moment, although with some differences in scale. It was observed that the right leg data showed a larger standard deviation, suggesting greater variability in the movements of this leg. However, when the CDSS Adjusted data was considered, the trajectories were more aligned with the MoCap values, showing greater consistency.

Analogous to the kinematics analysis, Table 18 presents the evaluation metrics of the joint moments calculated between the systems.

Table 18: Dynamic Evaluation Metrics Comparation.

	Max	**MAE**	**STD**	**RMSE**	**MSE**
CDSS vs Mocap - Left	2.68	1.20	0.61	1.35	1.83
CDSS Adjusted vs MoCap - Left	1.45	0.53	0.37	0.65	0.42
CDSS vs Mocap - Right	3.71	1.52	0.81	1.72	2.98
CDSS Adjusted vs MoCap - Right	1.50	0.41	0.31	0.51	0.26

The results in Table 18 show that CDSS presented minor variations compared to MoCap, which are

expected due to differences between the systems. For the left leg, the maximum error was 2.68 Nm, with a MAE of 1.20 Nm and an RMSE of 1.35 Nm. For the right leg, these values were slightly higher, with a maximum error of 3.71 Nm, MAE of 1.52 Nm, and RMSE of 1.72 Nm. Despite these differences, the values remain within an acceptable range for dynamic analyses.

With the application of the scaling adjustment in CDSS Adjusted, these variations were further reduced. For the left leg, the maximum error was reduced to 1.45 Nm, the MAE to 0.53 Nm, and the RMSE to 0.65 Nm. For the right leg, the maximum error decreased to 1.50 Nm, the MAE to 0.41 Nm, and the RMSE to 0.51 Nm. These improvements indicate that the adjustment applied to the CDSS not only enhanced kinematic accuracy but also strengthened dynamic accuracy, making CDSS Adjusted highly comparable to the gold standard established by MoCap.

Finally, to validate the use of the data in musculoskeletal simulations, a statistical analysis was performed on the correlations between the CDSS and MoCap data. Due to the non-normal distribution of the data, verified by the Shapiro-Wilk test, Spearman's correlation coefficient was used. This test is appropriate for data that do not follow a normal distribution and measures the strength and direction of the association between two ranked variables.

The statistical analysis yielded a Spearman's correlation coefficient of $r_s = 0.999$ for the left and right knee angles. For the joint moments, the correlations were $r_s = 0.985$ for the left leg and $r_s = 0.988$ for the right leg. These values indicate strongly positive correlations, suggesting that CDSS data are highly consistent with those of the MoCap. This confirms the feasibility of using these data in advanced musculoskeletal simulations, providing a solid foundation for future CDSS applications in clinical and research settings.

6.5.4 Comparison between Stimulation Modes

The comparison between the *Raising the Leg* and *Range of Angle* stimulation modes implemented in the CDSS aims to evaluate the precision of real-time controlled electrostimulation based on knee angles. Unlike commercial stimulators, which apply stimuli configured by time cycle, the modes developed in the CDSS use readings from IMU sensors, adjusting the stimulation signal according to joint movement in real-time.

The wearable system automatically logs the knee angles at the start and end of stimulation, allowing verification of whether the application follows the defined parameters. Figure 91 presents a box plot showing the start and end angles of stimulation for both modes, in both legs of the participants.

In the *Raising the Leg* mode, the stimulation was programmed to begin at 15° of knee angle and end at 60°. As shown in Figure 91, the stimulation started as expected, with no values below 15°, with a small

average delay of 0.4° and a maximum of 1.4°. The stimulation ended at an average of 61°, with a delay of up to 4°.

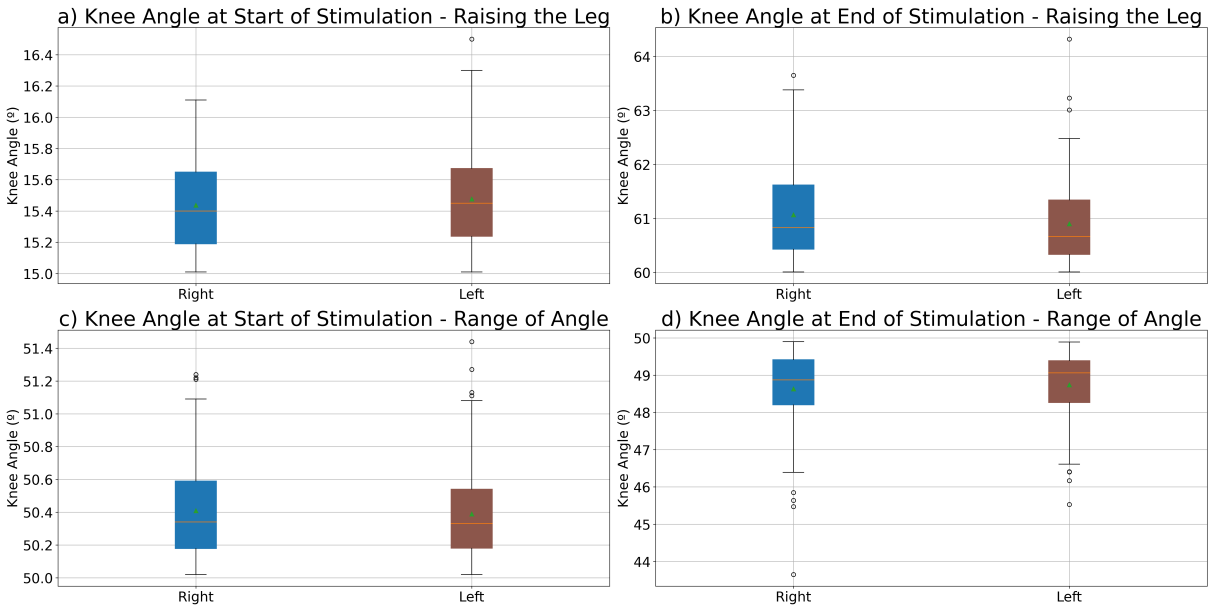


Figure 91: Knee angle at the start and end of stimulation modes..

In the *Range of Angle* mode, the stimulation was set to activate above 50°, without a defined upper limit, meaning the stimulation remained active at all angles above 50°. The average error at the start of stimulation was 0.4°, with maximum variations of 1.4°, and the end of stimulation showed delays of up to 4°, a pattern similar to founded in the first mode. The difference between the average errors at the start and end of stimulation can be explained by two main hypotheses. First, the downward movement of the leg is generally faster than the upward movement, which could lead to a delay in reading the angle when stopping the stimulus. The second hypothesis, and perhaps more pertinent, is the fact that the wearable system's processor has an additional task (the stimulation itself), which may introduce a greater delay in processing the angle reading.

In addition to the CDSS records, the EMG signal was analyzed to validate whether the stimulation modes were executed as intended. In Figure 92, the EMG signal is synchronized with the knee angle for the *Raising the Leg* stimulation mode, both normalized by the contraction cycle. In this mode, it is clear that the EMG signal increases only during the leg elevation phase and decreases significantly upon reaching approximately 60°, as expected.

Similarly, Figure 93 shows the EMG signal synchronized with the knee angle and normalized by the movement cycle for the *Range of Angle* stimulation mode. In this case, the EMG signal behaves differently from what was observed in Figure 92. The EMG signal gradually increases during the leg elevation phase

and after the knee reaches the 60° angle it remains at its maximum until the same angle is reached again during the lowering phase, confirming that the CDSS applied the stimulations as described in the protocol.

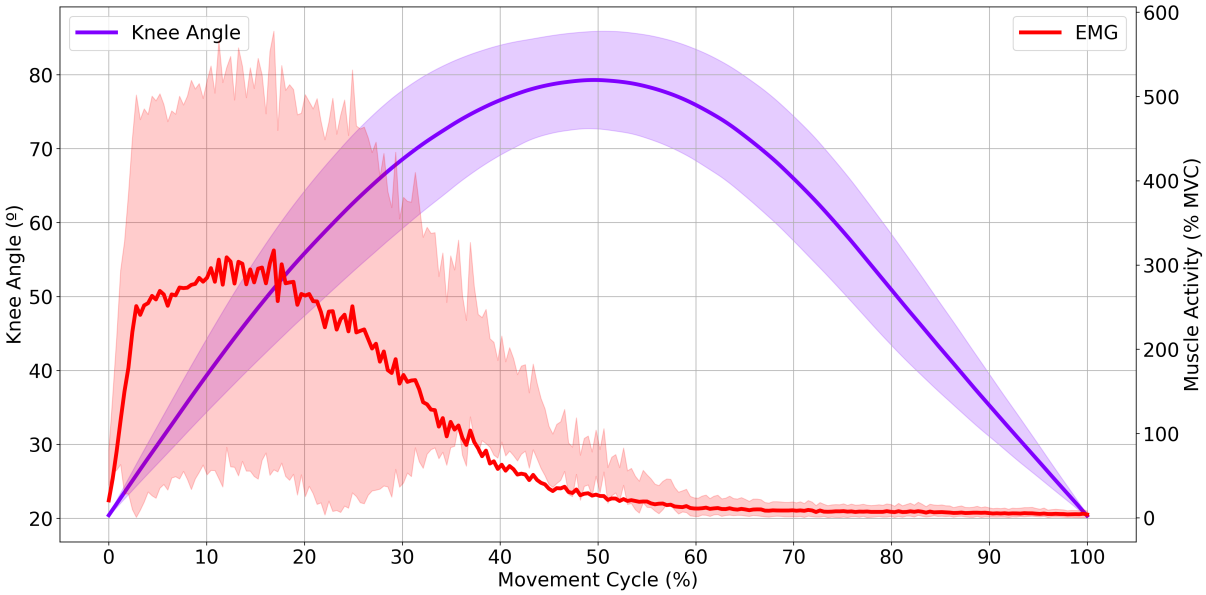


Figure 92: EMG signal during *Raising the Leg* stimulation.

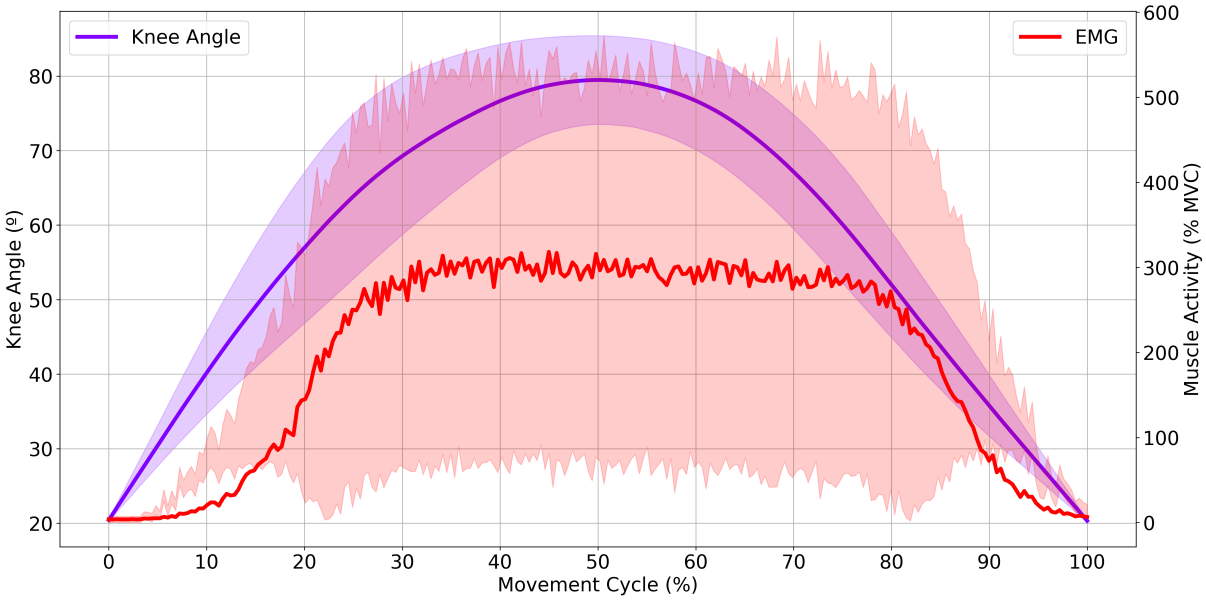


Figure 93: EMG signal during *Range of Angle* stimulation.

Self-Reported Feedback

As described in the protocol for this experimental study, after each series, participants were asked to answer two questions in the mobile app regarding their perceived comfort and fatigue using a 10-point

visual analog scale. For sessions without stimulation, participants completed 6 series per leg, while for sessions with stimulation, 3 series per leg were conducted.

The self-reported data indicate that participants did not experience high levels of fatigue, with the maximum recorded score being 6, reported by only one participant. Most participants rated their fatigue levels between 1 and 2, suggesting that although some experienced an increase in fatigue, none reached a state of exhaustion. Figure 94 shows the average variation in self-reported feedback from the first (green) to the last (red) response in each type of session.

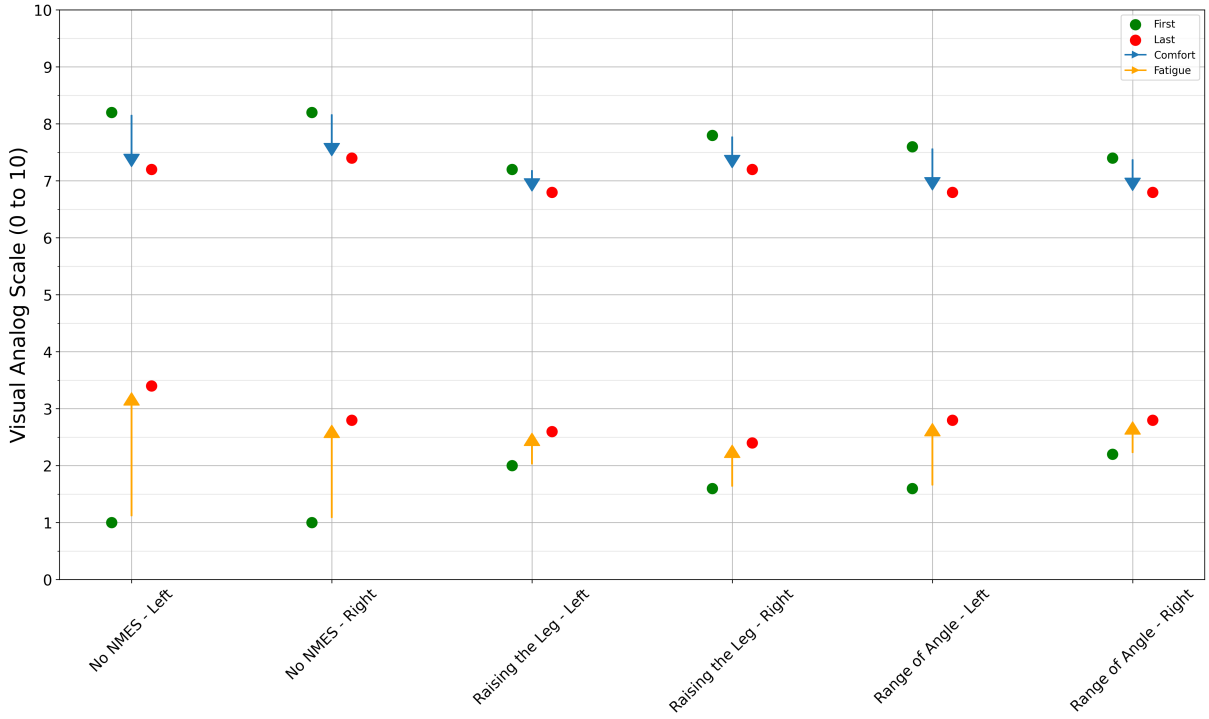


Figure 94: Self-Reported Feedback of Experiment 3.

As expected, the greatest variation in perceived fatigue was observed in the sessions without electrical stimulation, with a higher perception of fatigue in the left leg compared to the right. This is likely due to most participants having their right leg as their dominant leg, which may have made the left leg more prone to fatigue.

When comparing the stimulation modes, it can be observed that the *Raising the Leg* mode showed a lower average final fatigue level compared to the *Range of Angle* mode. However, in the initial sessions of the *Raising the Leg* mode, the perceived fatigue was slightly higher than in the *Range of Angle* mode, particularly in the left leg. This pattern did not occur in the right leg.

This difference may be related to the order of the sessions, as all participants performed the *Raising the Leg* mode first with the right leg and the *Range of Angle* mode first with the left leg. This trend becomes

clearer when observing that the initial fatigue in each leg's activities tends to increase progressively. To mitigate this bias, Table 19 presents the average variation in fatigue and comfort across the sessions.

Table 19: Average Variation in Fatigue and Comfort Across Experimental Sessions.

	Delta Fatigue	**Delta Comfort**
No NMES - Left	2.4	-1.0
No NMES - Right	1.8	-0.8
Raising the Leg - Left	0.6	-0.4
Raising the Leg - Right	0.8	-0.6
Range of Angle - Left	1.2	-0.8
Range of Angle - Right	0.6	-0.6

The analysis of the table reveals that the highest fatigue variation occurred in the sessions without electrical stimulation, with an increase of 2.4 points in the left leg and 1.8 points in the right leg. This supports the hypothesis that the left leg, being less dominant for most participants, tends to experience more fatigue. In terms of comfort, there was a slight decrease in the non-stimulation sessions, with a drop of 1.0 point in the left leg and 0.8 in the right, indicating a mild increase in discomfort over the course.

When comparing the stimulation modes, *Raising the Leg* showed less variation in fatigue compared to *Range of Angle*, especially in the left leg with the double of variation. This pattern suggests that although participants experienced slightly more fatigue in the *Range of Angle* mode, discomfort remained relatively low in both modes, with an average reduction in comfort of 0.4 to 0.8 points. These results indicate that while participants reported greater fatigue in the left leg, the *Raising the Leg* mode was slightly more comfortable and induced less fatigue than the *Range of Angle* mode.

Stimulation Noise in the EMG signal

The next step in the proposed analysis was to apply the knowledge gained from the first experimental study to clean the EMG signal by removing stimulation artifacts. However, the noise generated by the stimulator developed in the NanoStim project was significantly higher than the noise analyzed previously, which was caused by the commercial device.

In Figure 95, an example of the stimulation noise captured in the EMG signal during the two stimulation modes is shown. As can be observed, the noise presented is considerably different from that shown in Figure 55, making it impossible to logically separate the stimulation artifacts from the voluntary

muscle activity. As a result, it is not possible to filter the EMG signal from the experimental sessions with electrostimulation, preventing a meaningful analysis of muscle fatigue.

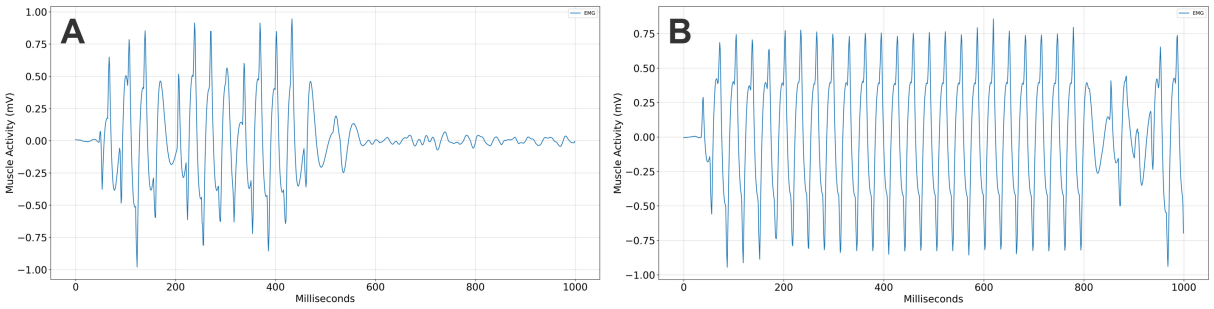


Figure 95: Stimulation Noise in the EMG signal. (A) *Raising the Leg* (B) *Range Of Angle*.

Upon investigating the reasons for the higher noise level and its difference from the commercial device, it was found that the issue is caused by the electronic components responsible for generating the stimulation pulses. Because the EMG acquisition circuit, which uses the analog-to-digital conversion of the ESP32, is soldered on the same PCB as the stimulation circuit without proper isolation, significant interference occurs.

To overcome this problem, it is necessary to develop a new PCB that adequately separates the two circuits to avoid interference. One possible solution is to convert the analog signals to digital immediately after they are read, using a dedicated AD converter. This would prevent interference until the data reaches the ESP32 microcontroller.

6.5.5 Muscle Fatigue Evaluation

In this subsection, the data analysis from the final experiment focused on evaluating muscle fatigue using the EMG signal collected by CDSS. The main objective is to investigate how muscle activity changed throughout the experimental session and to identify patterns related to muscle recruitment and fatigue.

In order to produce a more accurate comparison between participants, the EMG signal was normalized based on each individual's Maximum Voluntary Contraction and adjusted according to the knee extension movement cycle.

Figure 96 shows the muscle activity recorded in both legs of the participants during the experiment. By analyzing the data, it was observed that the right leg exhibited higher muscle activity compared to the left leg. At first glance, this finding seems to contradict the subjective data previously reported, where participants indicated greater difficulty performing exercises with the left leg.

To further explore this potential discrepancy and assess changes in muscle recruitment over time,

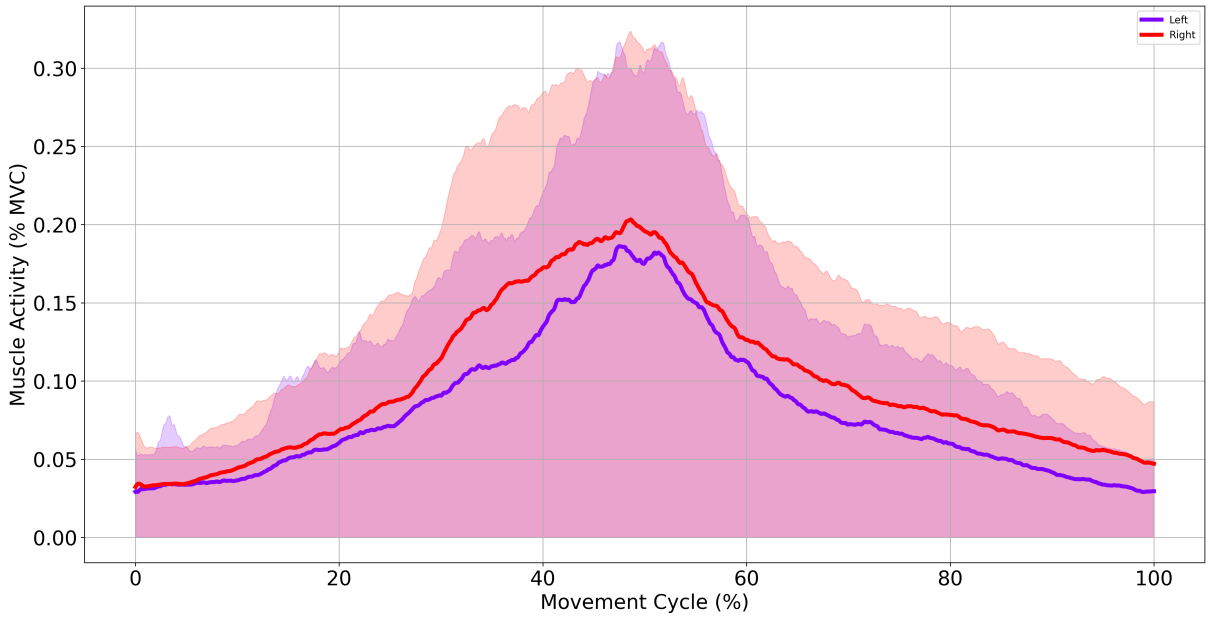


Figure 96: Muscle Activity in Both Legs - Experiment 3.

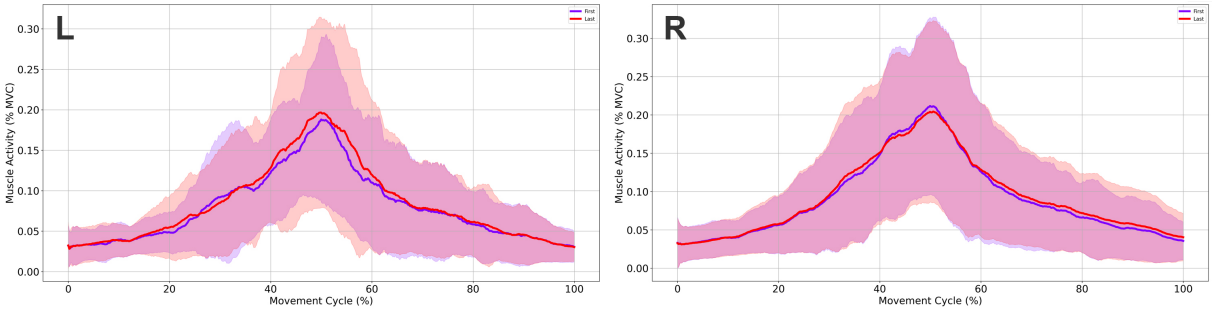


Figure 97: Muscle Activity Variation During Experimental Sessions in Both Legs - Experiment 3.

Figure 97 illustrates the variation in muscle activity between the beginning and the end of the experimental session without electrical stimulation.

In Figure 97, it can be noted that the average muscle activity in the participants' left leg performed indeed increase throughout the session, suggesting greater muscle recruitment at the end of the experiment. Conversely, this variation was less pronounced in the right leg, indicating that participants generally recruited more of the right muscle from the start. These results suggest that while the right leg showed higher overall muscle activity, the left leg progressively required more effort as the experiment advanced.

Fatigue Metrics

Similar to Experiment 2, the metrics related to muscle fatigue (Mean Frequency, Median Frequency, and RMS) were calculated for each contraction recorded in real-time by CDSS and later stored in the cloud. The results were normalized by each participant's standard deviation, allowing for a clearer analysis of

metric trends throughout the session.

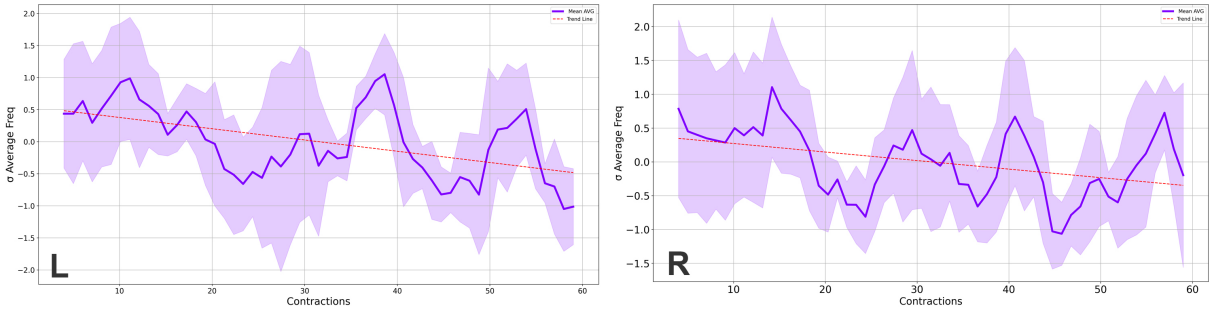


Figure 98: Trend of the Averange Frequency Metric - Experiment 3.

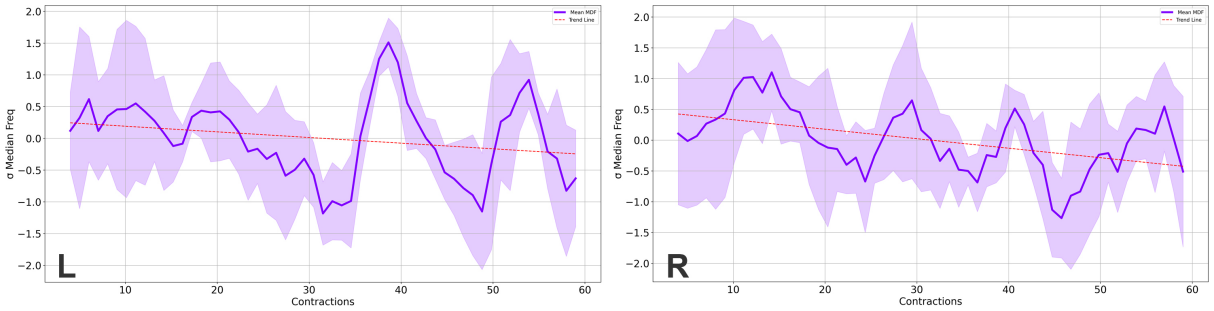


Figure 99: Trend of the Median Frequency Metric - Experiment 3.

In general, the frequency spectrum metrics, illustrated in Figures 98 and 99, showed a declining trend over the course of the experimental session. This is consistent with the downward wave-like behavior observed in Experiment 2. This decline reflects a reduction in the conduction velocity of muscle fibers, which is a characteristic sign of fatigue or adaptation to exercise.

The behavior of the Mean Frequency (avgFreq) and Median Frequency (MedFreq) metrics is quite similar, with a few subtle differences. First, the standard deviation of avgFreq is slightly higher than that of MedFreq in both legs. Additionally, the decline in avgFreq is steeper in the left leg compared to the right, whereas for MedFreq, the opposite occurs, with a slightly smaller decline in the left leg compared to the right.

Figure 100 illustrates the trajectory of RMS metric throughout the experimental session. Here, a contrasting behavior between the two legs can be observed: the left leg shows a positive slope, while the right leg shows a slight negative slope.

This difference suggests that participants experienced more fatigue in the left leg, requiring increased muscle recruitment as the session progressed. Given that the movement remained uniform throughout the session, the right leg data indicate that participants were able to control the exercise and even reduce muscle intensity over time.

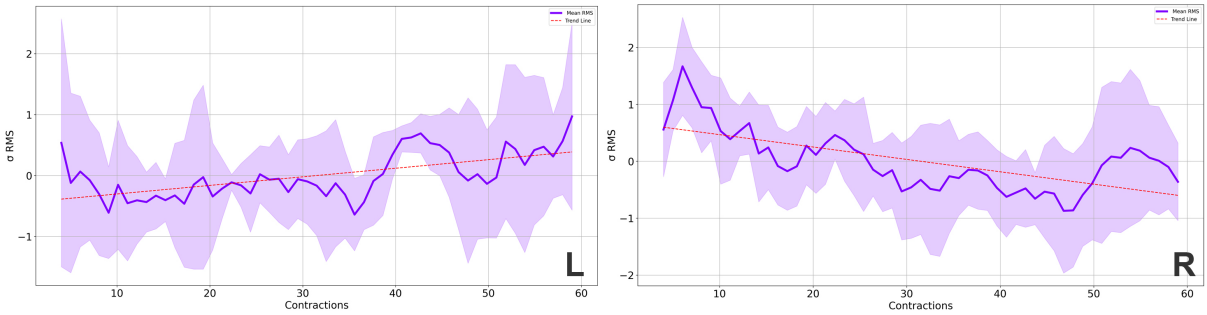


Figure 100: Trend of the RMS Metric - Experiment 3.

To provide a more detailed understanding of the behavior of MedFreq and RMS metrics in conjunction, the Joint Amplitude and Spectrum Analysis (JASA) method was applied. This method allows each contraction to be classified into four distinct physiological scenarios: increased muscle strength (Q1), recovery from fatigue (Q2), reduced muscle strength (Q3), and muscle fatigue (Q4). Figure 101 illustrates the application of the JASA method on the recognized contractions of both legs in Experiment 3. The points are color-coded in a gradient from red (early contractions) to green (later contractions).

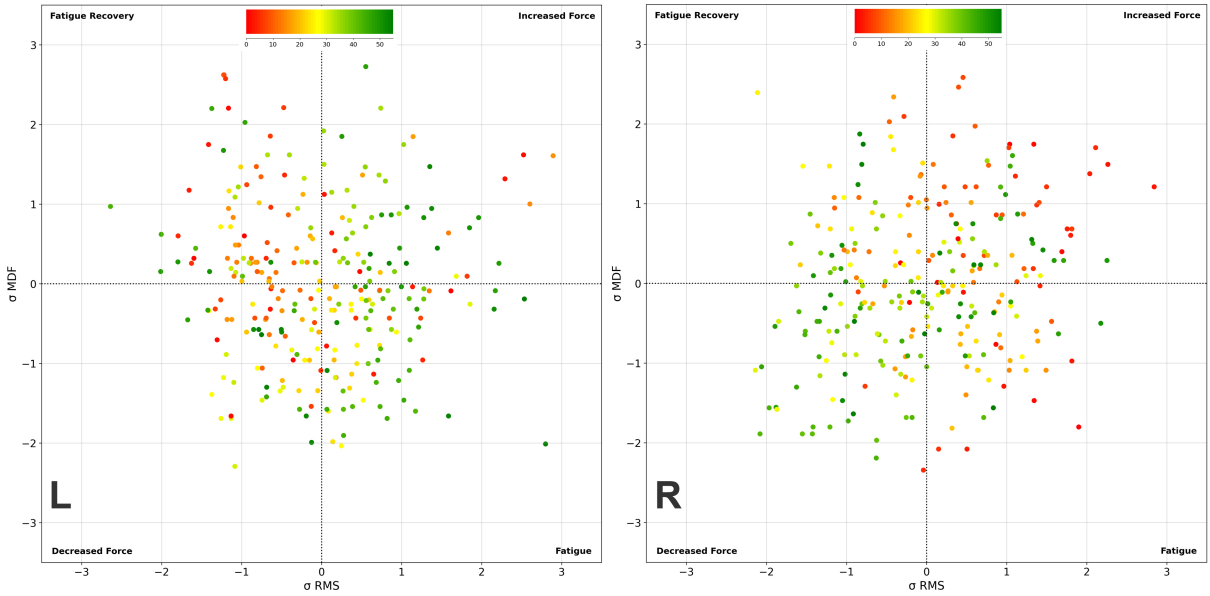


Figure 101: Joint Amplitude and Spectrum Analysis (JASA) - Experiment 3.

In the left leg, the JASA analysis reveals that most of the early contractions are found in quadrants Q2 (recovery from fatigue) and Q3 (reduction in muscle strength), suggesting that the muscles were adapting well to the exercise. However, as the session progressed, the points began to migrate toward quadrants Q1 and Q4, indicating increased strength and muscle fatigue in the final contractions.

On the other hand, in the right leg, most of the contractions from the middle to the end of the session were classified in quadrant Q3, related to reduced muscle strength. This suggests that participants main-

tained control of the movement with the right leg and reduced muscle activity to sustain the movement throughout the experimental session.

6.5.6 Fatigue Level Simulator vs Self-Report Feedback

The final analysis of Experiment 3 expands on the findings of Experiment 2, deepening the understanding of the behavior of the muscle fatigue level simulator. In this study, the focus is on analyzing the parametrization of the simulator and evaluating how it responds when applied to new experimental conditions and both legs. The central idea remains to precisely adjust the parameters so that the simulator individually adapts to each participant, using real-time fatigue metrics captured by CDSS as the basis.

In Experiment 3, in addition to using objective fatigue metrics, we conducted a direct comparison with participants' subjective feedback (self-report) in an effort to validate the simulator. Although the number of participants is still limited, this stage represents a significant advance in the ability to correlate personal perceptions of fatigue with the levels of fatigue detected by the simulator.

In this context, the simulator uses three main parameters, as detailed earlier. The first parameter (S) defines when the simulator starts counting occurrences of fatigue, eliminating possible initial muscle adaptations. The second parameter (F) refers to the number of fatigue occurrences required to change the level, and the third parameter (M) establishes the minimum intensity that an occurrence must have to be recorded as valid.

Based on previous results, in Experiment 3 we tested the same parameter combinations: $S = [5, 10, 20]$, $M = [1, 2, 3]$, and $F = [2, 3, 4]$, resulting in 27 different configurations. These configurations were applied to each session of each participant, generating the data analyzed below.

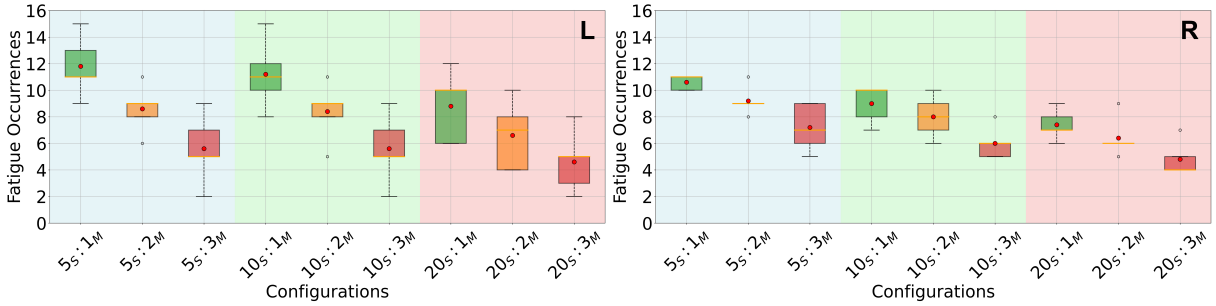


Figure 102: Fatigue Occurrences by Configuration in Both Legs - Experiment 3.

Figure 102 illustrates the number of fatigue occurrences considered in each configuration for both legs. It is observed that the variation of parameter M significantly impacts the number of occurrences in this experiment. In some cases, the average number of occurrences per participant increased by up to 4

when M was raised from 1 to 2. This variation indicates that the definition of parameter M substantially affects the number of occurrences recorded by the simulator and, consequently the level archived.

When comparing the right leg to the left leg, it is noted that for M values greater than 1, the average number of occurrences is quite similar for both legs. However, the left leg shows more significant variation in the number of occurrences than the right leg. This suggests that, despite similar averages, the left leg may experience more pronounced oscillations in fatigue.

In comparison with data from Experiment 2, participants in Experiment 3 exhibited a higher number of fatigue occurrences, with an average of 3 more occurrences for configurations where $M < 3$, considering the right leg results. This increase in the number of occurrences may indicate a greater sensitivity of the simulator in detecting fatigue under the new experimental conditions.

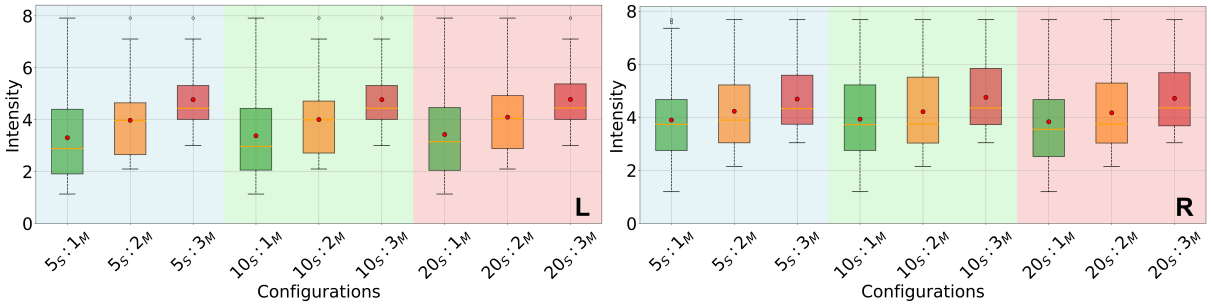


Figure 103: Intensity of Occurrences by Configuration in Both Legs - Experiment 3.

Figure 103 complements this analysis by displaying the average intensity of occurrences for each configuration. The results show that the average intensities were similar between the two legs, with slightly higher values in the right leg. This suggests that while fatigue intensity was similar for both legs, the left leg showed a higher number of occurrences with lower intensity throughout the session.

Figures 104 and 105 display the fatigue levels reached by participants, considering different numbers of occurrences required for a level change, for the left and right legs, respectively. Analyzing the charts, it becomes evident that the fatigue levels reached by the left leg were generally higher and showed more variation among participants compared to the right leg.

In the right leg, several configurations do not show a full boxplot, meaning that the mean and median were identical, indicating that almost all participants reached the same fatigue level. When compared to the data from Experiment 2, the fatigue levels in Experiment 3 were generally higher, supporting the hypothesis that participants in this experiment experienced more fatigue during the sessions.

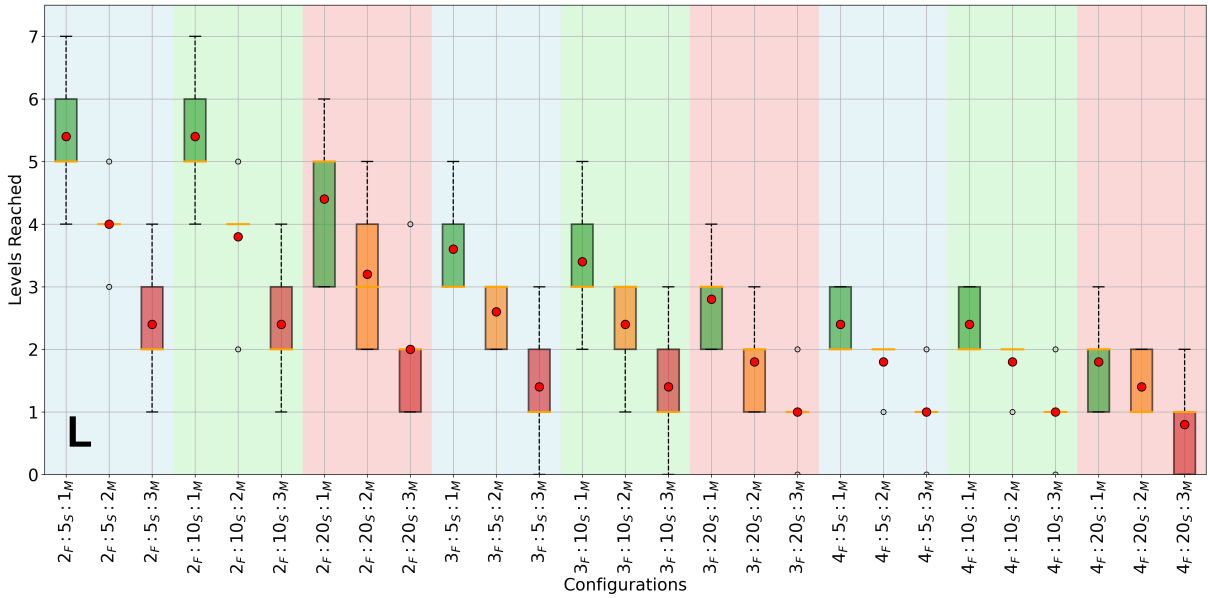


Figure 104: Fatigue Levels Achieved by Configuration on the Left Leg - Experiment 3.

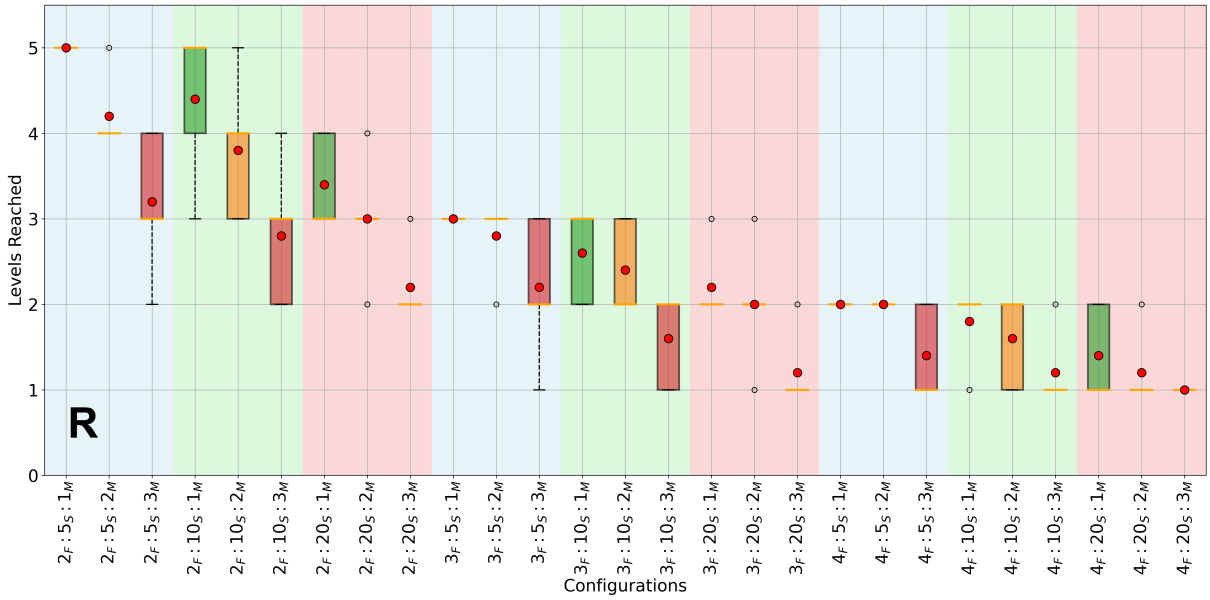


Figure 105: Fatigue Levels Achieved by Configuration on the Right Leg - Experiment 3.

The moment when each participant reached their first level of fatigue was also analyzed, as illustrated in Figures 106 and 107 for the left and right legs, respectively. The comparative analysis between the two legs reveals a significant difference in fatigue behavior. In the right leg, participants exhibited more instances of fatigue early in the session, suggesting faster muscular adaptation to the exercise. This could indicate that the right leg required greater initial effort to adjust to the movement, leading to an earlier muscular response, reflected in the first levels of fatigue.

On the other hand, the left leg showed more uniform behavior. The variation of parameter S, which defines when the simulator starts detecting fatigue, did not have a significant impact on the timing of the first level of fatigue. Regardless of high values for S, the first level was consistently reached between contractions 20 and 40. This pattern suggests that, unlike the right leg, the left leg experienced a more gradual difficulty, with fatigue manifesting more consistently and intensely in the middle of the session.

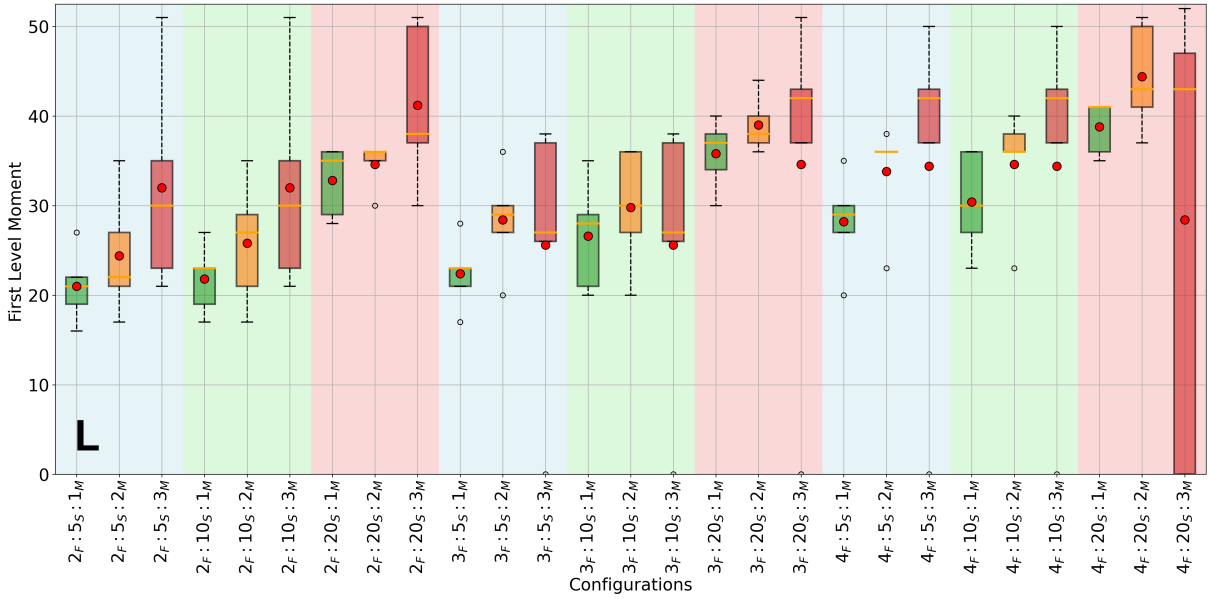


Figure 106: Contraction Number at First Fatigue Level Achieved on the Left Leg - Experiment 3.

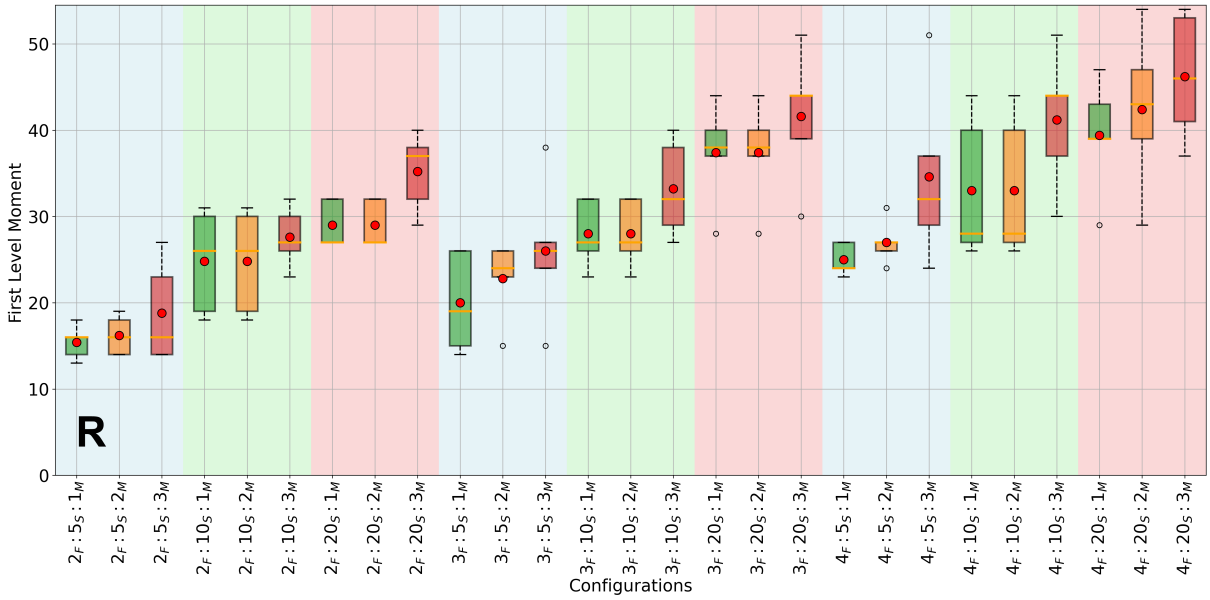


Figure 107: Contraction Number at First Fatigue Level Achieved on the Right Leg - Experiment 3.

Subjects Fatigue Evaluation

The $F = 3$, $S = 10$, and $M = 1$ configuration of the fatigue level simulator, as in experiment 2, proved effective in achieving a balance between sensitivity to muscle effort and the ability to monitor the progression of fatigue among participants. This configuration was chosen for representing a middle ground among the tested variations, allowing for more consistent analysis. Continuing the investigation, this configuration was applied to generate results that will be analyzed individually for each participant, comparing them with the subjective feedback (self-report) provided.

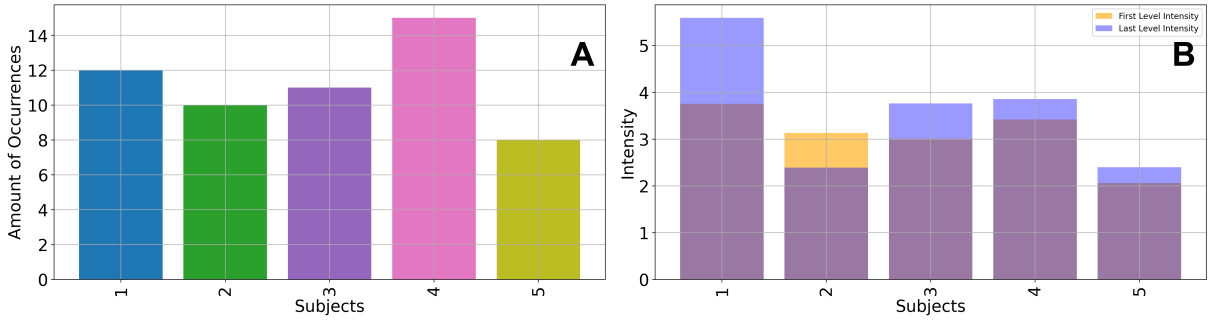


Figure 108: Amount of Fatigue Occurrences (A) and Intensity (B) by Subjects on the Left Leg.

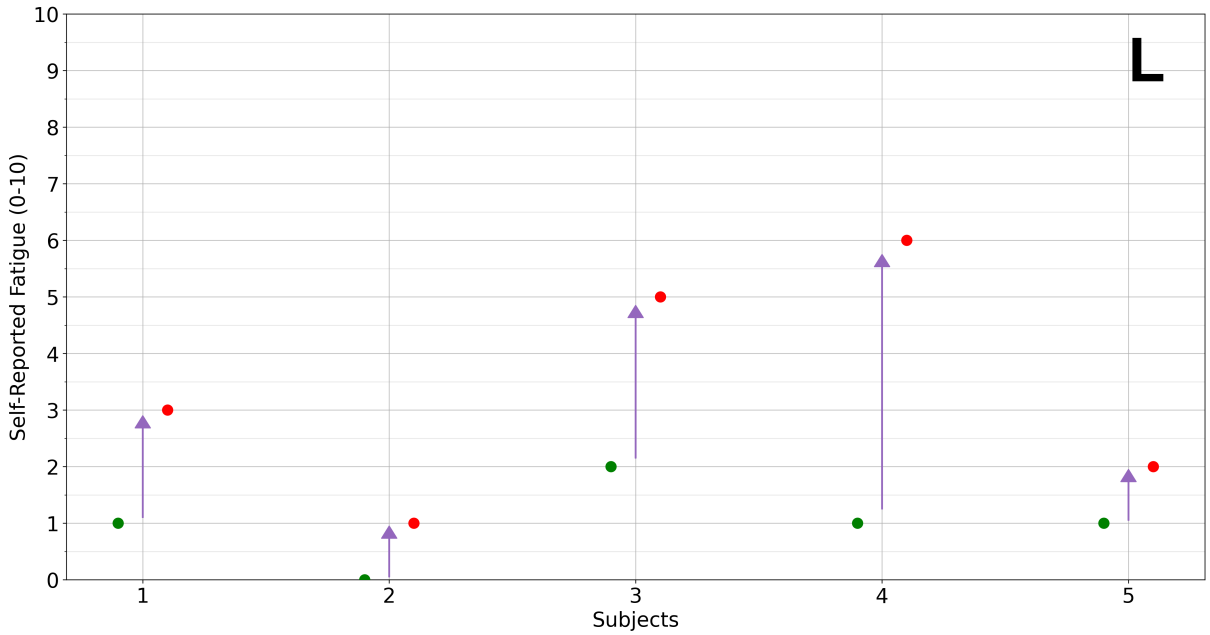


Figure 109: Evolution of Fatigue Perception in the Self-Report on the Left Leg.

In Figure 108A, the number of fatigue occurrences detected for each participant is shown, while Figure 108B presents the intensities of the first and last fatigue level reached for the left leg. It is observed that the participant with the highest number of occurrences was subject 4, recording 14 occurrences, followed

by subjects 1 and 3, with 12 and 10 occurrences, respectively. Subject 4, in addition to having the highest number of occurrences, exhibited one of the highest average fatigue intensities, with a clear increase between the first and last levels, indicating significant fatigue progression throughout the session. Although subject 1 recorded 12 occurrences, they displayed the highest initial and final intensity, suggesting that this participant experienced higher levels of fatigue from the beginning to the end of the session.

Subject 3, with an intermediate number of occurrences (10), showed fatigue intensities similar to subject 4 but with a less pronounced progression. In contrast, subjects 2 and 5 stood out as the most resistant to the exercise with the left leg, registering a lower number of fatigue occurrences. Subject 2, showed a reduction in fatigue intensity at the final level compared to the first, indicating that this participant not only experienced less fatigue but also adapted better to the exercise as the session progressed.

In Figure 109, the subjective feedback on muscle fatigue is illustrated for each participant. The green points indicate the first response, and the red points indicate the last, with the arrow representing the variation in perceived fatigue throughout the session. It is observed that participants 1, 4, and 5 began with a similar perception of fatigue (level 1), but each reported different final levels at the end of the experimental session. Participant 4, for example, reported the greatest increase in the sensation of fatigue by the end of the session, a perception that aligns with the simulator data, which also indicated the highest number of fatigue occurrences for this participant.

Similarly, subject 3, who reported the second-highest level of perceived fatigue, was identified by the simulator as one of those who experienced the most significant progression of fatigue throughout the session. Although subject 1 reported a moderate increase in perceived fatigue, they were also identified by the simulator as one of the most fatigued participants, completing the group of three participants with the highest fatigue levels. In contrast, subject 2 reported the lowest sensation of fatigue among all participants, a result consistent with the simulator data, which showed a lower number of fatigue occurrences and a decrease in intensity over the course of the session.

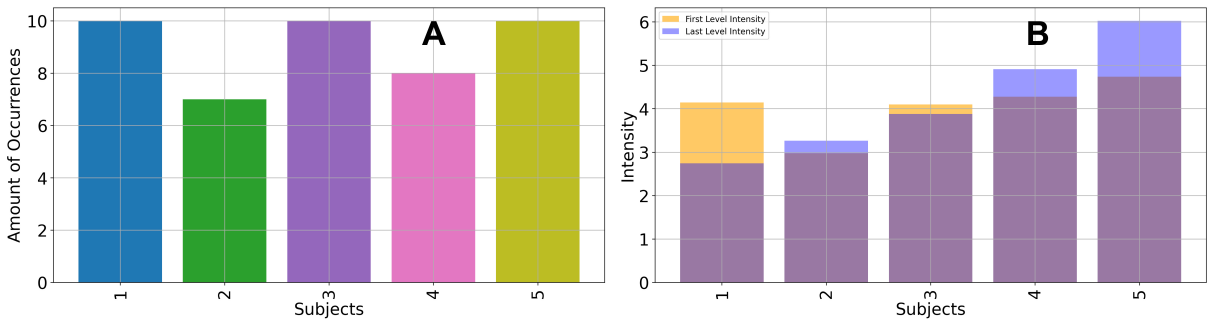


Figure 110: Amount of Fatigue Occurrences (A) and Intensity (B) by Subjects on the Right Leg.

Figure 110 presents the results of the fatigue level simulator for the right leg, using the same configuration ($F = 3$, $S = 10$, $M = 1$) applied in the previous analysis of the left leg. As seen in Figure 110A, the fatigue occurrences were more uniform among participants compared to the left leg. Three participants recorded 10 occurrences, while one participant had 8 and another had 7. This suggests a more balanced muscular response in the right leg across subjects.

In terms of intensity, shown in Figure 110B, the values were slightly higher than those observed in the left leg. However, an interesting point is that two participants had higher initial intensities compared to the final ones, indicating that they faced more difficulty at the beginning of the experiment but adapted throughout the session, resulting in less muscle fatigue by the end.

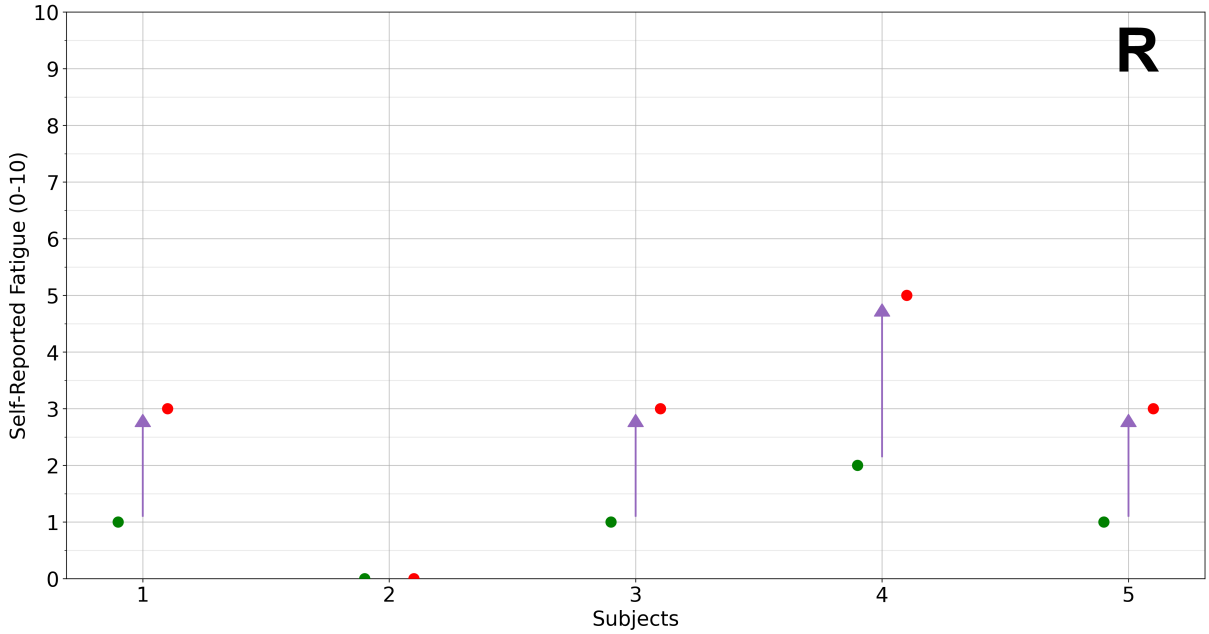


Figure 111: Evolution of Fatigue Perception in the Self-Report on the Right Leg.

Following the same logic, Figure 111 shows the self-reported fatigue feedback from participants during the session for the right leg. Participant 4, as in the left leg analysis, reported the highest perception of fatigue among all. However, when comparing the left leg to the right leg, it is evident that the perceived fatigue was lower in the right leg. Participant 4's fatigue perception increased from 2 to 5 in the left leg, while it varied from 1 to 6 in the right leg. This evidence aligns with the simulator's data, which indicated fewer fatigue occurrences in the right leg (8) compared to the left leg (14).

This consistency in results is also observed in other participants, such as participant 5, who reported a higher perception of fatigue in the right leg, contrary to the others. When analyzing the simulator's results for this participant, it is noticeable that there were 2 more fatigue occurrences in the right leg, and the initial and final intensity levels were significantly higher compared to the left leg, justifying the difference

in subjective feedback.

For participant 2, it is noteworthy that for the right leg, they consistently reported a fatigue level of 0. While it is unlikely that participant 2 experienced no fatigue at all, it is plausible that the fatigue felt was so minimal that it didn't significantly affect their self-reported fatigue index. However, in the left leg, the participant did report some variations in fatigue, indicating that fatigue was more pronounced in that leg. When analyzing the fatigue occurrences for participant 2, we see that there were 3 fewer occurrences in the right leg, with similar intensity levels between both legs, suggesting that these additional occurrences in the left leg likely contributed to the participant feeling more fatigue there.

Fatigue Reported vs Predicted Level

The final analysis conducted with the data from Experiment 3 aimed to evaluate the correlation between the fatigue levels predicted by the CDSS and the self-reported values provided by the participants during the series of each session. Since the fatigue level simulator was configured with a late start of 10 movements, the series analyzed began from the second, corresponding to the point at which the participants had already completed 20 movements.

Figure 112 illustrates the temporal evolution of self-reported and CDSS-predicted fatigue levels for each participant. The dotted lines represent the trend for each data set. A significant correlation is observed between the two sets, with all lines showing positive slopes. However, variations in slope between participants suggest that the perception of fatigue and its progression varied individually. This variability was well captured by the simulator, demonstrating its ability to adjust the level according to each subject's specific responses throughout the sessions.

In order to quantify this correlation, a statistical analysis was performed between the self-reported data and the levels predicted by the CDSS. Initially, the Shapiro-Wilk test was applied to check for data normality. When normality was confirmed for both sets, Pearson correlation was used to measure the linear relationship between the variables. Otherwise, the Spearman correlation was applied, which is more suitable for data that do not follow a normal distribution.

The interpretation of correlation strength followed the classification by Schober et al. (2018), where coefficients between 0 and 0.1 indicate negligible correlation, 0.1 to 0.39 indicate weak correlation, 0.4 to 0.69 moderate, 0.7 to 0.89 strong, and 0.9 to 1 very strong. A p-value below 0.05 was adopted for statistical significance, indicating that the probability of the result being due to chance is less than 5%.

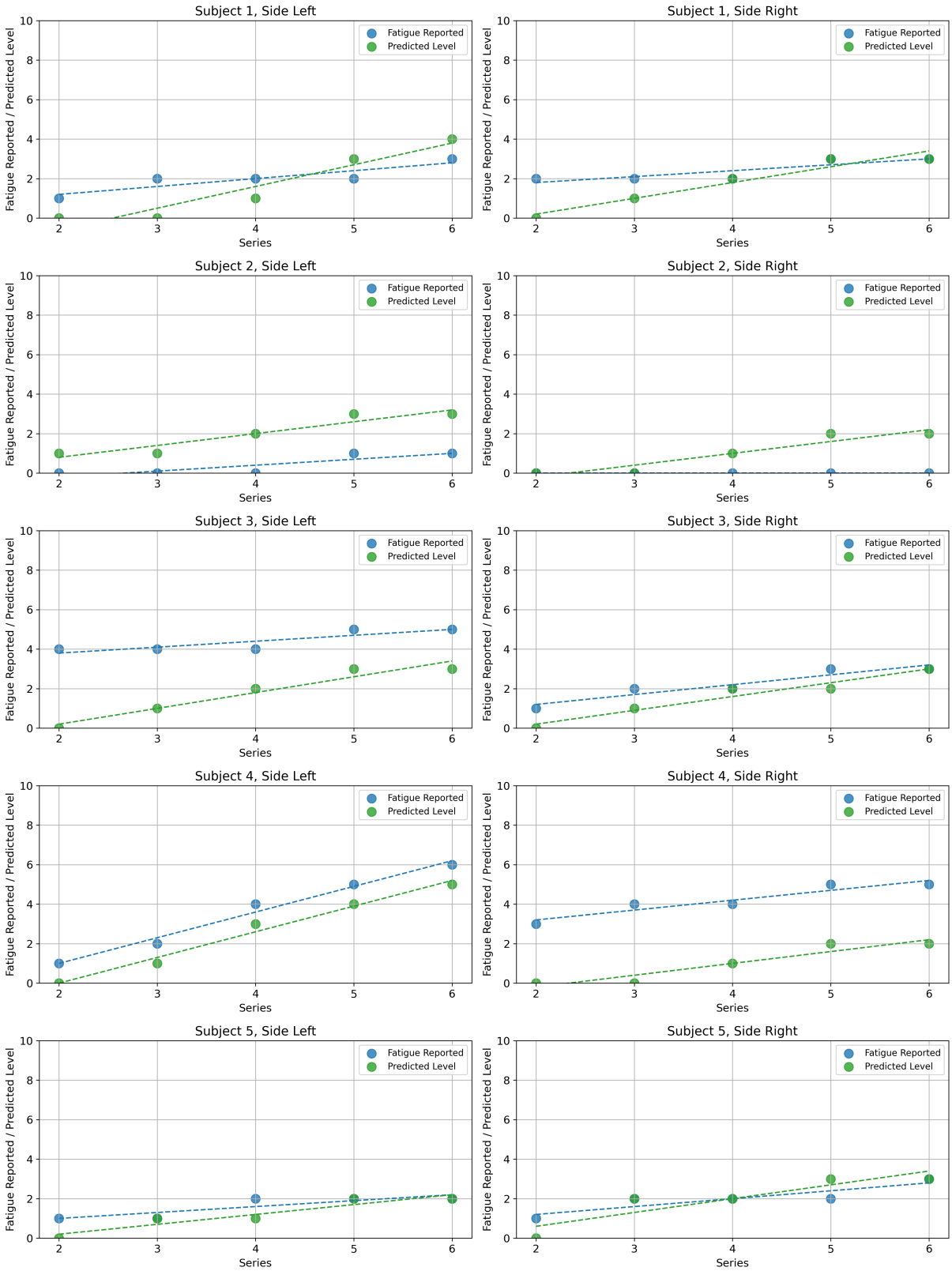


Figure 112: Comparison of self-report fatigue with predicted level by subject.

The correlations for each session of Experiment 3 are shown in Table 20. Except for subject 2, whose feedback remained constant, preventing correlation analysis, all other participants demonstrated strong

correlations between the predicted level and reported fatigue. Additionally, the correlation coefficients had an average of 0.868 $\pm$ 0.099 for the left leg and an average of 0.886 $\pm$ 0.013 for the right leg across participants. These average values are close to a very strong correlation (0.9) with low volatility.

In most sessions (6 out of 9), the correlation coefficients reached statistical significance, with subject 4 (left leg) showing a perfect correlation. Furthermore, Subject 5 on the right leg had a p-value of 0.058, slightly above 0.05. The two most distant results presented a 12.1% and 13.5% probability that the correlation was due to chance.

The average p-value was 0.066 $\pm$ 0.058 for the left leg, which is 1.6% above the threshold for statistical significance defined. The right leg's average p-value was 0.046 $\pm$ 0.008, indicating statistical significance with very low variability. These results suggest that while the right leg presented more consistent results regarding significant correlation, the left leg showed greater variability, although most cases still revealed a strong correlation.

Table 20: Correlations between predicted and self-reported fatigue levels.

Subject ID	**Correlation Coefficient**	**Strength**	**p-value**	**Significance**
		Left		
1	0.778	Strong	0.121	No
2	0.913	Very Strong	0.030	Yes
3	0.889	Strong	0.044	Yes
4	1.000	Very Strong	0.000	Yes
5	0.761	Strong	0.135	No
		Right		
1	0.889	Strong	0.044	Yes
2	0	Negligible	0	No
3	0.891	Strong	0.042	Yes
4	0.896	Strong	0.039	Yes
5	0.866	Strong	0.058	No

These findings indicate that the CDSS effectively predicted muscle fatigue progression in rehabilitation treatments, showing a strong correlation between simulated levels and the participants' subjective perceptions. However, more data is needed to validate the muscle fatigue simulation model better. The accuracy

and consistency observed thus far suggest that the CDSS can provide real-time biofeedback, allowing for dynamic and personalized adjustments in rehabilitation treatments.

6.5.7 Discussion Experiment 3

The third experimental study aimed to further evaluate the performance of CDSS in a more complex and technically advanced test environment, comparing its results with those obtained by the gold standard MoCap system, as well as investigating the effectiveness of the *Raising the Leg* and *Range of Angle* stimulation modes. This experiment was particularly significant as it incorporated, for the first time, data collection from both legs of the participants and enabled the exploration of musculoskeletal simulations using the OpenSim tool.

The first objective, which involved comparing CDSS and MoCap in capturing the movement's kinematics, revealed that although CDSS showed some small discrepancies in the measured angular values, especially the maximum angle, the results after applying the correction algorithm were quite consistent with MoCap system. The differences found in the raw values between both systems align with expectations, given that MoCap is widely recognized as a gold standard system. However, the correction applied to CDSS significantly aligned the data, demonstrating the system's effectiveness in monitoring real-time kinematics.

In addition, OpenSim was used to generate the knee joint dynamics from the captured data, allowing for the accurate calculation of joint moments (torques). The results obtained from the tool proved to be statistically similar between CDSS and MoCap, reinforcing the reliability of CDSS in musculoskeletal simulations. This advancement opens new possibilities for CDSS in broader applications, such as personalized rehabilitation treatments based on detailed computational simulations.

Regarding *Raising the Leg* and *Range of Angle* stimulation modes, the results were equally promising. Analyses showed that both stimulation modes were correctly applied according to the defined parameters, with minimal variations between the start and end angles of stimulation. The observed error differences can be attributed to both the speed at which participants performed the movements and the processor's response time in reading the sensors and activating stimulation. Compared to traditional electrostimulation methods, CDSS proved to be an effective alternative, offering dynamic stimulation control based on real-time knee angles.

The joint analysis of fatigue metrics once again highlighted CDSS's robustness in monitoring the progression of muscle fatigue throughout the session. The consistency of data between the right and left legs also contributed to validating the system, showing that even with individual variations, CDSS could capture

muscle fatigue differences accurately.

Another important aspect of this study was the analysis of fatigue levels. The fatigue simulator was directly compared with participants' self-reported feedback for the first time. This approach allowed for cross-validation between the objective data captured by the CDSS and the participants' subjective perceptions. The results indicated a strong correlation between the fatigue levels detected by the simulator and the participants' reported sensations of tiredness, especially in the later series of each experimental session. The fact that the simulator was able to track and reflect these perceived changes is a significant indication of its applicability in rehabilitation contexts, where real-time adjustment of stimulation is crucial.

However, some limitations were observed. One key factor to consider is the relatively small number of participants in the experiment, which may limit the generalization of the results. While the analyses were consistent, a study with a larger sample size would allow for a more comprehensive assessment of the system's effectiveness. Additionally, the interference generated by the electrostimulation system in the EMG signal was more pronounced than expected, limiting the direct analysis of muscle fatigue during stimulation.

Despite this challenge, a viable solution would be to incorporate non-stimulated repetitions into the treatment protocol throughout the session. This approach would allow for an accurate measurement of muscle fatigue without the artifacts caused by stimulation, providing a baseline for reactivating the stimulation more efficiently. While the noise generated by stimulation is inherent to the process and cannot be completely eliminated, this strategy can mitigate its effects and ensure that muscle fatigue analysis is conducted properly throughout the treatment.

Chapter 7

Conclusion

This doctoral dissertation presents the development of a Clinical Decision Support System for Electrostimulation Treatments for Muscle Rehabilitation in the Elderly, addressing the challenges of remote muscular rehabilitation and a low-cost wearable device as actuator. The work described in this document is a significant reference in the application of Industry 4.0 technologies to healthcare, specifically within the context of Health 4.0. This system was designed to meet the growing need for personalized and accessible treatments, particularly for the aging population, where conditions such as sarcopenia and knee osteoarthritis are prevalent.

The central concept of the NanoStim project incorporated the Internet of Things, biofeedback sensors, low-power microcontrollers, and Bluetooth Low Energy connectivity to develop an efficient, affordable, and portable wearable device. These technologies enable new approaches to home-based rehabilitation, offering significant benefits such as reducing clinic visits, lowering treatment costs, increasing accessibility, and enhancing patient well-being. However, this scenario is only feasible with a secure, efficient, and interoperable CDSS.

The main research question addressed in this dissertation is: *How can a Clinical Decision Support System be designed to support remote rehabilitation with electrostimulation using a wearable device?* In answering this question, one of the main outcomes of this dissertation was the development of a treatment scenario and a system architecture. The treatment scenario specifies a methodology for performing muscle rehabilitation with electrostimulation at the patient's home and in the clinic using a wearable device. The system architecture developed demonstrates how this treatment scenario can be feasible in terms of computing and technology.

Given that the system manages sensitive healthcare data, a key objective of this PhD work was to implement a robust data protection approach. This approach was analyzed in a Master's thesis, as described in section 6.2.2. Additionally, CDSS was submitted for approval to the Data Protection Officer (DPO) of the IPB, confirming that CDSS complies with the General Data Protection Regulation (GDPR) and can securely

handle personal and health-related data. Beyond its scientific validation, this achievement was a crucial step for submitting and approving ethical protocols that enable experimental studies with volunteers.

A notable aspect of this PhD journey was the collaboration with a second project called NanoID. This project had similar objectives to NanoStim in terms of muscle rehabilitation using electrostimulation and home-based treatment, but it aimed at improving the posture of elderly individuals and preventing falls. A new hardware was developed with 4 EMG sensors and four stimulators designed to be positioned on the abdomen and back of the patient. For this purpose, CDSS was adapted to manage this treatment in terms of data handling and information flow, ensuring data protection. Additionally, new types of stimulation, dependent on angles measured by an IMU sensor, were implemented in the mobile app. NanoID project concluded in June, 2023, providing further evidence that the proposed CDSS is interoperable and that the data processing methods developed are reliable.

The specific research question *How can real-time biofeedback from a wearable device be processed to accurately monitor and assess muscle fatigue during remote rehabilitation?* was addressed through a series of experiments. In the first experiment with volunteers, CDSS were tested to validate the synchronization of EMG and IMU data while applying electrostimulation via a commercial device. The results demonstrated that it was possible to filter stimulation artifacts from the EMG signal and cloud to calculate the muscle fatigue metrics, providing valuable information about muscle assessment. In the second experiment, the ability of CDSS to calculate metrics related to muscle fatigue in real time was evaluated. The implementation of the fatigue monitoring method in the mobile application, working in real-time, demonstrated similar results to the raw data processed in Python. This result is important evidence that CDSS can be used to support rehabilitation in remote settings. The third and most scientifically advanced experiment compared the CDSS with the gold standard MoCap system for motion capture. The results show that although small discrepancies in angular values were observed, the movement recognized by the CDSS has a statistical correlation of 0.999 with the MoCap system evidencing again its accuracy..

The specific research question *How can electrostimulation treatments be dynamically adjusted in real-time based on biofeedback data during a treatment session?* was addressed first by introducing innovative stimulation modes in the CDSS. *Raising the Leg* and *Range of Angle* modes proved to be effective in offering more refined and dynamic control of electrostimulation by adjusting to the patient's joint angles in real time. This approach significantly differs from commercial devices, providing a more responsive treatment tailored to the patient's muscle condition during the session.

The analysis of the fatigue level simulator performed in experimental studies 2 and 3 demonstrated the system's ability to estimate muscle fatigue during sessions. The results showed that the simulator is

versatile through its parameters to be adjusted to the reality expressed by the patient. As described in the treatment scenario, at each session the physician is in charge of analyzing and incorporating technical interpretation of the muscle response. Adjusting fatigue levels progression is an important step that involves the physician in the construction of the home treatment session.

The cross-validation between the fatigue simulator data and the subjective feedback of the participants in the third experiment is an important evidence of the rule-based reasoning functionality. This feature modifies the stimulation parameters when there is a change in fatigue levels calculated on the biofeedback processed in real-time. The statistical analysis showed a strong correlation between the fatigue levels measured by the CDSS and the subjective feedback of all participants. These results show that real-time adjustments of stimulation would be strongly correlated with the participants' perception, adapting according with their fatigue during the session, an essential requirement in remote treatments.

In summary, this PhD project contributes with a novel approach to remote muscle rehabilitation, integrating cutting-edge technologies into a secure and effective system for electrostimulation treatment. The CDSS not only facilitates personalized care but also expands access to rehabilitation, reducing the need for frequent clinical visits. It aligns with the World Health Organization's Decade of Healthy Aging goals by promoting affordable, accessible, and effective healthcare solutions for the elderly. The system's ability to process real-time biofeedback, adjust treatment parameters dynamically, and ensure data security places it as an important step forward in the future of personalized muscle rehabilitation, with the potential to significantly improve the quality of life for elderly patients.

7.1 Scientific Contributions

Throughout this doctoral project, significant contributions have been made to the advancement of science in the field of muscle rehabilitation using electrostimulation and Health 4.0 technologies. In addition to the system already described in this document, further contributions were made through the following publications and presentations:

7.1.1 Journal Papers

- Franco et al. (2022c) Motion Sensors for Knee Angle Recognition in Muscle Rehabilitation Solutions. Sensors 2022.

- Franco et al. (2024a) Biofeedback-based Method for Real-time Fatigue Monitoring of Knee Extension. International Journal of Online and Biomedical Engineering (iJOE), 2024.

- (submitted) Decision Support Systems for Lower Limb Rehabilitation Using Electrical Stimulation - A Review. Biomedical Engineering Advances, 2024.

7.1.2 Conference Papers

- Franco et al. (2021) Approaches to Classify Knee Osteoarthritis Using Biomechanical Data. In Proceedings of the International Conference on Optimization, Learning Algorithms and Applications (OL2A), Portugal, 2021.

- Franco et al. (2022b) System Architecture for Home Muscle Rehabilitation Treatment. In Proceedings of the 10th World Conference on Information Systems and Technologies (WorldCIST), Montenegro, 2022.

- Franco et al. (2022a) myHealth: A Mobile App for Home Muscle Rehabilitation. In Proceedings of the IEEE 9th International Conference on Serious Games and Applications for Health (SeGAH), Australia, 2022.

7.1.3 Doctoral Symposium

- Franco (2022) Decision Support System for NMES Treatments: A solution design. 17th Iberian Conference on Information Systems and Technologies (CISTI), Spain, 2022.

7.1.4 Extended Abstract in Conference

- Franco et al. (2024b) A preliminary comparative study of knee kinematics and dynamics with NanoStim and motion capture systems. In Proceedings of the 6th International Conference on NeuroRehabilitation (ICNR2024), Spain, 2024.

7.1.5 Co-authored Conference Papers

- Conselheiro et al. (2022) Titanium Based Dry Electrodes for Biostimulation and Data Acquisition. In Distributed Computing and Artificial Intelligence, 19th International Conference. Lecture Notes in Networks and Systems (DCAI), Italy, 2022.

- Sestrem. et al. (2022) Data acquisition, conditioning and processing system for a wearable-based biostimulation. In Proceedings of the 15th International Joint Conference on Biomedical Engineering Systems and Technologies (BIOSTEC), Online, 2022.

- Nunes et al. (2022) Anomaly Detection Using Smart Shirt and Machine Learning: A Systematic Review. In Proceedings of the International Conference on Optimization, Learning Algorithms and Applications (OL2A), Portugal, 2022.

7.1.6 Talks and Demos

- Seminar on Decision Support System to Electrical Stimulation Treatments at The Research Centre for Biomedical Engineering (CREB), Universitat Politècnica de Catalunya (UPC), held on May 23, 2024.
- Participation in the Encontro Ciência 2022 at the Lisbon Congress Center presenting the NanoStim project.
- NanoStim project was demonstrated on multiple occasions at the Research Centre in Digitalization and Intelligent Robotics (CeDRI) to national and international visitors.

7.1.7 Article in Online Newspaper

- IPB ajuda a desenvolver tecnologia pioneira para criar peça de vestuário com sensores que pode revolucionar a fisioterapia, published in Mensageiro de Bragança on May 4, 2023.

7.2 Future Perspectives

The future perspectives of this work point to several promising directions for expanding the system's capabilities and validating its effectiveness in real clinical settings. One important next step could be to conduct experimental studies with elderly patients diagnosed with sarcopenia and knee osteoarthritis, which may offer valuable insights into the effectiveness in populations that align with its target audience. Such advancements could be critical in demonstrating the applicability and benefits of the CDSS in clinical contexts, potentially validating its use in home-based muscle rehabilitation treatments.

Additionally, exploring the use of tools like OpenSim for musculoskeletal simulations prior to the application of electrostimulation could offer a valuable avenue for future research. Simulations might predict how patients' muscles and joints respond to electrostimulation under various conditions, allowing for more personalized treatments tailored to individual patients. Testing stimulation and fatigue configurations in a virtual environment could enhance treatment safety and effectiveness by predicting outcomes before real-world application.

Moreover, the rule-based system currently in place offers significant potential for the personalization of the electrostimulation parameters. Incorporating machine learning and artificial intelligence technologies into the CDSS could allow for more advanced analysis of fatigue patterns and enable adjustments of electrostimulation parameters based on the patient's biofeedback background. Such enhancements might lead to a more dynamic and personalized system that continually adapts to the patient's condition over time using many sessions, offering increasingly individualized treatment solutions.

Future efforts could also focus on improving real-time monitoring accuracy by addressing electromagnetic interference in EMG signals during electrostimulation. Advances in electronic circuits and signal processing methods may reduce noise generated during stimulation sessions, making the collected data more reliable. Furthermore, expanding the CDSS to new areas of rehabilitation, such as posture and balance improvement, could present additional opportunities for its application, aligning with the growing demand for digital health solutions in the Health 4.0 era.

Finally, this doctoral project has made significant contributions toward developing a robust, scalable CDSS for electrostimulation treatments using a wearable device. The system has overcome numerous technological challenges to create the scientific evidence presented in this dissertation that highlights its potential to enable effective remote rehabilitation.

Methodologically, this CDSS serves as a foundation for future remote rehabilitation systems, with the potential to incorporate the perspectives discussed to further advance and develop more sophisticated solutions. As the system continues to evolve, it promises to greatly improve the quality of life for elderly patients, aligning with global healthy aging initiatives and contributing to the advancement of healthcare technologies.

Bibliography

Aldrich, J. B. and Cousin, C. A. (2021). Smoothly switched adaptive torque tracking for functional electrical stimulation cycling. *IEEE Control Systems Letters*, 6:866–871.

Allen, B. C., Stubbs, K. J., and Dixon, W. E. (2022). Robust cadence tracking for switched fes-cycling using a time-varying estimate of the electromechanical delay. *Automatica*, 144.

Alter, S. (1980). Decision support systems: current practice and continuing challenges. *Addison-Wesley Reading, MA*, 157.

Anaya, F., Thangavel, P., and Yu, H. (2018). Hybrid fes-robotic gait rehabilitation technologies: a review on mechanical design, actuation, and control strategies. *International Journal of Intelligent Robotics and Applications*, 2:1–28.

Anisimova, A. S., Meerson, M. B., Gerashchenko, M. V., Kulakovskiy, I. V., Dmitriev, S. E., and Gladyshev, V. N. (2020). Multifaceted deregulation of gene expression and protein synthesis with age. *Proceedings of the National Academy of Sciences*, 117(27):15581–15590.

Arcolezi, H. H., Nunes, W. R., de Araujo, R. A., Cerna, S., Sanches, M. A., Teixeira, M. C., and de Carvalho, A. A. (2021). Rise controller tuning and system identification through machine learning for human lower limb rehabilitation via neuromuscular electrical stimulation. *Engineering Applications of Artificial Intelligence*, 102.

Aria, M. and Cuccurullo, C. (2017). bibliometrix: An r-tool for comprehensive science mapping analysis. *Journal of informetrics*, 11(4):959–975.

Arnott, D. and Pervan, G. (2005). A critical analysis of decision support systems research. *Journal of Information Technology*, 20:67–87.

Arnott, D. and Pervan, G. (2008). Eight key issues for the decision support systems discipline. *Decision Support Systems*, 44(3):657–672.

Arnott, D. and Pervan, G. (2014). A critical analysis of decision support systems research revisited: the rise of design science. *Journal of Information Technology*, 29(4):269–293.

Bao, X., Sheng, Z., Dicianno, B. E., and Sharma, N. (2020). A tube-based model predictive control method to regulate a knee joint with functional electrical stimulation and electric motor assist. *IEEE Transactions on Control Systems Technology*, 29(5):2180–2191.

Bause, M., Esfahani, B. K., Forbes, H., and Schaefer, D. (2019). Design for health 4.0: exploration of a new area. In *Proceedings of the Design Society: International Conference on Engineering Design*, pages 887–896. Cambridge University Press.

Catelli, D. S., Wesseling, M., Jonkers, I., and Lamontagne, M. (2019). A musculoskeletal model customized for squatting task. *Computer methods in biomechanics and biomedical engineering*, 22(1):21–24.

Cerone, G. L., Vieira, T. M., Botter, A., and Gazzoni, M. (2019). Design of a wireless, modular and programmable neuromuscular electrical stimulator. In *2019 41st Annual International Conference of the IEEE Engineering in Medicine and Biology Society (EMBC)*, pages 3815–3818. IEEE.

Chang, C.-H., Casas, J., Brose, S. W., and Duenas, V. H. (2022). Closed-loop torque and kinematic control of a hybrid lower-limb exoskeleton for treadmill walking. *Frontiers in Robotics and AI*, 8:702–860.

Chivers, I., Sleightholme, J., Chivers, I., and Sleightholme, J. (2015). An introduction to algorithms and the big o notation. *Introduction to Programming with Fortran: With Coverage of Fortran 90, 95, 2003, 2008 and 77*, pages 359–364.

Chodzko-Zajko, W. J., Proctor, D. N., Singh, M. A. F., Minson, C. T., Nigg, C. R., Salem, G. J., and Skinner, J. S. (2009). Exercise and physical activity for older adults. *Medicine & science in sports & exercise*, 41(7):1510–1530.

Cieza, A., Causey, K., Kamenov, K., Hanson, S. W., Chatterji, S., and Vos, T. (2020). Global estimates of the need for rehabilitation based on the global burden of disease study 2019: a systematic analysis for the global burden of disease study 2019. *The Lancet*, 396(10267):2006–2017.

Cifrek, M., Medved, V., Tonković, S., and Ostojić, S. (2009). Surface emg based muscle fatigue evaluation in biomechanics. *Clinical Biomechanics*, 24(4):327–340.

Coelho-Magalhães, T., Azevedo Coste, C., and Resende-Martins, H. (2022). A novel functional electrical stimulation-induced cycling controller using reinforcement learning to optimize online muscle activation pattern. *Sensors*, 22(23).

Conforto, S., Castronovo, A., De Marchis, C., Schmid, M., Bertollo, M., Robazza, C., Comani, S., and D'Alessio, T. (2014). The fatigue vector: a new bi-dimensional parameter for muscular fatigue analysis. In *XIII Mediterranean Conference on Medical and Biological Engineering and Computing 2013: MEDICON 2013, 25-28 September 2013, Seville, Spain*, pages 149–152. Springer.

Conselheiro, R., Lopes, C., Azevedo, N., Leitao, P., Agulhari, C., Veloso, H., Vaz, F., Gonçalves, J., Franco, T., and Sestrem, L. (2022). Titanium based dry electrodes for biostimulation and data acquisition. In *International Symposium on Distributed Computing and Artificial Intelligence*, pages 111–120. Springer.

Cousin, C. A., Deptula, P., Rouse, C. A., and Dixon, W. E. (2021). A switched lyapunov-passivity approach to motorized fes cycling using adaptive admittance control. *IEEE Transactions on Control Systems Technology*, 30(2):740–754.

Cruz-Jentoft, A. J., Bahat, G., Bauer, J., Boirie, Y., Bruyère, O., Cederholm, T., Cooper, C., Landi, F., Rolland, Y., Sayer, A. A., et al. (2019). Sarcopenia: revised european consensus on definition and diagnosis. *Age and ageing*, 48(1):16–31.

Cruz-Jentoft, A. J. and Sayer, A. A. (2019). Sarcopenia. *The Lancet*, 393(10191):2636–2646.

Dattani, S., Rodés-Guirao, L., Ritchie, H., Ortiz-Ospina, E., and Roser, M. (2023). Life expectancy. *Our World in Data*. https://ourworldindata.org/life-expectancy.

Delp, S., Anderson, F., Arnold, A., Loan, P., Habib, A., John, C. T., Guendelman, E., and Thelen, D. (2007a). Opensim: Open-source software to create and analyze dynamic simulations of movement. *IEEE Transactions on Biomedical Engineering*, 54:1940–1950.

Delp, S., Anderson, F., Arnold, A., Loan, P., Habib, A., John, C. T., Guendelman, E., and Thelen, D. G. (2007b). OpenSim: Open-Source Software to Create and Analyze Dynamic Simulations of Movement. *IEEE Transactions on Biomedical Engineering*, 54(11):1940–1950.

Duenas, V. H., Cousin, C. A., Ghanbari, V., Fox, E. J., and Dixon, W. E. (2020). Torque and cadence tracking in functional electrical stimulation induced cycling using passivity-based spatial repetitive learning control. *Automatica*, 115.

Dufaug, A., Barthod, C., Goujon, L., and Marechal, L. (2020). New joint analysis of electromyography spectrum and amplitude-based methods towards real-time muscular fatigue evaluation during a simulated surgical procedure: A pilot analysis on the statistical significance. *Medical Engineering & Physics*, 79:1–9.

Enoka, R. M. and Duchateau, J. (2008). Muscle fatigue: what, why and how it influences muscle function. *The Journal of physiology*, 586(1):11–23.

Estay, F. E., Rouse, C. A., Cohen, M., Cousin, C. A., and Dixon, W. E. (2019). Cadence and position tracking for decoupled legs during switched split-crank motorized fes-cycling. In *2019 American Control Conference (ACC)*, pages 854–859. IEEE.

Evans, W. J. and Lexell, J. (1995). Human aging, muscle mass, and fiber type composition. *The Journals of Gerontology: Series A*, 50A:11–16.

Fabbri, S., Silva, C., Hernandes, E., Octaviano, F., Di Thommazo, A., and Belgamo, A. (2016). Improvements in the start tool to better support the systematic review process. In *Proceedings of the 20th international conference on evaluation and assessment in software engineering*, pages 1–5.

Ferrari, F., Zimei, E., Gandolla, M., Pedrocchi, A., and Ambrosini, E. (2023). An emg-triggered cooperative controller for a hybrid fes-robotic system. In *2023 IEEE International Conference on Metrology for eXtended Reality, Artificial Intelligence and Neural Engineering (MetroXRAINE)*, pages 852–857. IEEE.

Franco, T. (2022). Decision support system for nmes treatments: A solution design. In *2022 17th Iberian Conference on Information Systems and Technologies (CISTI)*, pages 1–4. IEEE.

Franco, T., Henriques, P. R., Alves, P., Pereira, M. J. V., Sestrem, L., Leitão, P., and Silva, A. (2022a). myhealth: a mobile app for home muscle rehabilitation. In *2022 IEEE 10th International Conference on Serious Games and Applications for Health(SeGAH)*, pages 1–7.

Franco, T., Henriques, P. R., Alves, P., and Pereira, M. V. (2021). Approaches to classify knee osteoarthritis using biomechanical data. In *International Conference on Optimization, Learning Algorithms and Applications*, pages 417–429. Springer.

Franco, T., Henriques, P. R., Alves, P., Varanda Pereira, M. J., Leitão, P., and Azevedo, N. (2024a). Biofeedback-based method for real-time fatigue monitoring of knee. *International Journal of Online and Biomedical Engineering (iJOE)*, 20(13):60––83.

Franco, T., Henriques, P. R., Alves, P., Varanda Pereira, M. J., Pedrosa, T., Silva, F., Leitão, P., and Oliveira, L. (2022b). System architecture for home muscle rehabilitation treatment. In *Information Systems and Technologies*, pages 305–315. Springer International Publishing.

Franco, T., Peres, A., Font-Llagunes, J. M., and de Sousa, A. C. C. (2024b). A preliminary comparative study of knee kinematics and dynamics with nanostim and motion capture systems. In *Proceedings of the 6th International Conference on NeuroRehabilitation (ICNR2024)*.

Franco, T., Sestrem, L., Henriques, P. R., Alves, P., Varanda Pereira, M. J., Brandão, D., Leitão, P., and Silva, A. (2022c). Motion sensors for knee angle recognition in muscle rehabilitation solutions. *Sensors*, 22(19).

Ghanbari, V., Duenas, V. H., Antsaklis, P. J., and Dixon, W. E. (2019). Passivity-based iterative learning control for cycling induced by functional electrical stimulation with electric motor assistance. *IEEE Transactions on Control Systems Technology*, 27(5):2287–2294.

Gonçalves, J. L. (2023). Development of a transformer-based electrical stimulation driver for a wearable physiotherapy system. Master's thesis, Escola Superior de Tecnologia e Gestão. Instituto Politécnico de Bragança, Portugal.

Halaki, M. and Ginn, K. (2012). Normalization of emg signals: to normalize or not to normalize and what to normalize to. *Computational intelligence in electromyography analysis-a perspective on current applications and future challenges*, 10.

Hambly, M. J., de Sousa, A. C. C., and Pizzolato, C. (2024). Comparison of filtering methods for real-time extraction of the volitional emg component in electrically stimulated muscles. *Biomedical Signal Processing and Control*, 87.

Hassanlouei, H., Arendt-Nielsen, L., Kersting, U., and Falla, D. (2012). Effect of exercise-induced fatigue on postural control of the knee. *Journal of Electromyography and Kinesiology*, 22(3):342–347.

Hayashi, D., Roemer, F., and Guermazi, A. (2016). Imaging for osteoarthritis. *Annals of Physical and Rehabilitation Medicine*, 59(3):161–169. Special Issue: Osteoarthritis / Coordinated by Emmanuel Coudeyre and François Rannou.

Imoto, A. M., Peccin, M. S., Teixeira, L. E. P. d. P., Silva, K. N. G. d., Abrahão, M., and Trevisani, V. F. M. (2013). Is neuromuscular electrical stimulation effective for improving pain, function and activities of daily living of knee osteoarthritis patients? a randomized clinical trial. *Sao Paulo Medical Journal*, 131:80–87.

Isaly, A., Allen, B. C., Sanfelice, R. G., and Dixon, W. E. (2021). Encouraging volitional pedaling in functional electrical stimulation-assisted cycling using barrier functions. *Frontiers in Robotics and AI*, 8.

Jafari, E. and Erfanian, A. (2022). A distributed automatic control framework for simultaneous control of torque and cadence in functional electrical stimulation cycling. *IEEE Transactions on Neural Systems and Rehabilitation Engineering*, 30:1908–1919.

Jayaraman, P. P., Forkan, A. R. M., Morshed, A., Haghighi, P. D., and Kang, Y.-B. (2020). Healthcare 4.0: A review of frontiers in digital health. *Wiley Interdisciplinary Reviews: Data Mining and Knowledge Discovery*, 10(2).

Jwo, D.-J., Chang, W.-Y., and Wu, I.-H. (2021). Windowing techniques, the welch method for improvement of power spectrum estimation. *CMC-Computers Materials & Continua*.

Kellgren, J. H. and Lawrence, J. S. (1957). Radiological assessment of osteo-arthrosis. *Annals of the Rheumatic Diseases*, 16(4):494–502.

Kitchenham, B. and Charters, S. (2007). Guidelines for performing systematic literature reviews in software engineering. *EBSE Technical Report*, 2.3.

Kohn, M. D., Sassoon, A. A., and Fernando, N. D. (2016). Classifications in brief: Kellgren-lawrence classification of osteoarthritis. *Clinical Orthopaedics and Related Research®*, 474(8):1886–1893.

Langeard, A., Bigot, L., Chastan, N., and Gauthier, A. (2017). Does neuromuscular electrical stimulation training of the lower limb have functional effects on the elderly?: A systematic review. *Experimental Gerontology*, 91:88–98.

Lespasio, M. J., Piuzzi, N. S., Husni, M. E., Muschler, G. F., Guarino, A., and Mont, M. A. (2017). Knee osteoarthritis: a primer. *The Permanente Journal*, 21.

Liu, S.-H., Lin, C.-B., Chen, Y., Chen, W., Huang, T.-S., and Hsu, C.-Y. (2019). An emg patch for the real-time monitoring of muscle-fatigue conditions during exercise. *Sensors*, 19(14).

Lou, Z., Wang, L., Jiang, K., Wei, Z., and Shen, G. (2020). Reviews of wearable healthcare systems: Materials, devices and system integration. *Materials Science and Engineering: R: Reports*, 140.

Loya, S. R., Kawamoto, K., Chatwin, C., and Huser, V. (2014). Service oriented architecture for clinical decision support: a systematic review and future directions. *Journal of medical systems*, 38:1–22.

Lu, H., Halappanavar, M., and Kalyanaraman, A. (2015). Parallel heuristics for scalable community detection. *Parallel Computing*, 47:19–37. Graph analysis for scientific discovery.

Luttmann, A., Jäger, M., and Laurig, W. (2000). Electromyographical indication of muscular fatigue in occupational field studies. *International journal of Industrial ergonomics*, 25(6):645–660.

Lynch, C. L. and Popovic, M. R. (2008). Functional electrical stimulation. *IEEE Control Systems Magazine*, 28(2):40–50.

Lyu, C., Morim, P. T., Penzlin, B., Röhren, F., Bergmann, L., von Platen, P., Bollheimer, C., Leonhardt, S., and Ngo, C. (2023). Closed-loop fes control of a hybrid exoskeleton during sit-to-stand exercises: Concept and first evaluation. *Actuators*, 12 (8).

Maffiuletti, N. A. (2010). Physiological and methodological considerations for the use of neuromuscular electrical stimulation. *European journal of applied physiology*, 110(2):223–234.

Manini, T. M., Hong, S. L., and Clark, B. C. (2013). Aging and muscle: a neuron's perspective. *Current opinion in clinical nutrition and metabolic care*, 16(1).

McGinty, G., Irrgang, J. J., and Pezzullo, D. (2000). Biomechanical considerations for rehabilitation of the knee. *Clinical Biomechanics*, 15(3):160–166.

Molazadeh, V., Zhang, Q., Bao, X., and Sharma, N. (2021). An iterative learning controller for a switched cooperative allocation strategy during sit-to-stand tasks with a hybrid exoskeleton. *IEEE Transactions on Control Systems Technology*, 30(3):1021–1036.

Moznuzzaman, M., Khan, T. I., Neher, B., and Ide, S. (2021). Effects of lower limb muscle activities to osteoarthritic knees. In *2021 Joint 10th International Conference on Informatics, Electronics & Vision (ICIEV) and 2021 5th International Conference on Imaging, Vision & Pattern Recognition (icIVPR)*, pages 1–6.

Nekoukar, V. (2021). Control of functional electrical stimulation systems using simultaneous pulse width, amplitude, and frequency modulations. *Neuromodulation: Technology at the Neural Interface*, 24(8):1467–1474.

Nelson, A. (2018). Osteoarthritis year in review 2017: clinical. *Osteoarthritis and Cartilage*, 26(3):319–325.

Nelson, A. E. and Jordan, J. M. (2015). Osteoarthritis: Epidemiology and classification. In Hochberg, M. C., Silman, A. J., Smolen, J. S., Weinblatt, M. E., and Weisman, M. H., editors, *Rheumatology (Sixth Edition)*, pages 1433–1440. Mosby, Philadelphia.

Nishida, M., Tsuboyama, T., Moritani, T., and Arai, H. (2016). Review of the evidence on the use of electrical muscle stimulation to treat sarcopenia. *European Geriatric Medicine*, 7(3):267–271. SI: Sarcopenia.

Nunes, E. C., Barbosa, J., Alves, P., Franco, T., and Silva, A. (2022). Anomaly detection using smart shirt and machine learning: A systematic review. In *International Conference on Optimization, Learning Algorithms and Applications*, pages 470–485. Springer.

Obuz, S., Duenas, V. H., Downey, R. J., Klotz, J. R., and Dixon, W. E. (2019). Closed-loop neuromuscular electrical stimulation method provides robustness to unknown time-varying input delay in muscle dynamics. *IEEE Transactions on Control Systems Technology*, 28(6):2482–2489.

Olinski, M., Gronowicz, A., Ceccarelli, M., and Cafolla, D. (2017). Human motion characterization using wireless inertial sensors. In *New Advances in Mechanisms, Mechanical Transmissions and Robotics: Proceedings of The Joint International Conference of the XII International Conference on Mechanisms and Mechanical Transmissions (MTM) and the XXIII International Conference on Robotics (Robotics' 16)*, pages 401–408. Springer.

Page, M. J., McKenzie, J. E., Bossuyt, P. M., Boutron, I., Hoffmann, T. C., Mulrow, C. D., Shamseer, L., Tetzlaff, J. M., Akl, E. A., Brennan, S. E., et al. (2021). The prisma 2020 statement: an updated guideline for reporting systematic reviews. *International journal of surgery*, 88.

Papadopoulos, P., Soflano, M., Chaudy, Y., Adejo, W., and Connolly, T. M. (2022). A systematic review of technologies and standards used in the development of rule-based clinical decision support systems. *Health and Technology*, 12(4):713–727.

Peffers, K. (2008). Is research using theory from elsewhere. *Journal of Information Technology Theory and Application (JITTA)*, 9(2).

Popović-Maneski, L. and Mateo, S. (2022). Motimove: Multi-purpose transcutaneous functional electrical stimulator. *Artificial Organs*, 46(10):1970–1979.

Potvin, J. and Brown, S. (2004). Less is more: high pass filtering, to remove up to 99% of the surface emg signal power, improves emg-based biceps brachii muscle force estimates. *Journal of Electromyography and Kinesiology*, 14(3):389–399.

Power, D. J. (2002). *Decision support systems: concepts and resources for managers*. Greenwood Publishing Group.

Rahim, A. A., Che-Ani, A. I., Hussain, Z., Boudville, R., and Ahmad, K. A. (2019). Development of powered knee orthosis for fes-assisted knee swing. In *2019 9th IEEE International Conference on Control System, Computing and Engineering (ICCSCE)*, pages 209–214. IEEE.

Ricarte, G., de Macĕdo Pinheiro, L., and Bó, A. P. L. (2020). Intuitive and modular software architecture for functional electrical stimulation rehabilitation. In *2020 Latin American Robotics Symposium (LARS), 2020 Brazilian Symposium on Robotics (SBR) and 2020 Workshop on Robotics in Education (WRE)*, pages 1–6. IEEE.

Ritchie, H., Rodés-Guirao, L., Mathieu, E., Gerber, M., Ortiz-Ospina, E., Hasell, J., and Roser, M. (2023). Population growth. *Our World in Data*. https://ourworldindata.org/population-growth.

Rouse, C. A., Cousin, C. A., Allen, B. C., and Dixon, W. E. (2021). Shared control for switched motorized fes-cycling on a split-crank cycle accounting for muscle control input saturation. *Automatica*, 123.

Schober, P., Boer, C., and Schwarte, L. A. (2018). Correlation coefficients: appropriate use and interpretation. *Anesthesia & analgesia*, 126(5):1763–1768.

Sestrem., L., Kaizer., R., Gonçalves., J., Leitão., P., Teixeira., J., Lima., J., Franco., T., and Carvalho., J. (2022). Data acquisition, conditioning and processing system for a wearable-based biostimulation. In *Proceedings of the 15th International Joint Conference on Biomedical Engineering Systems and Technologies - BIODEVICES,*, pages 223–230.

Shaw, D., Singh, D., Kaur, M., Ahlawat, U. K., and Bhatia, D. (2020). Electromyographic activity of vastus lateralis muscle of dominant thigh (right) in relation to performance levels during the leg/knee extension exercise performance with 30 repetition maximum load. *BLDE University Journal of Health Sciences*, 5(2):194–199.

Shen, Y., Colloc, J., Jacquet-Andrieu, A., and Lei, K. (2015). Emerging medical informatics with case-based reasoning for aiding clinical decision in multi-agent system. *Journal of Biomedical Informatics*, 56:307–317.

Shoaip, N., El-Sappagh, S., Barakat, S., and Elmogy, M. (2019). Chapter 4 - reasoning methodologies in clinical decision support systems: A literature review. In Dey, N., Ashour, A. S., Fong, S. J., and Borra, S., editors, *U-Healthcare Monitoring Systems*, Advances in Ubiquitous Sensing Applications for Healthcare, pages 61–87. Academic Press.

Sijobert, B., Le Guillou, R., Fattal, C., and Azevedo Coste, C. (2019). Fes-induced cycling in complete sci: a simpler control method based on inertial sensors. *Sensors*, 19(19):42–68.

Silva, F. (2021). Arquitetura de segurança para aplicações clínicas inteligentes de tratamento no domicílio. Master's thesis, Escola Superior de Tecnologia e Gestão. Instituto Politécnico de Bragança, Portugal.

Sousa, A. C. C., Valtin, M., Bó, A. P., and Schauer, T. (2018). Automatic detection of stimulation artifacts to isolate volitional from evoked emg activity. *IFAC-PapersOnLine*, 51(27):282–287.

Sousa, A. S. and Tavares, J. M. R. (2012). Surface electromyographic amplitude normalization methods: a review. *Electromyography: new developments, procedures and applications*.

Sun, Z., Iyer, A., Lambeth, K., Cleveland, C., and Sharma, N. (2023). Knee extension tracking and fatigue regulation results using a robust mpc approach in a hybrid exoskeleton. *Control Engineering Practice*, 141.

Sutton, R. T., Pincock, D., Baumgart, D. C., Sadowski, D. C., Fedorak, R. N., and Kroeker, K. I. (2020). An overview of clinical decision support systems: benefits, risks, and strategies for success. *NPJ digital medicine*, 3(1).

Teodoro, R. G., Nunes, W. R., de Araujo, R. A., Sanches, M. A., Teixeira, M. C., and de Carvalho, A. A. (2020). Robust switched control design for electrically stimulated lower limbs: A linear model analysis in healthy and spinal cord injured subjects. *Control Engineering Practice*, 102.

Trygve, R. (2003). The model-view-controller (mvc) its past and present. *University of Oslo Draft*.

Valade, A., Acco, P., Grabolosa, P., and Fourniols, J.-Y. (2017). A study about kalman filters applied to embedded sensors. *Sensors*, 17(12).

van der Scheer, J. W., Goosey-Tolfrey, V. L., Valentino, S. E., Davis, G. M., and Ho, C. H. (2021). Functional electrical stimulation cycling exercise after spinal cord injury: a systematic review of health and fitness-related outcomes. *Journal of neuroengineering and rehabilitation*, 18(1).

Velickovski, F. (2016). *Clinical Decision Support for Screening, Diagnosis and Assessment of Respiratory Diseases: Chronic Obstructive Pulmonary Disease as a Use Case*. Phd thesis, Universitat de Girona. Escola Politècnica Superior.

Verma, D. (2022). *Using Case-based Reasoning for Creating Intelligent Systems in Healthcare*. Phd thesis, Norwegian University of Science and Technology, Norway.

Walmsley, C. P., Williams, S. A., Grisbrook, T., Elliott, C., Imms, C., and Campbell, A. (2018). Measurement of upper limb range of motion using wearable sensors: a systematic review. *Sports medicine-open*, 4:1–22.

Wannawas, N. and Faisal, A. A. (2023). Towards ai-controlled movement restoration: Learning fes-cycling stimulation with reinforcement learning. In *2023 International Conference on Rehabilitation Robotics (ICORR)*, pages 1–6. IEEE.

Wasylewicz, A. and Scheepers-Hoeks, A. (2019). Clinical decision support systems. *Fundamentals of clinical data science*, pages 153–169.

Watanabe, T. and Tadano, T. (2019). An examination of stimulation timing patterns for mobile fes cycling under closed-loop control of low cycling speed. In *International Conference on NeuroRehabilitation*, pages 1106–1110. Springer.

Welch, P. (1967). The use of fast fourier transform for the estimation of power spectra: a method based on time averaging over short, modified periodograms. *IEEE Transactions on audio and electroacoustics*, 15(2):70–73.

Wirth, R. and Hipp, J. (2000). Crisp-dm: Towards a standard process model for data mining. In *Proceedings of the 4th international conference on the practical applications of knowledge discovery and data mining*, volume 1. Springer-Verlag London, UK.

World Health Organization (2021). *Decade of healthy ageing: baseline report*. Geneva.

Yuan, S. and Larsson, S. C. (2023). Epidemiology of sarcopenia: Prevalence, risk factors, and consequences. *Metabolism*, 144.

Zeng, C., li, H., Yang, T., h. Deng, Z., Yang, Y., Zhang, Y., and h. Lei, G. (2015). Electrical stimulation for pain relief in knee osteoarthritis: systematic review and network meta-analysis. *Osteoarthritis and Cartilage*, 23(2):189–202.

Zhang, J., Zhang, L., Guo, S., Meng, W., Ai, Q., and Liu, Q. (2020a). Iterative learning control of functional electrical stimulation based on joint muscle model. In *Proceedings of the 2020 3rd International Conference on Computational Intelligence and Intelligent Systems*, pages 119–123.

Zhang, Q., Meng, Y., Wu, L., Xiang, X., and Xiong, C. (2020b). Artificially induced joint movement control with musculoskeletal model-integrated iterative learning algorithm. *Biomedical Signal Processing and Control*, 59.

Zhang, Y. and Jordan, J. M. (2010). Epidemiology of osteoarthritis. *Clinics in Geriatric Medicine*, 26(3):355–369.